

# Bases for Predicting the Earliest Penetrations Due to SCC for Alloy 600 on the Secondary Side of PWR Steam Generators

**Argonne National Laboratory**

**U.S. Nuclear Regulatory Commission  
Office of Nuclear Regulatory Research  
Washington, DC 20555-0001**



## AVAILABILITY OF REFERENCE MATERIALS IN NRC PUBLICATIONS

### NRC Reference Material

As of November 1999, you may electronically access NUREG-series publications and other NRC records at NRC's Public Electronic Reading Room at [www.nrc.gov/NRC/ADAMS/index.html](http://www.nrc.gov/NRC/ADAMS/index.html).

Publicly released records include, to name a few, NUREG-series publications; *Federal Register* notices; applicant, licensee, and vendor documents and correspondence; NRC correspondence and internal memoranda; bulletins and information notices; inspection and investigative reports; licensee event reports; and Commission papers and their attachments.

NRC publications in the NUREG series, NRC regulations, and *Title 10, Energy*, in the Code of *Federal Regulations* may also be purchased from one of these two sources.

1. The Superintendent of Documents  
U.S. Government Printing Office  
Mail Stop SSOP  
Washington, DC 20402-0001  
Internet: [bookstore.gpo.gov](http://bookstore.gpo.gov)  
Telephone: 202-512-1800  
Fax: 202-512-2250
2. The National Technical Information Service  
Springfield, VA 22161-0002  
[www.ntis.gov](http://www.ntis.gov)  
1-800-553-6847 or, locally, 703-605-6000

A single copy of each NRC draft report for comment is available free, to the extent of supply, upon written request as follows:

Address: Office of the Chief Information Officer,  
Reproduction and Distribution  
Services Section  
U.S. Nuclear Regulatory Commission  
Washington, DC 20555-0001  
E-mail: [DISTRIBUTION@nrc.gov](mailto:DISTRIBUTION@nrc.gov)  
Facsimile: 301-415-2289

Some publications in the NUREG series that are posted at NRC's Web site address [www.nrc.gov/NRC/NUREGS/indexnum.html](http://www.nrc.gov/NRC/NUREGS/indexnum.html) are updated periodically and may differ from the last printed version. Although references to material found on a Web site bear the date the material was accessed, the material available on the date cited may subsequently be removed from the site.

### Non-NRC Reference Material

Documents available from public and special technical libraries include all open literature items, such as books, journal articles, and transactions, *Federal Register* notices, Federal and State legislation, and congressional reports. Such documents as theses, dissertations, foreign reports and translations, and non-NRC conference proceedings may be purchased from their sponsoring organization.

Copies of industry codes and standards used in a substantive manner in the NRC regulatory process are maintained at—

The NRC Technical Library  
Two White Flint North  
11545 Rockville Pike  
Rockville, MD 20852-2738

These standards are available in the library for reference use by the public. Codes and standards are usually copyrighted and may be purchased from the originating organization or, if they are American National Standards, from—

American National Standards Institute  
11 West 42<sup>nd</sup> Street  
New York, NY 10036-8002  
[www.ansi.org](http://www.ansi.org)  
212-642-4900

Legally binding regulatory requirements are stated only in laws; NRC regulations; licenses, including technical specifications; or orders, not in NUREG-series publications. The views expressed in contractor-prepared publications in this series are not necessarily those of the NRC.

The NUREG series comprises (1) technical and administrative reports and books prepared by the staff (NUREG-XXXX) or agency contractors (NUREG/CR-XXXX), (2) proceedings of conferences (NUREG/CP-XXXX), (3) reports resulting from international agreements (NUREG/IA-XXXX), (4) brochures (NUREG/BR-XXXX), and (5) compilations of legal decisions and orders of the Commission and Atomic and Safety Licensing Boards and of Directors' decisions under Section 2.206 of NRC's regulations (NUREG-0750).

**DISCLAIMER:** This report was prepared as an account of work sponsored by an agency of the U.S. Government. Neither the U.S. Government nor any agency thereof, nor any employee, makes any warranty, expressed or implied, or assumes any legal liability or responsibility for any third party's use, or the results of such use, of any information, apparatus, product, or process disclosed in this publication, or represents that its use by such third party would not infringe privately owned rights.

# **Bases for Predicting the Earliest Penetrations Due to SCC for Alloy 600 on the Secondary Side of PWR Steam Generators**

---

---

Manuscript Completed: August 2001  
Date Published: September 2001

Prepared by  
Dr. Roger W. Staehle, Consultant  
22 Red Fox Road  
North Oaks, MN 55127

Under Contract to  
Argonne National Laboratory  
9700 South Cass Avenue  
Argonne, IL 60439

J. Muscara, NRC Project Manager

Prepared for  
Division of Engineering Technology  
Office of Nuclear Regulatory Research  
U.S. Nuclear Regulatory Commission  
Washington, DC 20555-0001  
NRC Job Code W6487



# **BASES FOR PREDICTING THE EARLIEST PENETRATIONS DUE TO SCC FOR ALLOY 600 ON THE SECONDARY SIDE OF PWR STEAM GENERATORS**

by

Dr. Roger W. Staehle  
Adjunct Professor  
University of Minnesota

## **ABSTRACT**

The purpose of this report is to define the bases for predicting the earliest failures in a set of tubes in steam generators where the mode of failure is stress corrosion cracking. By "earliest failure" is meant the first ones that occur at a probability in the range of 0.0001 to 0.01, depending on the number of tubes at risk for a particular mode-location failure. Such early failures are far removed from the mean time-to-failure where the probability of failure is 0.5. Most testing for the purpose of predicting performance is directed, intentionally or not, toward determining the mean; however, using the mean time-to-failure as a measure of design life implies that 50% of the tubes would have failed during the design life. Failure times at probabilities of 0.0001 to 0.01 may be less than  $10^{-4}$  to  $10^{-2}$  of the mean time-to-failure when the shape parameter of the Weibull distribution,  $\beta$ , is unity. In developing predictions of the earliest failures, knowledge of both the mean, whether measured as  $\mu$  or as the Weibull scale parameter,  $\theta$ , and the shape parameter,  $\beta$ , are necessary. In general, data obtained that are taken as the mean values are the same as correlations that are usually developed from testing; however, there are few data and no theory for predicting the shape parameter although certain inferences are possible with respect to the critical failure processes being random or subject to accumulation processes. To a first approximation, a conservative shape parameter for predicting the earliest failures is unity. However, larger shape parameters (an increasing shape parameter for the Weibull distribution means a narrower range of data) can be justified depending on the behavior of the most susceptible heats of material in a set. The capacity to predict the earliest failures depends on understanding the inherent variability, the metallurgically-induced variability, the environmentally-induced variability, and the effects of experimental methods on variability. Data for these contributions are analyzed. Information is available that permits developing useful inferences about the mechanistic bases for statistical parameters.

## TABLE OF CONTENTS

PAGE

<b>ABSTRACT</b> .....	iii
<b>FIGURES</b> .....	vii
<b>TABLES</b> .....	xvi
<b>SUMMARY AND CONCLUSIONS</b> .....	xvii
<b>ACKNOWLEDGMENTS</b> .....	xxi
<b>INTRODUCTION</b> .....	1
<b>1.1 Scope and Objectives</b> .....	1
<b>1.2 An Alternative Approach</b> .....	2
<b>1.3 Physical Bases</b> .....	3
<b>1.4 Problems with Arrays of Data</b> .....	3
<b>1.5 Geometries of Industrial Equipment: Nuclear         Steam Generators for PWRs</b> .....	5
<b>1.6 Examples of Statistical Descriptions</b> .....	6
<b>1.7 Domains of Initiation and Propagation</b> .....	7
<b>1.8 General Prediction of Dependencies of SCC-Modes and Submodes</b> .....	10
<b>1.9 Framework for Predicting Early Failures</b> .....	16
<b>1.10 Outline of the Approach</b> .....	16
<b>2.0 STATISTICAL DISTRIBUTIONS AND THEIR APPLICATIONS</b> .....	17
<b>2.1 Scope</b> .....	17
<b>2.2 The Distributions</b> .....	17
2.2.1 The Weibull Distribution .....	18
2.2.2 Exponential (Poisson) Distribution .....	22
2.2.3 Normal Distribution .....	24
2.2.4 Extreme Value Distribution .....	24
<b>2.3 Scatter: Coherent and Non-coherent Variability</b> .....	25
2.3.1 Coherent Variability .....	25
2.3.2 Non-coherent Variability .....	27
2.3.3 Contributions to Producing Non-coherent Variability .....	28
2.3.4 Minimizing Non-coherent Variability .....	29
2.3.5 Early Failures Relative to the Mean .....	30
<b>2.4 Properties of Distributions Related to <math>\beta</math> and the hf</b> .....	31
<b>2.5 The Coherent <math>\beta=1</math> (Poisson) and <math>\beta=4</math> Cases</b> .....	32
<b>2.6 The Mixed Condition Giving <math>\beta=1</math></b> .....	32
<b>2.7 Steep Dependencies of SCC Produce a <math>\beta=1</math> Result</b> .....	34
<b>2.8 Relative Influence of Stressors and Material</b> .....	35
<b>2.9 Relative Dominance of Initiation and Propagation</b> .....	37
<b>2.10 Insertion of Principal Variables into         Statistical Parameters, Stressors</b> .....	39
<b>3.0 INHERENT VARIABILITY</b> .....	41
<b>3.1 Scope</b> .....	41
<b>3.2 Components of Inherent Variability for the <math>\beta=1</math> Case</b> .....	42
<b>3.3 Components of Inherent Variability for the <math>\beta=4</math> Case</b> .....	43
<b>3.4 Bounding: Less Bounded and More Bounded</b> .....	44
<b>3.5 Conducting Experiments to Characterize Inherent Variability</b> .....	45

<b>4.0 METALLURGICAL VARIABILITY</b> .....	46
4.1 Scope .....	46
4.2 Alloy Composition .....	46
4.3 Structure Sensitive Effects .....	48
4.4 Orientation .....	52
4.5 Cold Work .....	53
4.6 Welds .....	54
4.7 Surface Treatments .....	55
<b>5.0 ENVIRONMENTAL VARIABILITY</b> .....	57
5.1 Scope .....	57
5.2 Chemical Effects .....	60
5.3 Temperature .....	63
5.4 Stress .....	67
<b>6.0 CRACK SHAPES AND FREQUENCY</b> .....	71
6.1 Scope .....	71
6.2 Frequency of Surface Micro-cracks .....	71
6.3 Effect of Pitting on SCC Initiation .....	73
<b>7.0 MEANS AND MEASUREMENT</b> .....	75
7.1 Scope .....	75
7.2 Types of Tests .....	75
7.3 Considerations in Means of Testing and Measurements .....	76
<b>8.0 MODELING AND APPLICATION</b> .....	79
8.1 Scope .....	79
8.2 Choosing $\theta$ for Estimating Earliest Failures with No Prior Failures .....	79
8.3 Evaluation of $t_0$ for Estimating Earliest Failures with No Prior Failures .....	80
8.4 Choosing $\beta$ for Estimating Earliest Failures with No Prior Failures .....	80
8.5 Dependencies of $\beta$ .....	82
8.5.1 General Features of $\beta$ .....	82
8.5.2 Analysis for Dependence of $\beta$ on Temperature and Stress .....	83
8.5.3 Alloy Dependence .....	84
8.5.4 Alloy Structure .....	84
8.6 Overall Problem with $\beta$ .....	84
8.7 Choosing Parameters After First Failures Have Occurred .....	85
8.8 Existing Patterns of Early Failures .....	86
8.9 Multiple Failures .....	86
8.10 Calculating the Probability of Failure Time Based on Initiation and Propagation .....	88
8.11 Calculating cdf with Changing Variables .....	89
8.12 Accelerated Testing and Extrapolating Results .....	90
8.13 Predicting Engineering Performance .....	91
<b>REFERENCES</b> .....	93

## FIGURES

PAGE

1. General relationship for the penetration of SCC following commonly accepted dependencies. Locations where principal variables enter this equation are noted..... 3
2. (a) Time-to-failure vs.  $1/T$  for 23 sets of data for stainless steels in boiling 35 to 45%  $MgCl_2$  solutions at open-circuit conditions. (b) Time-to-failure vs. stress for 40 sets of data measured for stainless steel in 42%  $MgCl_2$  at open-circuit conditions. From Jiang and Staehle.<sup>41</sup> ..... 4
3. (a) Available data for crack growth rates in a data base for sensitized Type 304 stainless steel\* exposed to boiling water nuclear reactor (BWR) environments. (b) Screened data applicable to the conditions noted on the figure. Bounding line shown. From Jansson and Morin.<sup>43</sup> ..... 5
4. (a) View of prototypic steam generator (SG) for pressurized water nuclear reactor (PWR) with vessel, tube sheet, tube supports, and a U-shaped tube, one of about 4000. (b) Tube in tube support. (c) Tube in tubesheet showing presence of deposits referred to as "sludge."... 6
5. (a) Probability vs. time since startup for SCC failure of welded stainless steel pipes from piping used in boiling water nuclear reactors (BWR). From Eason and Shusto.<sup>44</sup> (b) Probability vs. equivalent full power years (EFPY) for failures of tubing from a set of SGs in the Ringhals 4 PWR. Designations: TTS = "top of tube sheet." TS = "tubesheet." Circ. SCC = "circumferential SCC." P\* = special location where SCC is not serious. RT = "roll transition." AVB = "antivibration bars". (Unpublished data provided by L. Bjornkvist of Vattenfall and J. Gorman of Dominion Engineering.)..... 6
6. Nine segments of SCC: (1) Protective film adjusts to the environment; (2) chemical and/or mechanical perforation of protective film; (3) early penetration by pitting, intergranular corrosion, slip step dissolution, tunnels, dealloying and hydrogen embrittlement; (4) early SCC; (5) coalescence of small SCC; (6) propagation of coalesced SCC until  $K_{ISCC}$  reached; (7) stage I propagation; (8) stage II propagation; (9) stage III propagation. Overall stages of initiation and propagation shown. .... 7
7. (a) Schematic view of crack depth vs. time. From Andresen and Ford,<sup>68</sup> (b) Schematic view of crack velocity vs. time. Adapted from Parkins.<sup>69</sup> (c) Schematic view of penetration vs. time showing segments; solid lines indicate deterministic processes and dotted lines indicate stochastic processes; depths of pitting and SCC indicated. From Akashi and Nakayama.<sup>61</sup> (d) Schematic view of crack depth vs. time for materials of various susceptibilities to SCC. From Gras.<sup>70</sup> (e) Schematic view of open circuit potential vs. time showing locations associated with segments of SCC. Adapted from work of Hoar and Hines<sup>71</sup> and Hines.<sup>72</sup> (f) Crack depth vs. time for various stainless steels measured metallographically after exposure to boiling 42%  $MgCl_2$ . From Eckel.<sup>73</sup> ..... 9
8. Basis for distinguishing between initiation and propagation. (a) Schematic view of log stress vs. log of defect depth for cases of stresses on smooth surface specimens and the locus of points associated with  $K_{ISCC}$  as determined from pre-cracked specimens. (b) Graph for

determining the intersection of threshold stresses from smooth surface specimens with values of $K_{ISCC}$ . From Staehle. <sup>4</sup> .....	10
9. Maximum crack depth vs. exposure time for Alloy 600MA exposed to 10% NaOH at 315°C and +150 mV applied potential. Solid line and solid dots correspond to reference depth vs. time for SCC at the nominal conditions. Dotted lines and open circles represent the instances where the applied potential was removed at various times. Approximate regions of control by surface chemistry and crack tip chemistry are noted as they correspond to conditions of initiation and propagation. From Pessell. <sup>74</sup> .....	11
10. Five intrinsic modes of penetration by corrosion into solids: General corrosion (including chemical degradation, wear, erosion, and fretting), intergranular corrosion, pitting corrosion, stress corrosion cracking in transgranular and intergranular morphologies, and dry fatigue. ....	11
11. Schematic view of locations where submodes of SCC can occur relative to a polarization curve. Other submodes of pitting, general corrosion and passivity are noted. From Staehle. <sup>77</sup> .....	12
12. (a) Major submodes of SCC and IGC for Alloy 600 in sensitized and mill annealed conditions in the range of 280° to 350°C in aqueous solutions. Regions of SCC shown with respect to thermodynamic boundaries for iron and nickel species in water. Regions of SCC submodes shown are based on published experimental data. <sup>76</sup> LPSCC = "low potential SCC." HPSCC = "high potential SCC." AkSCC = "alkaline SCC." AcSCC = "acidic SCC." SN = "sensitized." MA = "mill annealed." P = "pure water." C = "contaminated." (b) Minor submodes of SCC shown with respect to the region around the Ni-NiO equilibrium. Minor submodes are shown relative to Ni/NiO line. ....	13
13. (a) Extent of LPSCC vs. applied potential for Alloy 600 at 350°C; note location of Ni/NiO equilibrium. Adapted from Totsuka and Szklarska-Smialowska. <sup>93</sup> (b) Type I dependence of SCC on potential with correlation equation noted. (c) Extent of HPSCC vs. potential for Alloy 600 at 288°C. Adapted from Shoji. <sup>94</sup> (d) Type II dependence of SCC on potential with correlation equation noted. (e) Maximum crack depth as a function of potential for Alloy 600 exposed to 10%NaOH at 315°C. Adapted from Pessall. <sup>74</sup> (f) Type III dependence of SCC on potential with correlation equation shown.....	14
14. (a) Potential vs. pH for iron in water. Shaded areas show locations for occurrence of SCC of low alloy steels exposed to different environments at room temperature except for one in high temperature water. Adapted from Congleton et al. <sup>96</sup> (b) Line shows potential below which hydrogen-related SCC occurs for various steels. Adapted from Parkins. <sup>95</sup> (c) Synthesis of data from Figures 14a and 14b. (d) Solubility of iron as a function of pH with the dotted line drawn from the minimum solubility to the region of no anodic SCC. Adapted from Pourbaix. <sup>97</sup> .....	15
15. (a) $f(t)$ vs. time for constant $\beta$ . (b) $f(t)$ vs. time for constant $\theta$ . (c) $F(t)$ vs. time for constant $\beta$ . (d) $F(t)$ vs. time for constant $\theta$ . (e) $h(t)$ vs. time for constant $\beta$ . (f) $h(t)$ vs. time for constant $\theta$ . (g) $dh(t)/dt$ vs. time for constant $\beta$ . (h) $dh(t)/dt$ vs. time for constant $\theta$ . $t_0$ taken as zero. ....	20



16. Probability vs. time for Type 304 stainless steel exposed to $MgCl_2$ solution at $126^\circ C$ and stressed at 100 MPa. Original observations shown in circles and points corrected with the location parameter, $t_o$ , are shown by triangles. Magnitude of $t_o$ is shown. Adapted from Shibata et al. <sup>101</sup> .....	22
17. (a) Shape parameter, $\beta$ , vs. mean failure time, $\mu$ , in terms of the Weibull distribution for experiments performed in pure water and NaCl solutions using sensitized stainless steel in the presence and absence of surface crevices in the temperature range of $30-80^\circ C$ . Adapted from Akashi and Nakayama. <sup>18</sup> (b) $H(t)$ vs. $t$ showing the intercept as it gives the location parameter, $t_o$ , and the slope as it gives the scale parameter, $\theta$ . Adapted from Akashi and Nakayama. <sup>18</sup> .....	23
18. Frequency vs. strength for the ultimate tensile and yield strengths for Alloy 690TT. From Balavage and Gardner. <sup>109</sup> .....	24
19. Range ratio (time for last specimen to fail/time for first specimen to fail), $t_N/t_1$ , vs. $\beta$ for three values of $N$ (number of specimens) based on Weibull distribution. ....	26
20. Probability vs. crack growth rate for Alloy 182 weld metal and wrought austenitic alloys exposed at $288^\circ C$ in low conductivity water. Data originally plotted as a log normal distribution. Adapted from Andresen. <sup>42</sup> .....	26
21. SCC growth rate vs. $1/T$ for data from six separate investigations of Alloy 600 where the LPSCC submode has been investigated. From Cassagne et al. <sup>116</sup> .....	27
22. (a) Aggregate $\beta_g$ vs. $\theta_H/\theta_L$ for local shape parameters of $\beta_L=1, 4$ and $10$ . Four equally spaced sets of data, on a logarithmic scale, are assumed for each calculation and five data points for each component distribution are taken. Based on Weibull distribution. (b) Example of method of calculation. $\theta_H$ and $\theta_L$ shown with four distributions, each with slopes $\beta_L$ , and the resulting $\beta_g$ calculated from aggregating the data for all slopes. ....	28
23. Components of coherent and non-coherent variability. ....	29
24. Early failure ratio, $t_1/t_\mu$ vs. $\beta$ for times at 0.0001, 0.001, 0.01 probabilities relative to the time for the mean at 0.5 probability using the Weibull distribution. ....	30
25. Schematic plot of probability of failure vs. time for field data and accelerated tests based on Weibull coordinates. N-1 corresponds to assumed field results; A-1 corresponds to assumed accelerated testing. ....	31
26. (a) cdf for $\beta=1$ and $\beta=4$ vs. time. (b) hf vs. time for $\beta=1$ and $\beta=4$ cases at $\theta=10$ and $t_o=0$ . (c) Possible contributions in the metal substrate, for a growing SCC, to the accumulation case for $\beta=4$ . (d) Possible contributions to the accumulation case $\beta=4$ from exterior of the metal surface with a superheated tube support geometry as in Figure 4. (e) Possible contributions to the $\beta=1$ case. ....	33
27. Probability vs. time for seven heats of Alloy 600 exposed to high purity water with hydrogen addition at $365^\circ C$ using reverse U-bend specimens where failure occurs by the LPSCC	

- submode. From Norring et al.<sup>117</sup> The detailed data were not published with these curves; thus, for analysis, each distribution was assumed to represent five data points, and the analysis of the aggregate distribution was based on this assumption. .... 34
28. (a) Schematic view of rate of SCC vs. potential similar to that for LPSCC as shown in Figure 13a and 13b and showing six arbitrary locations where distributions are obtained assuming that the SCC testing was performed at constant potential at these locations. (b) Schematic view of probability vs. time for  $\beta_L$  distributions at four locations with aggregate  $\beta_g$  shown. The aggregate is based on the idea that data came from four distributions that could not be distinguished in the final set of data.  $\beta_L$  slopes of 4 are typical of PWR primary water where (a) applies as indicated in Figure 52. (c) Schematic view of probability vs. time for three sets of data where the assumed rates are the same. .... 35
29. (a) Probability vs. time-to-failure for Zircaloy 2 exposed at 350°C to iodine gas. (b) Weibull parameters vs. hoop stress. Adapted from Shimada and Nagai.<sup>26</sup> Determination of curve dependencies from Fang and Staehle.<sup>118</sup> .... 36
30. (a) Probability vs. time for sensitized Type 304 stainless steel tested at 288°C in high purity oxygenated water. From Clark and Gordon.<sup>115</sup> (b) Probability vs. time for sensitized Type 304 stainless steel tested at 288°C in high purity oxygenated water. From Akashi and Ohtomo.<sup>119</sup> (c) Weibull parameters vs. stress from both the Clark and Gordon (CG) (dotted lines) and Akashi (A) (solid lines) distributions. .... 37
31. (a) Schematic illustration of the effects of temperature and stress on the  $\beta$  associated with time-to-failure as depending more on initiation or propagation. From Shibata and Takeyama.<sup>120</sup> (b) Probability vs. time for Type 304 stainless steel exposed to boiling  $MgCl_2$  at 154°C at various stresses. (c) Median values for upper and lower slopes vs. stress from (b). (d) Values of  $\beta$  for upper and lower vs. stress from (b). From Shibata and Takeyama.<sup>123</sup> (e) Data for  $t_p$ ,  $t_p'$ , and  $t_f$  for Type 304 stainless steel exposed to 30 w/o  $CaCl_2$  solution at a constant condition of 200 MPa and 100°C. From Shibata et al.<sup>121</sup> (f) Weibull calculation for (e). .... 38
32. (a) Probability vs. time for data determined for both initiation and propagation of a high strength steel exposed to a 3.5% NaCl solution at 40°C. From Ichikawa et al.<sup>124</sup> (b) Schematic illustration of the role of both initiation and propagation with the combined result. From Ichikawa et al.<sup>125</sup> .... 39
33. (a) Probability vs. pitting potential for Fe-Cr base alloys as determined at 30°C in 3.5w/o NaCl; solution  $N_2$  saturated. Pitting potentials measured with potentiometric scans of 16.7 mV/min. Data on the abscissa are adjusted for convenience of probability plotting by adding + 0.2V. The original data were plotted using normal probability coordinates. (b) Pitting potential at  $\theta$  from Figure 33a vs. chromium equivalent,  $Cr_{eq}$ . From Shibata.<sup>108</sup>  $\beta$  vs.  $Cr_{eq}$  from analysis for this report. .... 47
34. Probability vs. time for the SCC of Fe-Cr-Ni alloys containing fourth component additions tested in boiling  $MgCl_2$  at 90% of the yield stress. All specimens were annealed at 1150°C and were exposed in the form of 0.38 mm diameter specimens. From Staehle et al.<sup>126</sup> ..... 47

35. Grain boundary composition vs. distance from grain boundary. (a) Solute composition near a grain boundary for the case of forming a precipitate. Solute depleted regions and local accumulation due to rejection are shown. (b) Solute composition at a grain boundary associated with preferential adsorption or rejection for four cases. From Staehle. <sup>78</sup> .....	48
36. (a) Initiation time for LPSCC vs. annealing temperature for Alloy 600 in both MA and TT conditions. (b) Initiation time for LPSCC vs. extent of grain boundary carbides for MA and TT conditions. From Norring et al. <sup>117</sup> .....	49
37. (a) Probability vs. time for a reference Heat A and three heats where metallurgical structures have been produced that affect the distribution of carbides. Specimens exposed at 360°C in high purity water to produce LPSCC. From Webb. <sup>24</sup> (b) Probability vs. time comparing the LPSCC of mill annealed (MA) and thermally treated (TT) specimens in 360°C pure water with a partial pressure of hydrogen at 1.0 psia. Four heats of materials used. From Jacko. <sup>136</sup> .....	50
38. (a) Percent of tubes affected by LPSCC from the primary side of a PWR steam generator vs. heat number determined at roll transitions after approximately 40,000 hours of service. Primary surface temperature at this location is about 310°C. Environment is primary water as identified in Figure 4. (b) Percent of tubes affected by IGA and IGSCC vs. heat number from the secondary side of a PWR steam generator in heat transfer crevices after approximately 75,000 hours of service. Adapted from Scott. <sup>138*</sup> .....	51
39. LPSCC initiation time vs. water chemistry for four heats of Alloy 600 exposed at 330°C. From Jacko. <sup>91</sup> .....	51
40. Median times-to-failure vs. heats for sensitized Type 304 stainless steel tested in 288°C water. From Clarke and Gordon. <sup>115</sup> .....	52
41. (a) Probability vs. Pa from EPR test for as-welded Type 304 stainless steel piping. From Harris et al. <sup>140</sup> (b) Lower limit life vs. Pa from the EPR test for sensitized Type 304 stainless steel exposed to 3.5% NaCl solution at 80°C and to high-purity oxygenated water at 250°C. From Akashi and Nakayama. <sup>61</sup> .....	52
42. (a) Probability vs. time for the SCC of Type 310 stainless steel tested in boiling MgCl <sub>2</sub> at 154°C and stressed at 19,600 psi for five magnitudes of prestrain. From Cochran and Staehle. <sup>141</sup> (b) Correlation of $\theta$ , $\beta$ , and $t_o$ as a function of cold work from Figure (a). (c) Probability vs. time for the SCC of Alloy 600 tested in primary water at 360°C with 1.0 psia hydrogen for three magnitudes of cold work. Tubing was annealed and drawn to produce the cold work. From Jacko. <sup>137</sup> (d) Correlation of $\theta$ , $\beta$ , and $t_o$ as a function of cold work from Figure (c). .....	53
43. (a) Probability vs. time for SCC of Alloys 600B and 182B tested at constant load at 250°C with 8 ppm of dissolved oxygen in high purity water. From Akashi and Nakayama. <sup>142</sup> (b) Probability vs. time for the SCC of Alloy 600 compared with low carbon and high carbon welding material of EN82 tested in deoxygenated water at 360°C. From Webb. <sup>24</sup> (c) Lower limit lifetimes in a crevice bent beam experiment (CBB) for alloys exposed to high purity oxygenated water at 250°C. From Akashi. <sup>17</sup> .....	54

44. (a) Microhardness vs. distance for surfaces that have been machined and ground and only machined determined at the ID surface of a PWR reactor vessel closure penetration. From Rao.<sup>144</sup> (b) Microhardness vs. distance from the surface as affected by reaming at the ID surface of pressurizer heater sleeve penetration used in the pressurizer of a PWR primary system. From Rao.<sup>144</sup> ..... 55
45. (a) Probability vs. time for SCC for various surface preparations of Type 310 stainless steel tested in boiling  $MgCl_2$  at 154°C and stressed to 19,600 psi. From Staehle and Cochran.<sup>141</sup> (b) Probability vs. pitting potential for SCC, in 3.5% NaCl at 35°C and  $N_2$  saturated, of Types 304 and 316 stainless steel with 2/0 emery polishing or chemical etching (30%  $H_2SO_4$ , 35°C for 10 minutes). These data were originally plotted as a normal distribution (abscissa not adjusted from original). From Shibata and Takeyama.<sup>145</sup> ..... 56
46. (a) Concentration of soluble iron ions vs. pH for acidic and alkaline regions. Adapted from Pourbaix.<sup>97</sup> (b) Concentration of iron ions vs. potential at pH 5 and room temperature. Locations for the  $H_2O/H_2$  and  $O_2/H_2O$  equilibria are shown. Adapted from Pourbaix.<sup>97</sup> ..... 58
47. (a) Potential vs. oxygen concentration for stainless steel at 274°C. Relationship to the onset of IGSCC of sensitized stainless steel is shown based on testing with CERT specimens. Adapted from Indig and McIlree.<sup>147</sup> (b) Open circuit potential vs. time for platinum in flowing sea water From Salvago et al.<sup>148</sup> (c) Open circuit potential vs. time for sensitized Type 304 stainless steel exposed at 50°C in 0.35% NaCl at 1.75 $S_y$  with no crevices present. From Nakayama et al.<sup>105</sup> ..... 59
48. Estimated concentration in heated crevice of a SG geometry vs. bulk water chemistry. Concentration of anions and cations studied under conditions of SG secondary water chemistry at relevant heat fluxes. From Takamatsu et al.<sup>149</sup> ..... 60
49. (a) Probability vs. time for SCC of Type 304 stainless exposed to high concentrations of  $CaCl_2$  at 100°C and 200MPa. From Shibata et al.<sup>150</sup> (b) Correlation of data from (a). (c) Probability vs. time of sensitized Type 304 exposed to dilute solutions of chloride and stressed at 1.75 $S_y$  at 80°C in the creviced condition. Data originally plotted as linear H(t) vs. time-to-failure. From Nakayama et al.<sup>105</sup> (d) Correlation of data from (c). ..... 61
50. (a)  $\beta$  vs. concentration of  $CaCl_2$  for the failure times of SCC of Type 304 stainless steel at three temperatures. Adapted from Shibata et al.<sup>150</sup> (b) Median failure time vs. concentration of  $CaCl_2$  for the SCC of Type 304 stainless steel exposed to three temperatures. Adapted from Shibata et al.<sup>150</sup> (c)  $\beta$  vs. concentration for initiation and failure times as a function of  $CaCl_2$  for 100°C. Adapted from Shibata et al.<sup>121</sup> (d) Median failure time vs. concentration of  $CaCl_2$  for the SCC of Type 304 stainless steel. Adapted from Shibata et al.<sup>121</sup> ..... 61
51. Probability vs. time for the SCC of sensitized 304 stainless steel exposed to 0.35% NaCl at 30°C and a stress of 1.75 $S_y$ . Specimens tested in the creviced and crevice-free condition. From Nakayama et al.<sup>105</sup> ..... 62
52. (a) Probability vs. service time (equivalent full power years) for the LPSCC occurring on the primary side of tubes from operating SGs in PWRs. Temperatures are in the range of 315 to

- 320°C. (b) Probability vs. time for IGA/IGSCC occurring on the secondary side of tubes from operating SGs. SCC occurs at locations of heated crevices at tube supports, tube sheets and top of the tubesheet sludge piles as shown in Figure 4. From Staehle et al.<sup>27</sup> ..... 63
53. (a) Probability vs. pitting potential measured at flow velocities of 9.0, 11.3 and 14.6 cm/s. The specimens were pretreated at 3V in 0.5 H<sub>2</sub>SO<sub>4</sub> for 1 hour. Originally plotted as normal probability. From Shibata and Zhu.<sup>151</sup> (b) Correlation of data in (a). (c) Probability vs. service time for tubes plugged due to erosion-corrosion on the secondary side in a once-through steam generator. From Staehle et al.<sup>27</sup> ..... 64
54. (a) Probability vs. time for SCC failures as a function of temperature in stainless steel heat exchangers using industrial water in the chemical industry. Original data plotted as  $H(t)$  vs.  $t$  based on exponential distribution. (b) Correlation of  $\theta$  and  $\beta$  vs.  $1/T$ . From Shibata.<sup>16</sup> ..... 64
55. (a)  $\beta$  vs. temperature for initiation, propagation and failure of Type 304 stainless steel by SCC. (b)  $t_o$  vs. temperature for initiation, propagation and failure by SCC. (c) Mean time for initiation, propagation and failure vs. temperature. (d) Probability vs. time for times for initiation, propagation and failure at 126°C. Original data on Weibull coordinates as are the data in this figure. (e) Same as (d) for 138°C. (f) Same as (d) for 154°C. Data obtained in concentrated MgCl<sub>2</sub> solutions. From Shibata.<sup>16</sup> ..... 65
56. (a) Probability vs. time for  $t_i$  by SCC of Type 304 stainless steel exposed to a concentrated MgCl<sub>2</sub> solution. (b) Correlation of data for  $\theta$ ,  $\beta$ , and  $t_o$  vs. temperature. Original data plotted in exponential distributions. Adapted from Shibata.<sup>16</sup> ..... 65
57. (a) Normalized crack growth rate vs. temperature for sensitized Type 304 stainless steel exposed to high purity oxygenated water. Data analyzed by Eason and Padmanaban<sup>152</sup> and published by Andresen.<sup>42</sup> (b) Probability vs. normalized crack growth rate for temperatures from 25 to 300°C. (c) Correlation of data from (b) for  $\theta$ ,  $\beta$ , and  $t_o$  vs.  $1/T$ . ..... 66
58. LPSCC of Alloy 600 MA. (a) Probability vs. time to fail by LPSCC for a temperature range of 288 to 360°C for testing in high purity deoxygenated water containing a hydrogen concentration of 10-60 cc H<sub>2</sub>/kg H<sub>2</sub>O. From Webb.<sup>24</sup> (b) Correlation of data in (a) for  $\theta$ ,  $\beta$ ,  $t_o$  vs.  $1/T$ . (c) Probability vs. time to fail by LPSCC in high purity water and steam for 360 water and 400°C steam with 1 psia hydrogen in the former and 11 psia steam in the latter. From Jacko.<sup>153</sup> (d) Correlation of data in (c) for  $\theta$ ,  $\beta$ , and  $t_o$  vs.  $1/T$ . ..... 67
59. Probability vs. time for SCC of sensitized Type 304 stainless steel in the "Strauss Test" solution, a copper-copper sulfate-sulfuric acid solution (6 weight % CuSO and 16 weight % H<sub>2</sub>SO<sub>4</sub>), tested in uniaxial load at 100°C at four stresses. From Yamauchi et al.<sup>159</sup> (b) Correlation of  $\theta$ ,  $\beta$ ,  $t_o$  from (a) with stress. (c) Probability vs. time for SCC of sensitized Type 304 stainless steel exposed to a 0.35% NaCl solution at 80°C and no crevices present. From Nakayama et al.<sup>105</sup> Data originally plotted linearly as  $H(t)$  vs. time-to-failure (d) Correlation of data from (c). ..... 68
60. (a) Probability vs. time for SCC of Fe-17Cr-11Ni stainless steel exposed to boiling MgCl<sub>2</sub> at 154°C and tested at four stresses. These data are a three-parameter fit of the data shown in

Figure 31b. From Shibata and Takeyama. <sup>120</sup> (b) Probability vs. time for SCC of Type 310 stainless steel exposed to boiling $MgCl_2$ at $154^\circ C$ and tested at four stresses. Specimens were prestrained to 130% yield strength. From Cochran and Staehle. <sup>141</sup> (c) Correlation of $\theta$ , $\beta$ , $t_o$ vs. stress. ....	69
61. (a) Probability vs. time for SCC of Type 304 stainless steel tested in $MgCl_2$ at $138^\circ C$ tested at three stresses for the initiation stage. Data originally plotted in exponential coordinates as $R(t)$ . From Shibata et al. <sup>161</sup> (b) Correlation of $\theta$ , $\beta$ , $t_o$ vs. stress. ....	69
62. $\theta$ , $\beta$ , and $t_o$ for stainless steel at $138^\circ C$ vs. stress; data shown for initiation, propagation and total failure. (a) $\beta$ . (b) $t_o$ . (c) $\mu$ . From Shibata. <sup>16</sup> .....	70
63. (a) Probability vs. time for SCC of carbon steel weld metal tested at $250^\circ C$ in high purity water containing 8 ppm of dissolved oxygen. Tests conducted at constant load. Original data plotted as $H(t)$ vs. $t$ with exponential distribution. From Akashi and Nakayama. <sup>18</sup> (b) Correlation of $\theta$ , $\beta$ , $t_o$ for (a). (c) Probability vs. time for SCC of Alloy 750 in $350^\circ C$ water tested as tensile bars. From Blanchet et al. <sup>137</sup> (d) Correlation of $\theta$ , $\beta$ , and $t_o$ for (c). ....	70
64. (a) Normalized separation distance, $y/a$ , vs. normalized parallel approach distance, $x/a$ , relating to the critical conditions for the coalescence of small cracks. Data obtained from ferritic steel specimens exposed to $CO_3-HCO_3$ solution. From Parkins <sup>67</sup> and Parkins and Singh. <sup>161</sup> (b) Schematic illustration of the initiation of SCC from pits and coalescence; this is consistent with the model for initiation shown in Figure 7c. From Nakayama et al. <sup>105</sup> .....	71
65. (a) Number of cracks per mm vs. concentration of $CaCl_2$ for three temperature subjected to a constant applied stress of 200 MPa using a constant load apparatus with a hard spring. (b) Crack length vs. concentration of $CaCl_2$ . (c) and (d) Number of cracks related to their length for two concentrations of $CaCl_2$ . (e) Number of cracks per mm vs. $\beta$ for three temperatures and three concentrations of $CaCl_2$ . Adapted from Shibata et al. <sup>150</sup> .....	72
66. (a) Frequency vs. surface length of micro-cracks for sensitized Type 304 stainless steel exposed in a constant load test to $250^\circ C$ and 200 ppm dissolved oxygen. (b) Aspect ratio vs. crack depth for the same conditions as in (a). Adapted from Akashi and Nakayama. <sup>18</sup> .....	73
67. Frequency vs. depth of cracks for 0.1 and 0.3 $\mu S$ conductivity based on $Na_2SO_4$ addition tested at $0.2V_H$ . From Nakayama and Akashi. <sup>162</sup> .....	73
68. Results from exposure of stressed specimens of steel weld metal to $250^\circ C$ in high purity water with 8ppm dissolved oxygen. Specimens stressed with uniaxial constant load. (a) and (b) frequency vs. surface length of microcracks for two weld metals. (c) Length of microcracks vs. time. (d) Microcrack initiation rate vs. applied stress. From Nakanishi et al. <sup>107</sup> .....	74
69. (a) Stress vs. minimum pit diameter for SCC of carbon steel weld metal at $250^\circ C$ in high purity water with 8 ppm of dissolved oxygen. From Nakanishi et al. <sup>106</sup> (b) Stress intensity associated with pitting vs. duration of test that produces SCC as shown above the dotted line. From Nakayama et al. <sup>107</sup> .....	74

70. Principal types of tests for SCC and their applicability. ....	75
71. (a) Probability vs. time for two types of loading using Alloy 182 in high purity water at 288°C. CBB test with flow velocity of 0.056 cm/s. From Nakayama and Akashi. <sup>162</sup> (b) K threshold vs. ultimate strength for a 2 1/4Cr-1Mo steel measured using a crack opening displacement method (CMOD). Hydrogen charged thermally. From Gangloff. <sup>163</sup> .....	76
72. (a) Probability vs. time for various testing methods of Type 304 stainless steel compared with field experience. From Shibata. <sup>14</sup> (b) Probability vs. time comparing the CERT experiment on Type 304 stainless steel with results in (a). From Sato et al. <sup>164</sup> .....	77
73. (a) Probability vs. $\beta$ : for initiation, $\beta_i$ , propagation, $\beta_p$ , and failure, $\beta_f$ for data from various investigations in Prof. Shibata's laboratory. From Shibata. <sup>16</sup> (b) Shape parameter vs. median failure time for Type 304 stainless steel exposed to CaCl <sub>2</sub> at three temperatures and three concentrations. From Shibata et al. <sup>150</sup> .....	83
74. Schematic view of probability vs. time for case with early failure at 2000 hours and at 0.0005 probability showing options for extrapolating with slopes of $\beta=1$ and $\beta=4$ . ....	85
75. Probability vs. service time (equivalent full power years) for 0.1 or 1% for LPSCC at seven specific locations, using for each distribution data from SGs of multiple plants, each plot accounting for a single data point. Data adjusted to 316°C using an apparent activation energy of 50 kcal/mole. Adapted from Gorman et al. <sup>20</sup> .....	86
76. Schematic view of occurrence of different modes of SCC and localized corrosion at specific locations on the primary and secondary sides of PWR SGs. Details of SG locations shown in Figure 4. From Staehle. <sup>1</sup> .....	87
77. (a) pdfs for four separate failure modes occurring in the same subcomponent. Total pdf shown aggregating data from the four. (b) cdf for the four cases in (a) and the aggregate distribution is shown based on Eqn. (36). ....	88
78. (a) pdf for initiation, propagation and failure calculated numerically from Eqn. (38). (b) cdf for initiation, propagation, and failure calculated numerically from Eqn. (39). Dots show locations of numerical calculations. From Staehle and Stavropoulos. <sup>2</sup> .....	89
79. cdf calculated on the basis of temperature changing from T=100°C initially to T=20°C after 100 years following an exponential decay in temperature. From Stavropoulos et al. <sup>165</sup> .....	89
80. Schematic view of extrapolating statistical data obtained at accelerated conditions to the operating case. ....	90

## TABLES

1. Relationship of $\theta$ , $\beta$ , and $t_0$ to Temperature .....	80
2. Relationship of $\theta$ , $\beta$ , and $t_0$ to Stress .....	81



## SUMMARY AND CONCLUSIONS

The purpose of this report is to define a framework for predicting the earliest penetrations by stress corrosion cracking (SCC) in a set of tubes of Alloy 600 in a steam generator of a pressurized water reactor when the SCC occurs on the secondary side. Such early penetrations are those that can occur at times  $10^{-1}$  to  $10^{-4}$  of the mean time-to-failure; these early penetrations are not spurious but are a natural consequence of statistically distributed failure times. The occurrence of early penetrations is often regarded as out of the ordinary; however, such a predisposition results from the normal approach to obtaining data which emphasizes determining the mean failure time without giving attention to the natural dispersion of data. This report considers the following as they affect the earliest failures and their prediction: inherent variability, metallurgical variability, environmental variability, testing variability, and measurement variability. Finally, this report describes a stepwise framework for predicting the earliest failures.

For quantitative predictions of the earliest penetrations of SG tubes by SCC, this framework requires the insertion of modules that describe each of the submodes of SCC that can occur on the secondary side. These modules include such submodes as alkaline SCC, acidic SCC, low potential SCC, and lead SCC. These modules are subjects of subsequent reports. A final report will integrate the present framework with these modules to produce a quantitative model for predicting early penetrations. These modules will include the dependence of each submode upon the principal variables of SCC: pH, potential, species identity and concentration, alloy composition, alloy structure, temperature and stress.

The approach taken here is to develop a physically based statistical framework. Statistical methods by themselves do not account for the physical contributions of metallurgy, environments, methods of testing and variations among testing laboratories. Purely metallurgical testing to obtain mean values does not account for earliest failures. However, incorporating physical bases into a statistical framework provides a credible basis for predicting early failures.

An important objective of this work is predicting early penetrations as opposed to complete failures. Such early failure times would produce penetrations that are less than are conventionally measured by NDE of tubes in steam generators. However, most of the data in the relevant literature is available as times-to-failure or as crack velocity as functions of some set of principal variables. Therefore, in this report data are discussed mainly in terms of failure times. As the modeling is refined, the failure times will be used to define times for early penetrations. Such an approach will be based on the early penetrations being some fraction of total times for penetration.

Principal elements and considerations of the framework for prediction are as follows:

1. The Weibull distribution (Section 2.2) is used as a general framework. Generally, the Weibull distribution provides the consistently best fits to SCC data. Other distributions are available, which sometimes provide fits to the data equivalent to the Weibull distribution including the Gumbel, log normal, and normal. Sometimes, the exponential distribution, which is a special case of the Weibull distribution, is used because of its simplicity. However, these other distributions are not as flexible and as broadly applicable as the Weibull distribution.
2. The Weibull distribution (Section 2.2.1) contains three parameters which can be related directly to the quantitative dependencies of the submodes. These three parameters are: the scale parameter,  $\theta$ ; the shape parameter,  $\beta$ ; the location parameter,  $t_0$ .

3. The intensity of submodes of SCC (Section 1.8) can be connected to the Weibull distribution through modeling the Weibull parameters with the dependencies (Section 2.10) of the submodes on the principal variables of pH, potential (E), species (X), alloy composition (C), alloy structure (M), temperature (T) and stress ( $\sigma$ ). Thus, each of the Weibull parameters can be described, e.g.  $\theta = \theta(\text{pH}, E, X, C, M, T, \sigma)$ . While such dependencies are not well defined by existing experimental work, for each variable and for each submode, sufficient data are available in the literature to estimate most dependencies.
4. The submodes (Section 1.8) of SCC that are considered in this report are: low potential SCC (LPSCC), alkaline SCC (AkSCC), acidic SCC (AcSCC), high potential SCC (HPSCC), lead SCC (PbSCC), silica and alumina SCC (AlSiSCC), chloride SCC (ClSCC), lower valence sulfur SCC (S<sup>x</sup>SCC), copper SCC (CuSCC), doped steam SCC (DSSCC), and organic SCC (OgSCC). Some of these submodes may eventually become part of single submodes: e.g. the submodes of CuSCC, AcSCC, ClSCC are probably part of a single acidic submode. Further work will determine the extent to which such aggregations are compatible.
5. The procedures for incorporating the set of submodes into the Weibull parameters are being defined as the submodes are examined in this program.
6. Aside from problems of estimating the dependencies of submodes on principal variables there are three factors (Section 2.3) which produce variabilities that are difficult to quantify:
  - a. Heat-to-heat variations (Section 4.3) within a single specification for alloy composition and heat treatment can produce differences in  $\theta$  of about two orders of magnitude
  - b. Differences in surface finish (Section 4.6) and preparation can produce differences in  $\theta$  of at least an order of magnitude.
  - c. When the test or exposure environments are located in the region of a submode (Section 2.7) where there are large variations in rates, variations in  $\theta$  of about two orders of magnitude are possible.
7. The dependencies of  $\theta$  and  $t_o$  on principal variables (Section 8.2), which describe the respective submodes, follow patterns that are predictable. These patterns are the same ones that relate to the mean value dependencies for the submodes that are already well known.
8. The shape factor,  $\beta$ , is the most important consideration (Section 8.4) in predicting earliest failures. The value of the shape factor for practical purposes covers a range from  $\beta=1$  to  $\beta=4$  although shape factors outside this range are commonly observed. The importance of the shape factor is readily observed in Figure 24. Here, for a probability of failure of 0.0001, about one tube in 10,000 (three steam generators worth of tubes), a  $\beta=1$  corresponds to the first failure occurring at a time that is  $10^{-4}$  of the mean and a  $\beta=4$  corresponds to the first failure occurring at a time that is  $10^{-1}$  of the mean.
9.  $\beta$  does not follow the same dependencies on principal variables (Section 8.5) as  $\theta$  and  $t_o$  although it does follow regular dependencies. Properties and important considerations in selecting  $\beta$  for predicting early failures are as follows:
  - a. An important insight into the nature of  $\beta$  comes from its effect on the hazard function (Sections 2.2.1, 2.4, and 2.5) which is the probability of failure in the next interval,  $dt$ . For a  $\beta=1$ , the hazard function is constant in time, i.e. failure can occur any time and any place

where the  $\beta=1$  applies. For a  $\beta=4$ , the hazard function is negligible initially and then begins to increase sharply at about  $\text{time}=\theta/2$ .

- b. A  $\beta=1$  (intrinsic, i.e. with only a single heat) case corresponds to surface processes (Section 2.2.2) such as pitting, SCC initiation, and surface erosion being critical to the occurrence of SCC. These events are directly related to physical processes on the surface that include inclusions, grain boundaries, surface slip, surface stresses, and surface chemical reactions. See Figure 26. Generally, these are processes associated with SCC where the critical step is in the initiation stage.
  - c. A  $\beta=4$  (intrinsic, i.e. with only a single heat) corresponds to accumulation processes (Section 2.4) that are critical to the SCC. Such processes include accumulation of chemicals on the surface, diffusion into the surface, or migration and diffusion processes inside advancing SCC. See Figure 26.
  - d. The term "intrinsic" relative to the  $\beta=1, 4$  has the meaning that the value of the shape factors depends on a single heat tested in well controlled conditions. However, when multiple heats (Section 4.2) are tested in nominally the same environments and in nominally the same metallurgical condition, the value of  $\theta$  may vary at least two orders of magnitude. If these data are aggregated (Section 2.6), in view of their nominal similarity, the resulting value of  $\beta$  for the aggregation is much reduced. For example, when the individual sets of results have  $\beta=4$  values but the values of  $\theta$  are two orders of magnitude apart, the aggregated  $\beta=1$ . Thus, a value of  $\beta=1$  may result either from a mechanistic process that is controlled by surface factors or from the aggregation of data from different tests having nominally the same conditions but different values of  $\theta$ .
  - e. Some values of  $\beta$  seem to depend on the intensity of the testing stressors (Section 8.5): e.g. increasing stress, increasing temperature, increasing concentrations of chemical species. Thus, it seems reasonable that that data should be less dispersed, e.g. a higher value of  $\beta$ , when the intensities of stressors are increased. Some dependencies of  $\beta$  exhibit such trends. However, other dependencies of  $\beta$  follow mechanistic influences. Finally, still other values of  $\beta$  follow the decreasing patterns that result from aggregating tests.
10. Most of the work on the theory of SCC relates implicitly to the mean value dependencies. There is no mechanistic nor metallurgical theory for  $\beta$ . Thus, a major part of predicting the failure of tubes, when no initial data are available, is deciding on a value of  $\beta$ , especially since it produces such a large effect on the time of occurrence of the first failure relative to the mean value.
  11. There has been a great concern about reproducibility of data in connection with predicting early and later failures (Section 2.4). Typically, there is often large scatter in data that is obtained from good laboratories. However, scatter needs to be considered relative to the magnitude of  $\beta$  that is characteristic of the data. With a  $\beta=4$  the scatter of data is implicitly small. However, with a  $\beta=1$  the range of data is implicitly large. Nothing can change these ranges that depend on mechanisms that produce their unique values of  $\beta$ .
  12. Choosing values (Section 8.0) for predicting early failures via the parameters of  $\theta$ ,  $\beta$ , and  $t_o$ , in the absence of the more detailed work yet to be conducted in this program, should adopt the following approaches:

- a. Values of  $\theta$  (Section 8.2) should follow the existing dependencies of the mean value of submodes on the principal variables.  $\theta$  is essentially the same as the mean,  $\mu$ .
  - b. Values of  $t_o$  should be taken as  $0.1 \theta$  (Section 8.3).
  - c. Values of  $\beta$  should be taken (Section 8.4) as unity until the first failure occurs since this is the most reasonable as well as consistent with some field observations. After some early failures occur, a conservative value having substantial precedent is  $\beta=4$ .
13. There is no circumstance under which data would be perfectly reproducible (Section 1.4). It is the nature of SCC that results are distributed. The extent of the variability depends on the value of the shape parameter as affected by mechanistic or aggregation considerations.
  14. Predicting the earliest failures (Sections 2.8 and 8.11) from accelerated testing must consider not only the acceleration of the mean values but also the acceleration of the early failures such as those at probabilities of 0.0001. In cases where accelerated testing is used to predict performance, it must be recognized that the occurrence of failures in service will tend to follow low values of  $\beta$ , generally  $\beta=1$ , in view of the multiple heats and other factors that reduce values of  $\beta$ . On the other hand, accelerated testing is usually undertaken with single heats and at high values of stressors. These conditions tend to produce higher values of stressors, in the range of  $\beta=4$ . For such different values of  $\beta$ , between field experience and accelerated testing, the values of  $\theta$  may be a factor of 100 apart but at a 0.001 probability there is no acceleration as shown in Figure 25. Thus, the accelerated testing did not provide accelerated data for the early failure.
  15. In addition to the variability in times for SCC that is inherent (Section 2.0), variability is associated with multiple testing, relative contributions of initiation and propagation, metallurgical influences, environmental influences, method of testing, and methods of measurement.

## ACKNOWLEDGMENTS

It is a pleasure to acknowledge contributions from the following in preparing this report: Robert Abernethy of Weibull Risk and Uncertainty Analysis, Masatsune Akashi of IHI, Peter Andresen of General Electric, William Beggs of Bechtel Bettis Laboratory, James Benson of EPRI, Steve Bruemmer of PNL, Bruce Bussert of KAPL, John Congleton of the University of Newcastle upon Tyne, Dwight Diercks of ANL, Ernie Eason of Modeling and Computing Services, Jeffrey Gorman of DEI, Mac Hall of Bettis Atomic Power Laboratory, Robert Kelly of the University of Virginia, Jesse Lumsden of Rockwell, Al McIlree of EPRI, Joseph Muscara of the NRC, Kjell Norring of Studsvik, Redvers Parkins of the University of Newcastle upon Tyne, William Porr of Bechtel Bettis Laboratory, Gutti Rao of Westinghouse, Peter Scott of Framatome, John Scully of the University of Virginia, Masahiro Seo of Hokkaido University, Toshio Shibata of the University of Osaka, Tetsuo Shoji of the Tohoku University, Dino Stavropoulos formerly of DEI and Brian Woodman of APTECH Engineering.

I especially appreciate the work of Dr. Zhi Fang who performed the Weibull calculations and other analyses used in this report.

Finally, I am indebted to my staff who assisted me in organizing this report: Mary Elizabeth Ilg, Barbara Lea, Tim Springfield, and Erin Parrish-Siggelkow. Nancy Clasen obtained many of the documents upon which this report relies. I appreciate especially the work of John Ilg who prepared the figures and assembled the report.

## 1.0 INTRODUCTION

### 1.1 Scope and Objectives

The subject of this report, concerning the physical basis of statistical predictions of stress corrosion cracking, deals with the "statistical framework" part of the ten factors in the corrosion based design approach (CBDA) that I have described in detail elsewhere.<sup>1,2,3,4,5</sup> The main purpose of this report is to describe a framework for predicting the earliest failures that occur in tubing of steam generators. Such "early failures" are the first ones of thousands of similar tubes where the mechanism of the full array of failures can be the same. These earliest failures can occur in the range of  $10^2$  to  $10^4$  times earlier than the mean failure time. For this reason, the mean failure times that are usually determined are relevant to predicting performance only as they provide an index for a statistical distribution that models the occurrence of failures over time. However, despite its secondary importance to predicting the earliest failures, it is the mean value of failure times that is most often determined in experiments that are conducted to determine whether the design life can be met: i.e. the mean failure time is determined by conducting limited experiments and determining the mean value of failure times or some other index of failure.

This report is consistent with the urging of U. R. Evans in his remarks that were prepared for the meeting on Localized Corrosion held at Williamsburg Virginia in 1971:<sup>6</sup> "Perhaps these remarks may persuade someone present at Williamsburg to make a serious study of the subject of corrosion probability, which has much practical importance as well as much scientific interest."

The essence of the framework described here for predicting the earliest failures involves combining well-established statistical distributions with the physical processes that affect statistical parameters. Understanding the contributions of the physical processes that underlie the statistical parameters provides the most credible means for predicting early failures. Here, the physical aspects include both materials and environments.

Early failures do occur. A good example of one is associated with the weld sensitized 4" piping in the Dresden Nuclear Power Station in 1970.<sup>7,8</sup> There is a large literature on early failures due to stress corrosion cracking. Many of these are well known to the public. The subjects discussed in this report are relevant to all industries that are concerned with early and nominally premature failures.

Predicting the earliest failures is generally more important than predicting the mean time-to-failure. Reaching the latter means that half of the subcomponents, e.g. tubes in an SG, have failed. Such a result is not normally acceptable. Therefore, preoccupation with the mean value is misplaced as a base for predicting performance. Failed fractions in the range of 0.1 (10%) are usually the maximum acceptable for failures in SGs while 0.01, 0.001 and 0.0001 probabilities provide early warnings of impending failures.

Statistical distributions that describe the earliest failures depend on both the mean value of data and on the dispersion of such data over time. The mean value is the intercept that controls the position of a distribution; the statistical parameter concerned with modeling the dispersion of data is the "shape parameter." The extensive theory that has been developed for predicting and rationalizing SCC has been concerned implicitly with the mean value and not with the dispersion of data. There is, today, no theory for the dispersion of data; therefore, there is no theory that provides a basis for predicting the earliest failures.

The statistical bases for the framework being discussed here are not new and are used widely in modern technology as described in many texts;<sup>9,10,11,12,13</sup> however, the physical interpretation of statistical correlations is not significantly developed except for the work of Shibata,<sup>14,15,16</sup> Akashi,<sup>17,18,19</sup> Gorman,<sup>20,21</sup> Webb,<sup>22,23,24</sup> Shimada and Nagai,<sup>25,26</sup> Staehle,<sup>21,27</sup> and their co-workers.

The prediction of the earliest failures in a set of subcomponents has received extensive attention in the statistics community, especially in the framework of extreme value<sup>28,29,30</sup> and Weibull statistics.<sup>31,32,33,34</sup> Abernethy has prepared a useful text that describes the use and application of Weibull analysis.<sup>35</sup> However, there is a great need for *a priori* bases for predicting early failures; this can come only from insights into the physical bases for the early failures, which is emphasized here.

In this report, attention is focused primarily on the failure mode of stress corrosion cracking (SCC) since it is the most virulent of the various modes of degradation except for fast fracture. Pitting is considered to the extent that it is often, but not always, a precursor to SCC. This report concerns the statistical characterization of SCC.

This report is concerned primarily with the performance of tubing as it is used in steam generators. The performance of complex components and systems is not considered although these, too, have been successfully modeled with various statistical distributions.

The statistics community has been mainly concerned with developing functionalities for improving the precision and applicability of statistically based methods of predicting and analyzing behavior of systems including materials. On the other hand, the materials and design communities have been late to recognize the importance and utility of statistically based methods as they can be applied to understanding the occurrence of early failures. Data obtained by these latter communities are mainly interpreted in terms of mean values and often are sparse with respect to the implications of structure of materials and the subtleties of environments. Further, often, the apparently subtle influences of metallurgy and environments are sufficient to overwhelm the precision that can be obtained by refinements in statistical theory.

## 1.2 An Alternative Approach

The essential approach in this report involves connecting the physical description of SCC with statistical distributions; and, in this report, the Weibull distribution is used owing to its flexibility. Another approach to prediction is being developed by Wei and his co-workers.<sup>36,37,38,39,40</sup> In this approach, Wei starts from a description of the failure nucleus, e.g. a pit, and generates a physically-based statistical description, e.g. a Monte Carlo or other analysis. This approach has the same goal as that described here. Wei suggests that the nucleus-based approach provides a more credible base for projecting into the future. However, it is not clear that this approach can rationalize the broad range of metallurgical and environmental variability as discussed here although the physical origins of these variabilities are obscure. The present paper embraces the broad range of existing statistically-based descriptions of SCC. To develop a "nucleus based" physical description, as a basis for statistical prediction of all these systems, could require a large effort. Thus, the two approaches are complementary and jointly desirable for developing a framework for developing reliable predictions.

### 1.3 Physical Bases

What is meant here by the “physical bases” for statistical distributions includes the seven principal variables that affect corrosion: electrochemical potential, pH, identity and concentration of chemical species, metallurgical composition, metallurgical structure, stress, and temperature. These physical variables are illustrated in Figure 1 together with dependencies that are often observed. Within each of these seven categories of principal variables there are further substituents. For example, within the topic of “metallurgical structure” there is cold work, surface conditions, grain boundary composition, and distribution of second phases. The seven principal variables are assessed in this paper with respect to their influences on the parameters of statistical distributions.

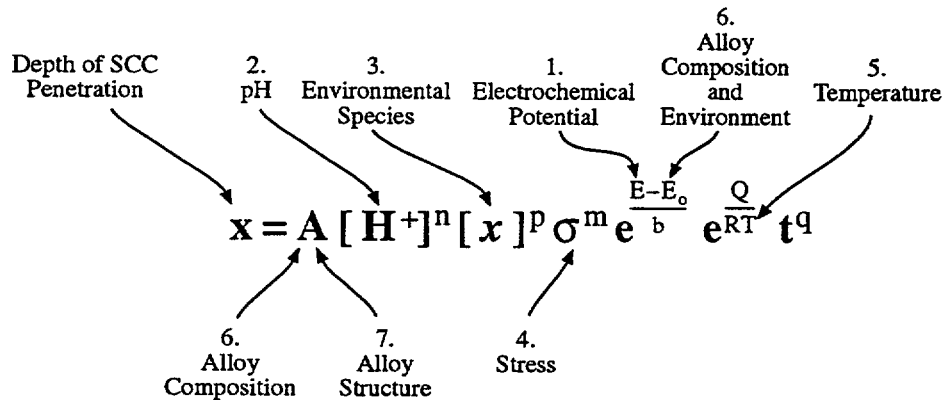


Figure 1: General relationship for the penetration of SCC following commonly accepted dependencies. Locations where principal variables enter this equation are noted.

Procedures for choosing optimum statistical distributions are not considered here; these are discussed extensively in statistical texts. In this report, the Weibull distribution is used predominantly because it is flexible and provides a basis for ready comparisons. The exponential distribution is often used when certain necessary conditions of randomness control the degradation phenomena; the exponential distribution is a special case of the Weibull distribution as is discussed in connection with Eqns. (11) to (16). The log normal distribution often fits failure data well but does not give the descriptive flexibility that the Weibull distribution provides; the log normal distribution is not used here. The normal distribution is often useful to characterize such features of materials as strength and chemical composition; pitting potentials have been modeled with normal distributions as shown in Figure 33 (data in this figure were originally modeled with a normal distribution but were re-modeled with a Weibull distribution for this report). Finally, extreme value distributions are useful in modeling certain degradation phenomena where the “worst of the worst” needs to be characterized.

### 1.4 Problems with Arrays of Data

While the theme of this report is the prediction of early failures, such predicting is sometimes confounded by multiple investigators obtaining nominally the same data from nominally similar combinations of materials and environments. Often, as the nominally same data are taken by an increasing number of investigators, the range of results increases beyond anything that can be described coherently. Figure 2 shows examples of sets of data that have been investigated by



numerous investigators where nominally the same materials and environments have been studied in a simple environment. The extents of the arrays of data are so broad as to provide no clear central tendency. These data can be treated only by some kind of bounding method depending on the requirements of the application.

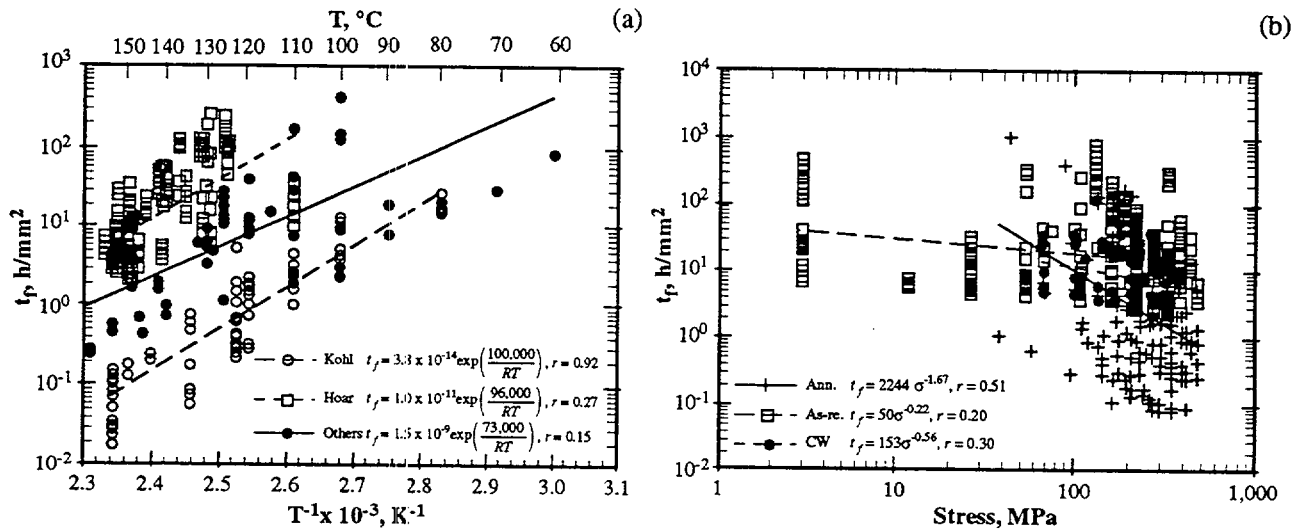


Figure 2: (a) Time-to-failure vs.  $1/T$  for 23 sets of data for stainless steels in boiling 35 to 45%  $\text{MgCl}_2$  solutions at open-circuit conditions. (b) Time-to-failure vs. stress for 40 sets of data measured for stainless steel in 42%  $\text{MgCl}_2$  at open-circuit conditions. From Jiang and Staehle.<sup>41</sup>

With respect to the broad arrays of data shown in Figure 2, one might conclude, facetiously, that the best data are the fewest. However, the broad array of these data suggests that relatively small changes in materials, environments, and testing can produce large and possibly unmanageable variability. Figure 2 suggests that data may need to be censored at least to the limits of the intended application. This is an approach suggested by Andresen.<sup>42</sup> Figure 3a shows data similar to Figure 2 but for the propagation of SCC in sensitized stainless steels exposed to pure oxygenated water in the range of 288 $^{\circ}\text{C}$ . Figure 3b shows data which have been censored from a population like that shown in Figure 3a. The screening in Figure 3b was based on selecting only those data that were relevant specifically to the performance of modern BWR nuclear plants. While the data are dispersed, they are less so than in Figure 3a. An upper design curve is shown, which is based on bounding the data rather on a statistically derived basis.

Thus, an important aspect of developing data for prediction involves considering the more precise relationship between the conditions under which data are obtained and the intended application for which the data are developed. This matter is not discussed in detail here; but censoring data is often necessary to provide reasonable bases for predictions.

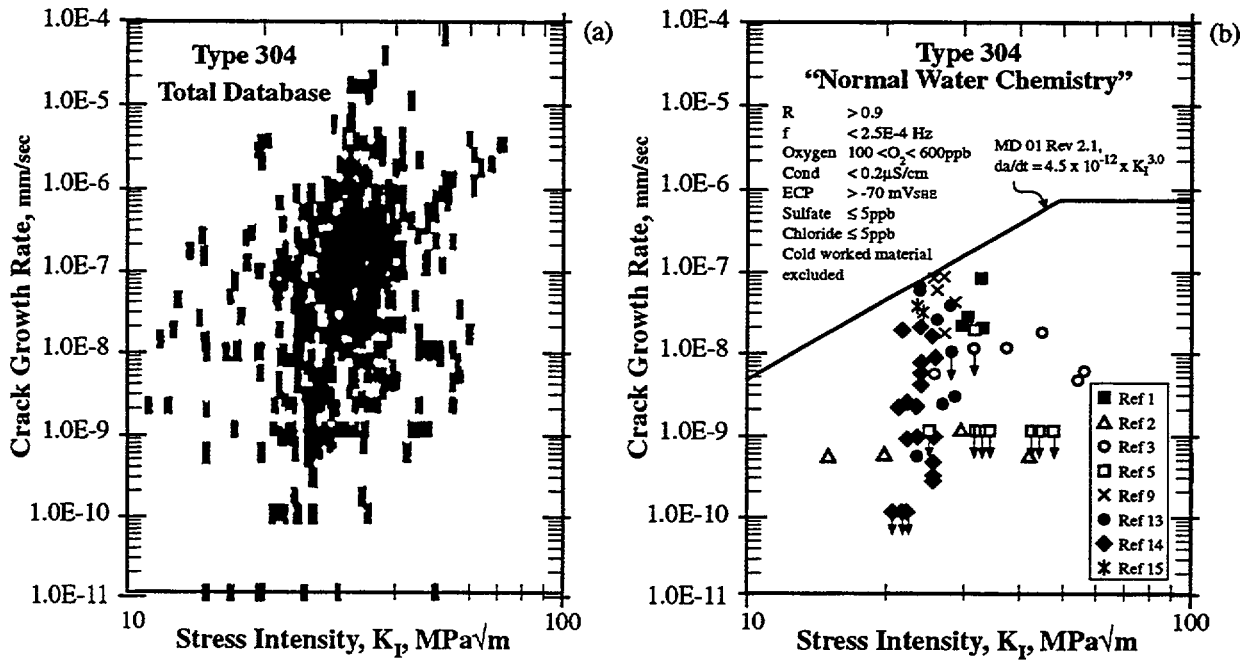


Figure 3: (a) Available data for crack growth rates in a data base for sensitized Type 304 stainless steel\* exposed to boiling water nuclear reactor (BWR) environments. (b) Screened data applicable to the conditions noted on the figure. Bounding line shown. From Jansson and Morin.<sup>43</sup>

### 1.5 Geometries of Industrial Equipment: Nuclear Steam Generators for PWRs

Many of the data used here as examples are taken from corrosion that has occurred in various components of steam generators (SG) of pressurized water cooled nuclear reactors (PWR); Figure 4 shows locations where corrosion is especially aggressive in steam generators. Through the early 1980s extensive corrosion has occurred in these SGs where Alloy 600 was used for tubing. On the inside of tubes (primary side) where the pure water from the reactor passes, SCC (identified as low potential SCC "LPSCC" in Figure 12) occurs at locations of high residual stresses such as at U-bends and in expansions near the tube sheet. On the outside of the tubes (secondary side), SCC occurs extensively in the heated crevices at tube supports (TSP) and at the tops of tube sheets (TSH). In these locations, chemicals are concentrated owing to the local superheat produced by crevices.

\* Various alloys are discussed in this report. Major chemical elements of these alloys are: (w/o)

Alloy	Fe	Cr	Ni	C	Other
Type 304 stainless steel	Bal.	18.0-20.0	8.0-10.5	0.08 max	
Type 304L stainless steel	Bal.	18.0-20.0	8.0-12.0	0.03 max	
Type 316 stainless steel	Bal.	16.0-18.0	10.0-14.0	0.08	Mo=2.0-3.0
Type 310 stainless steel	Bal.	24.0-26.0	19.0-22.0	0.25	
Alloy 800	Bal.	19.0-23.0	30.0-35.0	0.10 max	
Alloy 600	6.0-10.0	14.0-17.0	72.0	0.15 max	
Alloy 690	7.0-11.0	27.0-31.0	58.0 min	0.05 max	
Alloy 750	5.0-9.0	14.0-17.0	70.0 min	0.08 max	Ti=2.25-2.75, Al=0.40-1.0
Alloy 182 (weld metal)	10.0	13.0-17.0	59.0 min	0.10	Nb+Ta=1.0-2.5
Alloy 82 (weld metal)	3.0	18.0-22.0	67.0 min (Ni+Co)	0.10	Nb+Ta=2.0-3.0

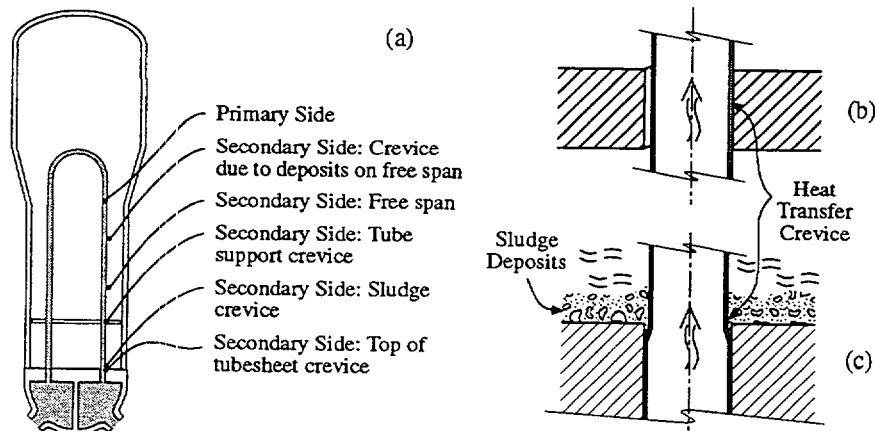


Figure 4: (a) View of prototypic steam generator (SG) for pressurized water nuclear reactor (PWR) with vessel, tube sheet, tube supports, and a U-shaped tube, one of about 4000. (b) Tube in tube support. (c) Tube in tubesheet showing presence of deposits referred to as "sludge."

## 1.6 Examples of Statistical Descriptions

The fact that SCC failures in components of operating equipment can be described well by statistical distributions is shown in Figure 5. Figure 5a shows the cumulative fraction of failures in stainless steel of boiling water reactor (BWR) plant piping due to SCC of welds from work of Eason and Shusto.<sup>44</sup> Figure 5b shows cumulative data obtained from the SCC in a SG of the type illustrated in Figure 4; these data are well described by Weibull distributions. Figure 5b also shows that SCC can occur simultaneously at several different locations in the same subcomponent, i.e. tubing; SCC is occurring on the inside of the tubes at locations of high residual stresses and on the outside of tubes at locations where heat transfer crevices accumulate high concentrations of chemicals as steam is produced in the supersaturated crevice conditions where flow is negligible.

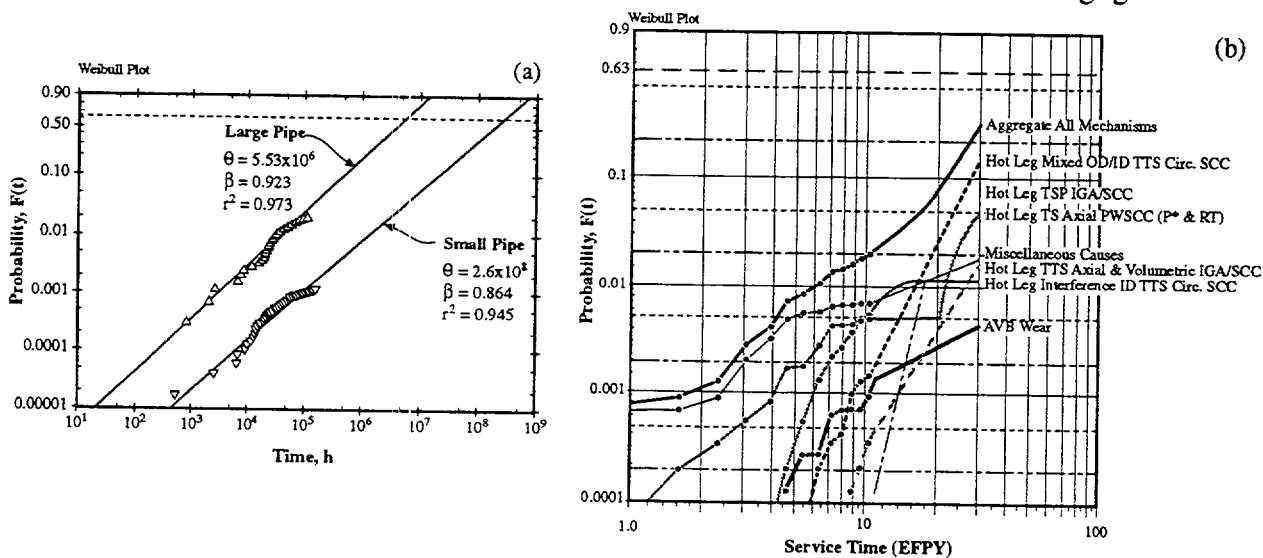


Figure 5: (a) Probability vs. time since startup for SCC failure of welded stainless steel pipes from piping used in boiling water nuclear reactors (BWR). From Eason and Shusto.<sup>44</sup> (b) Probability vs. equivalent full power years (EFPY) for failures of tubing from a set of SGs in the Ringhals 4 PWR. Designations: TTS = "top of tube sheet." TS = "tubesheet." Circ. SCC = "circumferential SCC." P\* = special location where SCC is not serious. RT = "roll transition." AVB = "antivibration bars".\*

\* Personal Communication from L. Bjornkvist, Vattenfall and J. A. Gorman, Dominion Engineering, April, 1999.

## 1.7 Domains of Initiation and Propagation

In order to appreciate what is being measured by data from SCC testing, Figure 6 shows the nine segments of SCC that occur in aqueous environments. These segments have been described by Staehle<sup>45</sup> and they are generally self evident in Figure 6. While the occurrence of these nine segments can be identified, it is not possible to model explicitly each of these nine steps. Rather, SCC is modeled here, as it is in most modeling, only as initiation and propagation segments. The initiation stage includes the first six steps shown in Figure 6, and the propagation stage includes the last three.

In Figure 6 the first segment involves the passive film adjusting to the environment; this adjustment usually exhibits itself as a change in open circuit potential over a period of time as studied by Hoar and Hines.<sup>46</sup> The second segment involves breaking the protective film either by chemical or mechanical processes. The conditions for chemical breakdown have been considered by many, and Engelhardt and Macdonald have described this process according to a point defect model<sup>47</sup> while Galvele has described it as a chemical dissolution process.<sup>48</sup> The conditions for mechanical breakdown have been considered by Lang et al.,<sup>49</sup> Latanision and Staehle,<sup>50,51</sup> Shibata and Staehle,<sup>52</sup> Swann and Nutting,<sup>53</sup> Ford and Andresen,<sup>54</sup> and Leach and Neufeld.<sup>55</sup> The third segment involves the earliest penetrations into the metal by either or some combination of intergranular penetration, slip step trenches,<sup>56,57,58</sup> tunnels,<sup>59,60</sup> pits,<sup>61</sup> breaking of brittle films produced by dealloying,<sup>62,63,64</sup> hydrogen-related degradation including the formation of hydrides and hydrogen bubbles at grain boundaries, grain boundary embrittlement<sup>65</sup> or other brittle films.<sup>66</sup>

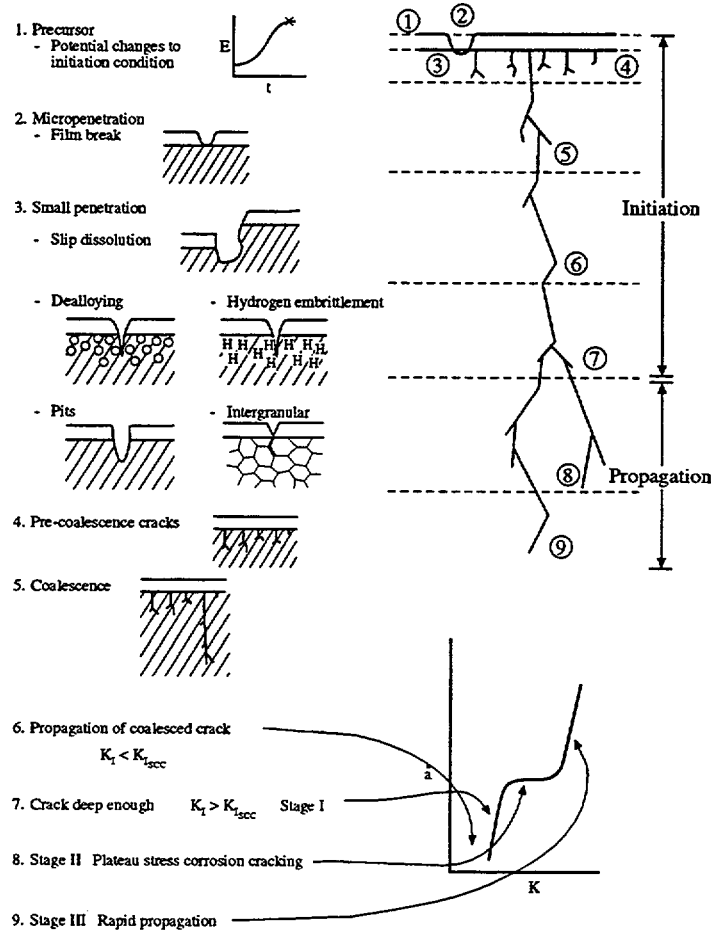


Figure 6: Nine segments of SCC: (1) Protective film adjusts to the environment; (2) chemical and/or mechanical perforation of protective film; (3) early penetration by pitting, intergranular corrosion, slip step dissolution, tunnels, dealloying and hydrogen embrittlement; (4) early SCC; (5) coalescence of small SCC; (6) propagation of coalesced SCC until  $K_{I,SCC}$  reached; (7) stage I propagation; (8) stage II propagation; (9) stage III propagation. Overall stages of initiation and propagation shown.

In the fourth segment of SCC shown in Figure 6 many, sometimes hundreds, of small cracks form. However, few, if any, of these small cracks propagate. Parkins<sup>67</sup> in Figure 64a has shown that some of these initial cracks coalesce to produce larger SCC which then can propagate. However, not all SCC follows this pattern, and initially formed cracks may propagate without the step of coalescence. In the sixth segment, these coalesced cracks propagate until they reach a point usually described by stage I of SCC. From this point, SCC propagates according to the stages I, II, and III as is conventionally described in the propagation of SCC and account for the seventh, eighth, and ninth segments.

The phenomenological evolution of the early stages of SCC has been described, and various views of these early stages are shown in Figure 7. Andresen and Ford<sup>68</sup> have proposed a model shown in Figure 7a where pitting is identified as a first step and the subsequent SCC grows at an increasingly rapid rate. They define initiation as the depth which can be discerned by inspection. Figure 7b shows the events proposed by Parkins<sup>69</sup> where he indicates a sequence similar to that in Figure 6. Akashi and Nakayama<sup>61</sup> in Figure 7c propose six steps with three being stochastic and three being deterministic; the sequence of events is similar to Figure 6. Figure 7d is proposed by Gras<sup>70</sup> and divides initiation and propagation into varying degrees of proneness to SCC. In general, the features of this figure are similar to those of Andresen in Figure 7a. Figure 7e shows a typical pattern for the open circuit potential vs. time as observed for stainless steels stressed and exposed in boiling  $MgCl_2$ .<sup>71,72</sup> Features of the open circuit potential vs. time can be correlated with certain segments of SCC as shown in the figure. This curve is the basis for many of the data obtained by Shibata discussed here. Figure 7f from the work of Eckel<sup>73</sup> shows the crack depth vs. time for six stainless steels exposed to boiling  $MgCl_2$ . These depths were determined metallographically and extrapolated to zero depth to determine the initiation times.

For the purposes of this report, only two stages of SCC are considered: initiation and propagation as shown in Figure 6. Figure 6 shows that initiation consists of the first six segments and propagation consists of the last three. Also, the general patterns shown in Figure 7 indicate that there is an initially slow stage followed by a more rapid second stage. The two inclusive steps of SCC, initiation and propagation, can be distinguished as shown in Figure 8. Generally, initiation is quantified by testing specimens with initially smooth surfaces where the minimum threshold stress for initiating SCC is determined. Propagation is quantified by testing with pre-cracked specimens where the velocity of the SCC is measured. Horizontal lines on Figure 8 identify thresholds for SCC of specimens with initially smooth surfaces; lines with a slope of  $-1/2$  identify loci of various values of  $K_{ISCC}$ . The intersection of horizontal and sloping lines identifies the transition between initiation and propagation. For example, for a threshold stress of 100 MPa and a  $K_{ISCC}$  of 5 MPa  $m^{1/2}$  the transition between initiation and propagation occurs at about 800  $\mu m$ . Initiation occurs below this transition and propagation occurs above.

The stages of initiation and propagation can also be differentiated by the method described by Pessell<sup>74</sup> who studied the SCC of Alloy 600 at 315°C in 10% NaOH with an applied potential of 150 mV. His results are shown in Figure 9. He first determined the characteristic development of SCC as depth vs. time in a test for seven days. This first experiment produced a reference. He then exposed specimens for lesser lengths of time and then removed the potential. The results in Figure 9 show that when the potential was removed after one day and two days the SCC did not propagate. After three days, when the potential was removed, the SCC continued to propagate but at a lower rate. When the potential was removed after four days, the SCC continued at the reference rate. The results in Figure 9 show that, when the SCC is less than about 500  $\mu m$ , progress of SCC depends on the applied potential. With deeper SCC, the SCC does not depend on the external potential and propagates without its continued application. The transition from the depth where the applied potential is necessary to where it is not is a transition from initiation or surface control to a condition of propagation or crack tip chemistry control. The transition from surface control to propagation control in Figure 9 is similar to the transition shown in Figure 8 for the case of 100 MPa and 5 MPa  $m^{1/2}$  which is typical of SCC of many stainless steels and high nickel alloys.

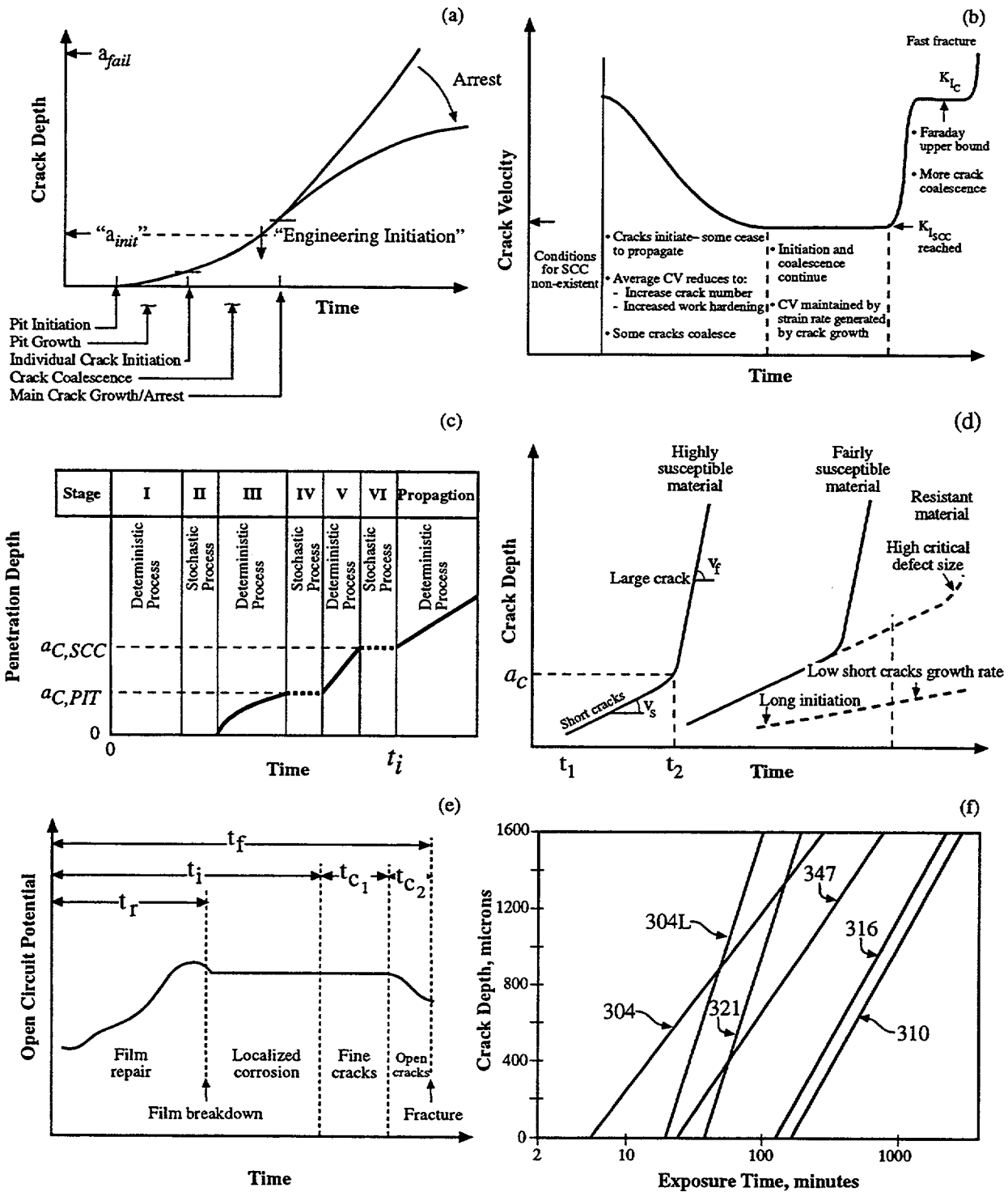


Figure 7: (a) Schematic view of crack depth vs. time. From Andresen and Ford,<sup>68</sup> (b) Schematic view of crack velocity vs. time. Adapted from Parkins.<sup>69</sup> (c) Schematic view of penetration vs. time showing segments; solid lines indicate deterministic processes and dotted lines indicate stochastic processes; depths of pitting and SCC indicated. From Akashi and Nakayama.<sup>61</sup> (d) Schematic view of crack depth vs. time for materials of various susceptibilities to SCC. From Gras.<sup>70</sup> (e) Schematic view of open circuit potential vs. time showing locations associated with segments of SCC. Adapted from work of Hoar and Hines<sup>71</sup> and Hines.<sup>72</sup> (f) Crack depth vs. time for various stainless steels measured metallographically after exposure to boiling 42%  $MgCl_2$ . From Eckel.<sup>73</sup>

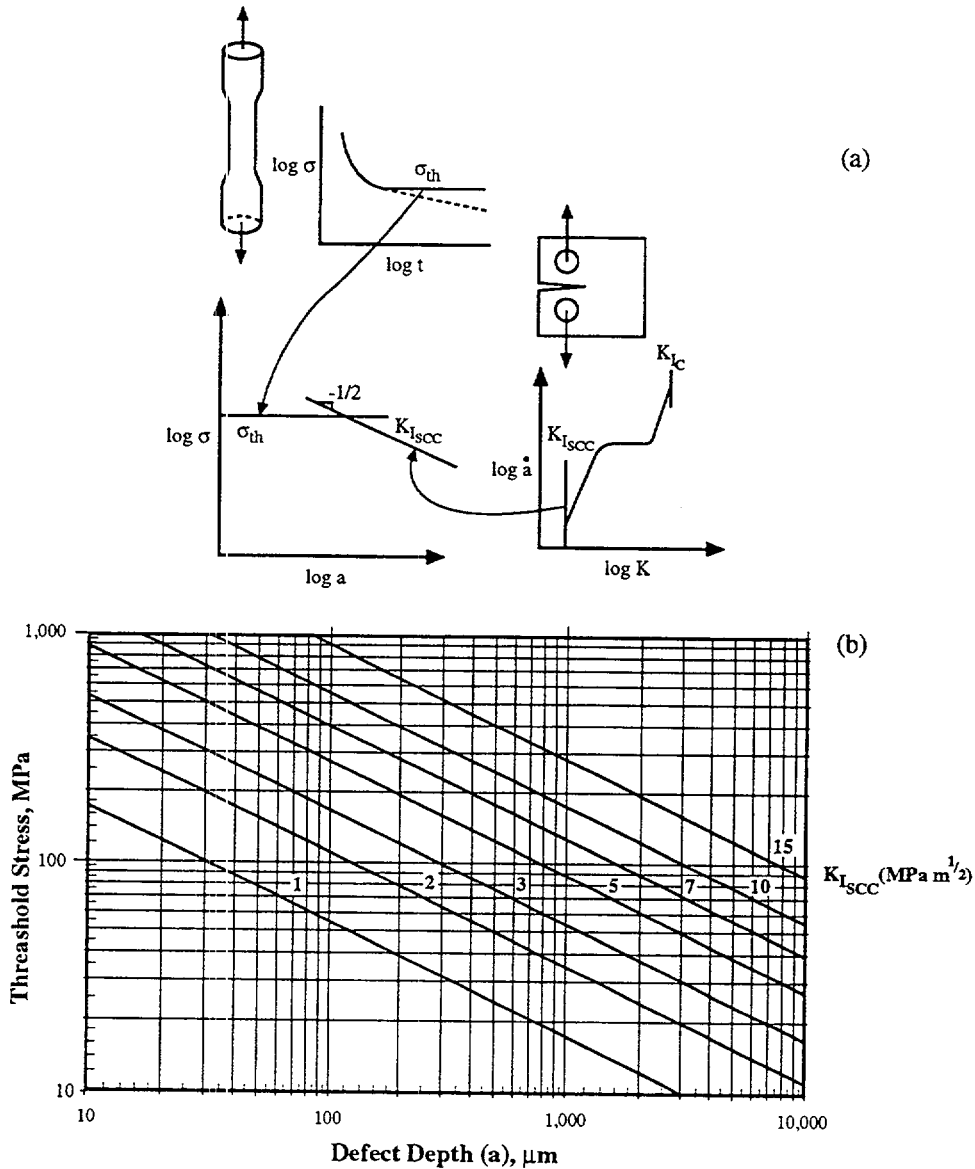


Figure 8: Basis for distinguishing between initiation and propagation. (a) Schematic view of  $\log$  stress vs.  $\log$  of defect depth for cases of stresses on smooth surface specimens and the locus of points associated with  $K_{I_{SCC}}$  as determined from pre-cracked specimens. (b) Graph for determining the intersection of threshold stresses from smooth surface specimens with values of  $K_{I_{SCC}}$ . From Staehle.<sup>4</sup>

### 1.8 General Prediction of Dependencies of SCC—Modes and Submodes

The consideration of initiation and propagation in Figures 6, 8 and 9 does not account for influences of metallurgy and environments on whether SCC actually occurs. In general, the intensity of SCC described in Figure 1 suggests that there are regions where no SCC occurs as the expression identifies negligible penetrations when the functions are minimal.

In this report, the terms “mode” and “submode” are used. The term, “mode,” is taken to mean the various morphologies that corrosion of solids produces as shown in Figure 10. The term, “submode,” refers to multiple occurrences of a single mode such as SCC where these occurrences, respectively, depend differently upon the principal variables of electrochemical potential, pH, species, alloy composition, alloy structure, stress and temperature.  $A_{kSCC}$  and  $A_{cSCC}$  as shown in Figure 12 are examples of separate submodes of SCC.

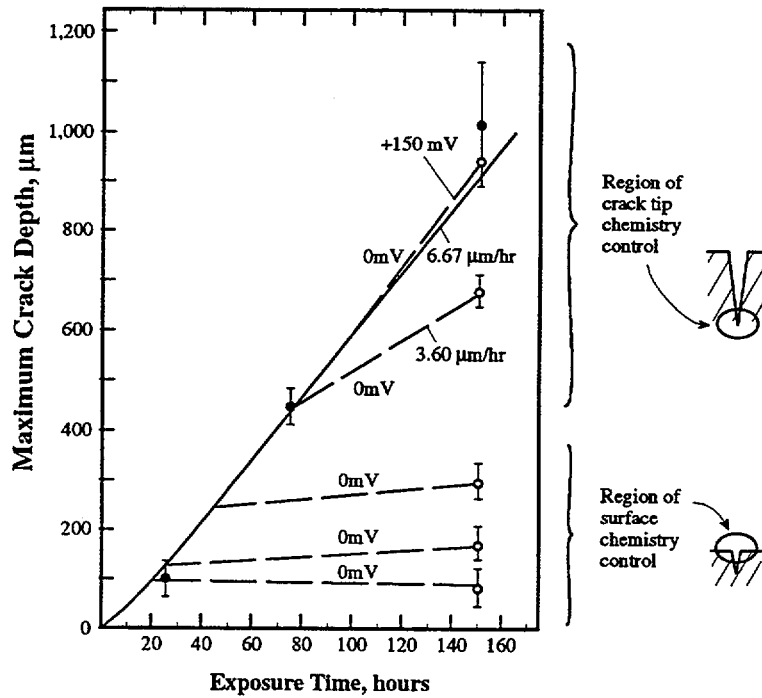


Figure 9: Maximum crack depth vs. exposure time for Alloy 600MA exposed to 10% NaOH at 315°C and +150 mV applied potential. Solid line and solid dots correspond to reference depth vs. time for SCC at the nominal conditions. Dotted lines and open circles represent the instances where the applied potential was removed at various times. Approximate regions of control by surface chemistry and crack tip chemistry are noted as they correspond to conditions of initiation and propagation. From Pessell.<sup>74</sup>

In aqueous environments, the occurrence of SCC often can be identified by features that are observed on polarization curves. A schematic view of a polarization curve is shown in Figure 11 based on the early suggestion of Staehle as later modified.<sup>75,76</sup> Superimposed on the polarization curve of Figure 11 are regions in which SCC is often found. Other regions of film-free corrosion, passivity, breakdown and pitting are also identified. At lower potentials, hydrogen evolution from the reduction of water occurs and sometimes contributes to hydrogen-related SCC. Figure 11 shows that SCC is most likely to occur in regions of passivity adjacent to regions of instability as well as in regions where hydrogen is produced; SCC should be expected adjacent to the active peak and adjacent to the breakdown of passive films. SCC in alkaline environments usually occurs immediately above the active peak; SCC of stainless steels in boiling MgCl<sub>2</sub> solutions often occurs in the region of the breakdown potential. Hydrogen embrittlement occurs when the hydrogen pressure increases with lowered potential in the range of the standard hydrogen equilibrium.

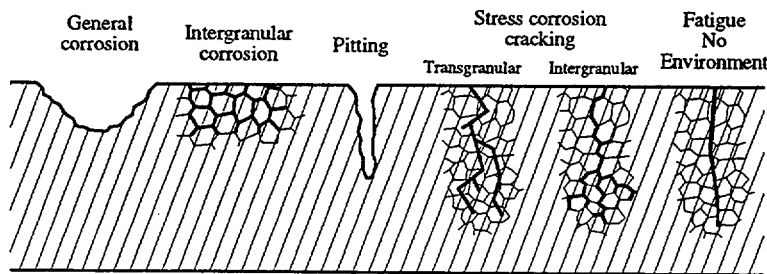


Figure 10: Five intrinsic modes of penetration by corrosion into solids: General corrosion (including chemical degradation, wear, erosion, and fretting), intergranular corrosion, pitting corrosion, stress corrosion cracking in transgranular and intergranular morphologies, and dry fatigue.



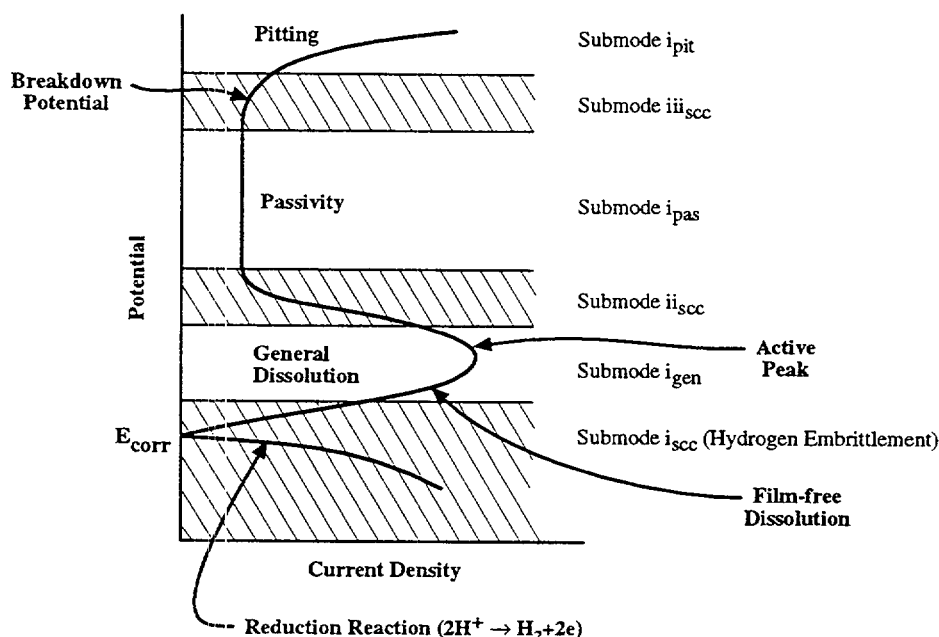


Figure 11: Schematic view of locations where submodes of SCC can occur relative to a polarization curve. Other submodes of pitting, general corrosion and passivity are noted. From Staehle.<sup>77</sup>

The most likely regions for the occurrence of SCC can be identified by conducting a polarization experiment and determining where these instabilities occur. The occurrence of SCC at these locations has been reported by many authors in many metal-environment systems.

A broader view of the occurrence of SCC can be organized by developing a mode diagram such as that in Figure 12.<sup>2,76</sup> Here, regions of SCC are identified based on experimental work reported by many authors.<sup>78</sup> Figure 12a describes four submodes of SCC that occur in Alloy 600 in the range of 300-350°C: alkaline SCC (AkSCC), low potential SCC (LPSCC), acidic SCC (AcSCC), and high potential SCC (HPSCC). The same four submodes occur in low alloy steels and stainless steels.

Figure 12b describes seven minor submodes:

- PbSCC in dilute lead-containing environments has been studied by many investigators, and failures in several operating SGs have been attributed to this submode. PbSCC was first studied by Copson and Dean<sup>79</sup> and since then has been studied by many authors including Miglin and Sarver,<sup>80</sup> Hwang et al.,<sup>81</sup> and Wright.<sup>82</sup> PbSCC produces SCC in Alloy 600, Alloy 690, Alloy 800, Monel 400, stainless steel, and 17-4PH and probably many more alloys. PbSCC occurs over the range of pH from alkaline, neutral, to acidic environments.
- SiAlSCC has been observed by Lumsden\* and occurs in mild alkalinities with silica and alumina present as low as about pH8; it is most rapid at about 150 mV above the standard hydrogen line.
- ClSCC has been reported for Alloy 600 in chloride solutions acidified with H<sub>3</sub>BO<sub>4</sub> by Berge and Donati,<sup>83</sup> and Berge et al.<sup>84</sup> contrary to the reports by Copson and Cheng who studied such alloys in boiling 42% MgCl<sub>2</sub>.<sup>85,86</sup> There is now little question that chloride produces SCC in Alloy 600. The possible occurrence of ClSCC is also supported by the work of Was et al. on the acuity of pitting as a function of chloride/sulfate ratio<sup>87</sup> as interpreted by Staehle.<sup>88</sup>
- S<sup>x</sup>SCC has been reported by Cassagne and Gelpi<sup>89</sup> to occur in alkaline solutions where S<sub>2</sub>O<sub>3</sub><sup>=</sup> is present; and similarly severe S<sup>x</sup>SCC in alloy 600 and 690TT has been reported to occur in Na<sub>2</sub>S and HS<sup>-</sup> but is not publicly reported. The possibility of S<sup>x</sup> SCC is also reported by Fang and Staehle.<sup>90</sup>

\* Personal Communication with J.B. Lumsden of Rockwell Science Center, June, 2001.

- AcSCC of Alloy 600 was first reported by Jacko.<sup>91</sup>
- CuSCC in mildly acidic sulfate solutions containing CuO has been reported by Pierson<sup>168</sup> who has shown that these environments produce SCC in both Alloy 600 and Alloy 690.
- DSSCC (SCC in doped steam environments) has been observed by Dehmlow<sup>92</sup> and others in steam where various concentrations of impurities at low concentrations have been added to the water producing the steam. This is referred to as the “doped steam” environment.

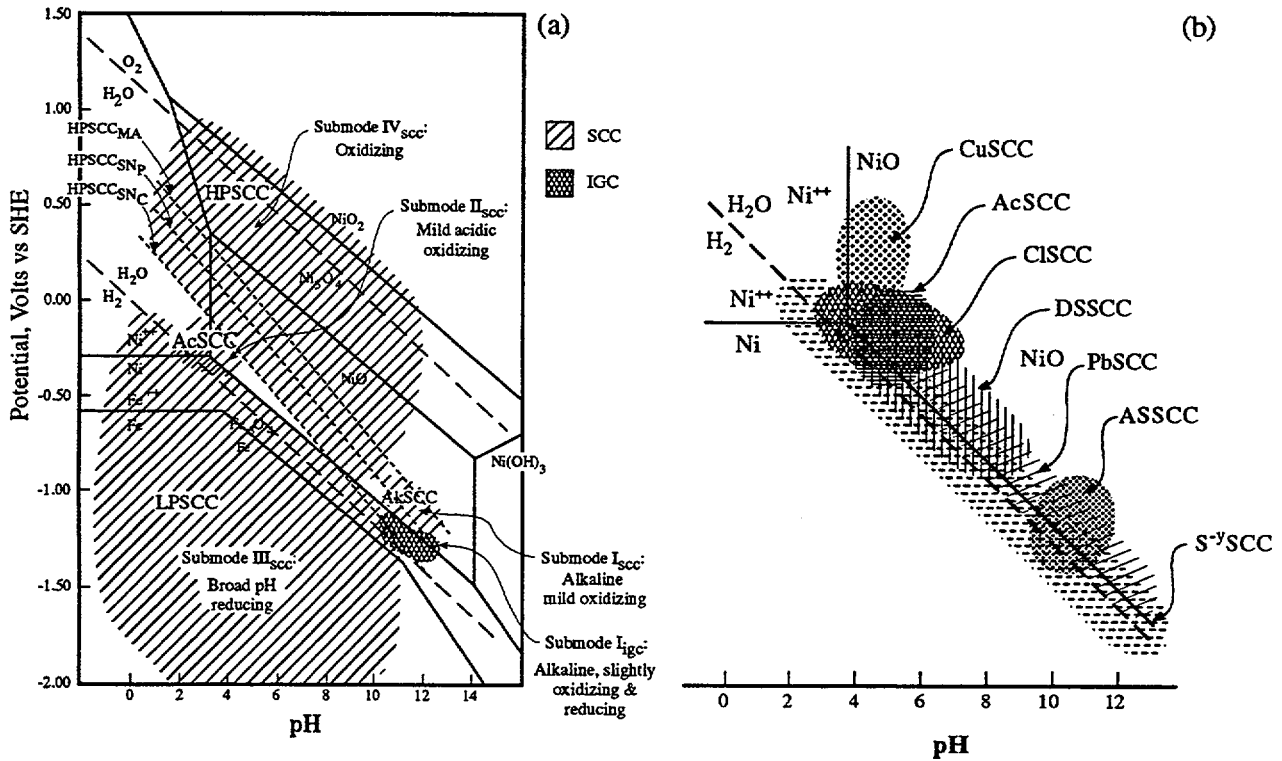


Figure 12: (a) Major submodes of SCC and IGC for Alloy 600 in sensitized and mill annealed conditions in the range of 280° to 350°C in aqueous solutions. Regions of SCC shown with respect to thermodynamic boundaries for iron and nickel species in water. Regions of SCC submodes shown are based on published experimental data.<sup>76</sup> LPSCC = “low potential SCC.” HPSCC = “high potential SCC.” AkSCC = “alkaline SCC.” AcSCC = “acidic SCC.” SN = “sensitized.” MA = “mill annealed.” P = “pure water.” C = “contaminated.” (b) Minor submodes of SCC shown with respect to the region around the Ni-NiO equilibrium. Minor submodes are shown relative to Ni/NiO line.

SCC is affected by the electrochemical potential according to three patterns as shown in Figure 13. In the case of LPSCC the intensity of SCC rises sharply in the negative direction at about the Ni/NiO equilibrium and remains generally constant to lower potentials as shown in Figures 13a and b. This is a type I dependence on potential. This rise occurs over a range of about 100 mV being negligible at higher potentials and fully developed at lower potentials. A similar but opposite pattern is associated with HPSCC and is shown in Figures 13c and d. This is a type II dependence on potential. Again, the rise in intensity as a function of potential is relatively steep and occurs over a range of about 100-200 mV. The third pattern, type III, which is typical of AkSCC and most likely AcSCC is shown in Figures 13e and f. Here, the SCC is maximum at some value and decreases at higher and lower potentials. This type III dependence is also observed for stainless steels in chloride solutions as shown for chloride-sulfate environments.<sup>76,78</sup> These prototypical dependencies of SCC on potential as illustrated in Figure 13 are one of the bases for the highly variable nature of SCC.

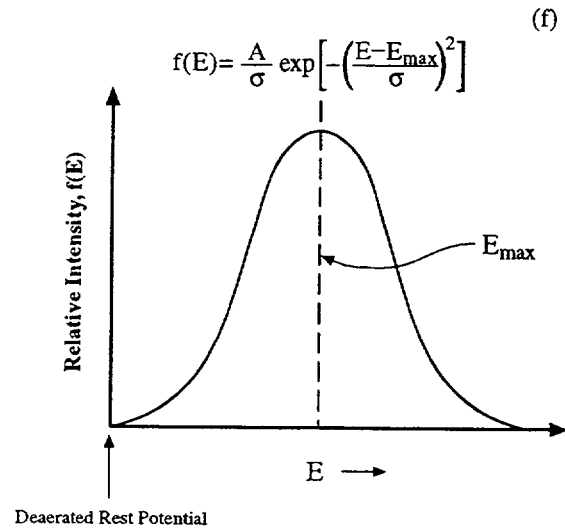
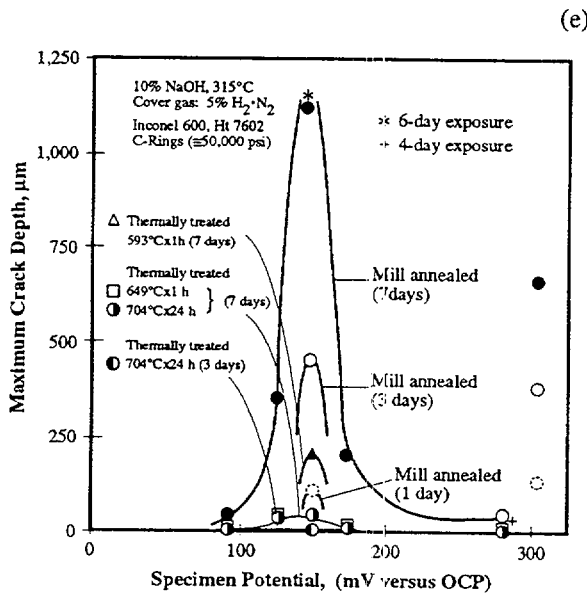
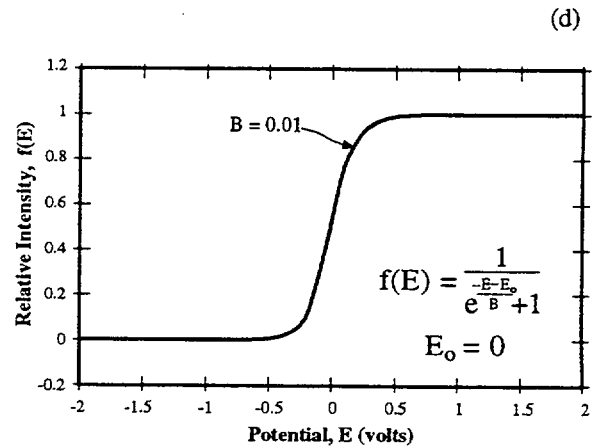
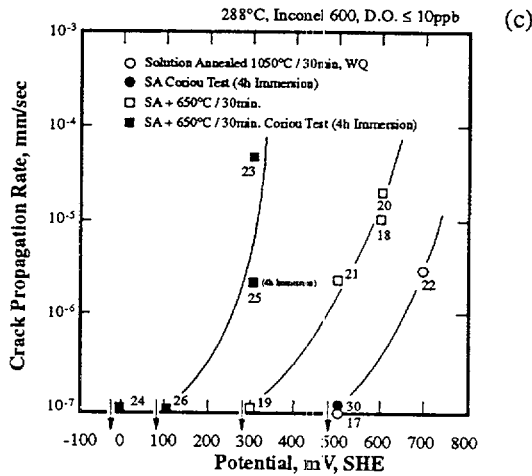
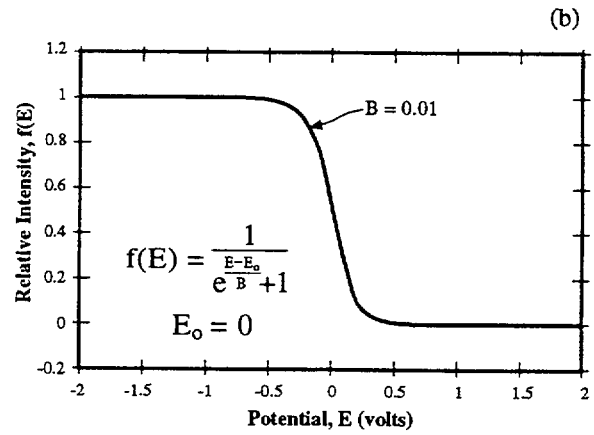
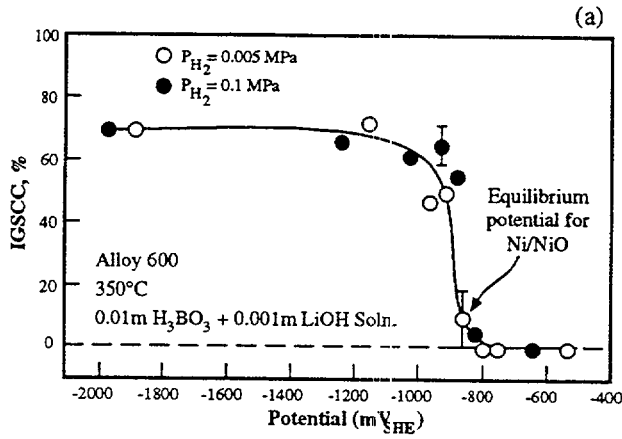


Figure 13: (a) Extent of LPSCC vs. applied potential for Alloy 600 at 350°C; note location of Ni/NiO equilibrium. Adapted from Totsuka and Szklarska-Smialowska.<sup>93</sup> (b) Type I dependence of SCC on potential with correlation equation noted. (c) Extent of HPSCC vs. potential for Alloy 600 at 288°C. Adapted from Shoji<sup>94</sup> (d) Type II dependence of SCC on potential with correlation equation noted. (e) Maximum crack depth as a function of potential for Alloy 600 exposed to 10%NaOH at 315°C. Adapted from Pessall.<sup>74</sup> (f) Type III dependence of SCC on potential with correlation equation shown.

Figure 14 shows a diagram for low alloy steels as developed by Parkins<sup>95</sup> and Congleton et al.<sup>96</sup> In this diagram a range of HPSCC is not shown but those for AkSCC, LPSCC, and AcSCC are evident. The middle of the AcSCC region follows the  $\text{Fe}_3\text{O}_4/\text{Fe}_2\text{O}_3$  equilibrium. This corresponds to the submode  $\text{ii}_{\text{SCC}}$  region of Figure 11. SCC centered about this equilibrium is consistent with the lack of protection provided by the  $\text{Fe}_3\text{O}_4$ . The data in Figure 14 show that the AcSCC region depends more on the pH and potential than on the specific chemistry of the test environments. The LPSCC region follows the general expectations for hydrogen-related SCC at lower potentials. The minimum in the continuum from AkSCC to AcSCC occurs at the same pH as the solubility minimum for iron in water as noted by comparing Figures 14c with 14d. This suggests that the SCC in the anodic regions depends strongly on the solubility of the metal oxide, as would be expected.

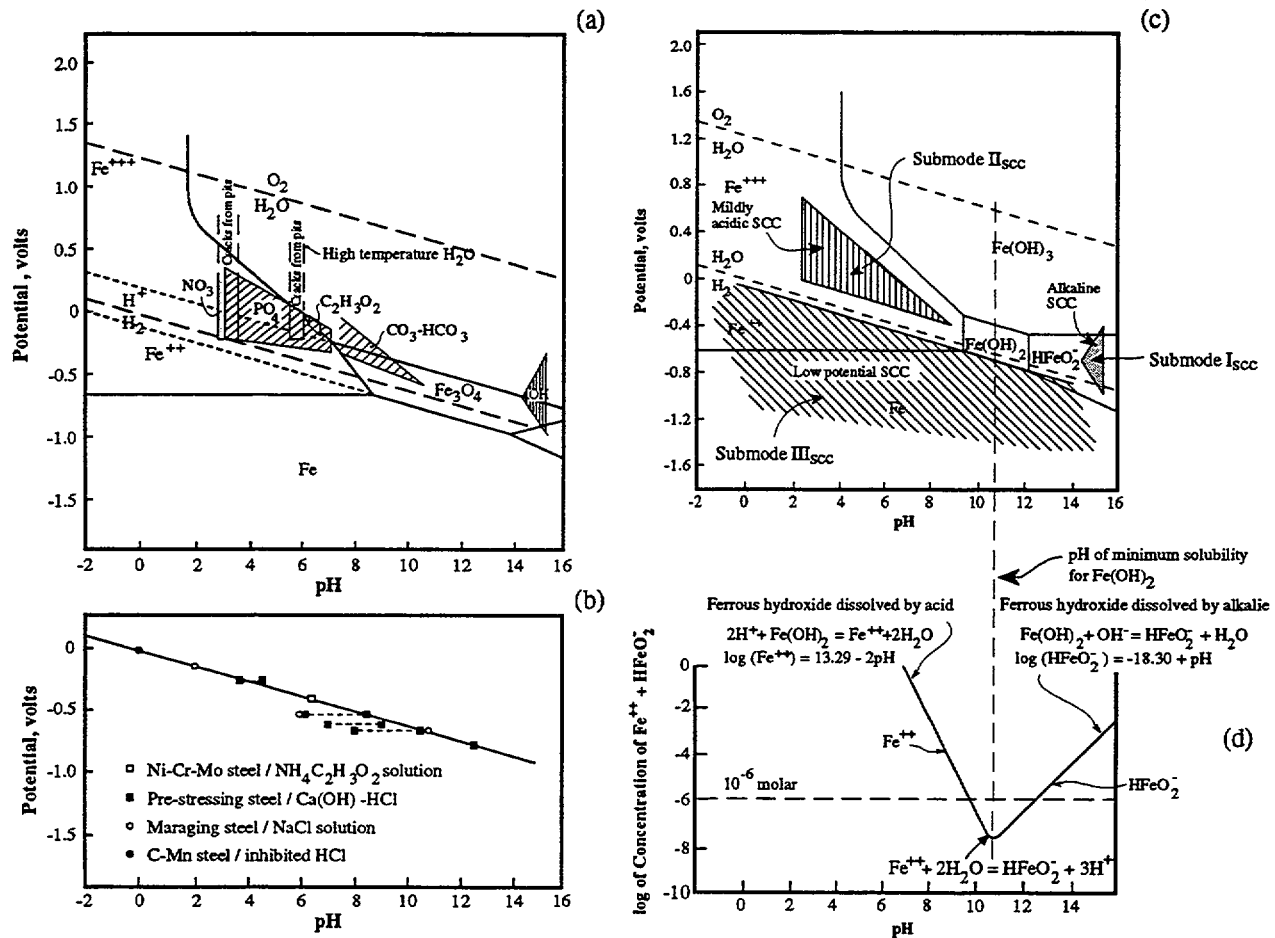


Figure 14: (a) Potential vs. pH for iron in water. Shaded areas show locations for occurrence of SCC of low alloy steels exposed to different environments at room temperature except for one in high temperature water. Adapted from Congleton et al.<sup>96</sup> (b) Line shows potential below which hydrogen-related SCC occurs for various steels. Adapted from Parkins.<sup>95</sup> (c) Synthesis of data from Figures 14a and 14b. (d) Solubility of iron as a function of pH with the dotted line drawn from the minimum solubility to the region of no anodic SCC. Adapted from Pourbaix.<sup>97</sup>

Figures 12 and 14 apply mainly to the conditions of initiation as defined in Figures 8 and 9 where the external environment can influence the chemistry of the early SCC. Propagation is mainly controlled by the chemistry at crack tips; chemistry at the tips of cracks is more controlled by local conditions at the crack tip and is less sensitive to the external bulk environments. Thus, propagation of SCC can sometimes continue in the presence of a broader range of bulk environments than those that control initiation as shown in Figures 12 and 14.

## 1.9 Framework for Predicting Early Failures

The main objective of this report is to enumerate and describe elements of a framework for predicting the earliest failures occurring by SCC. Principal considerations in this framework are:

- Emphasizing the importance of early failures that occur at low probabilities.
- Linking well known statistical distributions with physical factors that control SCC.
- Quantifying the scale, shape, and location parameters of statistical distributions by assessing their dependencies upon the seven principal variables of potential, pH, species, metallurgical composition, metallurgical structure, temperature and stress.
- Distinguishing the variabilities that are due to the inherent nature of the materials, the metallurgical or heat-to-heat effects, and the environmental effects.
- Screening non-relevant data.
- Identifying the variability that can be produced by methods of testing and by methods of measurement.
- Using the hazard function to identify physical influences on early failures.
- Identifying the leverage on variability produced by metallurgical and environmental effects.
- Developing an understanding of the dependencies of the shape parameter.

## 1.10 Outline of the Approach

This introduction defines the perspective of this report and introduces those aspects of SCC that affect predicting early failures. The introduction is followed by Section 2.0 that provides a perspective of statistical distributions as they are used to predict early failures and to interact with physical descriptions.

Subsequently, there are four sections that describe variabilities related to SCC: inherent variability (Section 3.0), metallurgically induced variability (Section 4.0), environmentally induced variability (Section 5.0), and statistical aspects of SCC morphologies (Section 6.0). Next, variability due to test methods and measurement are discussed (Section 7.0).

Finally, in Section 8.0, the combined considerations of statistical and physical factors are considered as they provide a framework for predicting the earliest failures. Approaches to developing such predictions are discussed.

## 2.0 STATISTICAL DISTRIBUTIONS AND THEIR APPLICATIONS

### 2.1 Scope

Predicting the earliest failures in this report relies on using well established statistical distributions that are applicable to modeling degradation processes and that can be connected with the physical bases of metallurgy and environment that influence the occurrence of SCC. This section describes the statistical distributions that are applicable to modeling SCC and pitting, bases for connecting them to the variables that affect SCC, problems of scatter of data, properties of statistical parameters as they relate to physical variables, and properties of early failures.

This section emphasizes the use of the Weibull distribution since it has been shown to model well various degradation phenomena. The Weibull distribution provides a good framework for illustrating the connection between statistical parameters and the principal variables that control SCC. Some data originally modeled by other distributions have been converted to the Weibull format. Aside from observing that the Weibull distribution is widely used, it is not intended to argue the relative merits of the various distributions.

The Weibull distribution was first developed empirically and published in 1951 by W. Weibull.<sup>31</sup> Weibull applied his distribution to a range of data including the variety of fly ash and the fiber strength of Indian cotton. Of more direct interest here, he applied the distribution to characterizing the strength of a Swedish steel and to the fatigue life of a steel. Gumbel<sup>28</sup> demonstrated that the Weibull distribution was one of the six asymptotic solutions to the system of extreme value statistics. Such a development is parallel to the early empirical development of the Tafel equation<sup>98</sup> in electrochemistry that was later shown to be on solid fundamental grounds from rate theory by Butler<sup>99</sup> and Erdey-Gruz and Volmer.<sup>100</sup> Gumbel, in commenting on Weibull's work, notes that "if the design of machinery is carried out in such a way that the stress does not exceed this value ( $t_0$  in the terminology used here, but the lower limit stress in Gumbel's discussion) the probability of rupture is zero. The impressive and promising work of Weibull requires systematic experiments designed according to his theoretical setup, which up to now have not, as far as I know, been fully carried out."<sup>\*</sup>

### 2.2 The Distributions

The Weibull and exponential distributions are described mainly. The following are described briefly for each distribution: probability density function,  $f(t)$ , (pdf); cumulative distribution function,  $F(t)$ , (cdf); reliability function,  $R(t)$ , (rf); hazard function,  $h(t)$ , (hf); and cumulative hazard function,  $H(t)$ , (chf). A consistent set of nomenclature and symbols is used. Symbols vary among texts and authors. In general, the formulations and nomenclatures by O'Conner,<sup>12</sup> Nelson,<sup>9</sup> and Abernethy<sup>35</sup> are used.

---

\* pp. 32 and 33 of Ref 29.

### 2.2.1 The Weibull Distribution\*

The most widely used and applicable distribution for describing the time-dependence of corrosion failures is the Weibull distribution. The pdf for the three parameter  $(\theta, \beta, t_o)$  Weibull distribution is given in Eqn. (1):

$$f(t) = \left[ \frac{\beta}{(\theta - t_o)^\beta} \right] (t - t_o)^{\beta-1} \exp \left[ - \left( \frac{t - t_o}{\theta - t_o} \right)^\beta \right], t > t_o \quad (1)$$

where:

$t$  = time

$t_o$  = location parameter or initiation time

$\theta$  = scale parameter or the Weibull characteristic. When  $\theta = t$ ,  $F(\theta) = 0.632$ .

$\beta$  = shape parameter or often called the "Weibull slope" as is evident when the linearized version of the cdf is discussed in Eqn. (8) and Figures 15c and 15d.

Figure 15 shows typical examples of the functions for the Weibull distribution: pdf, cdf, hf. Also the time derivative of the hf is shown. The derivative is used when mechanistic implications of the hf are discussed. The values used for these abscissas are arbitrary since the units can be any values so long as they are self consistent in units within the exponential; values for the equations are based on ones often observed in experimental and engineering experience. Figure 15 does not include values for the location parameter,  $t_o$ . An example of the application of  $t_o$  is shown in Figure 16.

The Weibull cdf is defined in Eqn. (2) and is shown in Eqn. (3). The cdf gives the probability that failure has occurred by a given time. Examples of cdfs corresponding to the pdfs are shown in Figure 15d.

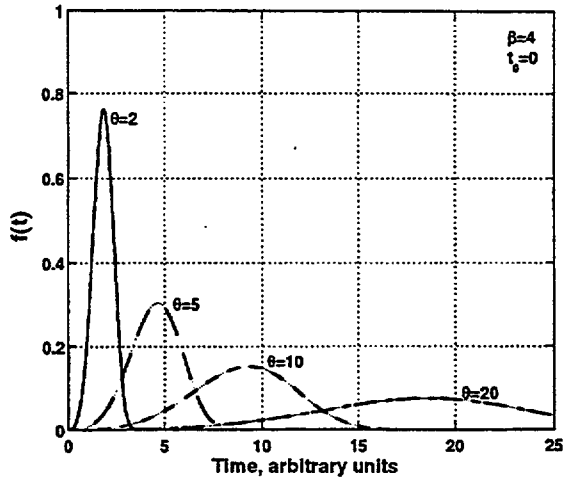
$$F(t) = P\{t' \leq t\} = \int_0^t f(t) dt \quad (2)$$

$$F(t) = 1 - \exp \left[ - \left( \frac{t - t_o}{\theta - t_o} \right)^\beta \right] \quad (3)$$

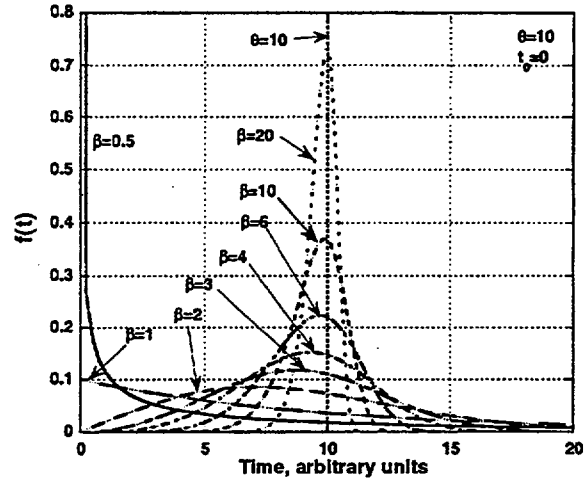
---

\* In this report most of the plots of cdfs are in terms of the Weibull format. Data from other formats including normal and exponential are converted into Weibull format. Also, the times are all converted to hours. All stresses are converted to MPa. The original formats are noted in the captions. Calculations for Weibull values in this report have been performed using the WINSMITH™ Weibull 3.0U. Where values of  $t_o$  are positive and non-negative, they are used rather than the two parameter fit. If the values of  $t_o$  are inconsequential, the two parameter fits are used. Reported on the figures is the value of  $F(\theta) = 0.632$  corresponding to the value for  $\theta = t$ . The value of 0.632 is shown as a dotted line on the Weibull plots. The Weibull software reports a value of  $\eta$ .  $\theta$  is the sum of  $t_o$  and  $\eta$ . i.e. the Weibull plots give  $\eta (\theta - t)$  vs.  $t$  or the relevant variable. The three parameter fit was not used for plots of probability vs. potential since the physical result was inaccurate. Where the number of points was less than about six, the two parameter fit was used. Data were obtained for all the plots taken from other authors by the program, Data Thief, Version 2, by K. Huyser and J. van der Laan, Computer Systems Group of the Nuclear Physics Section at the National Institute for Nuclear Physics and High Energy Physics, Amsterdam, 1991-95, that was downloaded from the Web.

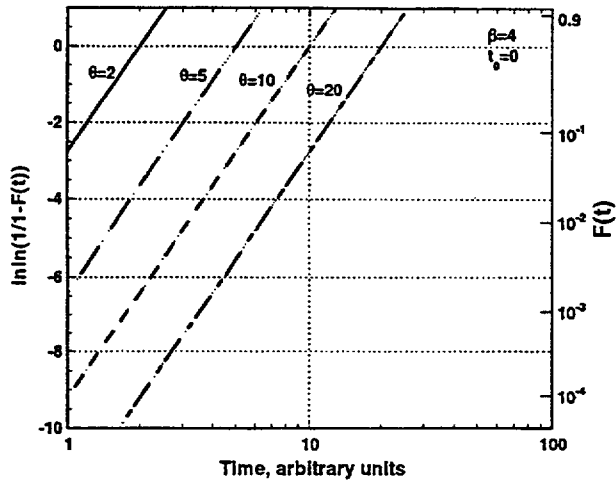
(a)



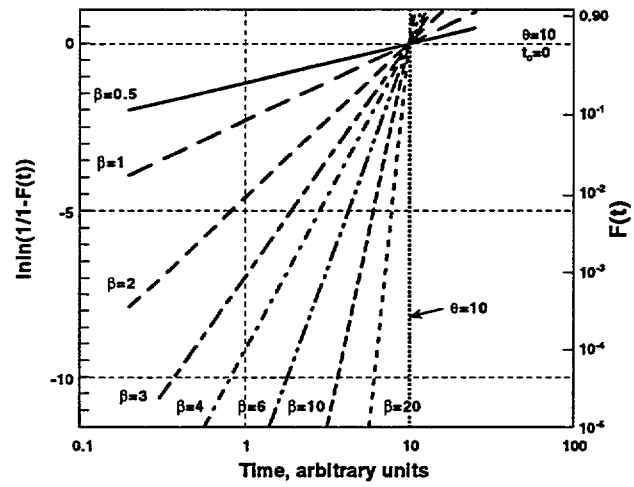
(b)



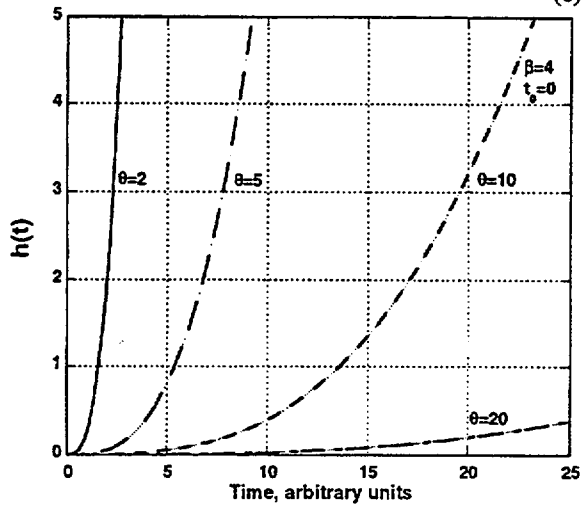
(c)



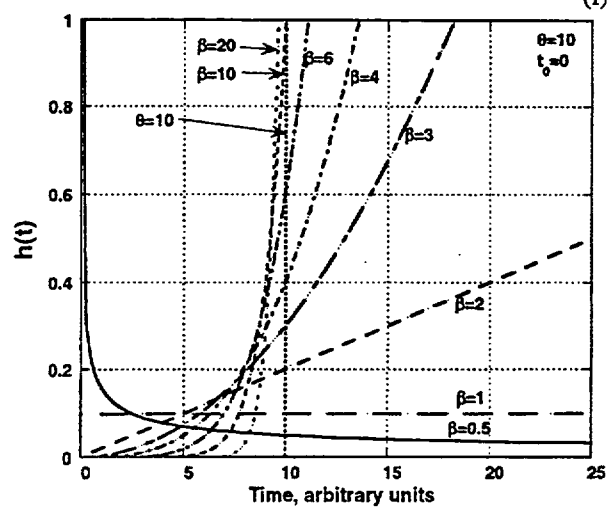
(d)



(e)



(f)





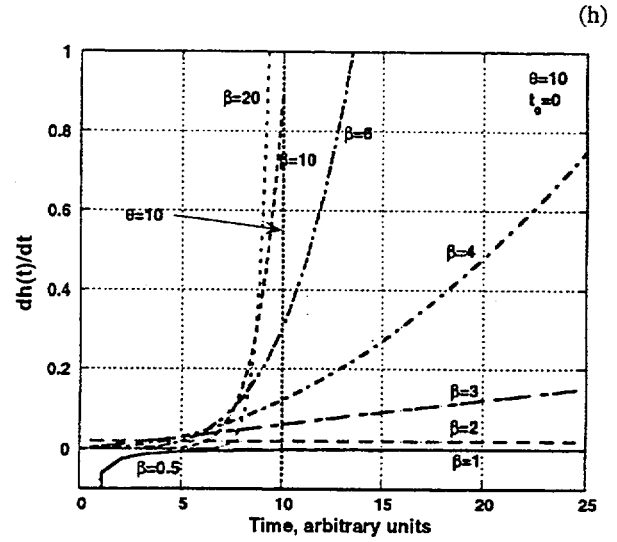
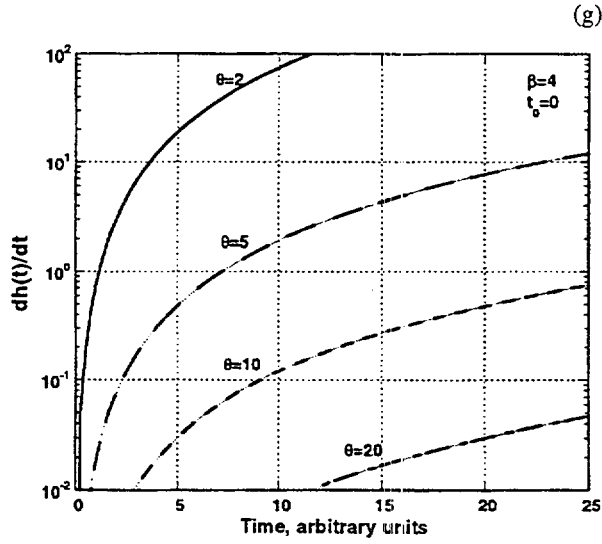


Figure 15: (a)  $f(t)$  vs. time for constant  $\beta$ . (b)  $f(t)$  vs. time for constant  $\theta$ . (c)  $F(t)$  vs. time for constant  $\beta$ . (d)  $F(t)$  vs. time for constant  $\theta$ . (e)  $h(t)$  vs. time for constant  $\beta$ . (f)  $h(t)$  vs. time for constant  $\theta$ . (g)  $dh(t)/dt$  vs. time for constant  $\beta$ . (h)  $dh(t)/dt$  vs. time for constant  $\theta$ .  $t_0$  taken as zero.

The hf is defined in Eqn. (4) and is given for the three parameter Weibull distribution in Eqn. (5). The hf is plotted in Figures 15e and 15f. The hf gives the probability that failure will occur in the next increment of time,  $dt$ . The hf is useful in distinguishing among whether the probability of failure is decreasing with time ( $\beta < 1$ ), is independent of time ( $\beta = 1$ ), or is increasing with time ( $\beta > 1$ ). Such trends are particularly useful for understanding the mechanistic processes that are critical to the initiation and propagation of SCC. Implications of the change in hazard functions with increasing values of  $\beta$  become important in assessing the physical bases for the shape parameter.

$$h(t) = \frac{f(t)}{1 - F(t)} \quad (4)$$

$$h(t) = \left( \frac{\beta}{\theta - t_0} \right) \left( \frac{t - t_0}{\theta - t_0} \right)^{\beta-1} = \frac{\beta}{(\theta - t_0)^\beta} (t - t_0)^{\beta-1} \quad (5)$$

The chf is defined in Eqn. (6) and is given in Eqn. (7) for the two parameter Weibull distribution:

$$H(t) = \int_0^t h(t) dt \quad (6)$$

$$H(t) = \frac{t}{\theta^\beta} \quad (7)$$

The cdf from Eqn. (3) is most useful when linearized, and the three parameter version is given in its linear form in Eqn. (8):

$$\ln \left[ \ln \left( \frac{1}{1 - F(t)} \right) \right] = \beta [\ln(t - t_0) - \ln(\theta - t_0)] \quad (8)$$

The reliability function or the survivorship function,  $R(t)$ , is given in Eqn. (9).  $R(t)$  gives the probability that failure will not occur at times greater than a value of  $t$ .

$$R(t) = P\{t' > t\} = \int_t^{\infty} f(t)dt = 1 - F(t) = \exp\left[-\left(\frac{t-t_o}{\theta-t_o}\right)^\beta\right] \quad (9)$$

Often, it is simpler and not necessary to include the location parameter,  $t_o$ ; and two parameter ( $t_o$  omitted) Weibull equations are often used. Omitting  $t_o$  implies that the damage process starts immediately. While  $t_o$  is sometimes called an initiation time, it is simply a fitting parameter; and any physical significance should not be assumed without careful consideration.  $t_o$  can provide a guide for when some stage of initiation could be expected. Any initiation time that is physically based would be a distributed variable and not a single value as noted in Figure 78 of Section 8.10.

The mean value of the Weibull distribution is given in Eqn. (10); however, the Weibull characteristic,  $\theta$ , is sufficiently close to the mean that it is considered interchangeable and is used here for relating to physical variables. The Weibull characteristic is evaluated where  $t=\theta$  corresponding to an  $F(t)$  of 0.632. Further, the mean is less straightforward to manipulate when incorporating the primary variables that affect SCC and when considering the connection between physical variables and the statistical parameters.

$$\mu(t) = (\theta - t_o) \Gamma\left[1 + \left(\frac{1}{\beta}\right)\right] + t_o \quad (10)$$

Figure 15 plus Eqns. (1) through (10) identify the following important features of the Weibull distribution:

- The shape parameter,  $\beta$ , greatly affects the difference between the earliest failures and the mean with lower values producing greater differences.
- Various values of the shape parameter can model decreasing probability of failure ( $\beta < 1$ ), time-independent probability of failure ( $\beta = 1$ ), and increasing probability of failure ( $\beta > 1$ ).
- The case for  $\beta = 1$  corresponds to the exponential distribution where the probability of failure is independent of time.
- Combining curves for  $\beta < 1$  with  $\beta > 1$  for the hf produce the well known bathtub curve of failures where some “startup” failures occur early, but their frequency decreases; while other failures, presumably due to operating conditions, begin to occur after some time.
- A  $\beta$  of about 3.4 gives a pdf that is similar to the normal probability.

With respect to evaluating the role of  $t_o$ , Figure 16 from Shibata et al.<sup>101</sup> illustrates how adding  $t_o$  improves the fit of data for a stainless steel exposed to a  $MgCl_2$  solution at 100 MPa and 126°C. Here, the initially curved fit of the data becomes a straight line with a  $t_o$  of 3.39 hours.

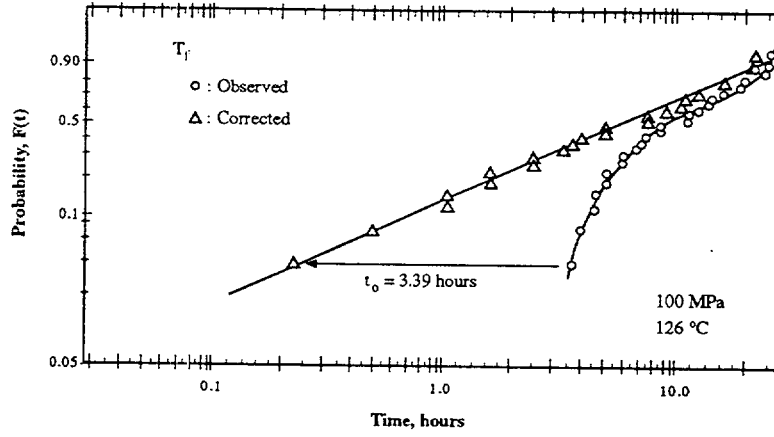


Figure 16: Probability vs. time for Type 304 stainless steel exposed to  $MgCl_2$  solution at  $126^\circ C$  and stressed at 100 MPa. Original observations shown in circles and points corrected with the location parameter,  $t_0$ , are shown by triangles. Magnitude of  $t_0$  is shown. Adapted from Shibata et al.<sup>101</sup>

### 2.2.2 Exponential (Poisson) Distribution

The exponential distribution is a special case of the Weibull distribution where  $\beta=1$ . The significance of this condition is apparent in Figure 15 where the pdf for the  $\beta=1$  case is an exponential decay, the cdf exhibits a relative shallow slope, and, most importantly, the hf is independent of time. While the exponential distribution is a special case of the Weibull distribution, its derivation comes from Poisson statistics. Poisson statistics are relevant to degradation processes because their derivation assumes that events being modeled occur randomly in time and space and that the potential number of occurrences is not limited. The parameters used for the exponential distribution are the same as those in the Weibull distribution owing to the connection for the case of  $\beta=1$ . The Poisson distribution is particularly applicable to SCC and pitting processes in the cases where failure is controlled mainly by surface (and therefore readily available) processes that occur at grain boundaries and inclusions; also, the initiation step of SCC is often usefully modeled by the exponential distribution. In contrast, for  $\beta>1$ , the Weibull distribution describes processes that appear to require accumulation of some quantity as indicated by the shapes of the hf in Figure 15f. The pdf, cdf, hf, chf, and mean for the exponential distribution are given in Eqns. (11) through (17), respectively. Here, the location parameter is included similarly to the approach for Eqns. (1) through (9) for the Weibull equations; the location parameter can be omitted to reduce the exponential distribution to a one parameter fit.

$$f(t) = \frac{1}{\theta - t_0} \exp\left[-\left(\frac{t - t_0}{\theta - t_0}\right)\right] = (\lambda) \exp[-(\lambda)(t - t_0)] \quad (11)$$

$$F(t) = 1 - \exp\left(-\frac{t - t_0}{\theta - t_0}\right) = 1 - \exp[-(\lambda)(t - t_0)] \quad (12)$$

$$h(t) = \frac{1}{\theta - t_0} = \lambda \quad (13)$$

$$H(t) = \frac{t - t_0}{\theta - t_0} = (\lambda)(t - t_0) \quad (14)$$

$$\mu(t) = \theta - t_0 = \frac{1}{\lambda} \quad (15)$$

where:

$\lambda$  = the time constant having units of  $\text{sec}^{-1}$  and also called the rate.  $\lambda$  is the reciprocal of the Weibull characteristic,  $\theta$ .

Further, the cdf can be simply related to the chf by Eqn. (16)

$$F(t) = 1 - \exp[-H(t)] \quad (16)$$

and the reliability or survivorship function is related to the cdf by Eqn. (17)

$$R(t) = \exp[-H(t)] = \exp\left[-\frac{t-t_0}{\theta-t_0}\right] = \exp[-(\lambda)(t-t_0)] \quad (17)$$

In the exponential distribution,  $\theta$  and  $t_0$  have the same meaning as in the Weibull distribution. For many practical cases  $t_0$  is taken as zero.

Akashi et al. have considered the properties of exponential distribution extensively.<sup>17,18,19,61,102,103,104,105,106,107</sup> Akashi has analyzed the shape parameter for a wide range of experiments using the Weibull distribution and has evaluated the shape parameter,  $\beta$ , for a range of mean failure times,  $\mu$ , for experiments conducted in pure water and NaCl. Results of his analysis are shown in Figure 17a. This plot shows that the shape parameters center about unity for a relatively large number of experiments. From these data, Akashi considers that using the exponential distribution broadly for analyzing pitting and SCC is justified. However, as shown in the Sections 4.0 and 5.0, there are many cases for the  $\beta > 1$  where the values are sufficiently large not to be considered close to unity. The significance of these differences in  $\beta$  are discussed in the Section 8.0.

In the context of using the exponential distribution, Akashi points out that it is possible to obtain values for the scale parameter explicitly using Eqns. (14) and (15) where the scale parameter,  $\theta$ , and location parameter,  $t_0$ , are obtained from the linear dependence of  $H(t)$  on  $t$  as shown in Figure 17b.

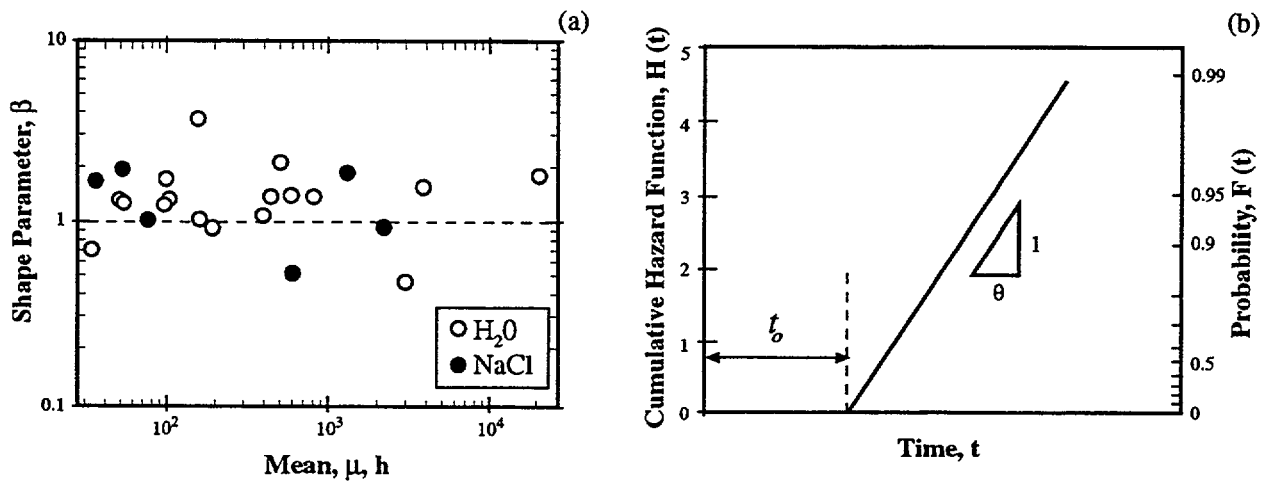


Figure 17: (a) Shape parameter,  $\beta$ , vs. mean failure time,  $\mu$ , in terms of the Weibull distribution for experiments performed in pure water and NaCl solutions using sensitized stainless steel in the presence and absence of surface crevices in the temperature range of 30-80°C. Adapted from Akashi and Nakayama.<sup>18</sup> (b)  $H(t)$  vs.  $t$  showing the intercept as it gives the location parameter,  $t_0$ , and the slope as it gives the scale parameter,  $\theta$ . Adapted from Akashi and Nakayama.<sup>18</sup>

### 2.2.3 Normal Distribution

While the normal distribution is not used in connection with predicting earliest failures and rarely used to model SCC, the distribution is useful as it models metallurgical properties and provides a reference. The pdf and cdf for the normal distribution are given in Eqns. (18), (19), and (20). The hf is defined by Eqn. (4) and the mean is  $\mu$ . Figure 18 shows normally distributed data for the ultimate and yield strengths of Alloy 690. The normal distribution has been used by Shibata to model pitting potentials.<sup>108</sup>

$$f(t) = \frac{1}{\sigma\sqrt{2\pi}} \exp\left[-\frac{1}{2}\left(\frac{t-\mu}{\sigma}\right)^2\right] \quad (18)$$

$$F(t) = P\{t \leq t\} = \int_{-\infty}^t (2\pi\sigma^2)^{-\frac{1}{2}} \exp\left[-\frac{1}{2}\left(\frac{t-\mu}{\sigma}\right)^2\right] dt \quad (19)$$

$$F(t) = \Phi(z) = \Phi\left(\frac{t-\mu}{\sigma}\right) \quad (20)$$

where:

- $\mu$  = mean
- $\sigma$  = standard deviation
- $\Phi(z)$  = available from standard tables

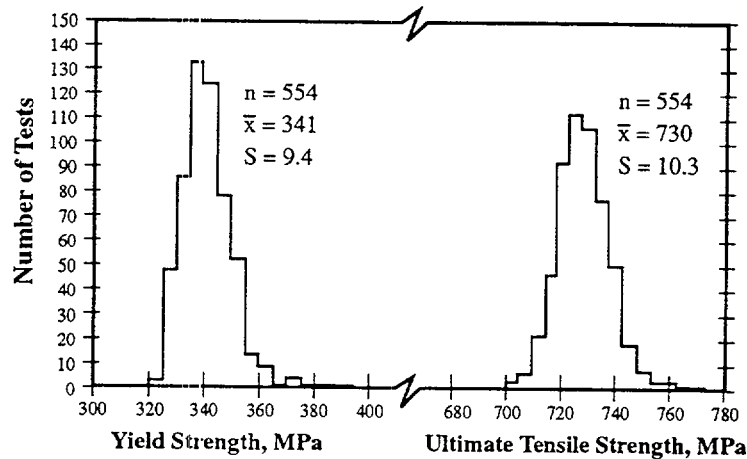


Figure 18: Frequency vs. strength for the ultimate tensile and yield strengths for Alloy 690TT. From Balavage and Gardner.<sup>109</sup>

### 2.2.4 Extreme Value Distributions

Extreme value statistics has been developed and refined by Gumbel.<sup>28,29</sup> Gumbel investigated extreme value statistical theory and found that there are three types of asymptotic distributions for which the forms of the cumulative distributions are shown in Eqns. (21), (22) and (23). Each of these types has a maximum and minimum form.

Type 1, Gumbel distribution:  $\exp[-\exp(-x)]$  (21)

Type 2, Cauchy distribution:  $\exp(-x^{-k})$  (22)

Type 3, Weibull distribution:  $\exp[-(x-\omega)^k]$  (23)

The maximum form of the Gumbel distribution is often used to model pitting. The minimum form of the Weibull distribution is the one referred to in this paper as “the Weibull distribution” and is generally much superior to the minimum form of the Gumbel distribution for characterizing small values. The Cauchy distribution is not useful in modeling failures.

Shibata et al.<sup>14,16,110,111,112,113,114</sup> have investigated extensively the application of extreme value statistics to pitting corrosion especially and to corrosion in general. Shibata finds that the maximum form of the Gumbel distribution, i.e. Eqn. (21) is useful in the study of pitting.

The approach to applying extreme value statistics might be useful for predicting the deepest SCC in a set. However, the kinetic aspects of pitting are different from those of cracking. Pitting follows a  $t^{1/3}$  pattern and tends to reach maximum depths. Nevertheless, such depths are relevant where SCC is initiated by pits as illustrated in Figure 7 and as they are discussed in connection with Figure 69.

### 2.3 Scatter: Coherent and Non-coherent Variability

When data, which are taken under identical circumstances, do not produce exactly the same results, they are sometimes thought to be faulty. In fact, it is the nature of measurements of SCC, as well as many other degradation phenomena, to exhibit variability. This variability is implicit in the multiple processes involved in the initiation and propagation of SCC as shown in Figure 6. However, different experimental procedures used in different laboratories often produce data that exhibit a further variability, in addition to the variability that is obtained in a single laboratory under well controlled conditions. Data taken under the most well-controlled conditions exhibit “coherent variability,” whereas, data taken under nominally similar but somewhat unique conditions at other laboratories exhibit “non-coherent” variability. Coherent variability of data taken at a reference laboratory provides an arbitrary reference.

The data in Figures 2 and 3a show examples of non-coherent variability. In both cases, similar materials and similar environments were tested by reputable investigators. However, the aggregate data is virtually unmanageable and does not provide rational bases for predicting performance.

There is a persistent hope that, if experiments were performed properly, there would be no scatter of data. Further, there are often suspicions that scatter is caused by shoddy experiments; this is not necessarily so. Scatter is implicit in phenomena such as SCC. Broader scatter is implicit in conducting nominally the same experiments in different laboratories.

#### 2.3.1 Coherent Variability

Coherent variability is essentially a reference set of data where a given laboratory has conducted a set of experiments under well controlled conditions. Other data, even equally well controlled, taken at other laboratories, will produce different results, sometimes with significant differences. The variability due to combining such multiple sets is “non-coherent,” whereas, the reference set is the “coherent set.”

Figure 19 illustrates the range of data that is expected as a function of the number of specimens and  $\beta$ . Here, the range is plotted in terms of the “range ratio,”  $t_N/t_1$ , where  $t_N$  refers to the last specimen to fail and  $t_1$  refers to the first. For a  $\beta=1$  in Figure 19, as identified by Akashi in Figure 17 as being a widely observed value, the range ratio is about 40 for ten specimens and about 800 for 100 specimens; for  $\beta=4$  the same range ratios are about 3 and 5, respectively. In general, values of  $\beta$  are not less than about unity for coherent variability owing to the mechanistic processes that produce variability in SCC. If the slopes are less than unity, non-coherent variability is likely. As shown in connection with the discussion of Figure 22, combining sets of nominally similar data always reduces the aggregate  $\beta$ .

To illustrate a case where data have been obtained under the nominally best possible conditions, Andresen<sup>42</sup> has reported measurements of the rate of crack growth at 288°C in low conductivity water for a welding alloy and wrought austenitic alloys, and the data are shown in Figure 20. Andresen considers these data to have been taken under well controlled conditions. The weld material exhibits a  $\beta=0.68$  and the wrought material a  $\beta=4.82$  with  $\theta=10^{-7}$  and  $1.4 \times 10^{-6}$  mm/sec, respectively. Comparing values of  $t_N$  and  $t_1$  for each set of data in Figure 20 shows that they exhibit results that are generally consistent with the behavior of coherent data as shown in Figure 19. The  $\beta$  for the 182 weld material,  $\beta=0.68$ , in Figure 20 is low relative, for example, to the case for  $\beta=1$  which is the lowest that coherent data should sustain.

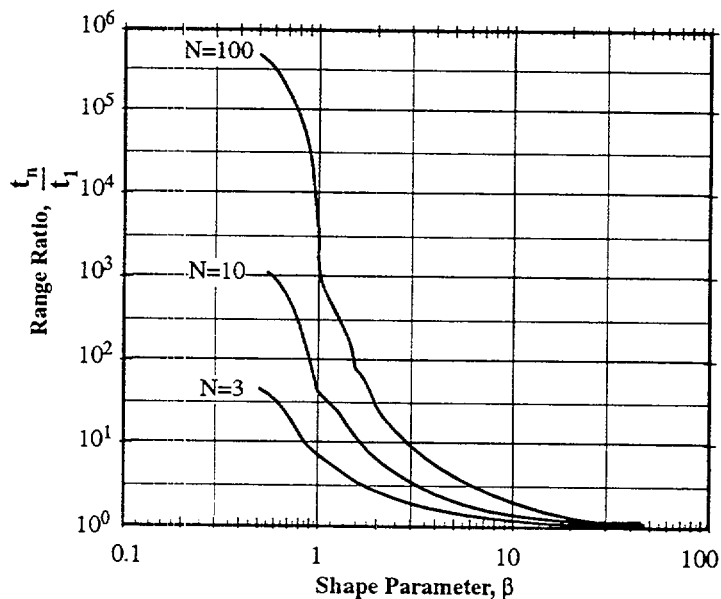


Figure 19: Range ratio (time for last specimen to fail/time for first specimen to fail),  $t_N/t_1$ , vs.  $\beta$  for three values of  $N$  (number of specimens) based on Weibull distribution.

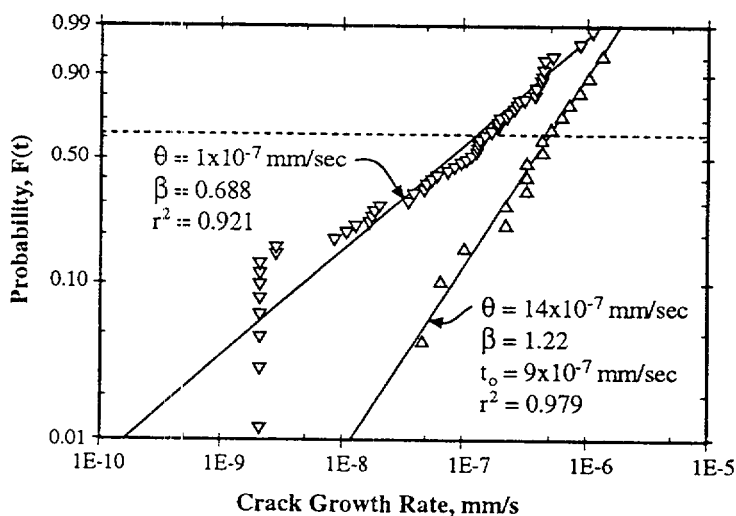


Figure 20: Probability vs. crack growth rate for Alloy 182 weld metal and wrought austenitic alloys exposed at 288°C in low conductivity water. Data originally plotted as a log normal distribution. Adapted from Andresen.<sup>42</sup>

Similar sets of coherent data are shown from the work of Webb and coworkers<sup>22,23</sup> in Figure 43b, Shimada and Nagai<sup>25</sup> in Figure 29, and Clarke and Gordon<sup>115</sup> in Figure 30. While such experiments were conducted under nominally well controlled reference conditions, some exhibit surprisingly low values of  $\beta$ , the meaning of which is discussed in connection with Figure 22.

### 2.3.2 Non-coherent Variability

Non-coherent variability results when data are obtained under conditions that are nominally the same but which are different in important details. Such differences usually result from tests conducted in different laboratories, by different investigators, and with different heats of material. Figure 21 from a review by Cassagne et al.<sup>116</sup> shows results from six separate investigations of LPSCC (this submode is shown in Figure 12) where the crack growth rates are plotted vs.  $1/T$ . While these data are not shown statistically nor were they obtained on that basis, they exhibit about two and a half orders of magnitude difference despite being conducted in nominally the same environments and with nominally the same materials. The data were taken by two different testing techniques in six different laboratories. Had these data been analyzed statistically as a single group, they would have exhibited a low  $\beta$ , less than unity. These data, taken as a group, are similar qualitatively to those in Figures 2 and 3a.

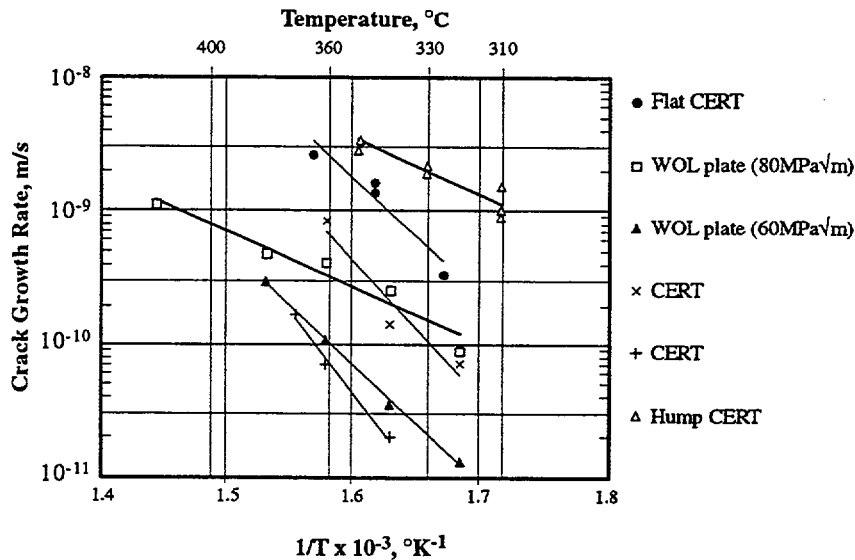


Figure 21: SCC growth rate vs.  $1/T$  for data from six separate investigations of Alloy 600 where the LPSCC submode has been investigated. From Cassagne et al.<sup>116</sup>

The effect of non-coherent variability on the value of  $\beta$  is illustrated in Figure 22. Here, arbitrary data, with ratios of the highest  $\theta$ ,  $\theta_H$  to the lowest  $\theta$ ,  $\theta_L$  of 1, 5, 10, 100, and 1000 and each with  $\beta$  of 1.0, 4.0 and 10.0, are assumed and plotted; each data point includes calculations for four Weibull distributions where the values of  $\theta$  are equidistant in the logarithmic scale. Two parameter Weibull fits were used. The four different values of  $\theta$  in each calculation are prototypic of non-coherent data from multiple laboratories or from other influences that produce ranges of  $\theta$  as discussed in connection with Figure 27; these data are typical of the spread of results obtained by different laboratories and different heats of material where the nominal alloy, heat treatment, test environment, and method of measurement are the same. In Figure 22 the aggregate shape parameter,  $\beta_g$ , is plotted vs. the ratios of the highest to lowest values of  $\theta$ , i.e.  $\theta_H/\theta_L$ . Figure 22 defines terms,  $\beta_g$  and  $\beta_L$ , for “aggregate  $\beta$ ” and “local  $\beta$ .” The  $\beta_g$  results from combining groups of data with different values of  $\beta_L$ . These terms are not applied in all cases in this discussion, but are used when the respective effects need to be distinguished.

The data of Figure 22 show how the aggregation of nominally similar sets of data can produce lower aggregate values of  $\beta$ . Figure 22 applies to many of the data discussed in this paper and can explain how data with a  $\beta_L=4$  based on coherent variability can appear to have a much lower value



of  $\beta_g$  when data from various sources, using nominally similar conditions, are aggregated. This effect of aggregation also explains how separate sets of data, individually with a value of  $\beta=1$ , can produce a lower value of  $\beta$  as shown in Figure 20.

### 2.3.3 Contributions to Producing Non-coherent Variability

Contributions to the variability of data that give non-coherent results are shown schematically in Figure 23. These contributions are as follows:

- Inherent variability where the data exhibit scatter under the best conditions of testing. Such variability is inherent in the multiple paths that SCC can take as illustrated in Figure 6 and as discussed in Section 3.0.
- The complexity of initiation and propagation segments interacting where the former is often more variable than the latter as illustrated in Figures 31 and 32.

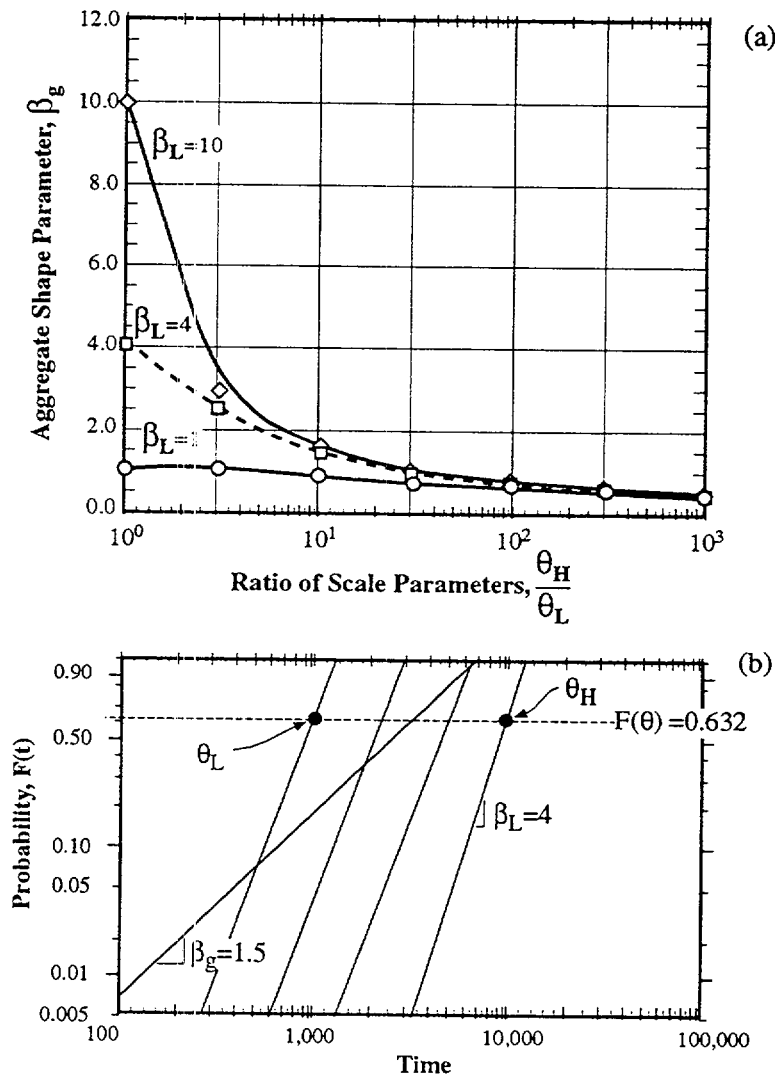


Figure 22: (a) Aggregate  $\beta_g$  vs.  $\theta_H/\theta_L$  for local shape parameters of  $\beta_L=1, 4$  and  $10$ . Four equally spaced sets of data, on a logarithmic scale, are assumed for each calculation and five data points for each component distribution are taken. Based on Weibull distribution. (b) Example of method of calculation.  $\theta_H$  and  $\theta_L$  shown with four distributions, each with slopes  $\beta_L$ , and the resulting  $\beta_g$  calculated from aggregating the data for all slopes.

- Metallurgical variability that is due generally to the structure-sensitive properties of materials as they are affected by thermal and mechanical processing. This contribution to variability is often called “heat-to-heat variability.” This is discussed in the section on metallurgical variability and in connection with the data of Norring, et al.<sup>117</sup> in Figure 27. Early failures due to heat-to-heat variation are often, and usually erroneously, said to be caused by “bad heats” of material.
- Surface condition as affected by surface treatments, corrosion, abrasion, polishing, grinding, type of machining (e.g. reaming vs. drilling). This is discussed in the Section 4.0.
- Small changes in environments, especially pH, potential, and certain impurities at ppb to ppm concentrations. These small changes produce large variabilities owing to the highly leveraged effects of environmental changes on the intensity of SCC as discussed in the Section 5.0.
- Methods of testing. Statically loaded U-bends relax even at room temperature differently from specimen to specimen; and crack velocities obtained from constant extension rate testing are not the same as crack velocities determined by compact tension specimens.
- Methods of obtaining data. Obtaining data from operating systems, e.g. the SG shown in Figure 4, depends on the detection of cracks which, in turn, is affected by both the operator of the NDE and the equipment being used. Also, visual inspections of surfaces even in laboratory experiments do not always detect SCC. In the NDE community there is a concept called “probability of detection” (POD) that treats the capacity to detect existing defects.
- Non-applicable data that are sometimes included in data sets used for prediction. For example, SCC in BWR nuclear plants is sensitive to conductivity of the solution as noted in Figure 67. Data obtained at high conductivities are sometimes included in the data base for predicting performance for this application, even though the data are not applicable. To avoid non-applicable variability, data are sometimes censored as in Figure 3b.

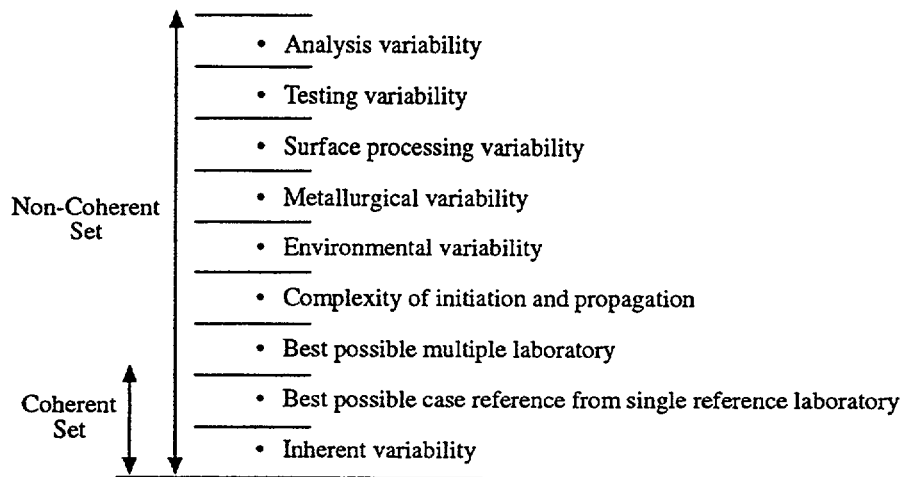


Figure 23: Components of coherent and non-coherent variability.

### 2.3.4 Minimizing Non-coherent Variability

There are three approaches to minimizing non-coherent variability. First, especially among laboratories where similar experiments are undertaken, substantial attention should be given to assuring the similarity of testing condition. Second, with respect to a given application, the existing data may derive from too broad a base; and the data should be screened as shown in Figure 3. Third, the nature of the non-coherence can be examined to determine whether it needs to be accepted since a given application may incorporate multiple heats of material that will lead to low aggregate values of  $\beta_g$ .

### 2.3.5 Early Failures Relative to the Mean

An important objective of this discussion is predicting the earliest failures. Such early failures, for example at an 0.0001 probability (i.e. about one tube in the SG of Figure 4), are evident in the cdfs shown in Figures 15c and 15d and especially as the shape parameter,  $\beta$ , decreases. However, most corrosion testing implicitly obtains information about the mean time-to-failure and little about the shape parameter. Yet, once sufficient time has elapsed for the mean to occur, the equipment is decimated. Thus, the mean value is useful only as it provides an intercept for the dependence of probability upon time. Figure 24 shows the ratio of the time at which failures occur for a low probability such as 0.0001, 0.001 and 0.01 relative to the mean time as a function of  $\beta$ . This is the "early failure ratio,"  $t_i/t_\mu$ , where  $t_i$  corresponds to the least time of failure at the 0.0001, 0.001 or 0.01 probabilities relative to the  $t_\mu$ , the mean time, e.g. the time for failure at 0.5 probability. It is clear that, for the nominally same mechanistic process (i.e. on the same line), the mean value is largely irrelevant for most practical applications especially as  $\beta$  decreases. Figure 24 indicates that determining both the shape parameter and the mean value is necessary for predicting early failures; however, the shape parameter dominates the process of predicting early failures.

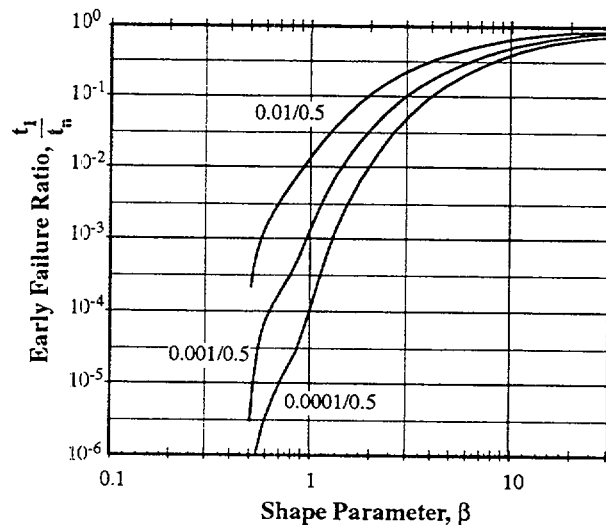


Figure 24: Early failure ratio,  $t_i/t_\mu$  vs.  $\beta$  for times at 0.0001, 0.001, 0.01 probabilities relative to the time for the mean at 0.5 probability using the Weibull distribution.

The possibly large differences between  $t_i$  and  $t_\mu$  in Figure 24 affects the applicability of experimental data obtained from accelerated testing for assuring performance of the design life of equipment. Conducting accelerated testing in support of assuring performance for relatively long design lives must consider three important influences:

- First, failures in service may occur very much earlier than the mean as noted in Figure 24.
- Second, construction of engineering equipment utilizes multiple heats of material which usually, while nominally purchased to the same specification, exhibit different values of  $\theta$  and  $\beta$ . An order of magnitude difference or more in  $\theta$  among the heats, as suggested in Figure 21, is not uncommon. As described in detail in Section 4.0, when the overall distribution applicable to all the heats is developed, its slope is likely to be in the range of unity despite the individual heats having much higher slopes. This effect is discussed in connection with Figures 22 and 27.
- Third, accelerated testing is often conducted on material from a single heat and often at conditions that are more intense than the application, e.g. higher stresses and temperatures. The

combined influence of a single well behaved heat, together with more intense testing conditions, sometimes combine to produce a relatively high  $\beta$  as illustrated in Figure 25.

Figure 25 illustrates the consequences of these three influences. Two distributions are shown schematically. One corresponds to field experience, (N-1), with a  $\beta=1$ ; such a distribution is consistent with the data from Figure 5a. It is also consistent with the overall distribution comprised of data from multiple heats in Figure 27. The other steeper distribution corresponds to a typical slope often determined in accelerated tests where a single heat is used, tests are performed in a single laboratory, and more intense conditions are applied. Such results might typically exhibit values of  $\beta$  in the range of 5. Since the tests to assure performance for the design life are accelerated, often by a factor of 100, by comparing the mean values as shown here, the tests seem legitimately accelerated. However, the acceleration occurs only for the mean; at an 0.001 probability lines N-1 and A-1 cross, and there is no acceleration. The intersection of lines N-1 and A-1 shows that accelerated testing cannot predict early failures unless the nature of the shape parameter is accounted for.

It is traditionally required that the accelerated tests study the same failure mechanism that is expected in service. A corollary mandate should require that the shape parameter determined in accelerated testing be related to the shape parameter of failures expected during operation.

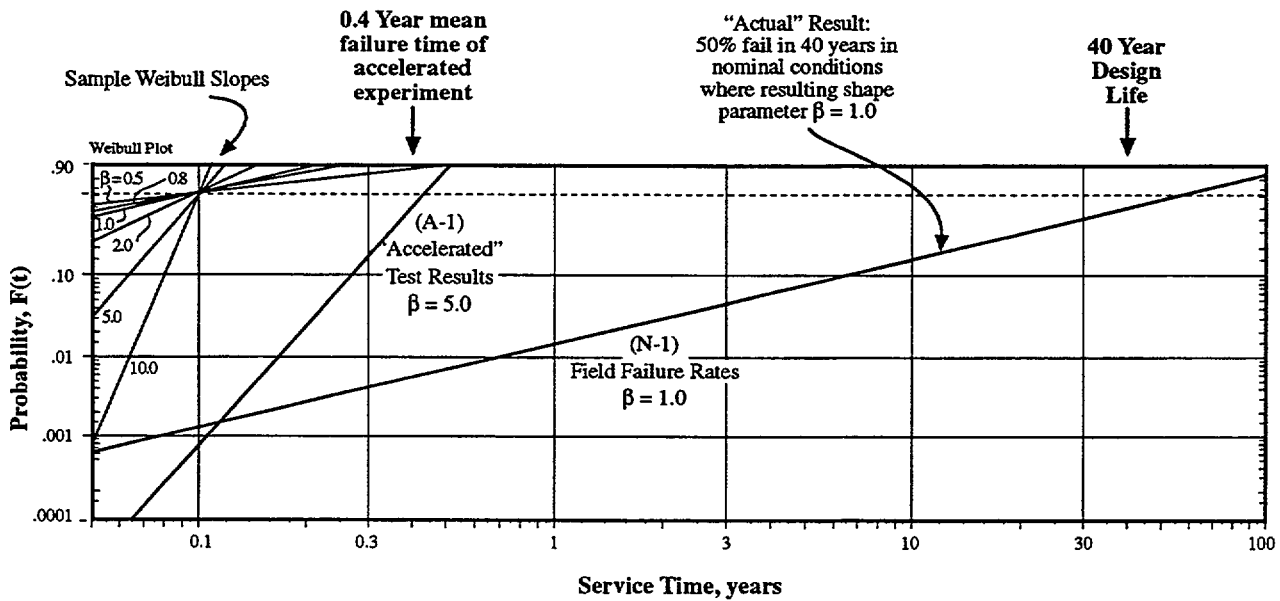


Figure 25: Schematic plot of probability of failure vs. time for field data and accelerated tests based on Weibull coordinates. N-1 corresponds to assumed field results; A-1 corresponds to assumed accelerated testing.

## 2.4 Properties of Distributions Related to $\beta$ and the hf

Knowledge of the shape parameter,  $\beta$ , provides the most important contribution to understanding and predicting early failures at low probabilities as illustrated in Figures 15 and 24. Therefore, understanding the factors that produce the lower slopes is important to the main objective of this paper.

For illustrative purposes, this discussion considers the  $\beta=1$  and  $\beta=4$  cases as prototypic of the important classes of data. The data discussed in Sections 4.0 and 5.0 show numerous cases of both types as well as intermediate ones.

There are two classes of conditions that produce the  $\beta=1$  case:

- The “coherent case” where the critical physical processes that produce failure are completely random in space and time, but where data are gathered in a well-characterized set of tests. Such

conditions are associated with pitting and initiation of SCC where both are related to easily accessible critical processes on surfaces. These accessible surface processes produce the conditions to which the Poisson, or exponential, distribution applies.

- The “mixed condition” case where the subcomponents exhibit substantially different scale parameters and possibly different shape parameters although, taken as a group, the data are taken from the same nominal material and the same test or exposure environment. This circumstance is illustrated in Figure 22. These different conditions may involve different heats of the same nominal material and different laboratory test conditions used for the same heat. Combining the data from these different conditions with different values of  $\theta$  and  $\beta$  produces an overall value of  $\beta$  that approaches unity or less. Such a circumstance is discussed in connection with Figure 27.

The two separate classes of the “coherent case” and the “mixed condition” are entirely different in their origin but produce distributions that appear to be the same, i.e. a  $\beta$  in the range of unity.

Conditions that produce the  $\beta=4$  case are possibly less diverse as there is no analog to the “mixed condition” except as data with higher values of  $\beta_L$  combine but with different values of  $\theta$  as illustrated in Figure 22a. First, the  $\beta=1$  (Poisson) and  $\beta=4$  cases are considered together. Next the mixed case is considered.

## 2.5 The Coherent $\beta=1$ (Poisson) and $\beta=4$ Cases

Referring to Figure 15f, the hf for  $\beta=1$  is independent of time; whereas, the hf for  $\beta=4$  curves sharply upward at about half the value of  $\theta$ , meaning that the failure probability remains low early but then rises sharply. Also, for the  $\beta=4$  case, as shown in Figure 15h, the first derivative of the hf begins to increase significantly. These two cases are compared schematically in Figure 26a.

In view of the significant differences in the  $\beta=1$  and  $\beta=4$  cases as illustrated in Figure 26a, there must be quite different physical processes associated with these cases. The principal feature of Poisson processes is the randomness in space and time. Failure can occur any place and any time. Physical processes that are relevant to these conditions include pitting and the initiation of SCC as shown in Figure 26e. Pitting is clearly related only to surface features such as grain boundaries, precipitates and surface slip. It is well known, for example, that high purity alloys do not sustain pitting in many cases. Initiation of SCC also involves surface-related processes. If the initiation processes are slow relative to propagation, then the surface-related processes, and hence the Poisson condition, would dominate the value of  $\beta$ .

In contrast, the  $\beta=4$  case must relate to some kind of accumulation processes. The value of the hf, or probability of failure, remains low until a time of about half of  $\theta$ ; then, the hf increases sharply. This pattern implies that certain conditions must accumulate, at which point the SCC accelerates. Only such accumulation of conditions could account for the sharp rise in the hf as illustrated in Figures 15f and 26b. However, there are numerous accumulation processes that could be associated with SCC. Considering the geometry of Figure 4, SCC from the primary side, which exhibits  $\beta=4$  behavior in laboratory and field applications, as in Figure 52, must be related to processes such as diffusion into the surface or into the crack or the accumulation of creep damage at the crack tip. On the secondary side a significant accumulation process is associated with the concentration of chemicals at the heat transfer crevices as shown in Figures 4b and 4c, Figure 26d, and Figure 48.

Possible physical processes associated with the Poisson  $\beta=1$  and  $\beta=4$  cases are illustrated in Figures 26c, d, and e. While the options in Figures 26c, d, and e indicate possible physical processes that might explain the  $\beta=1$  and  $\beta=4$  cases, it is not possible to be more precise as to mechanistic details based only on the shapes of the hf.

## 2.6 The Mixed Condition Giving $\beta=1$

The mixed condition that also produces a  $\beta$  in the range of unity, while component data is character-

ized by higher values of  $\beta$ , is best illustrated by the work of Norring, et al.<sup>117</sup> as shown in Figure 27. Norring et al. obtained data for the LPSCC of seven heats of Alloy 600, each with nominally the same heat treatment. As shown in Figure 27, the values of  $\theta$  vary from 987 to 6958 hours. Slopes for the individual heats are in the  $\beta=4$  range, from 1.73 to 7.1. The aggregate distribution has a  $\beta=1.50$  and an intermediate value of  $\theta=3509$  hours. This relationship among slopes of the component sets and the aggregate distribution is typical of the patterns calculated in Figure 22. In fact, it is reasonable to aggregate the data in Figure 27 since they were tested by the same laboratory, were the same alloy, were exposed to about the same environment, and were subjected to the same heat treatments. The resulting aggregated  $\beta$  in Figure 27 is, in fact, the aggregated  $\beta_g$  for the non-coherent case.

It is quite likely that the  $\beta=0.92$  and  $0.86$  shape parameters with  $\theta=5.53 \times 10^6$  and  $2.6 \times 10^8$  hours for the SCC of large and small diameter BWR pipes, respectively, as shown in Figure 5a, is a case of multiple heats similar to Figures 22 and 27 since each weld must have a slightly different material property.

Thus, the appearance of the  $\beta=1$  shape parameters can be produced either by Poissonian processes, as illustrated in Figure 26 where  $\beta$  is generally unity as suggested by Akashi and Nakayama in Figure 17, or by the aggregation of data where the values of  $\theta$  for individual heats are sufficiently different thereby producing the lower values of  $\beta_g$  as shown in Figure 22.

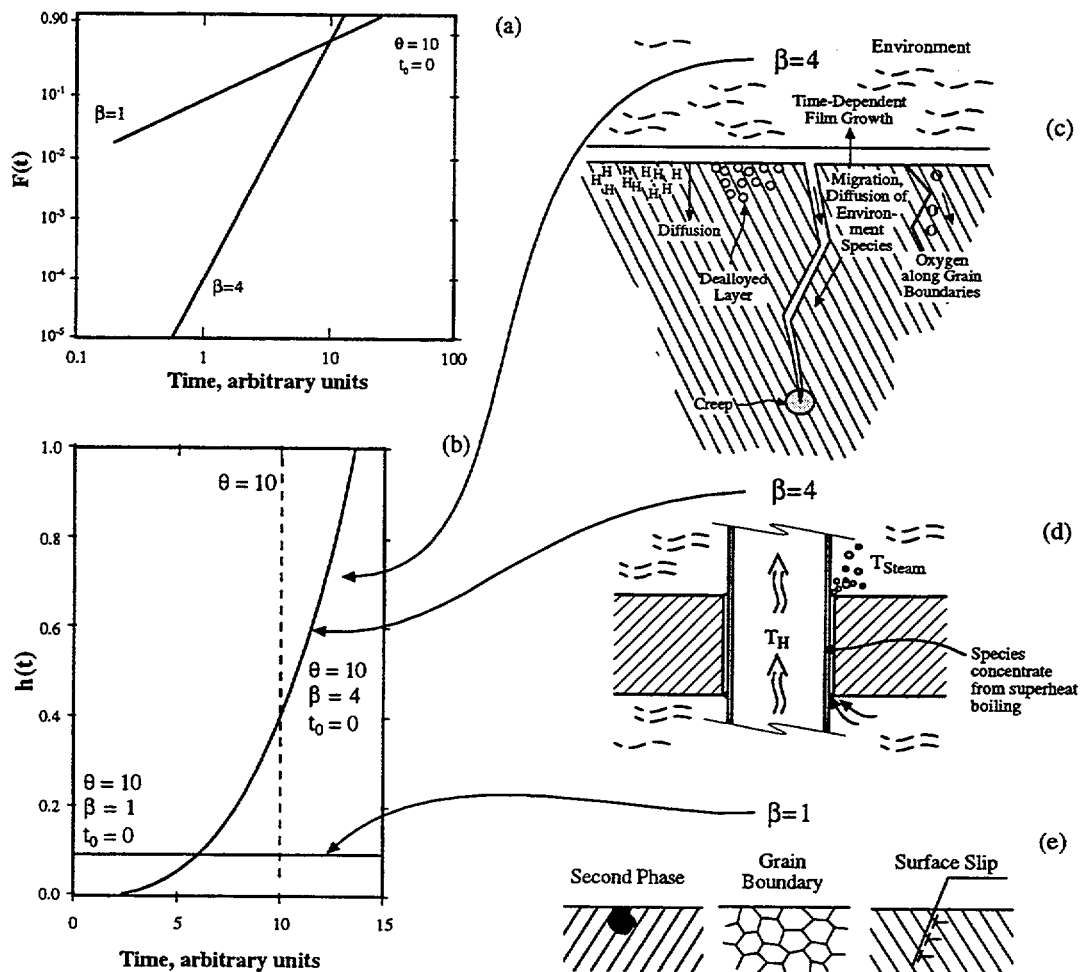


Figure 26: (a) cdf for  $\beta=1$  and  $\beta=4$  vs. time. (b) hf vs. time for  $\beta=1$  and  $\beta=4$  cases at  $\theta=10$  and  $t_0=0$ . (c) Possible contributions in the metal substrate, for a growing SCC, to the accumulation case for  $\beta=4$ . (d) Possible contributions to the accumulation case  $\beta=4$  from exterior of the metal surface with a superheated tube support geometry as in Figure 4. (e) Possible contributions to the  $\beta=1$  case.

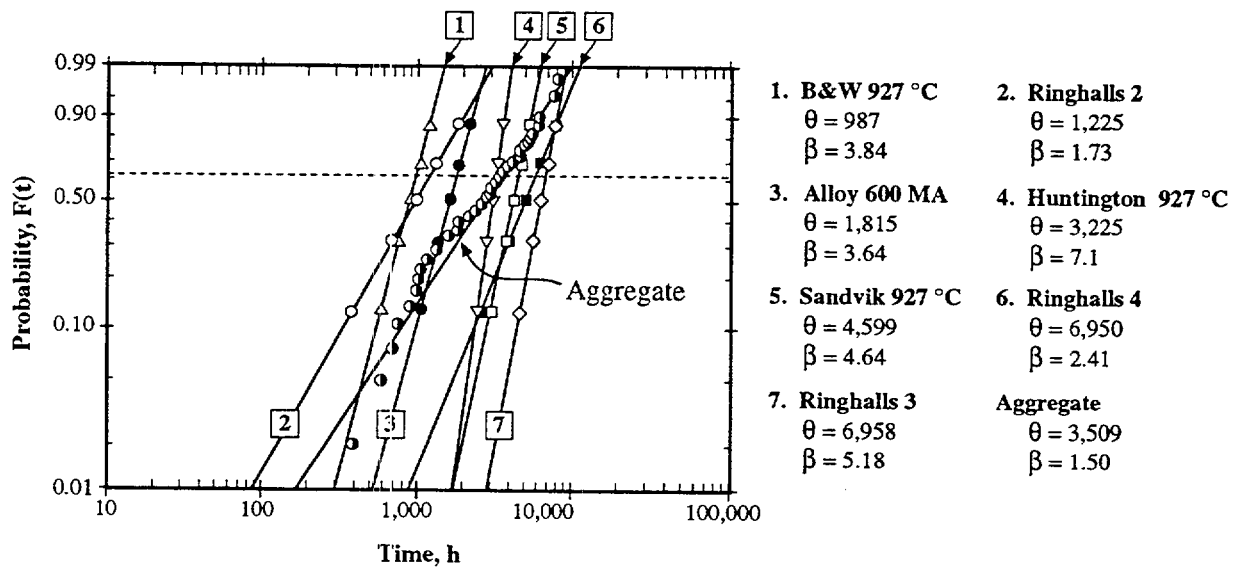


Figure 27: Probability vs. time for seven heats of Alloy 600 exposed to high purity water with hydrogen addition at 365°C using reverse U-bend specimens where failure occurs by the LPSCC submode. From Norring et al.<sup>117</sup> The detailed data were not published with these curves; thus, for analysis, each distribution was assumed to represent five data points, and the analysis of the aggregate distribution was based on this assumption.

## 2.7 Steep Dependencies of SCC Produce a $\beta=1$ Result

Figures 22 and 27 show that the overall slope is lowered when the component data come from relatively separated values of  $\theta$ . A similar trend can result from the fact that the value of  $\theta$  depends, in some submodes, strongly on environmental factors such as electrochemical potential and pH as described in Section 5.0. The sharp dependence of SCC upon potential is shown in Figure 13 where three types of potential dependence of SCC are illustrated and where large changes can occur over relatively small ranges of potential, e.g. 100 to 200 mV.

Figure 28 shows schematically the effects on  $\theta$  of testing conducted at different potentials. This analysis assumes that a change in  $\theta$  or  $\mu$  corresponds, and is directly proportional to, effects of principal variables as in Figure 1, i.e. a variation of 100 on the rate of SCC as a function of potential, for example in Figure 13b, would correspond to a variation in  $\theta$  of the same magnitude. A variation of 100 in the rate of SCC, as shown in Andresen's data in Figure 20, is not unusual for SCC processes. Thus, if sets of experiments were conducted at designated locations in Figure 28a e.g. at (3), (4), (5), (6), the values of  $\theta$  would vary over two orders of magnitude owing to the effect of potential on  $\theta$ . If the results of these experiments are then aggregated, assuming that a single phenomenon had been studied, and neglecting the possible influences of relatively small differences in potential, the  $\beta_g$  from the four experiments would produce a lower slope, as in Figure 28b, similar to the patterns in Figures 22 and 27. It is assumed that the slopes of the separate experiments would be similar since the mechanistic details would remain the same. If the data from locations (1), (2), and (3) are aggregated, where the rates are the same at each potential of different tests, the  $\beta_g$  is the same as  $\beta_l$  as shown in Figure 28c.

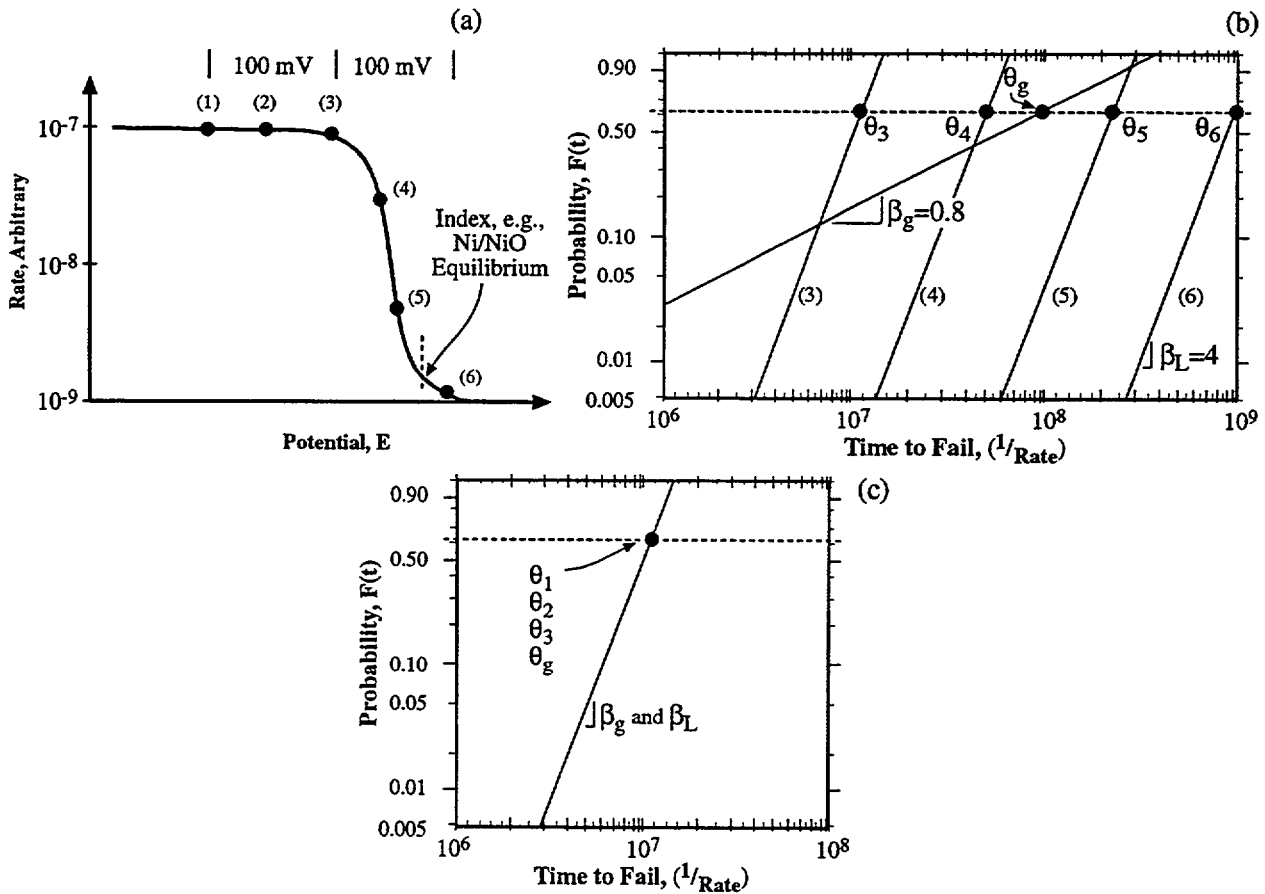


Figure 28: (a) Schematic view of rate of SCC vs. potential similar to that for LPSCC as shown in Figure 13a and 13b and showing six arbitrary locations where distributions are obtained assuming that the SCC testing was performed at constant potential at these locations. (b) Schematic view of probability vs. time for  $\beta_L$  distributions at four locations with aggregate  $\beta_g$  shown. The aggregate is based on the idea that data came from four distributions that could not be distinguished in the final set of data.  $\beta_L$  slopes of 4 are typical of PWR primary water where (a) applies as indicated in Figure 52. (c) Schematic view of probability vs. time for three sets of data where the assumed rates are the same.

Thus, the appearance of a  $\beta=1$  value, following the illustration of Figure 28, can result from conducting experiments or operating an application where there is a steep dependency of SCC on a variable such as potential or pH and where the environmental conditions cannot be precisely controlled. The aggregated  $\beta_g$  result is similar to that for multiple heats in Figures 22 and 27. The same  $\beta_L$  is assumed on all the component distributions in Figure 28 since the mechanism is the same, and only the principal variable of potential is changed; however, the  $\beta_L$  values do not have to be the same for the lowering of  $\beta_g$ .

## 2.8 Relative Influence of Stressors and Material

It seems reasonable that increasing the magnitude of a stressor would cause the value of  $\beta$  to increase, i.e. increasing the stress or temperature would cause all the specimens to fail closer to the same time. Such a pattern is evident in Figure 29 from the work of Shimada and Nagai.<sup>25</sup> Here, a



zirconium alloy, Zircaloy 2, was exposed to iodine gas at 350°C at different stresses. The cdf for each stress is plotted in Figure 29a. Values of  $\theta$ ,  $\beta$ , and  $t_o$  are plotted as a function of stress in Figure 29b.  $\theta$  and  $t_o$  decrease with increasing stress in an expected pattern.  $\beta$  increases with stress according to the expectation that increasing intensities of the stressor would cause results to occur closer to the same time.

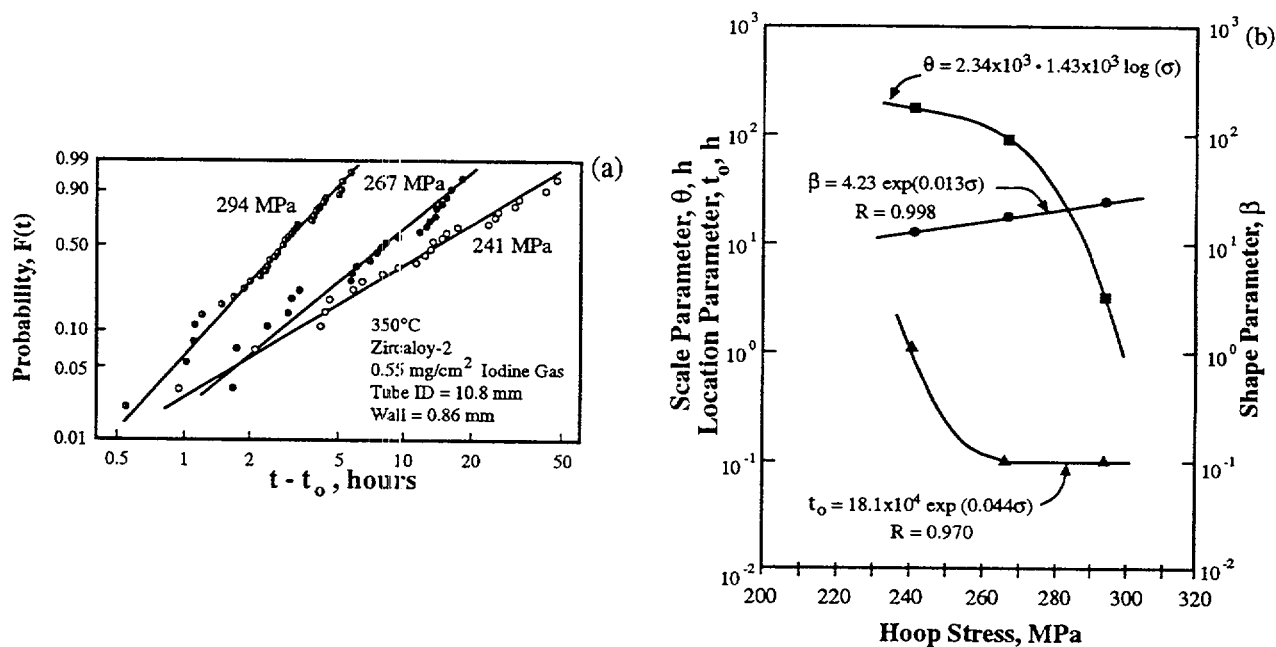


Figure 29: (a) Probability vs. time-to-failure for Zircaloy 2 exposed at 350°C to iodine gas. (b) Weibull parameters vs. hoop stress. Adapted from Shimada and Nagai.<sup>26</sup> Determination of curve dependencies from Fang and Staehle.<sup>118</sup>

In contrast to the pattern for increasing  $\beta$  with increasing stress shown in Figure 29, results from Akashi and Ohtomo<sup>17,119</sup> and from Clarke and Gordon<sup>115</sup> show the opposite effect of stress in Figures 30a and 30b where the SCC of sensitized Type 304 stainless steel was studied at 288°C in high purity oxygenated water. The effects of stress on the Weibull parameters from the data in Figures 30a and 30b are shown in Figure 30c. In both cases  $\theta$  decreases with increasing stress. Also,  $t_o$ , which could be determined only for the Gordon and Clark experiments, decreased with increasing stress. However, in both cases the  $\beta$  exhibited downward trends in contrast to the dependencies of  $\beta$  on stress in Figure 29 for Zircaloy 2 in iodine gas. The general mechanistic problem of dependencies of  $\beta$  on physical variables is discussed in Section 8.5.

The causes of the opposite trends for  $\beta$  in Figures 29 and 30 are not clear. However, the downward trend with increasing stress in Figure 30 might be explained by the progressive opening of cracks at higher stresses which would permit the surface environment to enter more readily, thereby approaching the more Poisson-like surface condition. On the other hand, the experiments in Figure 29 were conducted in gas; therefore, the environment did not change with the deepening of cracks, as would occur in an aqueous environment. The relatively high  $\beta$  in Figure 29 is unusual and suggests that the conditions of the experiments were quite similar in the sense suggested by Figure 28c.

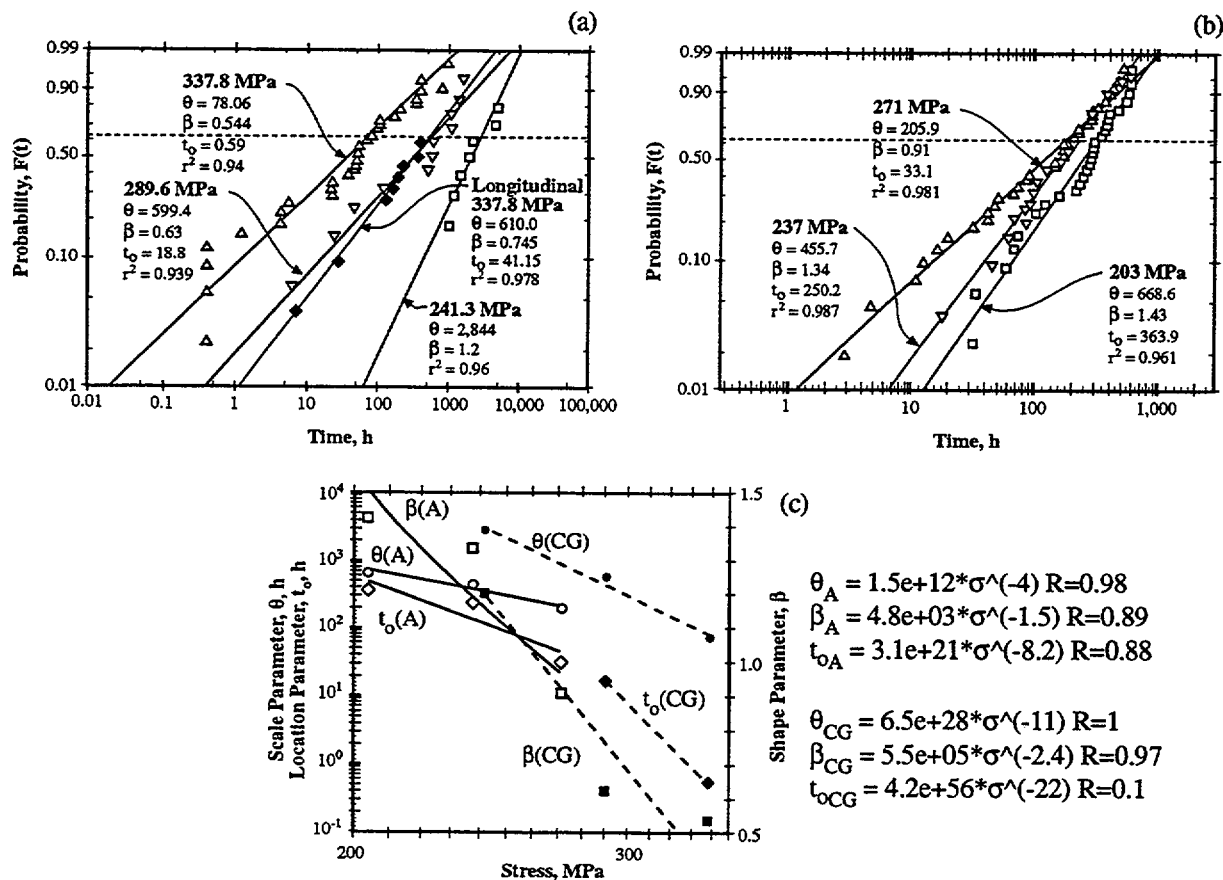


Figure 30: (a) Probability vs. time for sensitized Type 304 stainless steel tested at 288°C in high purity oxygenated water. From Clark and Gordon.<sup>115</sup> (b) Probability vs. time for sensitized Type 304 stainless steel tested at 288°C in high purity oxygenated water. From Akashi and Ohtomo.<sup>119</sup> (c) Weibull parameters vs. stress from both the Clark and Gordon (CG) (dotted lines) and Akashi (A) (solid lines) distributions.

A comparison of the data from Figures 29 and 30 suggests that the relative magnitude of the stressors may be less important than the experimental methods or the mechanistic processes.

## 2.9 Relative Dominance of Initiation and Propagation

Since the shape parameter,  $\beta$ , for initiation and propagation tend toward the  $\beta=1$  and  $\beta=4$  values, respectively, time-to-failure data which are dominated by initiation will tend toward the former and those dominated by propagation will tend toward the latter. This possibility was first suggested by Shibata and Takeyama<sup>120</sup> through Figure 31a. Here, they suggested that there are certain conditions where the initiation time would dominate the time-to-failure, which would lead to time-to-failure data where  $\beta=1$ . Other conditions would be dominated by propagation and would lead to a higher  $\beta$ , in the  $\beta=4$  category. The patterns illustrated in Figure 31a generally suggest that bi-modal distributions should be observed. In fact, such distributions are observed as illustrated in Figure 31b. Figures 31c and 31d show that the slopes for the upper and lower segments correspond to initiation and propagation domination, respectively, as indicated by the slopes being of the  $\beta=1$  and  $\beta=4$  types. Here the “2” subscript refers to the upper more shallow data and the “1” refers to the earlier and steeper data. Figure 31e shows prototypic data taken by Shibata et al.<sup>121</sup> indicating how his use of electrochemical methods, shown in Figure 7e, produced data for distinguishing initiation from propagation data. Figure 31f shows the result of analyzing these data using the Weibull software.<sup>8</sup> Here the  $\beta_i$  is 4.62,  $\beta_p$  for propagation is 4.81 and  $\beta_i$  for initiation is 1.76, which is high for a purely initiation process.

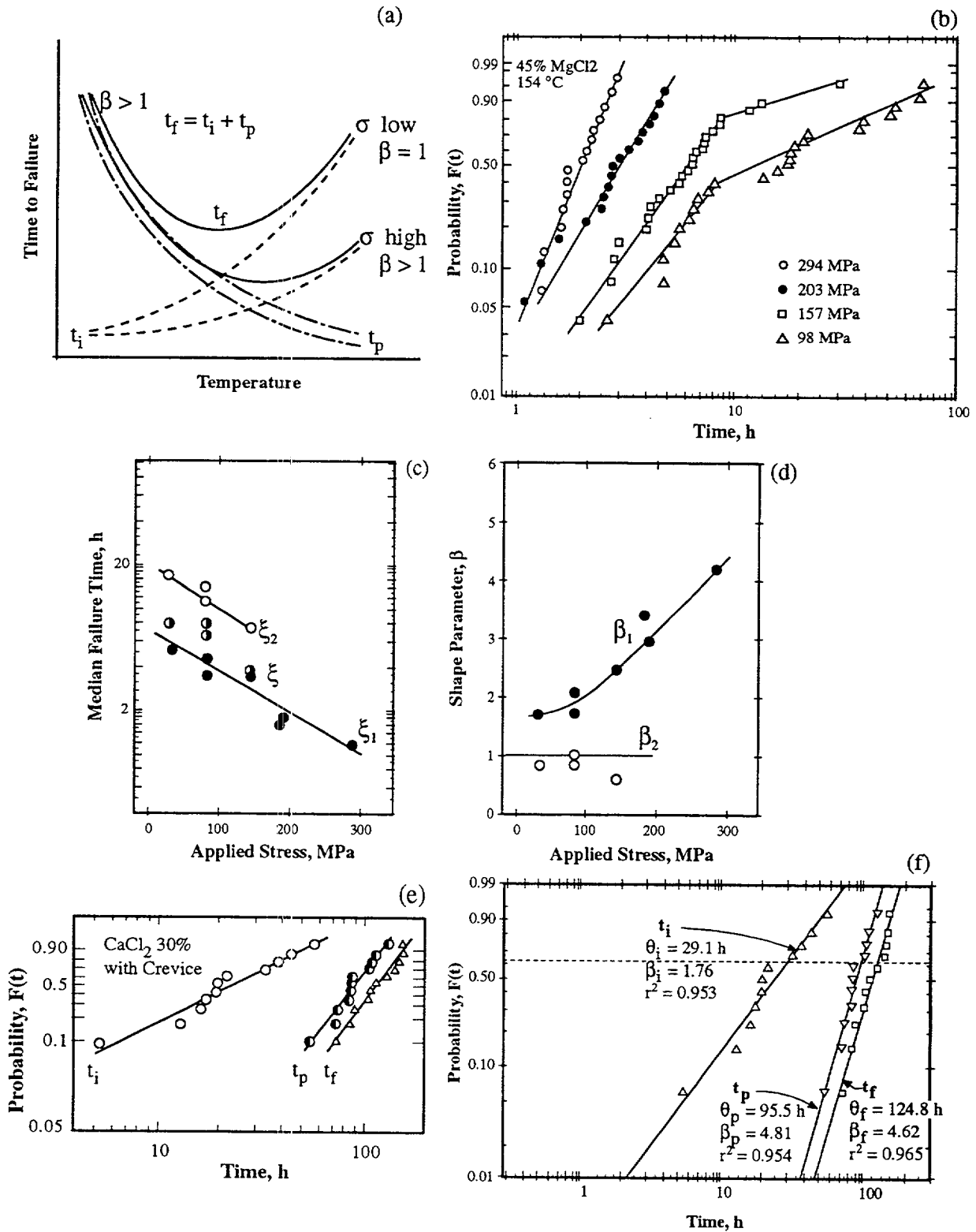


Figure 31: (a) Schematic illustration of the effects of temperature and stress on the  $\beta$  associated with time-to-failure as depending more on initiation or propagation. From Shibata and Takeyama.<sup>120</sup> (b) Probability vs. time for Type 304 stainless steel exposed to boiling  $MgCl_2$  at  $154^\circ C$  at various stresses. (c) Median values for upper and lower slopes vs. stress from (b). (d) Values of  $\beta$  for upper and lower vs. stress from (b). From Shibata and Takeyama.<sup>123</sup> (e) Data for  $t_i$ ,  $t_p$ , and  $t_f$  for Type 304 stainless steel exposed to 30 w/o  $CaCl_2$  solution at a constant condition of 200 MPa and  $100^\circ C$ . From Shibata et al.<sup>121</sup> (f) Weibull calculation for (e).

Ichikawa et al.<sup>124,125</sup> studied initiation and propagation processes in high strength steel exposed to a 3.5%NaCl at 40°C temperature using an approach similar to Figure 31. Their data are shown in Figure 32a and their interpretation is shown in Figure 32b. They found the same bi-modal results as shown in Figure 31b.

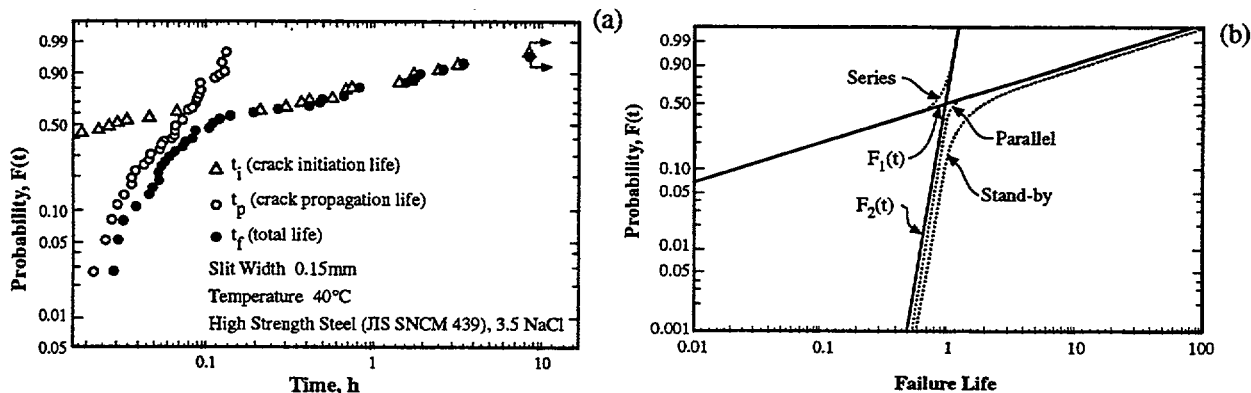


Figure 32: (a) Probability vs. time for data determined for both initiation and propagation of a high strength steel exposed to a 3.5% NaCl solution at 40°C. From Ichikawa et al.<sup>124</sup> (b) Schematic illustration of the role of both initiation and propagation with the combined result. From Ichikawa et al.<sup>125</sup>

The bimodal pattern exhibited by some data most likely results from the relative dominance of initiation or propagation processes. The values of  $\beta$  for each mode can be analyzed as relating to initiation and to propagation processes separately. The initiation processes in such bi-modal results show the lower values expected of initiation processes which follow Poisson statistics. The propagation processes exhibit higher values of  $\beta$ , in the  $\beta=4$  category. Possible physical processes associated with initiation and propagation are described in Figure 26.

## 2.10 Insertion of Principal Variables into Statistical Parameters, Stressors

In Figure 1, general dependencies of SCC on principal variables are shown. This equation then applies directly to the scale parameter,  $\theta$ , which is essentially the mean in the Weibull distribution as indicated in Eqn. (24). Similar relationships can be initially assumed for the other Weibull parameters,  $\beta$  and  $t_o$  as in Eqns. (25) and (26).

$$\theta = A_{\theta} [H^+]^{h_{\theta}} [x]^{p_{\theta}} [M]^{r_{\theta}} \sigma^{m_{\theta}} e^{\frac{E-E_{\theta\theta}}{b_{\theta}}} e^{-\frac{Q_{\theta}}{RT}} \quad (24)$$

$$\beta = A_{\beta} [H^+]^{h_{\beta}} [x]^{p_{\beta}} [M]^{r_{\beta}} \sigma^{m_{\beta}} e^{\frac{E-E_{\theta\beta}}{RT}} e^{-\frac{Q_{\beta}}{RT}} \quad (25)$$

$$t_o = A_{t_o} [H^+]^{h_{t_o}} [x]^{p_{t_o}} [M]^{r_{t_o}} \sigma^{m_{t_o}} e^{\frac{E-E_{\theta t_o}}{b_{t_o}}} e^{-\frac{Q_{t_o}}{RT}} \quad (26)$$

Where:

A = constant

H<sup>+</sup> = hydrogen ion activity

x = concentration of active species (possibly more than one)

- M = metallurgical factor such as associated with sensitization
- $\sigma$  = stress
- E = electrochemical potential
- $E_0$  = electrochemical constant being either the corrosion potential or the thermodynamic equilibrium potential
- b = electrochemical constant
- Q = apparent activation energy
- R = gas constant
- T = absolute temperature
- n, p, m, r, q = constants

The patterns for the statistical parameters in Figures 29 and 30 show that they depend on the variable of stress. The dependencies of these statistical parameters on other principal variables are discussed in Sections 4.0, 5.0, and 8.0. The framework provided by Eqns. (24)-(26) is a basis for predicting the early failures as discussed in Section 8.0.

In general, the scale parameter,  $\theta$ , can be expected to follow well known correlations based upon mean behavior. Gorman and coworkers,<sup>20,21</sup> for example, have shown that Weibull distributions can be adjusted for temperature and stress using well known apparent activation energies and stress exponents for the purpose of normalizing data.

The location parameter,  $t_0$ , follows expected patterns in that it decreases with increasing intensities of stressors as shown also in Figures 29 and 30.

However, the shape parameter,  $\beta$ , seems to depend as much on mechanistic features as on the magnitude of stressors since its dependence, at least on stress from Figures 29 and 30, does not follow the expectation that it should increase with decreasing  $\theta$ . While  $\beta$  depends on physical and mechanistic influences as illustrated in Figure 26, its meaning is also confounded by the mixed effects as discussed in connection with Figures 22, 27, and 28.

The extent to which these dependencies of Eqns. (24) through (26) can be incorporated into statistical parameters permits their application over changing circumstances. For example, the cdf can be predicted as the temperature changes over time as in Figure 79.

### 3.0 INHERENT VARIABILITY

#### 3.1 Scope

Design requires some credible reference upon which to estimate performance. It would be desirable if there were some kind of perfect test that would produce base line results where the data exhibited no variability. Unfortunately, such a perfection does not exist nor is it implicit in corrosion processes.

If this perfection cannot be achieved, it would be desirable to establish a reference and a basis for the minimum variability as applied to SCC. Such a reference would then provide the basis for systematically incorporating metallurgical and environmental influences in order to organize a framework for predicting early failures. This reference should identify variability that is inherent in the material-environment system without the confounding element of non-coherency.

For the purpose of this paper, a quantitative measure of variability is taken as the range ratio,  $t_N/t_1$ , which is discussed in connection with Figure 19. The range ratio defines the ratio of the longest failure time to the shortest. The usual measure of dispersion, the standard deviation, for the Weibull distribution, is in Eqn. (27) but this is more cumbersome than the range ratio:

$$\sigma = (\theta - t_o) \sqrt{\Gamma\left(1 + \frac{2}{\beta}\right) - \left[\Gamma\left(1 + \frac{1}{\beta}\right)\right]^2} \quad (27)$$

where:  $\sigma$  = the standard deviation. This is the same symbol as conventionally used, as here, for stress. However, the context prevents any misunderstanding.

There are some problems in developing an ideal minimum variability as a reference. Principal among these are the following:

1. The first significant problem is that the range of data depends on the value of  $\beta$ . For the  $\beta=4$  case, as shown in Figure 24, the variability is relatively low. For the  $\beta=1$  case the variability is relatively high. However, there is nothing that can be changed since the value of  $\beta$  depends on the mechanism of SCC, excluding the mixed condition and non-coherency case. As a minimum, then, the variability is fixed by the critical mechanism that controls the mechanism of SCC as the mechanism affects  $\beta$ .
2. The second significant problem is the inevitability of the mixed condition case that produces lower values of  $\beta_g$  as illustrated in Figures 22, 27, and 28. The effective  $\beta$ , then, depends mainly on the diversity of the  $\theta$ s among various laboratories or among various tests. Further, in any application, multiple heats or multiple lots of material are used with the inevitable result of a lower  $\beta$ .
3. The mixed condition case includes the following as they produce essentially multiple values of  $\theta$ :
  - Heat to heat variation as described in Figure 27 and in Figures 38, 39 and 40.
  - Variation over ranges of potential or pH where the intensity of SCC varies sharply as illustrated in Figure 28.

- Variations in environmental conditions such as pH, potential, conductivity, stress, temperature, and concentrations of species in deposits where small changes are highly leveraged with respect to producing SCC.
4. The data obtained depend on the experimental methods. For example, a statically loaded experiment produces much different results from the pulse loaded experiment as described in Figure 71a. The crack growth in CERT specimens, see Figure 72, produces quite different results from compact tension specimens. Further, applied stresses relax with time.
  5. The usefulness of data depends on the application. This is the basis for the screening illustrated in Figure 3.

The idea of the reference case having minimum inherent variability depends on a set of experiments conducted in some chosen laboratory using a set of presumably well characterized materials with a chosen method of testing. Thus, inherent variability is not a theoretical construction but rather an experimental one. This implies that such a reference has to be chosen by some consensus process. Approaches to such a goal often involve “round robin” testing although results from such programs often have to be censored.

Principal features of inherent variability are the following:

1. SCC data are inherently variable because of the multiple paths involved in the nine segments of SCC as shown in Figure 6. It is not possible that SCC in any way can be deterministic or single valued.
2. The concept of inherent variability is experimentally defined by a set of experiments ideally conducted under coherent, well defined, well controlled and well monitored conditions.
3. The nature of inherent variability and the important physical bases depend on the nature of the shape factor that is unique to the material-environment system being studied. For the prototypic cases of  $\beta=1$  and  $\beta=4$  as illustrated in Figure 26, the associated and critical physical processes are quite different.
4. A reference set of experiments for establishing inherent variability produces the largest value of  $\beta$  that is unique to the conditions considered. Additional experiments, with different values of  $\theta$  decreases the aggregate  $\beta_g$ .

### 3.2 Components of Inherent Variability for the $\beta=1$ Case

The  $\beta=1$  case is based on the principal features that underlie Poisson statistics where events are random and can occur at any time and any place independent of the time duration. The quantitative implication of Poisson statistics is shown by the constancy of the hazard function, in Figure 15f, over time. It is implicit in these conditions that the critical processes associated with the  $\beta=1$  case occur at the surface. The fact that many occurrences of SCC exhibit  $\beta=1$  behavior is illustrated by the work of Akashi and Nakayama<sup>18</sup> in Figure 17.  $\beta=1$  behavior is also evident in the mixed dispersions in Figures 31 and 32 where part is dominated by  $\beta=1$  behavior and part by  $\beta=4$  behavior. Differences between the  $\beta=1$  and  $\beta=4$  cases are illustrated schematically in Figure 26. Physical

factors on surfaces, which can provide critical nuclei favoring  $\beta=1$  behavior for SCC include:

- Grain boundaries.
- Grain boundaries as affected by compositional changes due to precipitation and/or adsorption as shown in Figure 35.
- Second phases in the grain matrix.
- Location of the pitting potential with respect to the open circuit potential.
- Concentrations and variability of species, e.g. Cl<sup>-</sup>, as they promote pitting or inhibit pitting.
- Dependence of properties of passive film as affected by potential and pH.
- Grain size as it affects pile-up stresses.
- Variability of surface stresses as affected by relative grain orientations.
- Grain orientation with respect to favorable slip.
- Stacking fault energy as it affects the geometry of surface slip.
- Alloy composition as it affects surface processes of embrittlement such as dealloying.
- Diffusion of environmental species inward including hydrogen and oxygen.

These factors are sufficiently variable individually that their contributions to critical processes in SCC would vary randomly over time.

### 3.3 Components of Inherent Variability for the $\beta=4$ Case

The  $\beta=4$  case is characterized by the sharp rise in the hf that begins at about half the value of  $\theta$ . This characteristic implies that the  $\beta=4$  case depends on accumulation processes as illustrated in Figure 26. Accumulation processes seem more likely to relate to processes associated with the growth of SCC. However, there are certain surface processes for which accumulation is a necessary first step. Accumulation processes which can contribute to the  $\beta=4$  case are the following:

- Migration of critical species along the SCC.
- Buildup of corrosion products inside the SCC.
- Deformation at the tip of the crack.
- Chemical alteration of grain boundaries including adsorption and precipitation.
- Diffusion of environmental species into the crack tip including hydrogen and oxygen.



- Coalescence of short cracks to produce longer ones.
- Development of local constraints of stress on short cracks.
- Strength and distribution of hydrogen traps.
- Accumulation of species on heat transfer surfaces and in crevices such as those illustrated in Figure 48.
- Diffusion of species from the environment, such as hydrogen and oxygen, into the metal.
- Preferential dissolution of active components from active-noble alloys.

### 3.4 Bounding: Less Bounded and More Bounded

While the nature of the hf for  $\beta=1$  and  $\beta=4$  cases indicates random and accumulation aspects, respectively, these cases differ also in the extent to which they are bounded or can be specified fundamentally.

For the  $\beta=1$  case conditions on the surface are less easily bounded and involve at least the following considerations:

- Electrochemical potentials change locally and, on the average, with time as shown in Figure 47. The potential has a large leverage on the intensity of SCC as shown in Figures 13 and 28.
- pH changes similarly to the potential.
- Local flow of the environment changes the rate of arrival of reducible species and removes pre-existing species.
- Deposits form over time that produce local cells where separated alkalinity and acidity develop.
- Local stresses on the surface can vary from the nominal bulk stress by at least a factor of three at various locations.

As these processes interact with the variable character of susceptibility to SCC, as illustrated in Figure 28, bounding its occurrence in modeling is increasingly difficult. This “unboundedness” is different in detail but similar in general to the random requirement for Poisson statistics.

As SCC propagates, the conditions affecting the propagation of the crack are more bounded as follows:

- The local chemistry is circumscribed by conditions of the local SCC enclave. Here, environments tend to become saturated; they are oxygen deficient, the local open circuit potential at the crack tip is less variable and is controlled by the local mixed electrodes; deposits of corrosion products in the crack minimize rapid chemical changes at the crack tip.

- Stresses at the crack tip are more constant becoming a zone of cold work that is generally constant in its properties.

These more bounded conditions inside an advancing SCC should produce less variability. This boundedness may also contribute to the lower variability aside from the implication of the accumulation nature of the  $\beta=4$  case.

### 3.5 Conducting Experiments to Characterize Inherent Variability

Since defining inherent variability depends on the experiments, precautions for conducting experiments to obtain a reference case should be taken. Andresen<sup>42</sup> has enumerated precautions for minimizing variability. Precautions for developing a reference case for inherent variability include the following:

- Use a single heat of material where the processing has been homogeneous and well controlled in temperature and deformation.
- Use specimens where stresses do not relax and can be reproducibly controlled.
- Control the test environment to maintain constant chemistry, minimize buildup of surface contamination, and prevent galvanic reactions.
- Use surface preparations on specimens which, in themselves, produce minimum variability, noting the influences of surface treatment in Figure 45a.
- Confine the experiment to either fully initiation or fully propagation control.
- Employ a single operator for the experiments.
- Conduct self-consistent and adequately sensitive examinations of progress of SCC.
- Use *in situ* methods of measurement to avoid periodic removal of specimens at intermediate times.

Clearly, obtaining a good reference for inherent variability could be relatively expensive. However, such a reference is required for predictions. With a credible reference in place, effects of other important variables can be incorporated more credibly.

## 4.0 METALLURGICAL VARIABILITY

### 4.1 Scope

The subject of metallurgical variability refers to the effects of metallurgical factors on statistical distributions. These metallurgical factors include alloy composition, structure, and surface condition. While some of the metallurgical factors produce important effects, they are not readily quantified, i.e. how is the large effect of heat treatment placed into a numerical framework? Nonetheless, in order to account for the effects of metallurgical structure, it needs to be quantified so that they can be included in the quantitative framework of Eqns. (24)-(26). While the data from investigations is not extensive in support of a characterizing metallurgical variability, there is a sufficient body of work to provide directions.

Metallurgical variability generally influences SCC through the complexities of structure-sensitive properties. This is evident from Figure 27. The early SCC failures are usually attributed either to "bad heats" or to "contamination." Rarely is either of these attributions justified. Rather, the early failures are those that should be expected at the 0.0001 or 0.001 probability. Considering the various ways that composition of material and structure could interact to produce variability, SCC seems impossibly complex. It is surprising that there is as much order as occurs. The topics considered in this section include alloy composition, structure sensitive properties as affected by heat treatment, cold work, orientation, welding, and surface condition.

### 4.2 Alloy Composition

Effects of variations in the average alloy composition have not been studied extensively with respect to effects on the probability of SCC because small variations in the average alloy composition do not seem as important as grain boundary effects, small concentrations of impurities, and aspects of structure including transformations and multiple phases.

Figure 33a<sup>108</sup> shows the effect of alloy composition on the probability of pitting as a function of potential. The effects of alloy composition are correlated in Figure 33b and follow generally well known patterns. In addition, the effect of alloy composition on the value of  $\beta$  is shown to be linear, increasing with increasing  $Cr_{eq}$ . Of particular interest here is the dispersion of data for the pitting potential. Once the pitting potential is exceeded, the passive film is rapidly perforated and reactivity increases significantly as suggested on Figure 11. The correlation with  $\beta$  indicates that increasing  $Cr_{eq}$  reduces the variability. These influences on the pitting potential and  $\beta$  should affect SCC to the extent that pitting is part of the initiation process.

The effect of fourth component alloy additions on the SCC of a Fe-15Ni-20Cr alloy tested in boiling  $MgCl_2$  is shown in Figure 34 from the work of Staehle et al.<sup>126</sup> The acceleration by additions of platinum metals has been rationalized by Staehle,<sup>77</sup> and similar results have been published by van Rooyen.<sup>127</sup> The addition of platinum provides efficient local cathodes for the reduction of water and for increasing the potential into the upper SCC region shown in Figure 11 as rationalized by Staehle.<sup>77</sup> The accelerating effects of molybdenum have been studied by Barnartt, Stickler, and van Rooyen;<sup>128</sup> the accelerating effects of nitrogen have been studied by Uhlig et al.;<sup>129,130,131</sup> and the accelerating effects of phosphorous have been studied by Lang<sup>132</sup> and by Bond and Dundas.<sup>133</sup> The mechanisms of these accelerations have been attributed to effects on stacking fault energy by Swann and Nutting<sup>134</sup> and Douglass et al.<sup>135</sup>

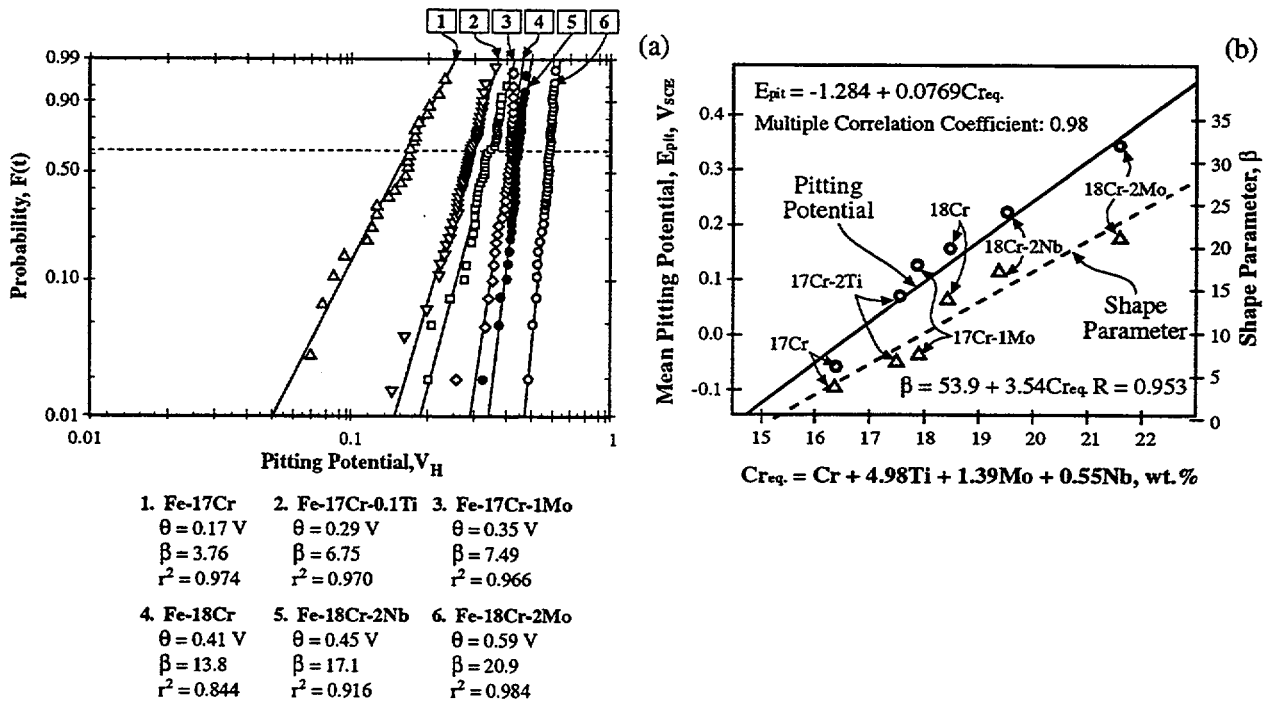


Figure 33: (a) Probability vs. pitting potential for Fe-Cr base alloys as determined at 30°C in 3.5w/o NaCl; solution  $N_2$  saturated. Pitting potentials measured with potentiometric scans of 16.7 mV/min. Data on the abscissa are adjusted for convenience of probability plotting by adding + 0.2V. The original data were plotted using normal probability coordinates. (b) Pitting potential at  $\theta$  from Figure 33a vs. chromium equivalent,  $Cr_{eq}$ . From Shibata.<sup>108</sup>  $\beta$  vs.  $Cr_{eq}$  from analysis for this report.

The relatively greater slopes in Figure 34 due to molybdenum and nitrogen additions are probably due to the lack of dispersion of conditions for the SCC of these materials in accordance with the pattern suggested in Figure 28.  $t_o$  is positive for all alloys. The relatively high values of  $t_o$  suggests that an accumulation process is involved in this SCC as suggested in Figure 26. Except for the molybdenum and phosphorus, the values of  $\beta$  are in the range of unity, which suggests that the SCC is dominated by surface processes and are consistent with Poisson statistics.

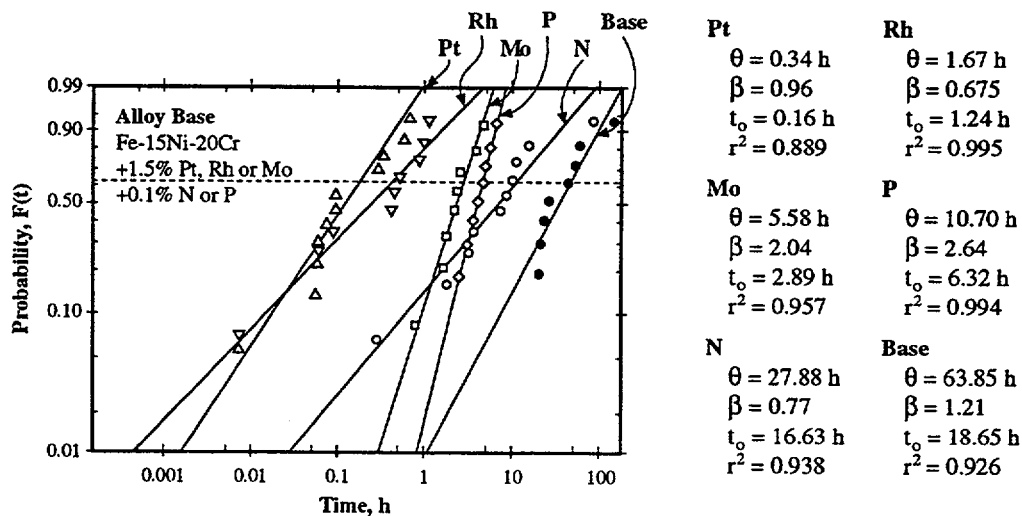


Figure 34: Probability vs. time for the SCC of Fe-Cr-Ni alloys containing fourth component additions tested in boiling  $MgCl_2$  at 90% of the yield stress. All specimens were annealed at 1150°C and were exposed in the form of 0.38 mm diameter specimens. From Staehle et al.<sup>126</sup>

### 4.3 Structure Sensitive Effects

This section evaluates the effects of alloy structure on statistical distributions. The experience with effects of heat treatment generally show that heat-to-heat variations produce large variations in  $\theta$  as indicated in Figure 27. Despite extensive work, there is no satisfactory explanation for the effects of alloy structure on the SCC of Alloy 600 and similar materials. The data discussed here illustrate the large variabilities due to alloy structures, but the mechanisms by which thermal and mechanical processes exert such large effects are not discussed.

An important path of SCC is intergranular as illustrated in Figure 10. This is often related, especially in stainless steels, to "sensitization" caused by the depletion of chromium at grain boundaries due to the well known formation of chromium carbides under certain conditions of heat treatment. Similar sensitization occurs for the high nickel alloys, but the chemistry of the depleted region is nickel- rather than iron-rich as for the stainless steels. This process of forming precipitates and depleting adjacent regions is illustrated in Figure 35a. Not only does the formation of precipitates change the chemistry at grain boundaries, but adsorption of species to grain boundaries produces changes up to  $10^6$  relative to the bulk concentration as shown in Figure 35b. Such accumulations, as well as rejections, provide preferential paths for SCC, IGC and for initiating pitting. Four adsorption processes involving impurities and alloy elements are illustrated in Figure 35b.

Figure 36 shows examples of the influence of processing as it affects the distribution of carbides on LPSCC in high purity water from the work of Norring et al.<sup>117</sup> Figure 36a shows the effect of mill annealing temperature on the initiation time of LPSCC. The ratio of the earliest to latest SCC in this figure is approximately 20. Such ranges of mill annealing temperatures have not been uncommon in the past in the production of Alloy 600 and similar alloys. Figure 36b shows how the initiation of SCC is affected by the extent of carbides at the grain boundaries. In general, for LPSCC of Alloy 600, as well as for other of the submodes shown in Figure 12, increasing the extent of carbides that form at grain boundaries increases the SCC resistance.

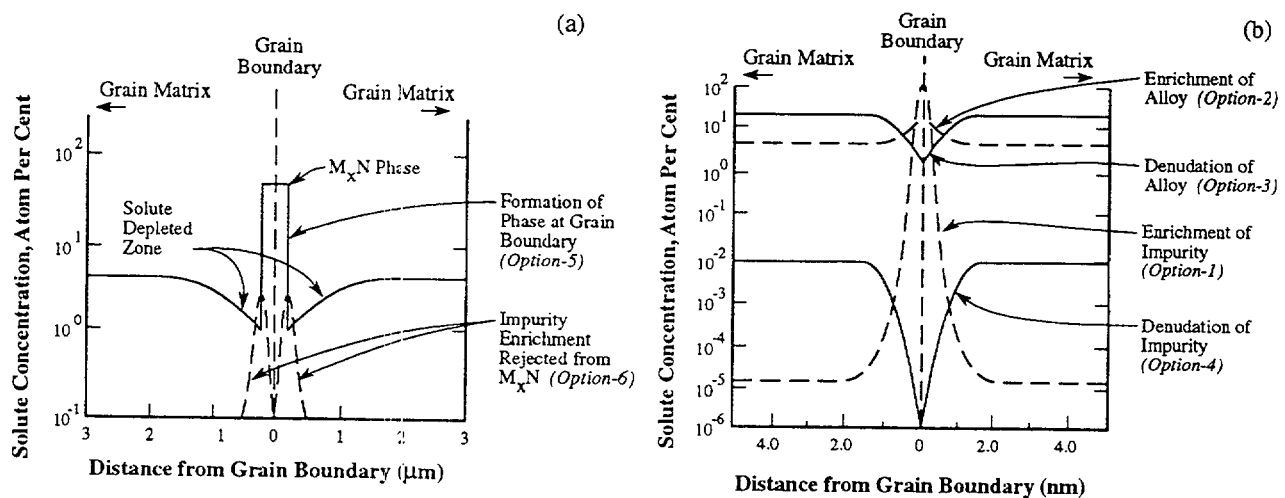


Figure 35: Grain boundary composition vs. distance from grain boundary. (a) Solute composition near a grain boundary for the case of forming a precipitate. Solute depleted regions and local accumulation due to rejection are shown. (b) Solute composition at a grain boundary associated with preferential adsorption or rejection for four cases. From Staehle.<sup>78</sup>

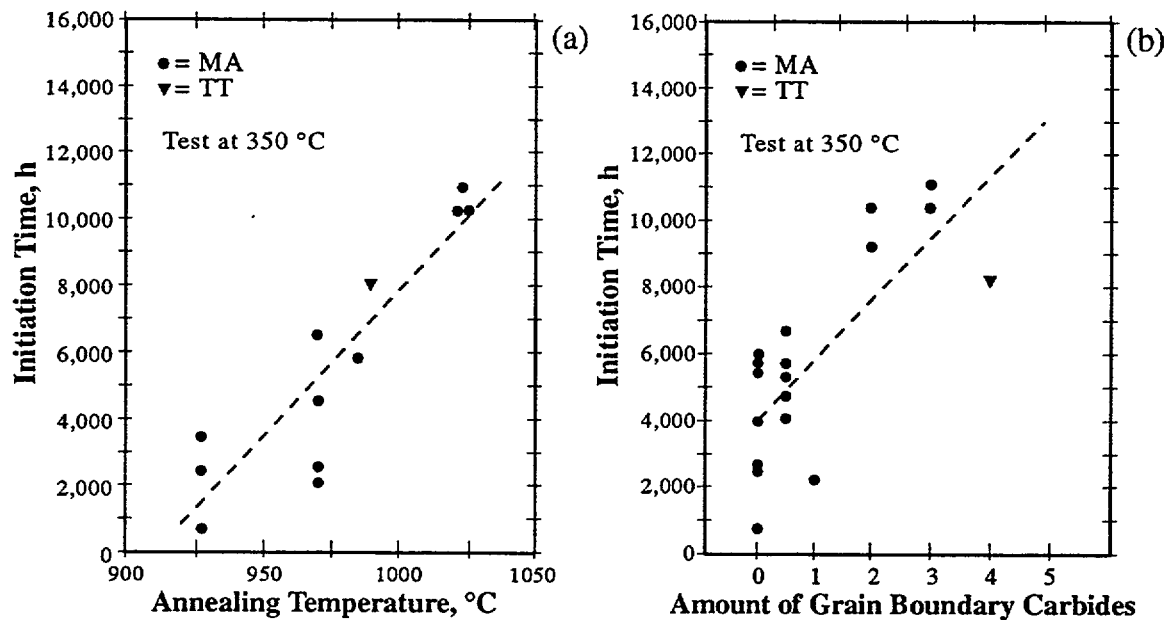


Figure 36: (a) Initiation time for LPSCC vs. annealing temperature for Alloy 600 in both MA and TT conditions. (b) Initiation time for LPSCC vs. extent of grain boundary carbides for MA and TT conditions. From Norring et al.<sup>117</sup>

The general influences shown in Figure 36 have been studied more quantitatively in the LPSCC submode with statistical distributions by Webb<sup>24</sup> as shown in Figure 37a. Here, effects of three heat treatments are compared with a reference “Heat A.” The density of carbides at grain boundaries increases the resistance to SCC by a factor of 110 comparing the Heat A with the HW and annealing condition. Such variations in the SCC even among commercial heats are common. Except for heat A the slopes are typical of the  $\beta=4$  case.

Results from the work of Norring et al.<sup>117</sup> in Figure 27 show values of  $\beta_L$  and ranges of  $\theta$  similar to the results in Figure 37. This relatively large range of values for  $\theta$  would produce an overall effect of reducing the aggregate value of  $\beta$  as illustrated in Figure 27 as well as in Figure 22.

Figure 37b compares the MA and TT conditions. While the TT heat treatment was developed to increase the resistance to SCC, the effect is not large and is within the range of Figure 37a. This heat treatment was developed based on the work of Blanchet et al.<sup>137</sup> who showed that a sensitizing heat treatment would minimize LPSCC.

An important confirmation of the laboratory data from Figures 36 and 37, is provided by Scott in his 2000 Speller award lecture.<sup>138</sup> Figure 38, adapted from Scott’s paper, shows results taken from the primary and secondary sides of operating PWRs (see Figure 4 as reference); Scott has analyzed the percent occurrence of SCC for each of the heats used in a single steam generator, and these percentages are plotted as bars vs. the heat number. The heat numbers along the abscissa are in the order of production of the heats. The number of tubes used in the steam generator from each heat is shown at the top of each bar. These data show that a relatively few heats produce most of the SCC on both primary and secondary sides. This trend is consistent with the laboratory data in Figures 36 and 37.

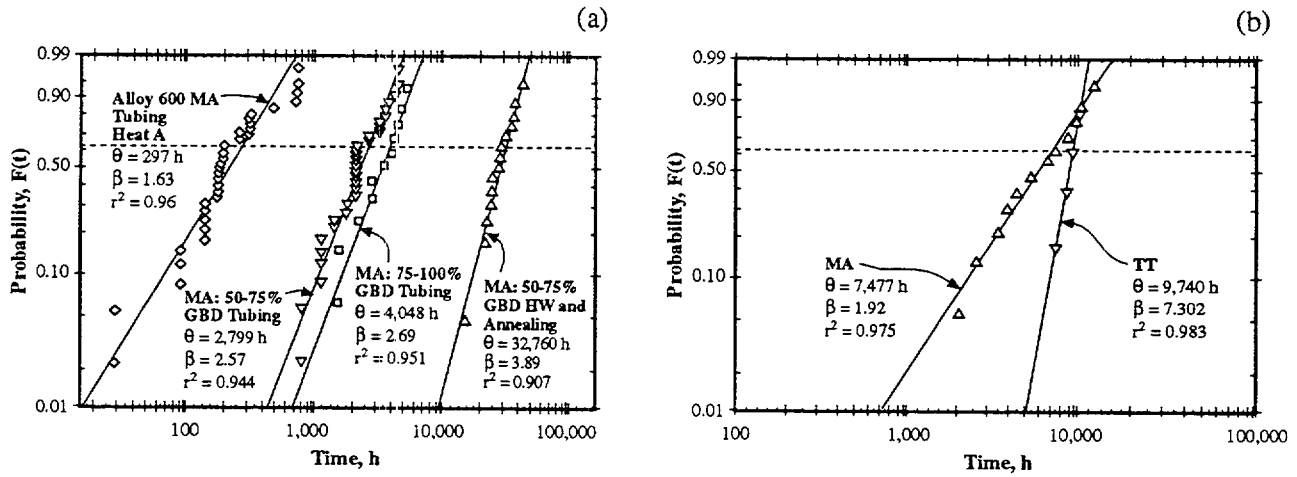


Figure 37: (a) Probability vs. time for a reference Heat A and three heats where metallurgical structures have been produced that affect the distribution of carbides. Specimens exposed at 360°C in high purity water to produce LPSCC. From Webb.<sup>24</sup> (b) Probability vs. time comparing the LPSCC of mill annealed (MA) and thermally treated (TT) specimens in 360°C pure water with a partial pressure of hydrogen at 1.0 psia. Four heats of materials used. From Jacko.<sup>136</sup>

Scott's data from operating equipment together with laboratory data in Figures 27 and 37 imply that metallurgical structures are critical in developing predictions for the earliest failures. The range of values of  $\theta$  implicit in Scott's results together with the laboratory data imply that values of  $\beta$  for the aggregate will become unity or less following the predictions of Figures 22, 27, and 28. The overall result is the large variability implicit in low values of  $\beta_g$ . This is not the coherent Poissonian variability but rather the non-coherent and mixed variability.

The effect of heat-to-heat variability was also investigated by Jacko<sup>91</sup> who studied the LSPCC behavior of Alloy 600 of four heats over a range of water chemistries used in the primary systems of PWRs. His results in Figure 39 show initiation time vs. five different water chemistries and with the four heats of material. One standard deviation for the data is noted. This implies that the earliest failures would be about two standard deviations from the mean. However, the data in Figure 39 show that there is about two orders of magnitude difference in the means. The range ratio for the set would be much greater.

Stainless steels used in piping of BWRs shown in Figure 5a exhibit the same heat-to-heat variability as Alloy 600 as shown in Figure 40 from the work of Clarke and Gordon.<sup>115</sup> The results for this Type 304 stainless steel exhibit a range of failure times in high purity 288°C water over a factor of 600. This result is consistent with the results in Figures 36 and 37 for Alloy 600.

Sensitization can be quantified by the EPR test.<sup>139</sup> This test determines the magnitude of coulombs produced in a cyclic polarization experiment as the difference between forward and reverse scans. The number of coulombs in this difference is proportional to the degree of sensitization. Figure 41a shows the probability vs.  $P_a$  which provides an insight into the range of sensitizations that are observed in commercial heats of sensitized stainless steel. Figure 41b<sup>61</sup> shows a clear relationship between the  $P_a$  and the lower limit lifetime for sensitized Type 304 stainless steel exposed to a 3.5% NaCl solution at 80°C and a high purity water solution at 280°C. The results show similar trends.

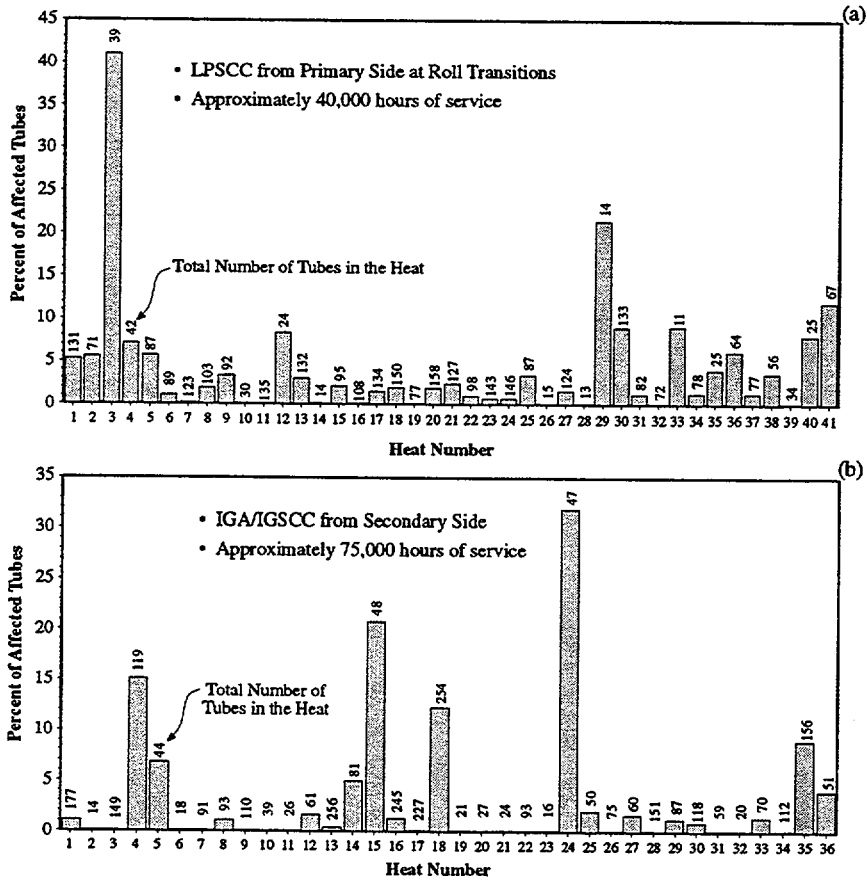


Figure 38: (a) Percent of tubes affected by LPSCC from the primary side of a PWR steam generator vs. heat number determined at roll transitions after approximately 40,000 hours of service. Primary surface temperature at this location is about 310°C. Environment is primary water as identified in Figure 4. (b) Percent of tubes affected by IGA and IGSCC vs. heat number from the secondary side of a PWR steam generator in heat transfer crevices after approximately 75,000 hours of service. Adapted from Scott.<sup>138\*</sup>

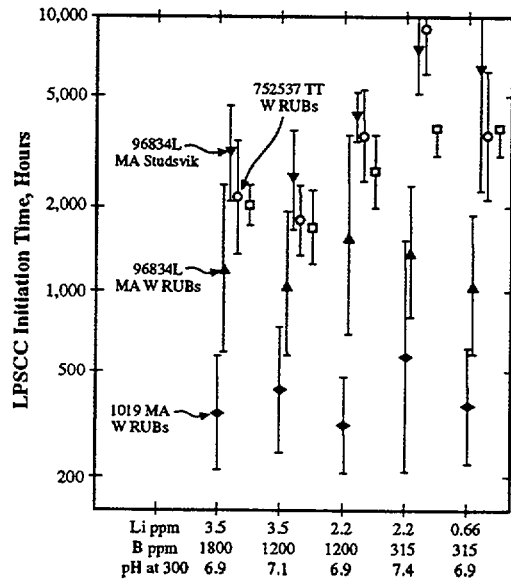


Figure 39: LPSCC initiation time vs. water chemistry for four heats of Alloy 600 exposed at 330°C. From Jacko.<sup>91</sup>

\* Personal Communication with P.M. Scott, Framatome, January, 2001.



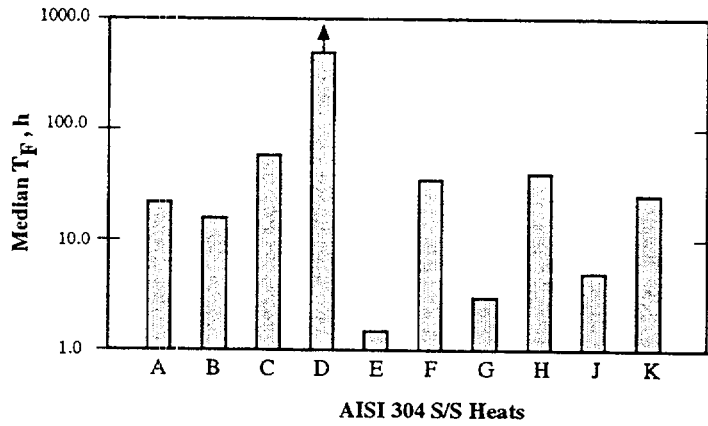


Figure 40: Median times-to-failure vs. heats for sensitized Type 304 stainless steel tested in 288°C water. From Clarke and Gordon.<sup>115</sup>

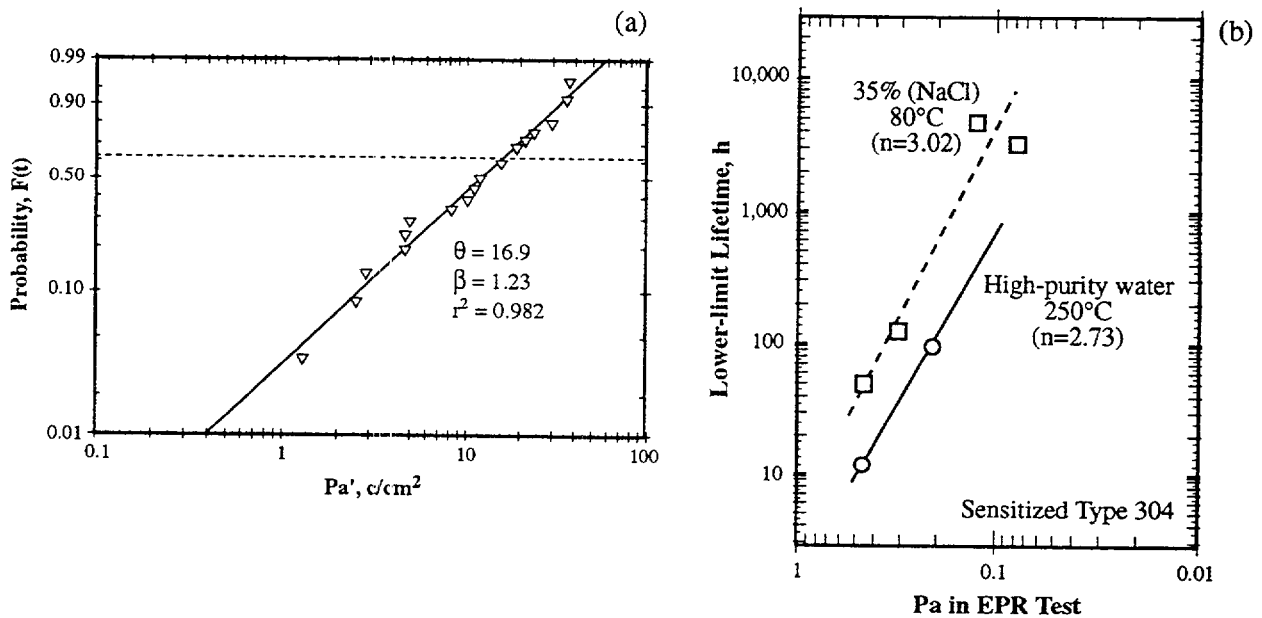


Figure 41: (a) Probability vs.  $P_a$  from EPR test for as-welded Type 304 stainless steel piping. From Harris et al.<sup>140</sup> (b) Lower limit life vs.  $P_a$  from the EPR test for sensitized Type 304 stainless steel exposed to 3.5% NaCl solution at 80°C and to high-purity oxygenated water at 250°C. From Akashi and Nakayama.<sup>61</sup>

#### 4.4 Orientation

One set of data shown in Figure 30a is available to show the effects of specimen orientation on SCC. Figure 30a compares SCC in the transverse and longitudinal directions at 338 MPa. For transverse and longitudinal data the values of  $\theta$  and  $\beta$  are 78.6 and 610.0 hours and 0.54 and 0.75, respectively. The values of  $\beta$  are similar, but  $\theta$  is 8 times longer for the longitudinal orientation. The heat from which the specimens were taken was the same. The similarity of slopes suggests that the mechanisms are the same. However, these low values, according to the discussion of Figures 22 and 27, may indicate nothing about the mechanism but rather about the non-coherency of the testing. These slopes are less than can be attributed to a single coherent mechanism.

## 4.5 Cold Work

Cold work exerts important but varying effects on the SCC distributions as shown in Figure 42. Here, the work of Cochran and Staehle, as shown in Figures 42a and 42b,<sup>141</sup> used Type 310 stainless steel exposed to boiling  $MgCl_2$  at  $154^\circ C$ . They identify a minimum in  $\theta$  at 6% vs. the magnitude of cold work. The value of  $\beta$  is also minimum at the same point. This pattern in  $\beta$  suggests a significant change in mechanism associated with 6% cold work involving a surface-critical condition at 6% and more accumulation-like processes at high and lower magnitudes of cold work similar to the processes identified in Figure 26.

At the higher magnitudes of cold work for the Alloy 600, shown in Figures 42c and 42d, increasing cold work decreases the value of  $\theta$  and  $\beta$ . The low  $\beta$  at 35% cold work suggests a non-coherency pattern and not a mechanistically-related cause. The increase in  $t_0$  with increasing cold work is opposite to the expected trend. However, it is not clear what should be expected from cold work owing to the combination of increases in surface sites, high residual stresses and dynamic local slip.

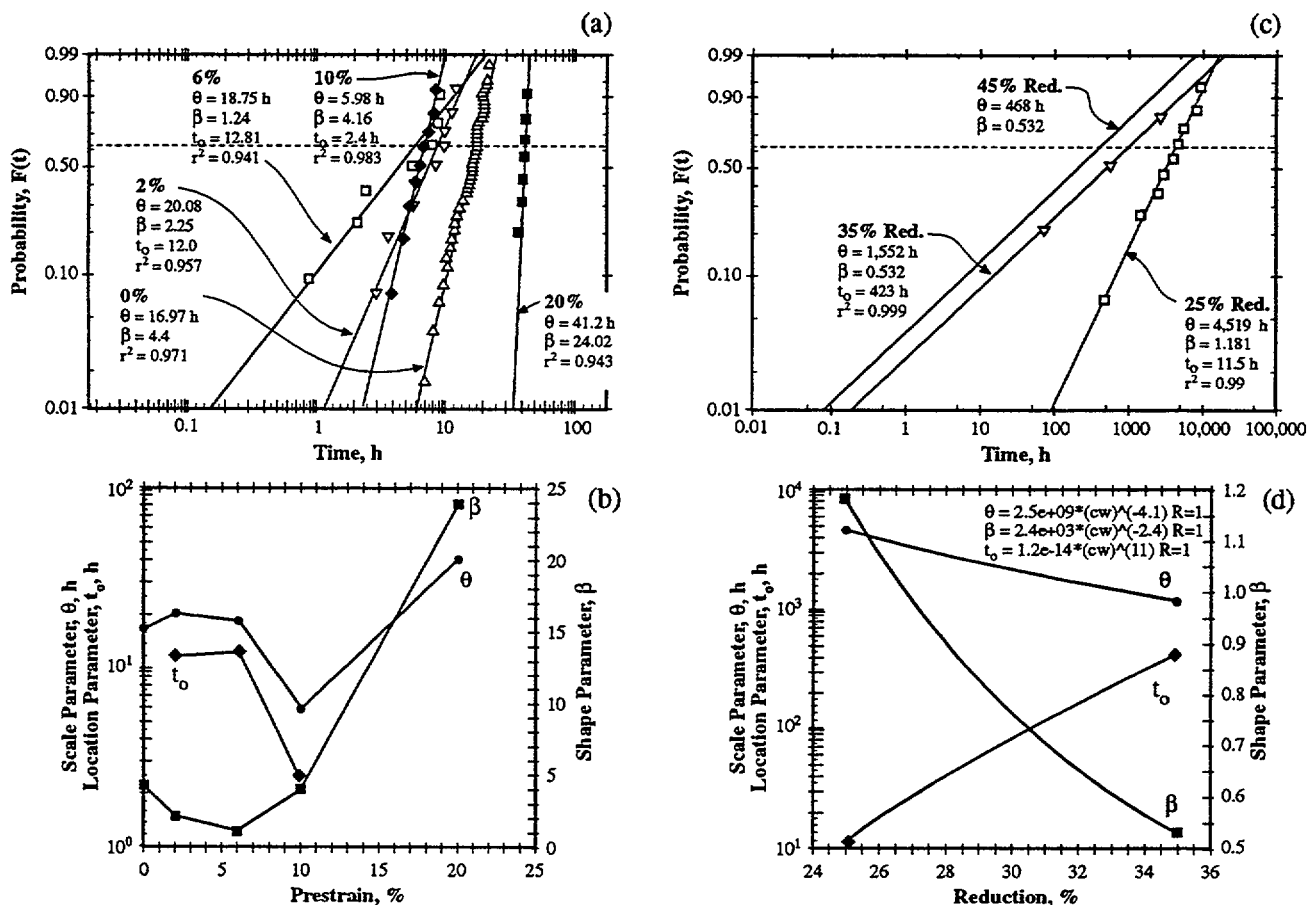


Figure 42: (a) Probability vs. time for the SCC of Type 310 stainless steel tested in boiling  $MgCl_2$  at  $154^\circ C$  and stressed at 19,600 psi for five magnitudes of prestrain. From Cochran and Staehle.<sup>141</sup> (b) Correlation of  $\theta$ ,  $\beta$ , and  $t_0$  as a function of cold work from Figure (a).\* (c) Probability vs. time for the SCC of Alloy 600 tested in primary water at  $360^\circ C$  with 1.0 psia hydrogen for three magnitudes of cold work. Tubing was annealed and drawn to produce the cold work. From Jacko.<sup>137</sup> (d) Correlation of  $\theta$ ,  $\beta$ , and  $t_0$  as a function of cold work from Figure (c).\*

\* In these plots, and the following ones where the statistical parameters are correlated, there are often limited data so that plots using two or three entries may be misleading. However, these data are the only ones available.

## 4.6 Welds

Distributions of data from welding and weld metal have been investigated with inconsistent results. Figure 5a shows results from welds in stainless steel pipes in a BWR application where the environment is oxygenated high purity water in the range of 288°C. Here,  $\beta$  for the aggregate is 0.86 to 0.93 with this range most likely due to non-coherency if the welds are considered to be a series of different heats of material according to the pattern of Figure 22. Alloy 182B weld metal is compared with Alloy 600 in Figure 43a.  $\theta$  of the 182B is larger and the slope is steeper. The lower slopes,  $\beta=0.50$  and 1.14 for the Alloy 600B and 182B, respectively, suggest mixing conditions according to Figure 22 rather than coherency. Slopes in Figure 43b, comparing Alloy 82 weld metal with two carbon concentrations with Alloy 600, show that the weld metals exhibit higher values of  $\theta$  but lower slopes of  $\beta=1.04$  and 1.11 for the low and high carbon weld metals, respectively. The reasons for the opposite effects of the weld metals in the two figures may relate to the Alloy 182 being tested in BWR conditions of high temperature oxygenated water at 288°C while the Alloy 82 was tested at high purity water at 360°C in deoxygenated conditions. The results of both sets of data are within the range shown in Figure 37a for structures involving carbides at grain boundaries. Figure 43c compares the lower limit lifetime for three weld metal alloys with that of Alloy 600 according to a composition index and shows that the behavior, in what is effectively  $\theta$ , is consistent with the average alloy compositions.

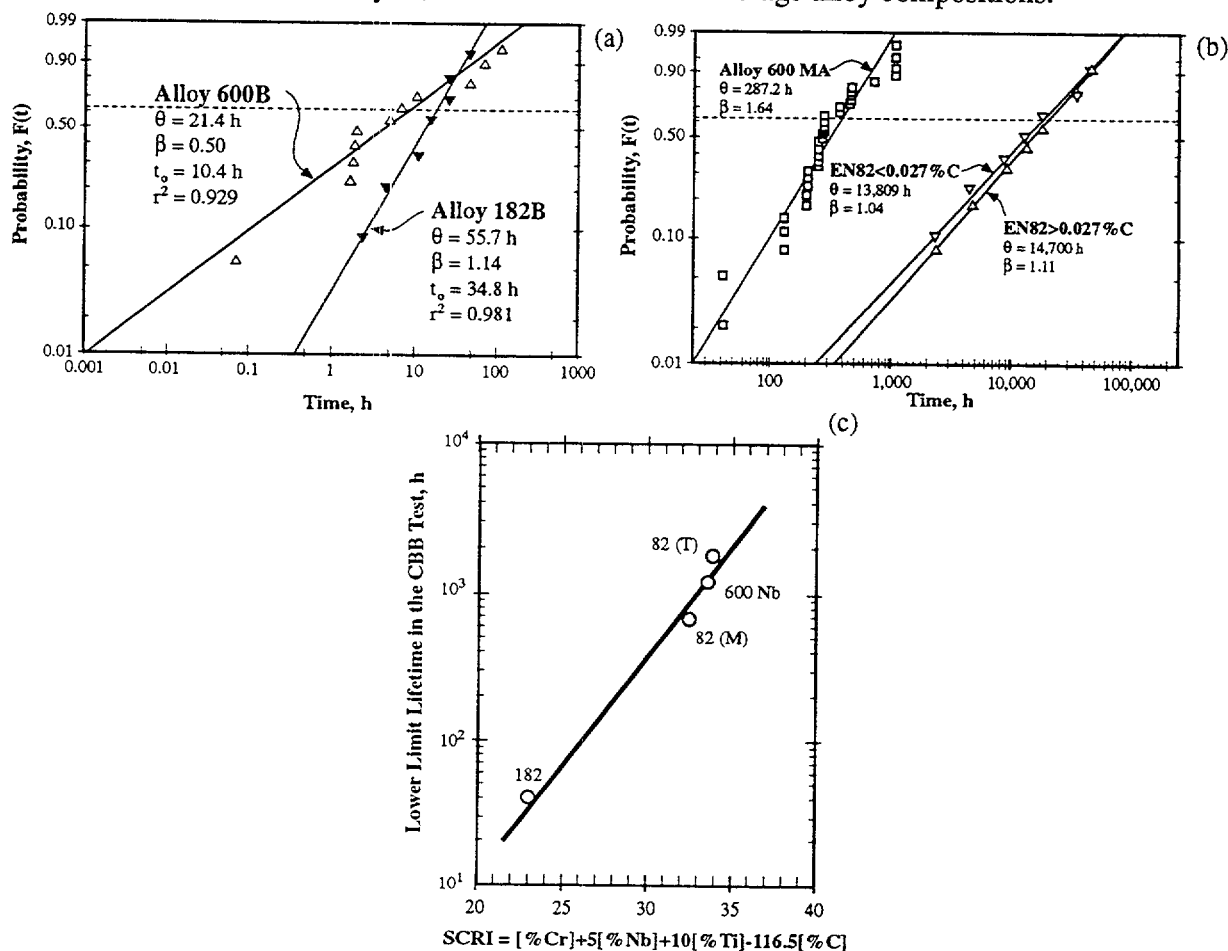


Figure 43: (a) Probability vs. time for SCC of Alloys 600B and 182B tested at constant load at 250°C with 8 ppm of dissolved oxygen in high purity water. From Akashi and Nakayama.<sup>142</sup> (b) Probability vs. time for the SCC of Alloy 600 compared with low carbon and high carbon welding material of EN82 tested in deoxygenated water at 360°C. From Webb.<sup>24</sup> (c) Lower limit lifetimes in a crevice bent beam experiment (CBB) for alloys exposed to high purity oxygenated water at 250°C. From Akashi.<sup>17</sup>

## 4.7 Surface Treatments

Surface preparation is well known to affect the intensity of SCC. Rentler and Welinsky<sup>169</sup> showed that etching the surface of Alloy 600 greatly accelerates SCC in the LPSCC mode. Berge<sup>143</sup> demonstrated that the SCC of alloy 600 in operating PWRs is greatly affected by the method of machining. Surface preparation can produce confounding effects that obscure effects of alloy composition and structure as well as environments on SCC. Surface grinding was shown to accelerate the occurrence of SCC in the BWR piping described in Figure 5a.

Figure 44 shows the effect of surface preparations on the hardness of the near surface region for Alloy 600 from the work of Rao.<sup>144</sup> This increase in hardness may accelerate the initiation of SCC according to effects of cold work discussed in connection with Figure 42, it may change the surface stresses, or it may increase the number of sites for initiation.

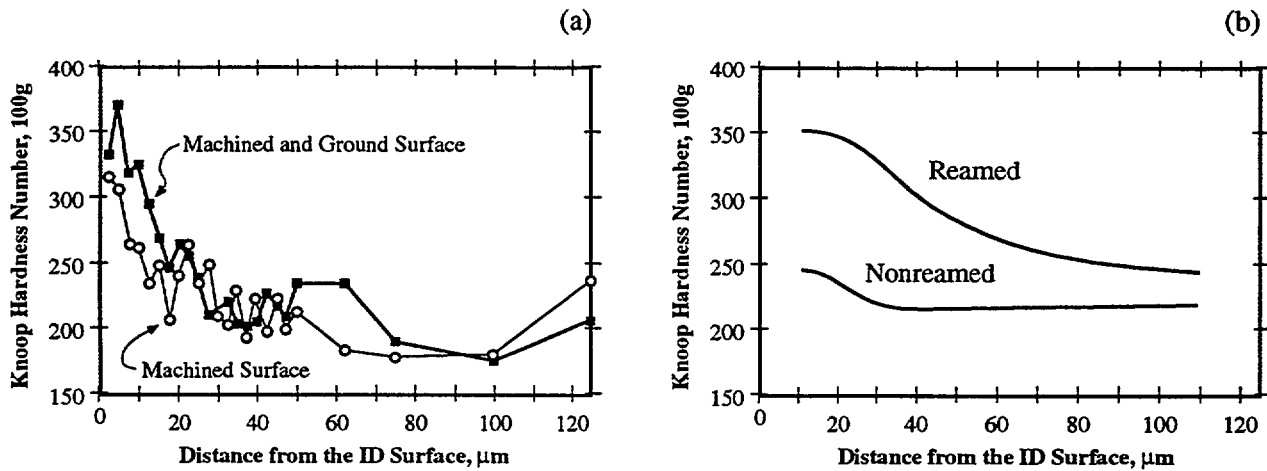


Figure 44: (a) Microhardness vs. distance for surfaces that have been machined and ground and only machined determined at the ID surface of a PWR reactor vessel closure penetration. From Rao.<sup>144</sup> (b) Microhardness vs. distance from the surface as affected by reaming at the ID surface of pressurizer heater sleeve penetration used in the pressurizer of a PWR primary system. From Rao.<sup>144</sup>

Variability such as that introduced by the processes studied in connection with Figure 44 has been studied by Cochran and Staehle<sup>141</sup> and by Shibata and Takeyama.<sup>145</sup> Their results are shown in Figure 45. Cochran and Staehle investigated effects of mechanical and chemical treatments on the SCC of Type 310 stainless steel tested in boiling  $MgCl_2$  at 150°C. They used three intensities of mechanical preparations as smooth (SMP), medium (MMP) and rough mechanical polish (RMP) that were achieved by using various grits; they also studied the vacuum annealed condition and chemical and electrochemical polishing. The results in Figure 45a exhibit a range of values for  $\theta$  of 3.79 to 15.9 hours and values of  $\beta$  from 1.1 to 4.7.

Shibata and Takeyama<sup>145</sup> have compared the pitting potential of Types 304 and 316 stainless steel as shown in Figure 45b for surfaces that have been prepared by emery polishing and chemical etching. The specimens were exposed to 30%  $H_2SO_4$  at 35°C for 10 minutes. At least for the Type 316, the chemical etch produces a more resistant surface in terms of increased pitting potential indicated by a  $\theta$  of 0.95 volts compared to the emery polish at 0.47 volts; the values of  $\beta$  of 3.6 and 11.8, respectively, show that there is greater variability introduced by the etching process.

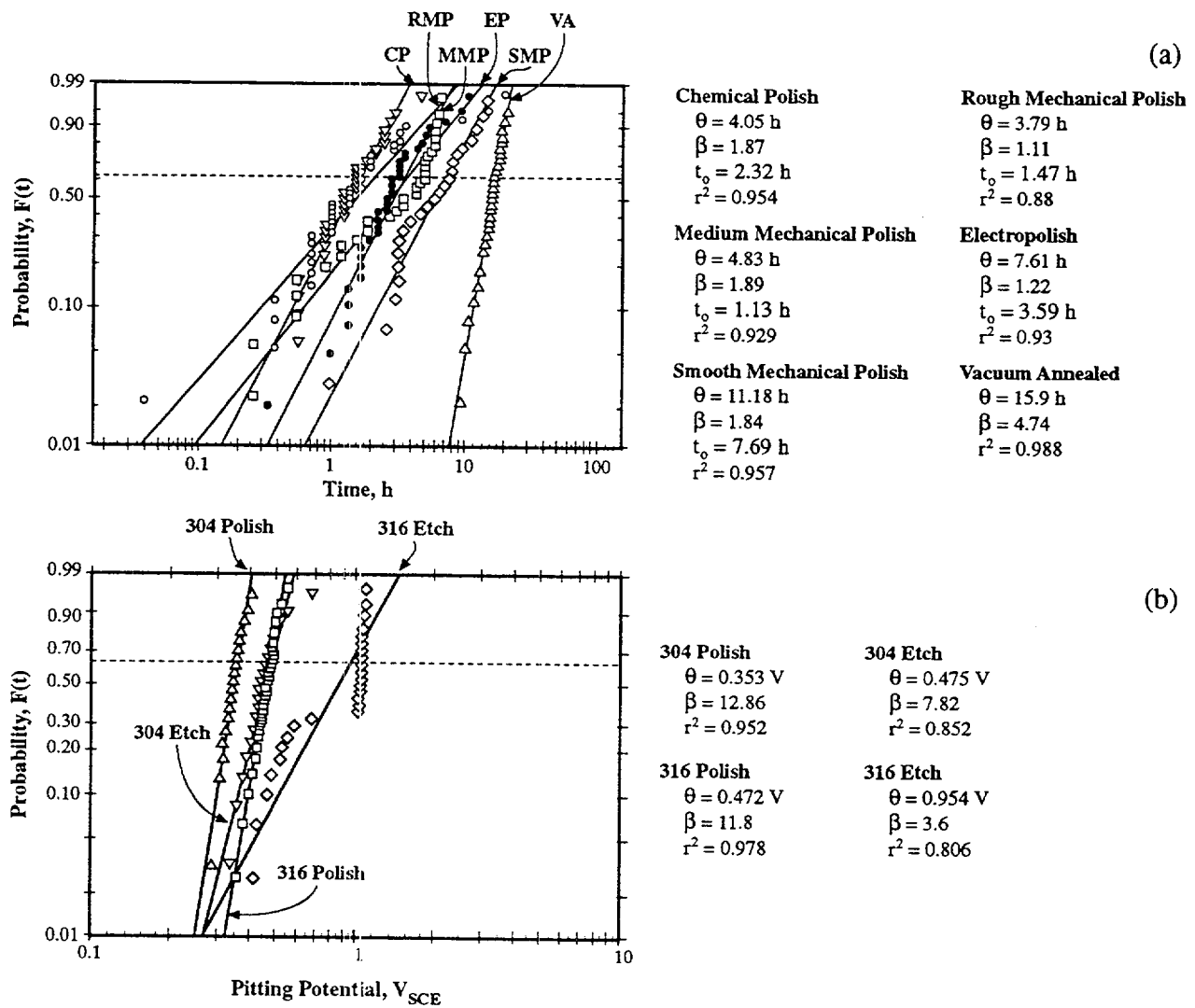


Figure 45: (a) Probability vs. time for SCC for various surface preparations of Type 310 stainless steel tested in boiling  $MgCl_2$  at  $154^\circ C$  and stressed to 19,600 psi. From Staehle and Cochran.<sup>141</sup> (b) Probability vs. pitting potential for SCC, in 3.5% NaCl at  $35^\circ C$  and  $N_2$  saturated, of Types 304 and 316 stainless steel with 2/0 emery polishing or chemical etching (30%  $H_2SO_4$ ,  $35^\circ C$  for 10 minutes). These data were originally plotted as a normal distribution (abscissa not adjusted from original). From Shiba and Takeyama.<sup>145</sup>

## 5.0 ENVIRONMENTAL VARIABILITY

### 5.1 Scope

Environmental variability refers to the effects of environments on the statistical distributions. Environments, as identified in the CBDA, include chemistry, stress, temperature, and flow. The chemical environment here includes the electrochemical potential, pH, and chemical species. The environmental variables, unlike the metallurgical variables, are more readily quantified. These variables can also enter the dependencies of the statistical parameters as identified in Eqns. (24)-(26).

Environmental variables affect SCC in two ways: First, the occurrence of SCC depends upon interactions between the metal and environment as illustrated in Figures 11-14; second, the environment controls whether conditions can activate SCC by some variable, such as the potential, being in the range of a SCC submode as illustrated in Figure 13. Environments exert strong leverages on the occurrence of SCC in the following ways:

- The large changes in solubility of protective films that result from relatively small changes in pH and potential as indicated in Figures 14 and 46.
- The large stress exponent as illustrated by the work of Webb et al.<sup>22,23,24</sup> and van Rooyen<sup>127</sup> for the behavior of Alloy 600 in the LPSCC mode.
- High activation energies for the temperature effect as described by Rebak and Szklarska Smialowska.<sup>146</sup>
- The sharp changes with potential of the intensity of SCC as shown in Figures 13 and 28.
- The sharp change in reactivity at the pitting potential as indicated in Figure 11 and Figure 33a.
- The large effects of potential on the thermodynamic pressure of hydrogen.
- Large effects due to the low concentrations of some species, e.g. chloride and lead as indicated in Figure 12b.
- Capacity of environment to concentrate on surfaces due to heat transfer or adsorption effects.
- The effect of separate anodic and cathodic reactions associated with deposits or crevices in producing separated locations of acidity alkalinity at different locations.

Further, these relatively high leverages often produce variable results as they interact with sharp transitions in the intensity of SCC as illustrated in Figure 28.

Figure 46 shows the effects of pH and potential on the solubility of iron oxides at 25°C. Here, it is evident that relatively small changes in pH and potential change the solubility by relatively large amounts. A consequence of this effect is illustrated in Figure 14 where the SCC of steel is negligible at the solubility minimum. Metallurgical chemistry which produces increasingly insoluble oxides, e.g.  $\text{Cr}_2\text{O}_3$ , as illustrated in Figure 33a, also participates in reducing the rate of pitting and sometimes of SCC.

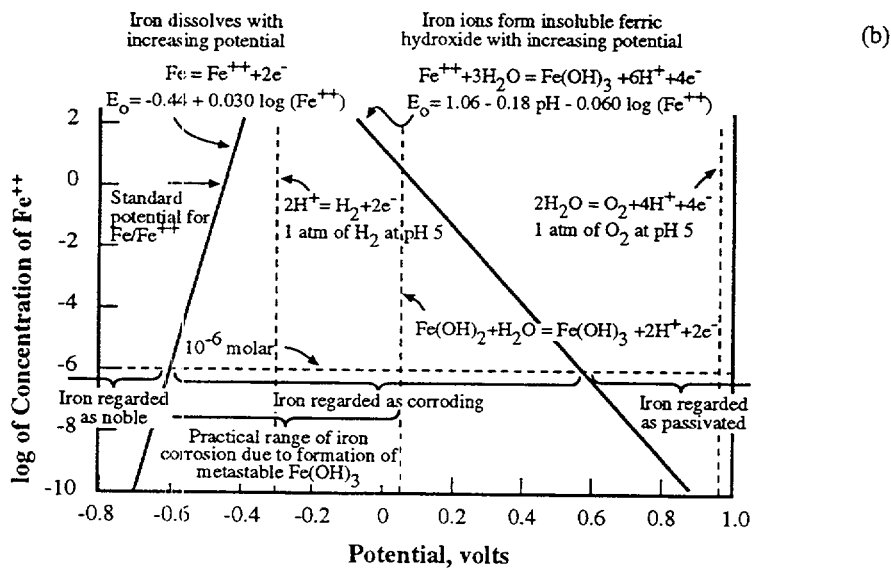
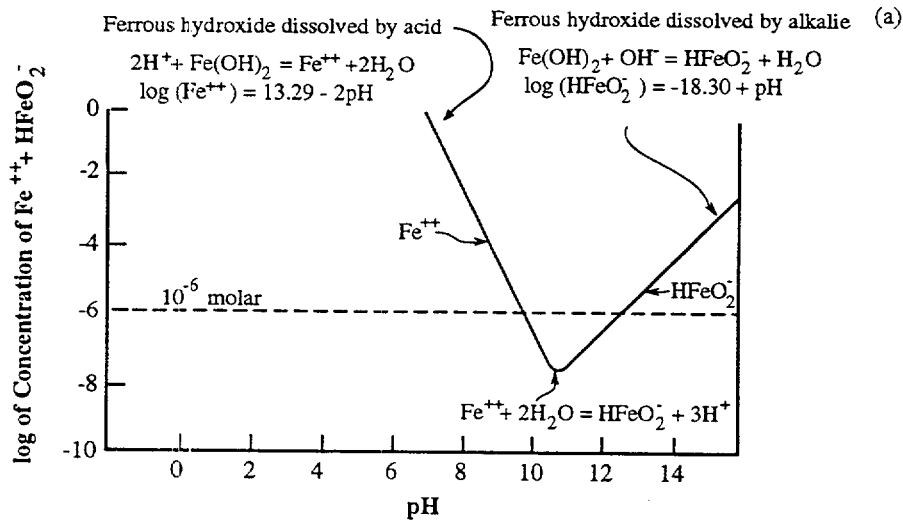


Figure 46: (a) Concentration of soluble iron ions vs. pH for acidic and alkaline regions. Adapted from Pourbaix.<sup>97</sup> (b) Concentration of iron ions vs. potential at pH 5 and room temperature. Locations for the  $\text{H}_2\text{O}/\text{H}_2$  and  $\text{O}_2/\text{H}_2\text{O}$  equilibria are shown. Adapted from Pourbaix.<sup>97</sup>

With respect to the sometimes sharp boundaries where SCC occurs, as illustrated in Figures 11-14, normal environments are quite variable. Figure 47 shows three examples of such highly variable behavior. Figure 47a shows the effect of oxygen on the potential at 274°C from the work of Indig and McIlree.<sup>147</sup> Many others have found the same results. This figure shows that the open circuit potential can increase by about 700 mV when the dissolved oxygen is changed from 1 ppb to 1 ppm. Such a large effect is the basis for many of the oscillations in potential in commercial equipment using aqueous environments. Figure 47b shows the variation of potential measured in sea water on a platinum electrode over a period of 13,000 hours.<sup>148</sup> Figure 47c shows how the open circuit potential on the surface of sensitized 304 stainless steel varies in a 0.35% NaCl solution at 50°C when the specimen is stressed to 1.7 Sy without a crevice geometry. Interactions of such variable potentials with the relatively narrow ranges and sharp transitions, as in Figure 13, over which SCC occurs, indicates why the occurrence of SCC is so variable in operating equipment.

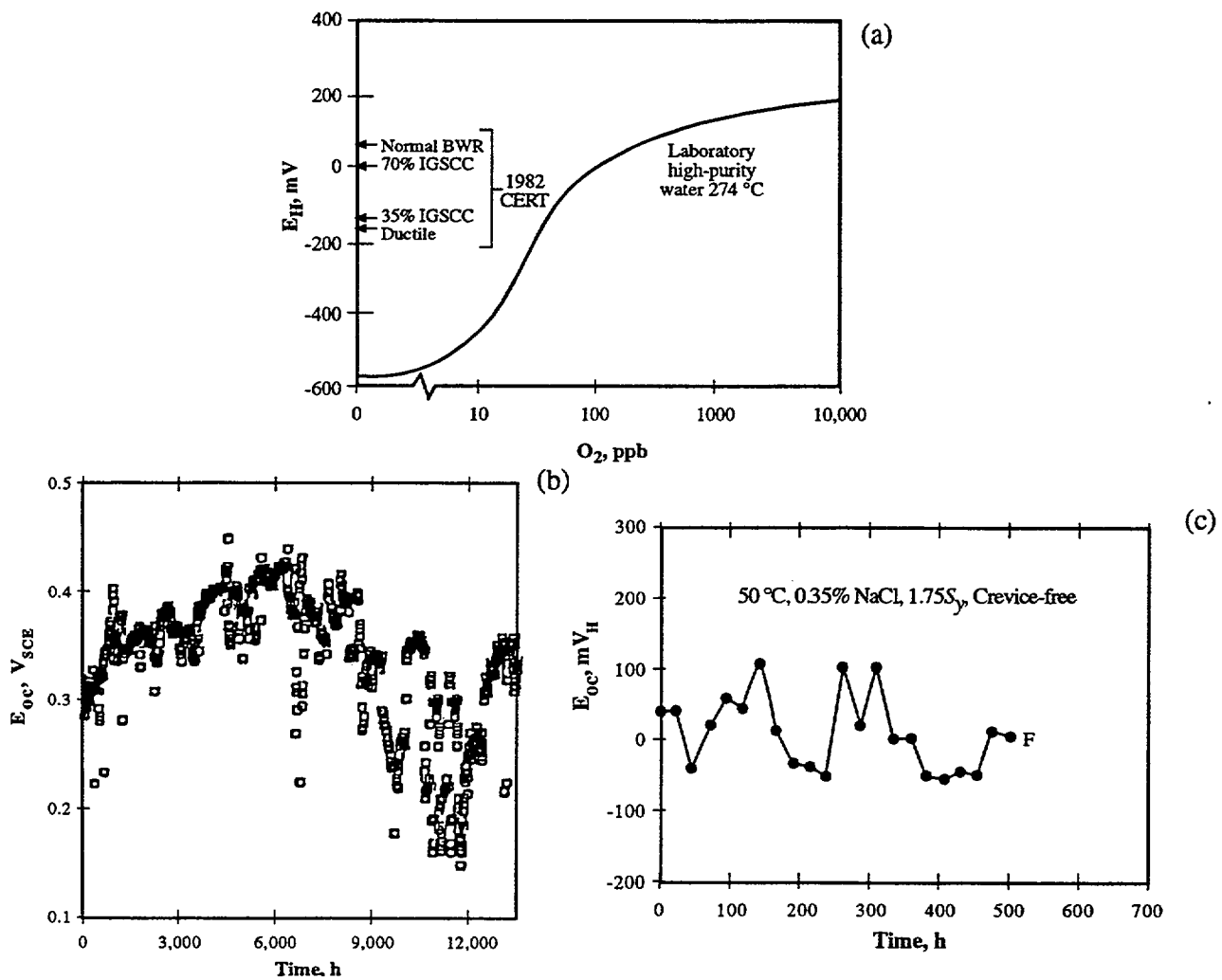


Figure 47: (a) Potential vs. oxygen concentration for stainless steel at 274°C. Relationship to the onset of IGSCC of sensitized stainless steel is shown based on testing with CERT specimens. Adapted from Indig and McIlree.<sup>147</sup> (b) Open circuit potential vs. time for platinum in flowing sea water. From Salvago et al.<sup>148</sup> (c) Open circuit potential vs. time for sensitized Type 304 stainless steel exposed at 50°C in 0.35% NaCl at 1.75S<sub>y</sub> with no crevices present. From Nakayama et al.<sup>105</sup>

The effectiveness of heat transfer crevices, such as those shown in Figure 4, in concentrating species from even nominally pure environments is shown in Figure 48 from the work of Takamatsu et al.<sup>149</sup> Such concentration processes are part of the accumulation of the  $\beta=4$  pattern shown in Figure 26d. Here, in Figure 48, concentration factors up to  $10^4$  are shown for the cations Na<sup>+</sup> and K<sup>+</sup> while concentration factors of  $10^3$  are shown for anions, Cl<sup>-</sup> and F<sup>-</sup>. These concentrations occur after exposures of from 17 to 1650 hours to heat fluxes of  $7.5$  to  $9.3 \times 10^4$  kcal/m<sup>2</sup>hr. Surface temperatures are in the range of SG operating conditions, and the environments are obtained from a side stream from an operating SG. These concentrations change the local chemistry to which tube surfaces are exposed and permit modes of SCC which could not occur in the pure bulk water.



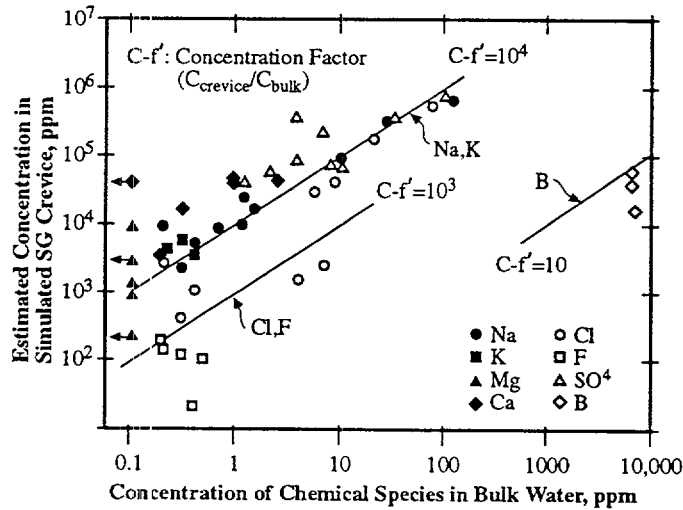


Figure 48: Estimated concentration in heated crevice of a SG geometry vs. bulk water chemistry. Concentration of anions and cations studied under conditions of SG secondary water chemistry at relevant heat fluxes. From Takamatsu et al.<sup>149</sup>

## 5.2 Chemical Effects

Effects of chloride concentration on the distribution of data for the SCC of stainless steels is shown in Figure 49 for both concentrated and dilute solutions. Figures 49a and 49b show the effects of concentrated solutions of  $\text{CaCl}_2$  on the SCC of 304 stainless steel. The data of Figure 49a are correlated in Figure 49b. The expected trends of decreasing  $\theta$  and  $t_o$  are evident. The large decrease in  $\beta$  is contrary to the expectation that increasing the stressor should increase  $\beta$ . However, it is clear that such an expectation is not well founded as indicated for the opposite effects of another stressor, stress, in comparing the dependencies of  $\beta$  on stress in Figures 29 and 30. The decrease in  $\beta$  with increasing concentration suggests that the initiation of SCC is progressively more dominant as illustrated in Figure 31 and 32.

For the dilute chloride solutions in Figure 49c and d, the concentration of chloride produces an opposite effect on  $\beta$  compared with the concentrated  $\text{CaCl}_2$ . Here, the  $\theta$  decreases with increasing concentration.  $t_o$  decreases with increasing concentration, which is an expected result.  $\beta$  increases significantly with increasing concentration, indicating that the SCC is much more controlled by propagation than initiation.

Shibata et al.<sup>121</sup> have correlated the effects of concentration and temperature of  $\text{CaCl}_2$  on the SCC of Type 304 stainless steel and have also determined the effect of concentration on the times for initiation, propagation and failure; values of  $\beta$  have also been determined. These results are shown in Figure 50. Figure 50b shows that increasing concentrations and temperatures at first lower the median time-to-failure; at about 15 w/o  $\text{CaCl}_2$ , the median time-to-failure is independent of concentration. For the total time-to-failure,  $\beta$  increases with increasing concentration as shown in Figure 50a; and the initially low values, typical of Poisson behavior, increase with increasing concentrations, indicating propagation control. This pattern is opposite to that in Figure 49a. Figure 50a shows that  $\beta$  for the initiation stage is unity in accordance with expectations for a surface-related process. The higher values of  $\beta$  for the total failure indicate that it is dominated by propagation. The separation of initiation and propagation stages and the relative magnitudes of the initiation stage is consistent with the examples of Figure 31 and 32.

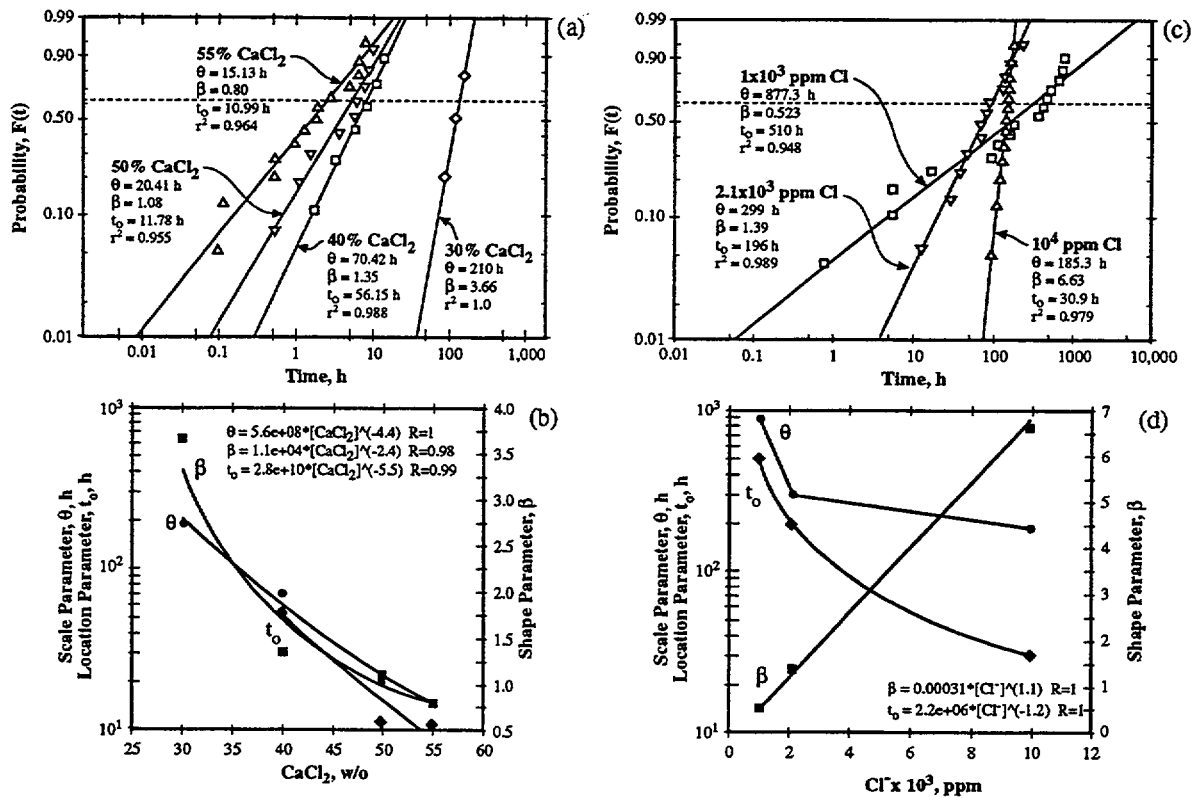


Figure 49: (a) Probability vs. time for SCC of Type 304 stainless exposed to high concentrations of  $\text{CaCl}_2$  at 100°C and 200MPa. From Shibata et al.<sup>150</sup> (b) Correlation of data from (a). (c) Probability vs. time of sensitized Type 304 exposed to dilute solutions of chloride and stressed at 1.75 $S_y$  at 80°C in the creviced condition. Data originally plotted as linear  $H(t)$  vs. time-to-failure. From Nakayama et al.<sup>105</sup> (d) Correlation of data from (c).

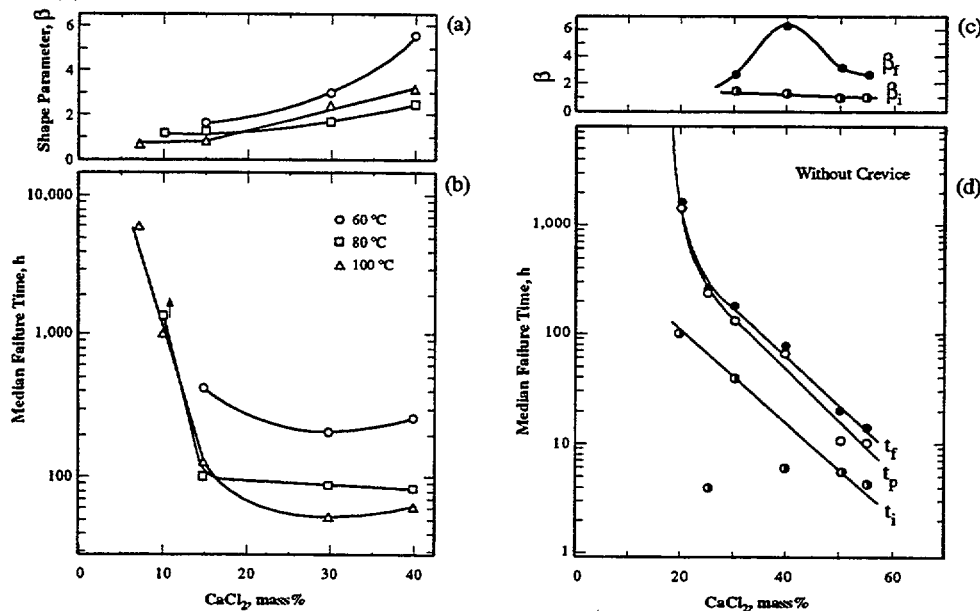


Figure 50: (a)  $\beta$  vs. concentration of  $\text{CaCl}_2$  for the failure times of SCC of Type 304 stainless steel at three temperatures. Adapted from Shibata et al.<sup>150</sup> (b) Median failure time vs. concentration of  $\text{CaCl}_2$  for the SCC of Type 304 stainless steel exposed to three temperatures. Adapted from Shibata et al.<sup>150</sup> (c)  $\beta$  vs. concentration for initiation and failure times as a function of  $\text{CaCl}_2$  for 100°C. Adapted from Shibata et al.<sup>121</sup> (d) Median failure time vs. concentration of  $\text{CaCl}_2$  for the SCC of Type 304 stainless steel. Adapted from Shibata et al.<sup>121</sup>

The distribution of SCC data in the presence and absence of crevices has been investigated by Nakayama et al.,<sup>105</sup> and their results are shown in Figure 51. The values of  $\theta$  are not significantly different; however,  $\beta$  values show that outside the crevice the conditions are more random and unbounded and favor an interpretation of the  $\beta=1$  condition. The  $\beta=1.49$  for the creviced case relative to the  $\beta=0.87$  of the non-crevice case suggests that the crevice case involves some accumulation processes possibly similar to those in Figure 48.

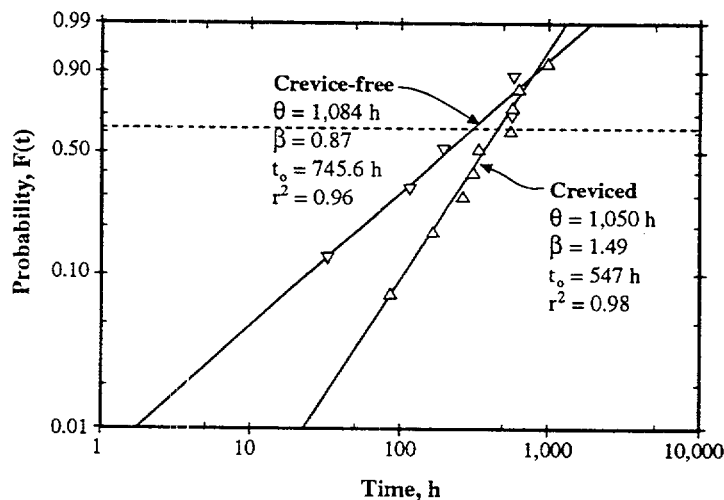


Figure 51: Probability vs. time for the SCC of sensitized 304 stainless steel exposed to 0.35% NaCl at 30°C and a stress of 1.75S<sub>y</sub>. Specimens tested in the creviced and crevice-free condition. From Nakayama et al.<sup>105</sup>

In contrast to the generally concentrated environments studied in Figures 49-51, extensive monitoring of SGs for PWR plants has provided data sufficient to determine the distributions of SCC on primary and secondary sides as shown in Figure 52. The data in this figure were shown originally on separate figures<sup>27</sup> and is collected in Figures 52a and 52b for primary and secondary sides, respectively. Figure 52a shows that values of  $\beta$  are mostly in the  $\beta=4$  range with one at 1.36. Data in Figure 52b for the secondary side also show values of  $\beta$  in the range from 4.45 to 5.86. Taken together, these data indicate high slopes in spite of the possible lowering of slopes as indicated by the processes Figures 22 and 27. These high slopes might be associated with early failures due to the high susceptibility of certain heats as suggested by the data of Figure 38. The data in Figure 5b are similar to those shown in Figure 52 except that the latter data show SCC at multiple locations.

Increasing flow of the environment increases the pitting potential, and this effect on the distribution of data has been studied by Shibata and Zhu<sup>151</sup> for Type 304L stainless steel in 3.5% NaCl solution with nitrogen saturation at 35°C. Potentials were measured at a scan rate of 480 mV/min. The effect of flow on the pitting potential is shown in Figure 53a, and the data are correlated in Figure 53b. Increasing flow by a factor of five increases the pitting potential about 90 mV. Values of  $\beta$  are high, between 9.71 and 15.5, indicating that the data are not significantly dispersed.

Whereas, increasing flow decreases the tendency for pitting, high velocities sometimes produce erosion corrosion. Figure 53c shows the distribution of data for the erosion of tubes on the secondary side of a once-through steam generator. The  $\beta$  for this process is unity, as would be expected for a totally surface related process.

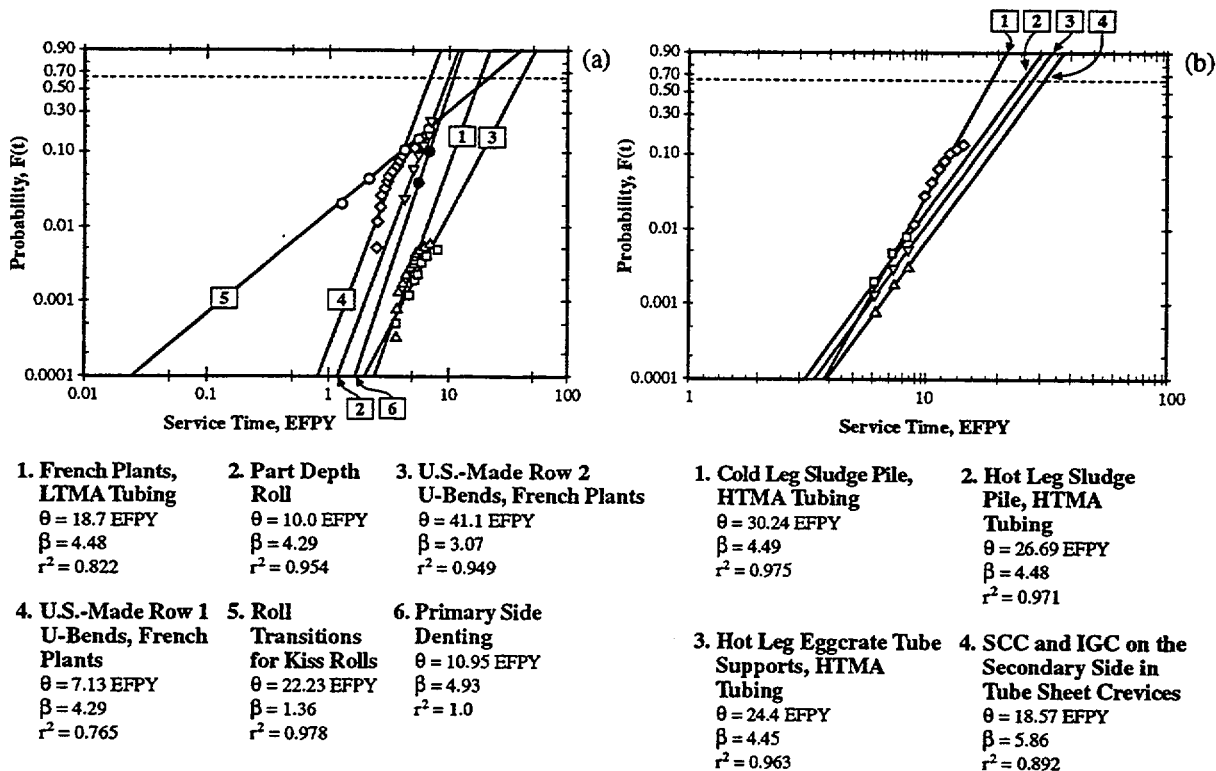


Figure 52: (a) Probability vs. service time (equivalent full power years) for the LPSCC occurring on the primary side of tubes from operating SGs in PWRs. Temperatures are in the range of 315 to 320°C. (b) Probability vs. time for IGA/IGSCC occurring on the secondary side of tubes from operating SGs. SCC occurs at locations of heated crevices at tube supports, tube sheets and top of the tubesheet sludge piles as shown in Figure 4. From Staehle et al.<sup>27</sup>

### 5.3 Temperature

The distribution of data for the occurrence of SCC-related failure in operating heat exchangers from 50 to 200°C is shown in Figure 54a, and the data are correlated in Figure 54b. Here,  $\theta$  increases with  $1/T$  as expected. The increase of  $\beta$  with  $1/T$  is opposite to expected behavior. However, this expected trend with increasing value of stressors seems not to be a good generalization as indicated by comparing data that show opposite effects of stress in Figures 29 and 30.

The effect of temperature, in a temperature range similar to that in Figure 54, has been studied in the laboratory where stainless steel has been exposed to concentrated  $MgCl_2$  at temperatures between 126 and 154°C. These data are shown in Figures 55 and 56. Figure 55 shows data from Shibata<sup>16</sup> where he has determined the initiation and propagation behavior for Type 304 stainless steel in concentrated  $MgCl_2$  as a function of temperature. Figure 55c shows that the overall time-to-failure is generally constant, while the mean time to initiation increases; and the mean time for propagation decreases. In accordance with this pattern, the values of  $\beta$  for initiation are about unity and the values for propagation are generally higher except at the lower temperature.  $t_0$  increases for initiation and for the overall time-to-failure; whereas,  $t_0$  for propagation is lower. This behavior fits the pattern predicted by Shibata in Figure 31a. The  $\beta=1$  behavior for initiation is consistent with surface-related processes discussed in connection with Figure 17.

The data in Figure 55 for  $t_0$  have been re-analyzed and are shown in Figure 56 for the Weibull three-parameter fit using the methods in this report. The distributions are shown in Figure 56a, and the correlations are shown in Figure 56b. The results are generally similar to those in Figure 55.  $\theta$  decreases with  $1/T$  and  $\beta$  also increases with  $1/T$ . The trend of  $t_0$  in Figure 56b is the same as that in Figure 55b, increasing as the temperature increases. It should be noted that the plots in Figure 56 show  $t - t_0$  and  $\theta - t_0$ .

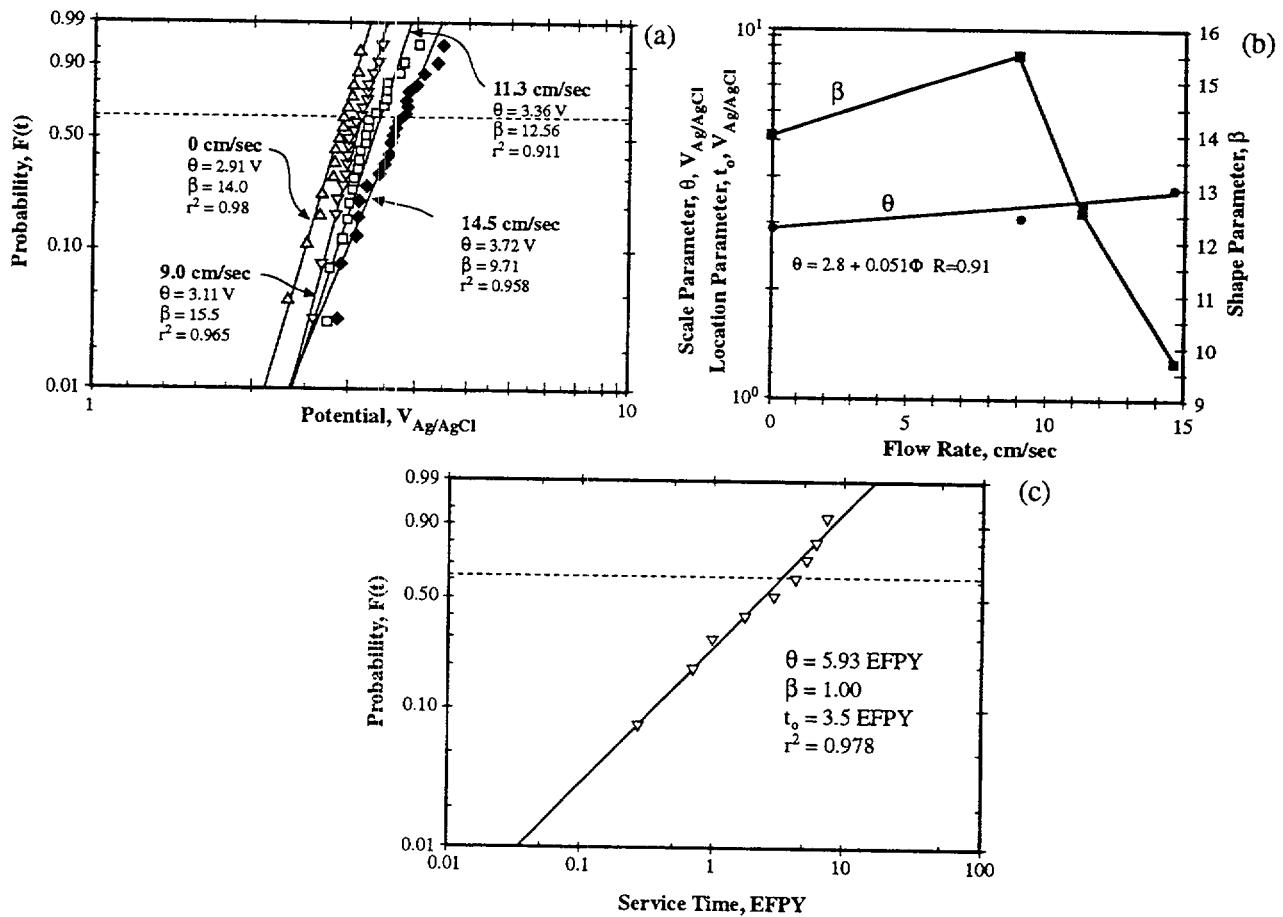


Figure 53: (a) Probability vs. pitting potential measured at flow velocities of 9.0, 11.3 and 14.6 cm/s. The specimens were pretreated at 3V in 0.5  $H_2SO_4$  for 1 hour. Originally plotted as normal probability. From Shibata and Zhu.<sup>151</sup> (b) Correlation of data in (a). (c) Probability vs. service time for tubes plugged due to erosion-corrosion on the secondary side in a once-through steam generator. From Staehle et al.<sup>27</sup>

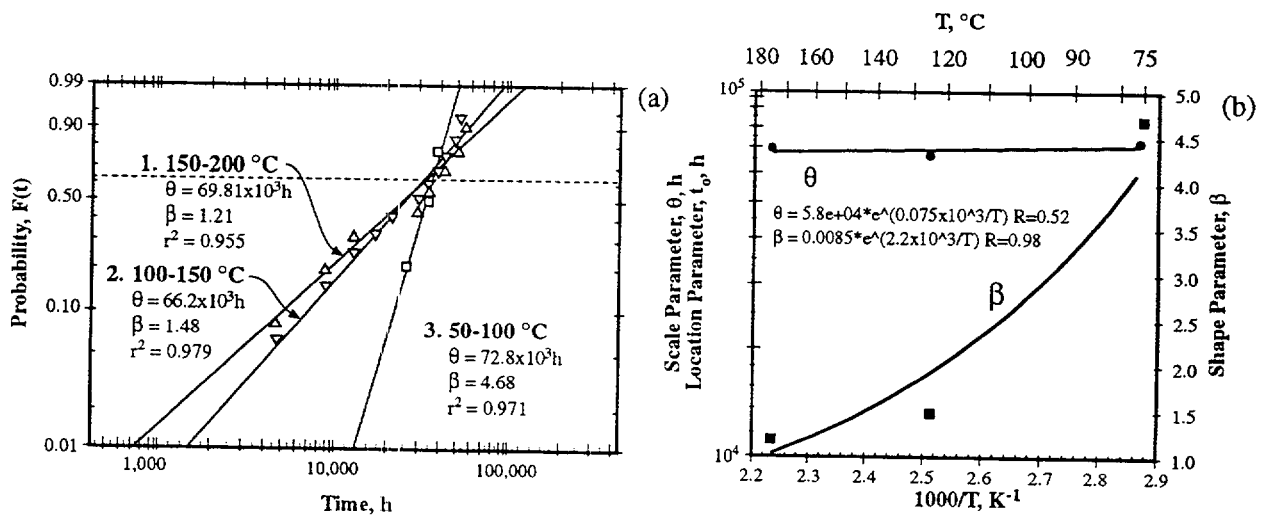


Figure 54: (a) Probability vs. time for SCC failures as a function of temperature in stainless steel heat exchangers using industrial water in the chemical industry. Original data plotted as  $H(t)$  vs.  $t$  based on exponential distribution. (b) Correlation of  $\theta$  and  $\beta$  vs.  $1/T$ . From Shibata.<sup>16</sup>

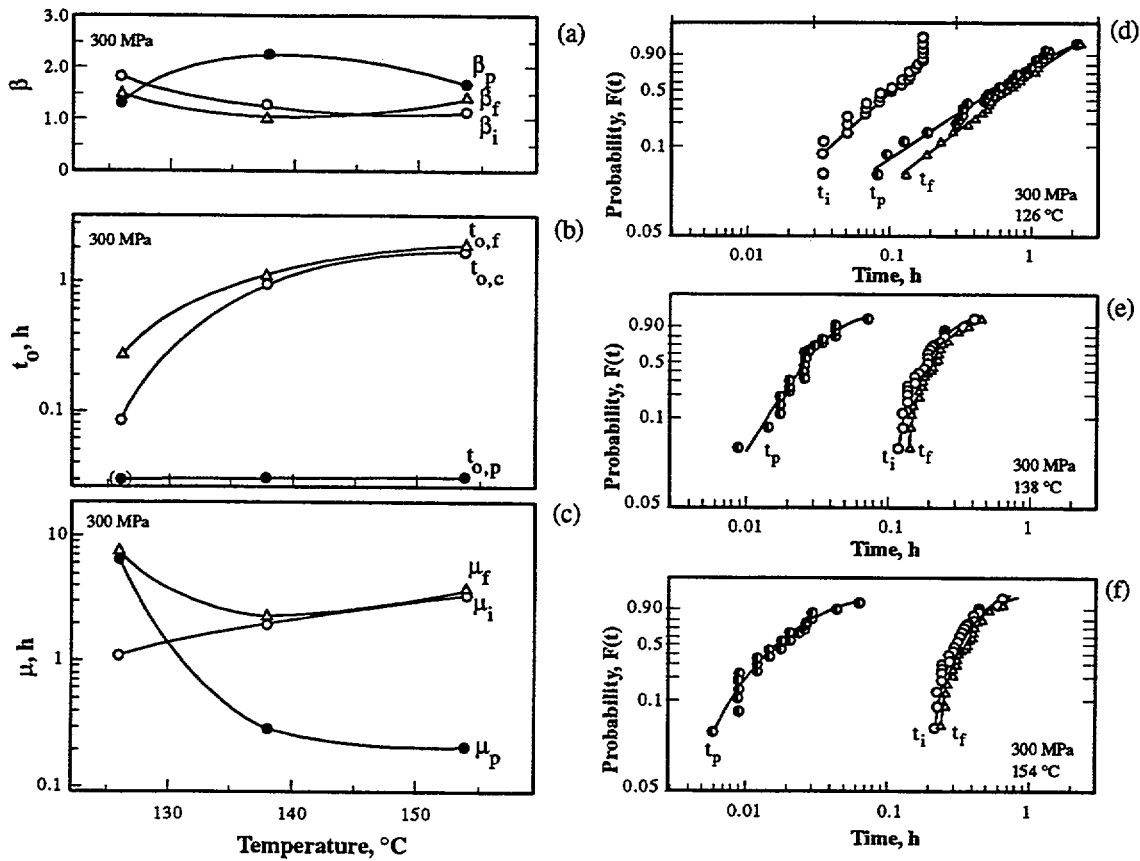


Figure 55: (a)  $\beta$  vs. temperature for initiation, propagation and failure of Type 304 stainless steel by SCC. (b)  $t_o$  vs. temperature for initiation, propagation and failure by SCC. (c) Mean time for initiation, propagation and failure vs. temperature. (d) Probability vs. time for times for initiation, propagation and failure at 126°C. Original data on Weibull coordinates as are the data in this figure. (e) Same as (d) for 138°C. (f) Same as (d) for 154°C. Data obtained in concentrated  $MgCl_2$  solutions. From Shibata.<sup>16</sup>

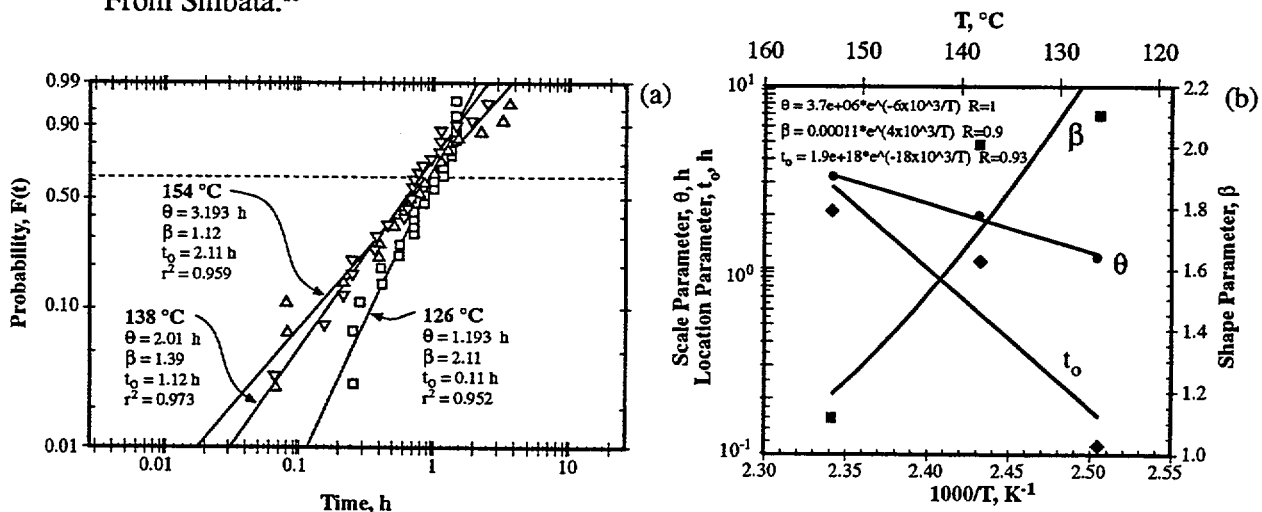


Figure 56: (a) Probability vs. time for  $t_i$  by SCC of Type 304 stainless steel exposed to a concentrated  $MgCl_2$  solution. (b) Correlation of data for  $\theta$ ,  $\beta$ , and  $t_o$  vs. temperature. Original data plotted in exponential distributions. Adapted from Shibata.<sup>16</sup>

The effect of temperature has been studied over a wider range in high purity water<sup>42,153</sup> from 25 to 300°C for sensitized stainless steel as shown in Figure 57. The original plot of data is shown in

Figure 57a. Here, a range of data was correlated for the rate of SCC as a function of temperature. The distribution of these data is shown in Figure 57b and the correlation of  $\theta$ ,  $\beta$ , and  $t_0$  is shown in Figure 57c. In Figure 57c the normalized propagation rates, as  $\theta$ , increase with increasing temperature as shown in Figure 57a. Values of  $t_0$  are generally constant except for a lower value at 50°C.  $\beta$  decreases monotonically with increasing temperature, suggesting, nominally, that the processes of SCC are becoming more Poissonian; however, since these data are an aggregation, it is more reasonable that the decrease in  $\beta$  results from the mixing effect shown in Figures 22 and 27. Andresen suggests that this “scatter” in his terms is due to the inter-dependency among parameters. It is more likely an effect due to non-coherency.

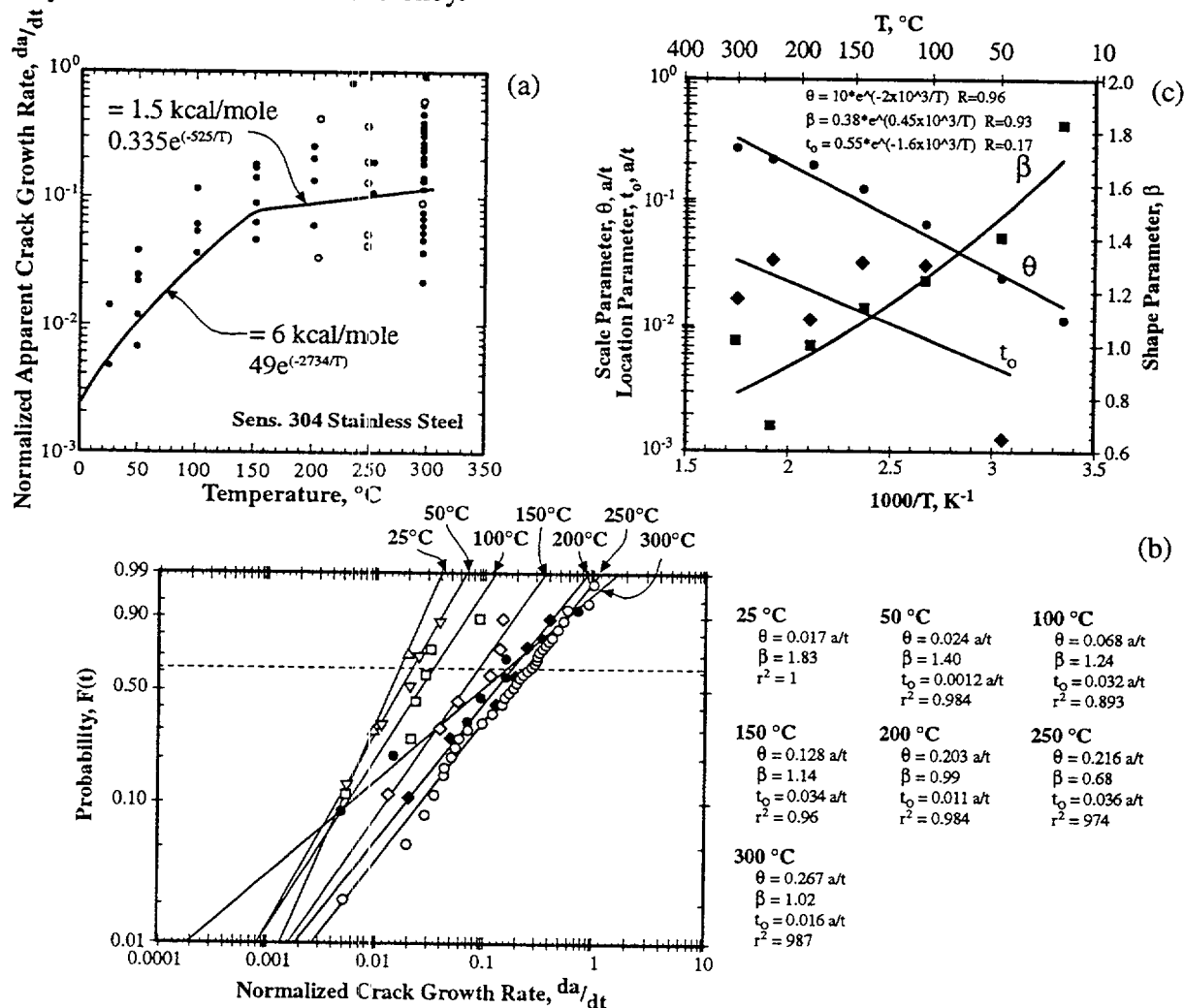


Figure 57: (a) Normalized crack growth rate vs. temperature for sensitized Type 304 stainless steel exposed to high purity oxygenated water. Data analyzed by Eason and Padmanaban<sup>152</sup> and published by Andresen.<sup>42</sup> (b) Probability vs. normalized crack growth rate for temperatures from 25 to 300°C. (c) Correlation of data from (b) for  $\theta$ ,  $\beta$ , and  $t_0$  vs.  $1/T$ .

Data from the higher end of the temperature range are shown in Figure 58 from studies of LPSCC in high purity and deoxygenated water applicable to the primary side of PWRs. Here, distributions obtained over temperatures from 288 to 400°C are shown from two investigations. Figures 58a and 58b from the work of Webb,<sup>24</sup> include data that have been taken in aqueous solutions; Figures 58c and 58d are taken from both water at 360°C and steam at 400°C.  $\theta$  for time-to-failure in Figure 58b increases linearly vs.  $1/T$  and follows an expected pattern.  $\beta$  decreases with  $1/T$ , which is consistent with the expectation from the effect of stressors, although this is opposite to the patterns

exhibited at lower temperatures in Figures 54 and 56 as well as for the crack growth rate over temperature in high purity oxygenated water shown in Figure 57. The same trends are exhibited by the work of Jacko<sup>153</sup> in Figure 58c and d although there are only two data points.

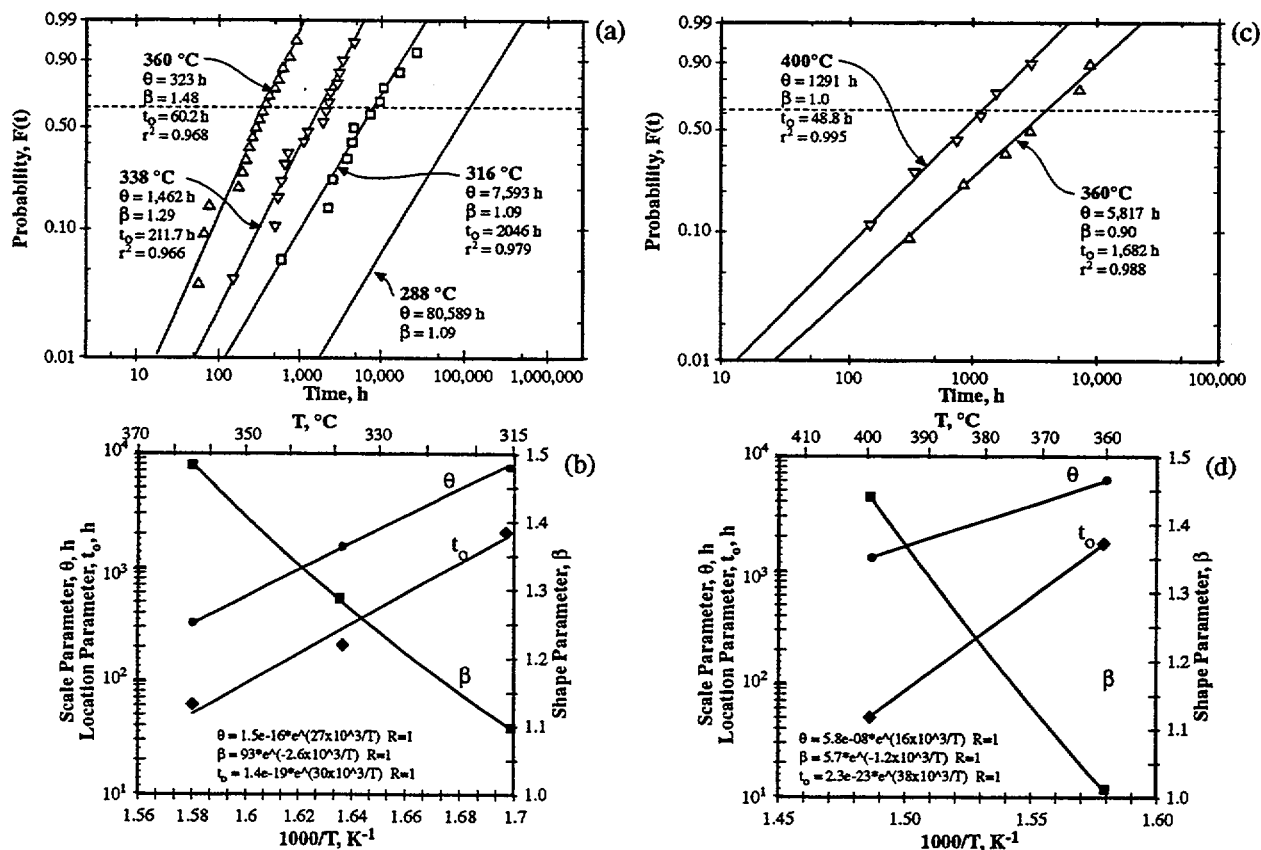


Figure 58: LPSCC of Alloy 600 MA. (a) Probability vs. time to fail by LPSCC for a temperature range of 288 to 360°C for testing in high purity deoxygenated water containing a hydrogen concentration of 10-60 cc  $H_2$ /kg  $H_2O$ . From Webb.<sup>24</sup> (b) Correlation of data in (a) for  $\theta$ ,  $\beta$ ,  $t_0$  vs.  $1/T$ . (c) Probability vs. time to fail by LPSCC in high purity water and steam for 360°C water and 400°C steam with 1 psia hydrogen in the former and 11 psia steam in the latter. From Jacko.<sup>153</sup> (d) Correlation of data in (c) for  $\theta$ ,  $\beta$ , and  $t_0$  vs.  $1/T$ .

## 5.4 Stress

Most of the distributions concerned with the effect of stress have been obtained with initially smooth surfaces as occur in tensile bars, CERT tests, U-bends, C rings, and stressed tubes. Thresholds for SCC of smooth surfaces on alloys described in this report have been determined by many authors including van Rooyen,<sup>9</sup> Webb,<sup>24</sup> Scott et al.<sup>155</sup> Theus,<sup>156</sup> Magdowski and Speidel,<sup>157</sup> Shoji,<sup>94</sup> Amzallag et al.<sup>158</sup> The existing data for the effect of stress on SCC in  $MgCl_2$  environments are summarized in Figure 2 where the stress exponents vary from 0.5 to 9.

Sensitized Type 304 stainless steel has been exposed to the solution specified for the "Strauss Test," a copper-copper sulfate-sulfuric acid solution (6 weight %  $CuSO$  and 16 weight %  $H_2SO_4$ ), and the distribution of failures have been measured as a function of applied stress.<sup>159</sup> These results are shown in Figure 59. Figure 59a shows the distributions and Figure 59b shows the correlations of statistical parameters with stress.  $\theta$  exhibits a stress exponent of -3.8 and  $t_0$  a stress exponent of -2.8. This test environment is aggressive to sensitized stainless steel, and the possible effects of intergranular corrosion seem important at the low stresses. However, at higher stresses the SCC seems less connected to surface processes based on the increasing values of  $\beta$ . The parallel decrease in  $t_0$  with  $\theta$  is expected although there is no more formal basis for this expectation than for the dependencies of  $\beta$  on stressors.



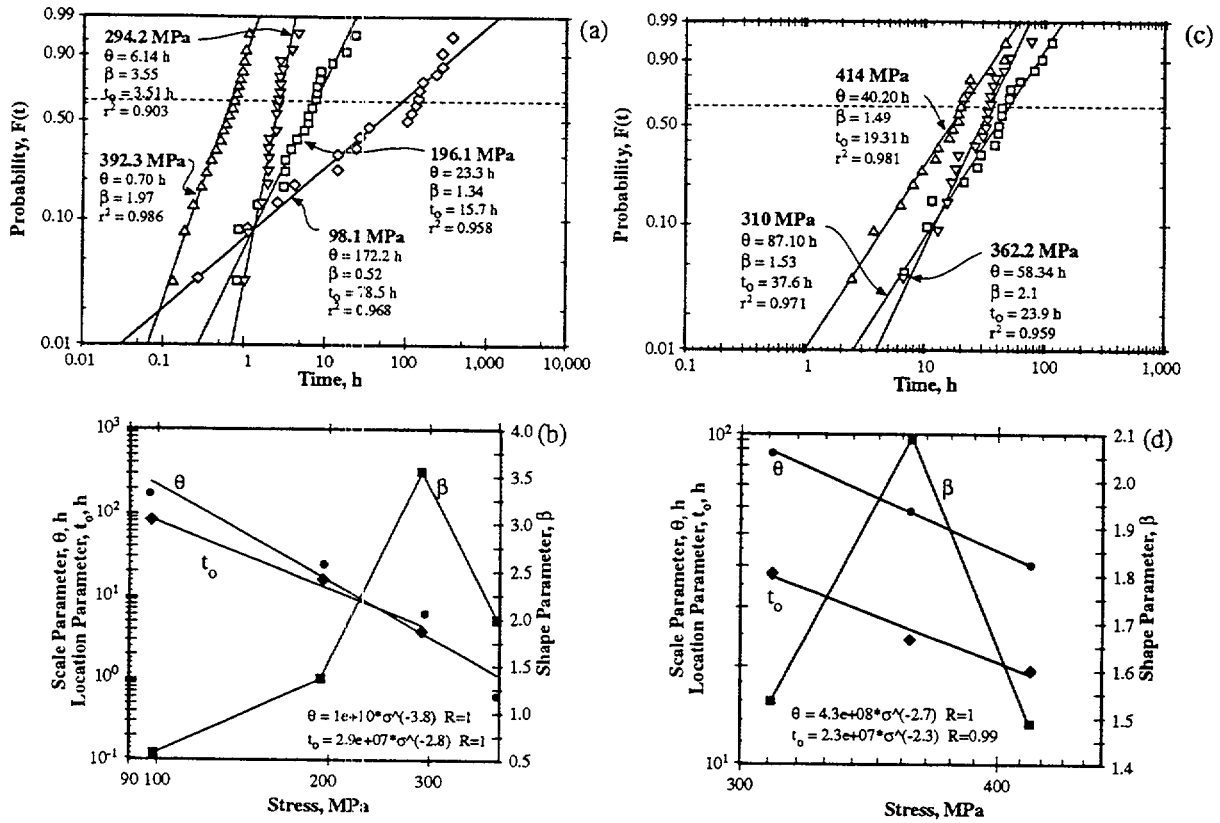


Figure 59: Probability vs. time for SCC of sensitized Type 304 stainless steel in the “Strauss Test” solution, a copper-copper sulfate-sulfuric acid solution (6 weight % CuSO and 16 weight % H<sub>2</sub>SO<sub>4</sub>), tested in uniaxial load at 100°C at four stresses. From Yamauchi et al.<sup>159</sup> (b) Correlation of  $\theta$ ,  $\beta$ ,  $t_0$  from (a) with stress. (c) Probability vs. time for SCC of sensitized Type 304 stainless steel exposed to a 0.35% NaCl solution at 80°C and no crevices present. From Nakayama et al.<sup>105</sup> Data originally plotted linearly as  $H(t)$  vs. time-to-failure (d) Correlation of data from (c).

Figure 59c and 59d show distributions from the same range of temperature as for Figure 59a. The  $\theta$  and  $t_0$  as in Figure 59b have parallel slopes both decreasing with increasing stress. The stress exponent for  $\theta$  and that of  $t_0$ , -2.7 and -2.3 respectively, are in the same range as for Figure 59b. The increase and decrease of  $\beta$  in Figure 59d provide no obvious clue to its pattern.

Increasing the temperature to 154°C in boiling MgCl<sub>2</sub>, Figure 60 shows two sets of data for Type 304 and Type 310 stainless steel from Shibata and Takayama<sup>120</sup> and Cochran and Staehle,<sup>141</sup> respectively. The distributions are shown in Figures 60a and 60b, and the correlations with  $\theta$ ,  $\beta$ , and  $t_0$  are shown in Figure 60c. For the Type 304,  $\theta$  exhibits a slope of -2.1, somewhat lower than in Figure 59 but the  $\theta$  for Type 310 is more shallow.  $t_0$ , for both alloys is generally parallel to the  $\theta$ . Values of  $\beta$  for the two alloys seem consistent in the sense that the peaks somewhat overlap; the peak in  $\beta$  in the mid-range of testing temperature seems to be consistent and suggests a significant although not understood effect. This peak is similar to that in Figure 49d for the chloride solution at 80°C. This mid-range of temperature favors a more propagation-dominated pattern of  $\beta$  in view of the higher values.

Figure 61 shows results from a set of experiments conducted by Shibata et al.<sup>160</sup> on Type 304 stainless steel exposed to boiling MgCl<sub>2</sub> but only for the initiation stage. In this case the final failure is dominated by the initiation stage so that the results of Figure 61, which are nominally for data for initiation, may be taken as similar to failure.\* The distribution is shown in Figure 61a, and the correlation of statistical parameters is shown in Figure 61b. The slope for  $\theta$  is -1.2, somewhat more shallow than those in Figure 59 and 60. The slope and values of  $t_0$  do not suggest a special pattern. No  $t_0$  is available from the 100 MPa stress. In Figure 61b the  $\beta$  exhibits the same peak as shown in Figure 60 suggesting that there is some validity to such peaks.

\* Personal Communication with Prof. T. Shibata, Osaka University, November 27, 2000.

An integrated view of the effect of stress on  $\theta$ ,  $\beta$ , and  $t_0$  is shown in Figure 62 for Type 304 stainless steel in boiling  $MgCl_2$ . Here, the mean values of failure time are close to the mean time for initiation, and the mean times for propagation are relatively short. The failure time is dominated by initiation.  $t_0$  for failure decreases with increasing stress, but the separate values for propagation and initiation are different. The  $\beta$  for final failure increases with stress and suggests progressively more involvement of propagation; however, this is not supported by the pattern of  $t_0$  and the value of  $\mu$ .

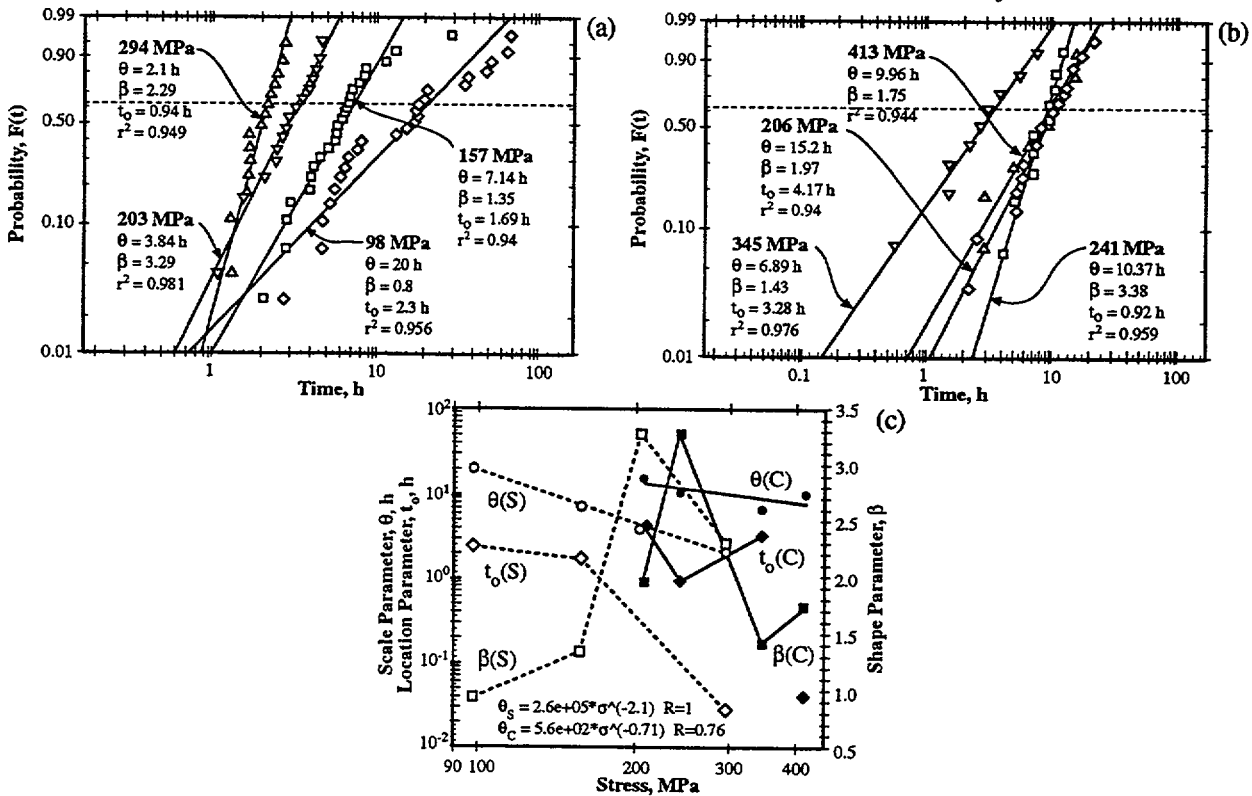


Figure 60: (a) Probability vs. time for SCC of Fe-17Cr-11Ni stainless steel exposed to boiling  $MgCl_2$  at 154°C and tested at four stresses. These data are a three-parameter fit of the data shown in Figure 31b. From Shibata and Takeyama.<sup>120</sup> (b) Probability vs. time for SCC of Type 310 stainless steel exposed to boiling  $MgCl_2$  at 154°C and tested at four stresses. Specimens were prestrained to 130% yield strength. From Cochran and Staehle.<sup>141</sup> (c) Correlation of  $\theta$ ,  $\beta$ ,  $t_0$  vs. stress.

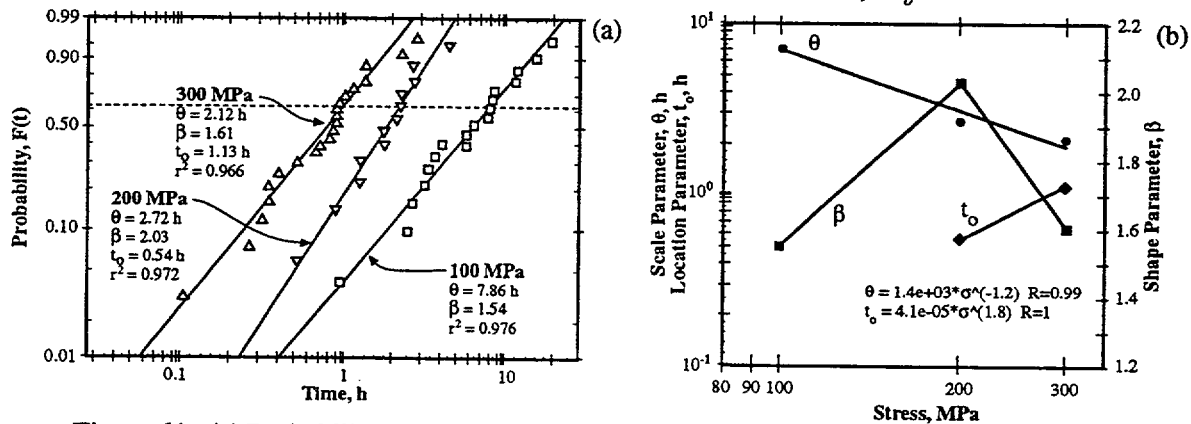


Figure 61: (a) Probability vs. time for SCC of Type 304 stainless steel tested in  $MgCl_2$  at 138°C tested at three stresses for the initiation stage. Data originally plotted in exponential coordinates as  $R(t)$ . From Shibata et al.<sup>160</sup> (b) Correlation of  $\theta$ ,  $\beta$ ,  $t_0$  vs. stress.

Distributions for various stresses for carbon steel and Alloy 750 are shown in Figure 63a and 63c. Correlations are shown in Figures 63b and 63d. In both cases the stressed alloys are exposed to

high purity water. For the carbon steel the water is pure but oxygenated; for the Alloy 750 the water is pure and deoxygenated. The slopes are similar and are -3 and -3.7, respectively. In both cases the values for  $t_o$  decrease generally parallel to the values of  $\theta$ . Values for  $\beta$  in both cases are irregular; however, there is a general trend for  $\beta$  to decrease with increasing stress.

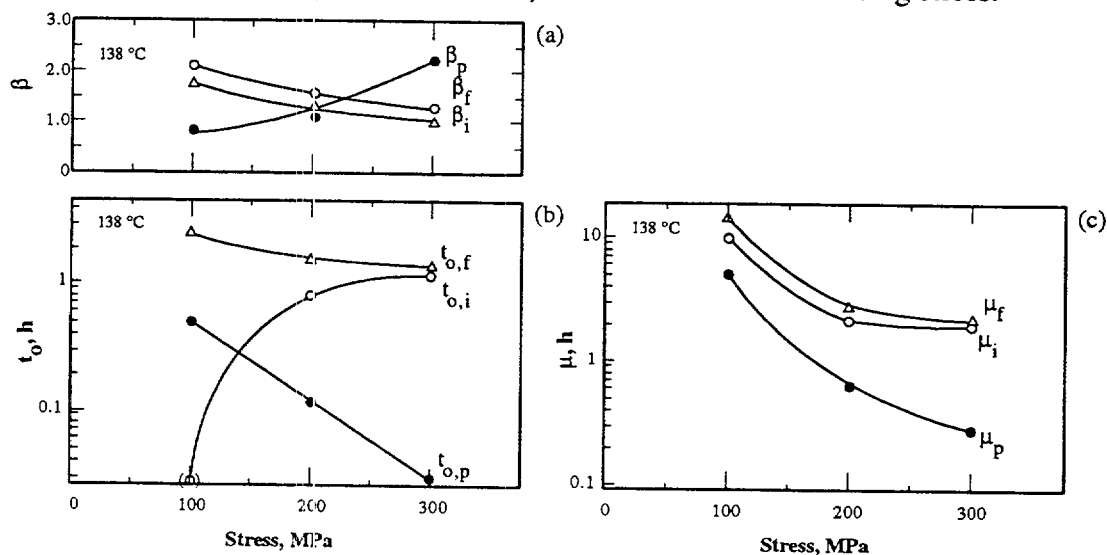


Figure 62:  $\theta$ ,  $\beta$ , and  $t_o$  for stainless steel at 138°C vs. stress; data shown for initiation, propagation and total failure. (a)  $\beta$ . (b)  $t_o$ . (c)  $\mu$ . From Shibata.<sup>16</sup>

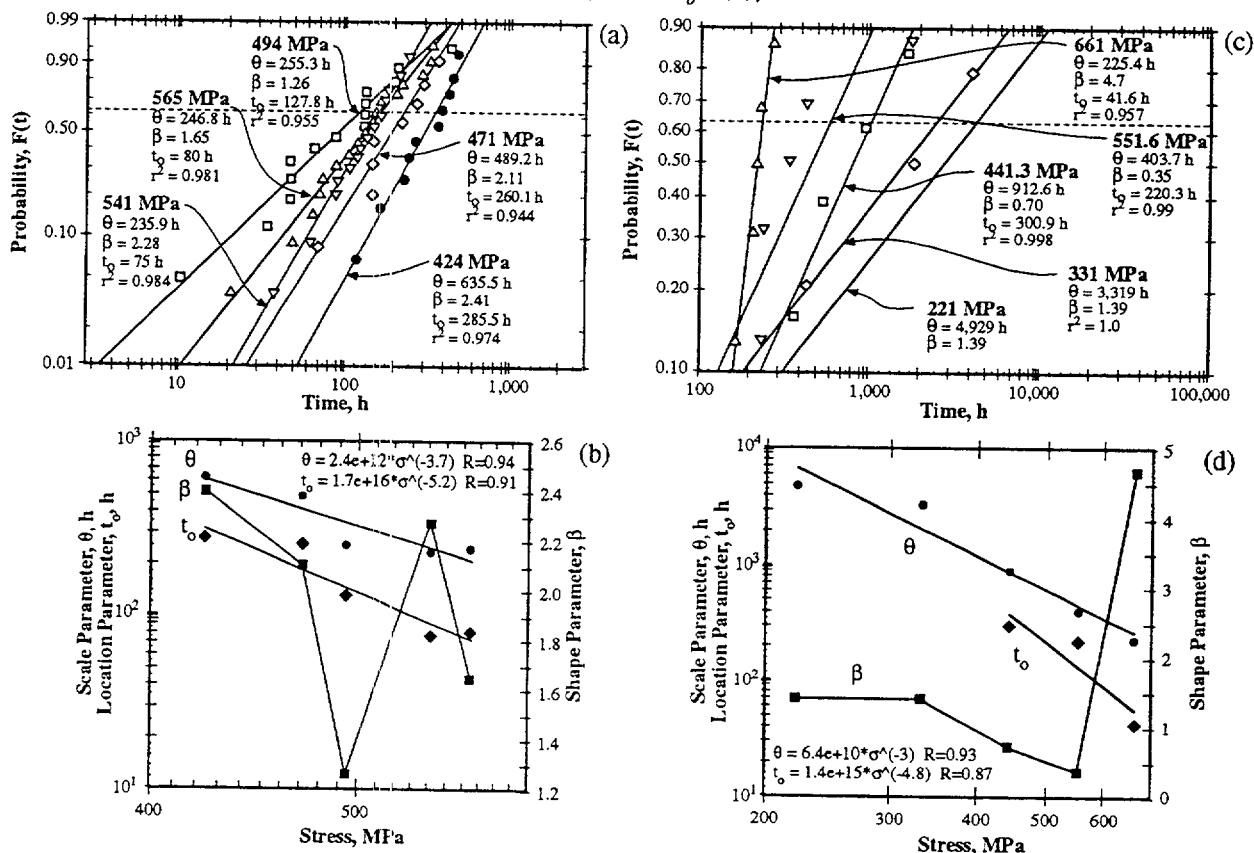


Figure 63: (a) Probability vs. time for SCC of carbon steel weld metal tested at 250°C in high purity water containing 8 ppm of dissolved oxygen. Tests conducted at constant load. Original data plotted as  $H(t)$  vs.  $t$  with exponential distribution. From Akashi and Nakayama.<sup>18</sup> (b) Correlation of  $\theta$ ,  $\beta$ ,  $t_o$  for (a). (c) Probability vs. time for SCC of Alloy 750 in 350°C water tested as tensile bars. From Blanchet et al.<sup>137</sup> (d) Correlation of  $\theta$ ,  $\beta$ , and  $t_o$  for (c).

## 6.0 CRACK SHAPES AND FREQUENCY

### 6.1 Scope

Figure 6 indicates that the early stages of SCC involve the nucleation of many small cracks. Figure 26 indicates that the formation of early and later steps relate to the values of  $\beta$ . Lower values of  $\beta$  indicate processes that occur at the surface; higher values of  $\beta$  indicate processes that relate to deeper cracks or to some kind of accumulation processes. Some work has been conducted to characterize the dimensions and frequency of occurrence of these early cracks.

Figure 64a shows results from a study by Parkins<sup>67</sup> of the conditions for coalescence of cracks. The results in Figure 64a show that well defined conditions of separation and approach favor coalescence. Figure 64b from Nakayama et al.<sup>105</sup> characterize their observations of the initiation SCC from pits and their subsequent coalescence.

The statistical aspects of the early stages of SCC are discussed here.

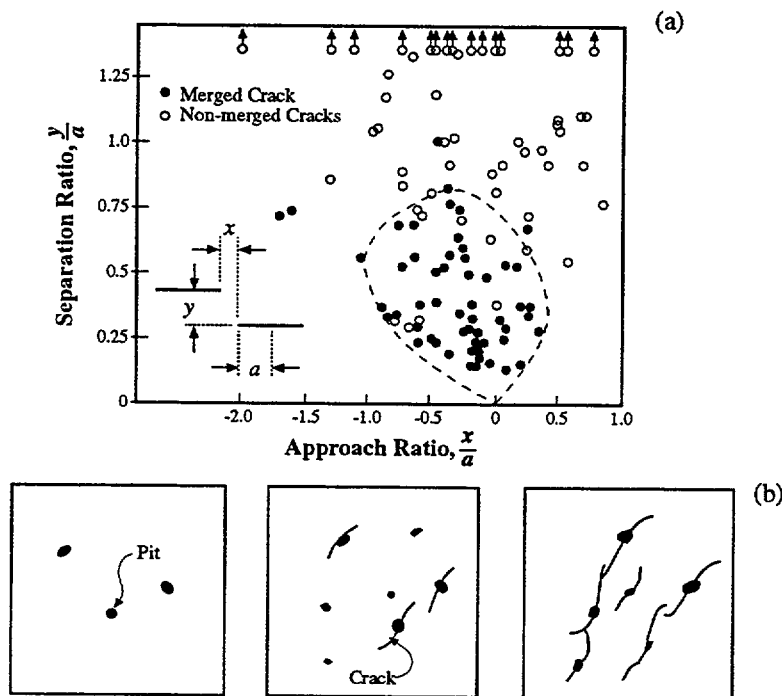


Figure 64: (a) Normalized separation distance,  $y/a$ , vs. normalized parallel approach distance,  $x/a$ , relating to the critical conditions for the coalescence of small cracks. Data obtained from ferritic steel specimens exposed to  $\text{CO}_3\text{-HCO}_3$  solution. From Parkins<sup>67</sup> and Parkins and Singh.<sup>161</sup> (b) Schematic illustration of the initiation of SCC from pits and coalescence; this is consistent with the model for initiation shown in Figure 7c. From Nakayama et al.<sup>105</sup>

### 6.2 Frequency of Surface Micro-cracks

The frequency and dimensions of surface micro-cracks formed during the early stage of SCC, through the fourth segment of Figure 6, have been studied by Shibata et al.<sup>150</sup> for Type 304 stainless steel in three concentrations of  $\text{CaCl}_2$  and at three temperatures. The results of these studies are shown in Figure 65. These results show that the density of cracks increases with concentration of  $\text{CaCl}_2$  but decreases slightly with increasing temperature although this influence seems minor. Figure 65 shows that the crack length decreases with increasing concentration of  $\text{CaCl}_2$  and also decreases with increasing temperature. Figure 65e shows that the density of cracks is related to  $\beta$  with there being an increasing density of cracks with increasing  $\beta$ .

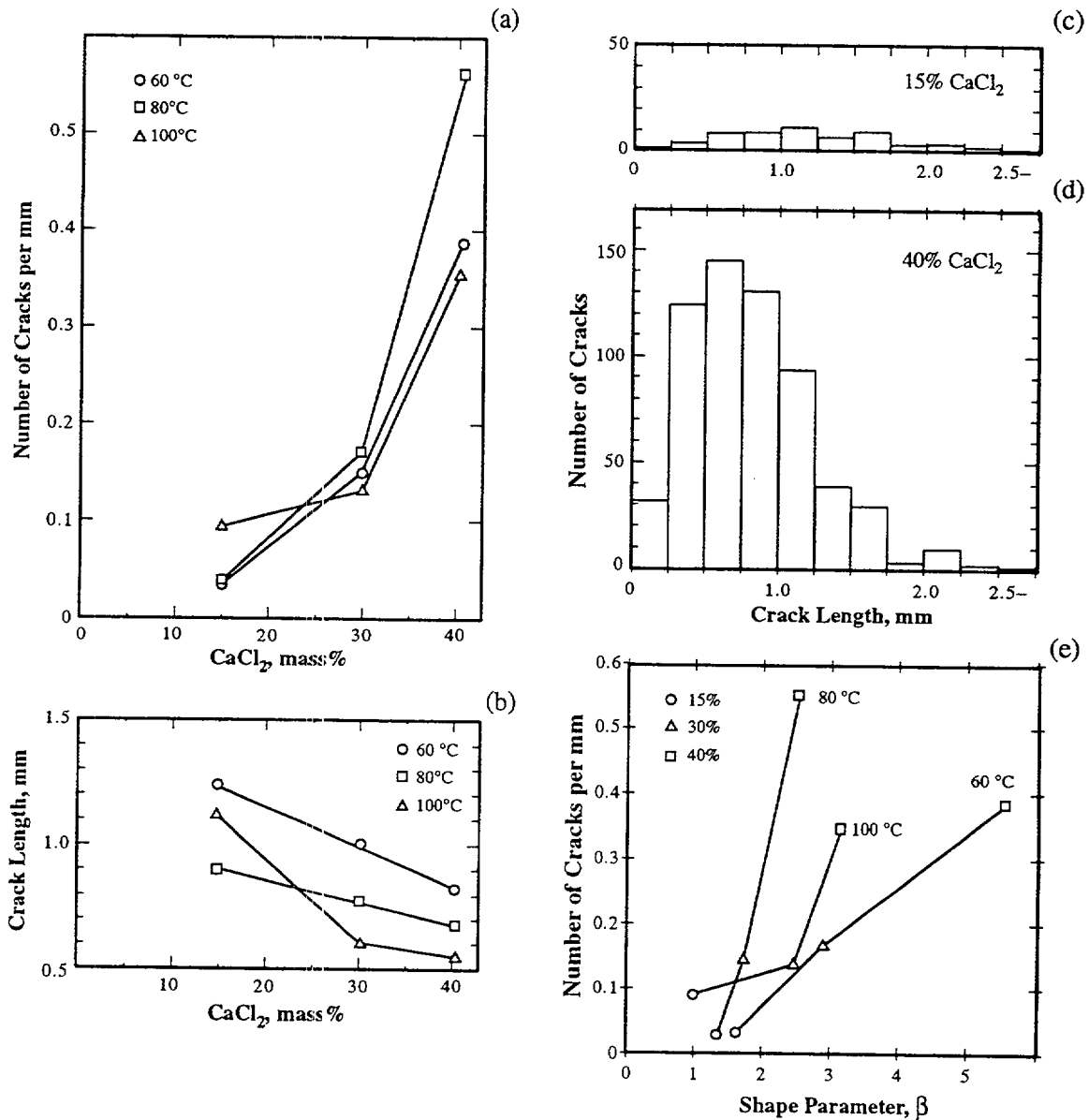


Figure 65: (a) Number of cracks per mm vs. concentration of CaCl<sub>2</sub> for three temperatures subjected to a constant applied stress of 200 MPa using a constant load apparatus with a hard spring. (b) Crack length vs. concentration of CaCl<sub>2</sub>. (c) and (d) Number of cracks related to their length for two concentrations of CaCl<sub>2</sub>. (e) Number of cracks per mm vs.  $\beta$  for three temperatures and three concentrations of CaCl<sub>2</sub>. Adapted from Shibata et al.<sup>150</sup>

The frequency and dimensions of early SCC have been studied for Type 304 stainless steel exposed at 250°C with 20 ppm dissolved oxygen. Results are shown in Figure 66 from the work of Akashi and Nakayama.<sup>18</sup> The aspect ratio seems to remain constant at least to depths of 1200  $\mu\text{m}$ . The length of small cracks in this higher temperature environment is about a factor of 10 smaller than those formed in CaCl<sub>2</sub> shown in Figure 65.

The frequency of cracks is affected by small changes in the conductivity of pure deoxygenated water as shown in Figure 67 from the work of Nakayama and Akashi.<sup>162</sup> Here, sensitized Alloy 182 weld metal was exposed to 288°C for 500 hours in a crevice bent beam (CBB) test at an applied potential of  $0.2V_{\text{H}}$ . At the larger depths of cracks there is almost an order of magnitude of increase in the frequency for the higher conductivity environment.

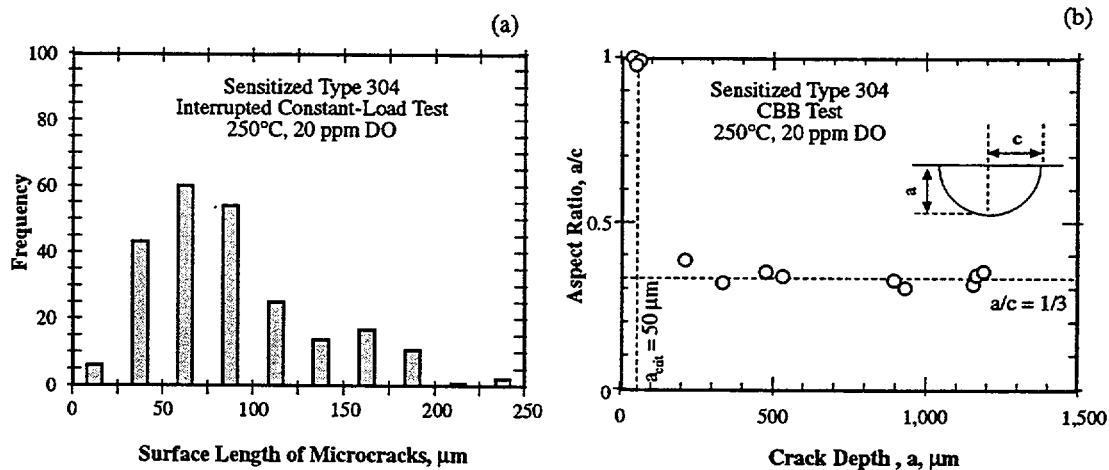


Figure 66: (a) Frequency vs. surface length of micro-cracks for sensitized Type 304 stainless steel exposed in a constant load test to 250°C and 200 ppm dissolved oxygen. (b) Aspect ratio vs. crack depth for the same conditions as in (a). Adapted from Akashi and Nakayama.<sup>18</sup>

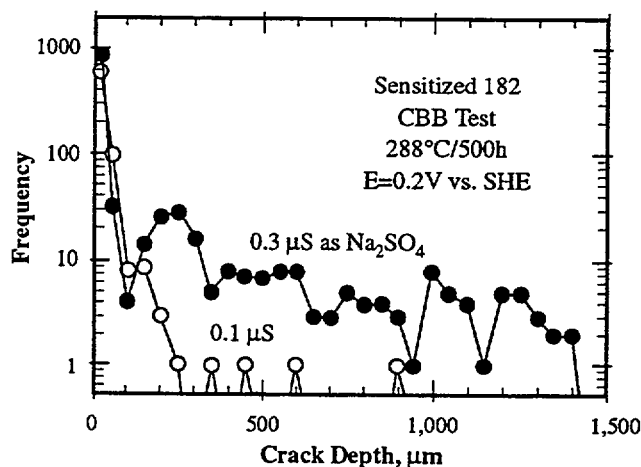


Figure 67: Frequency vs. depth of cracks for 0.1 and 0.3  $\mu\text{S}$  conductivity based on  $\text{Na}_2\text{SO}_4$  addition tested at 0.2V<sub>H</sub>. From Nakayama and Akashi.<sup>162</sup>

In general, it appears that the aspect ratio of cracks remains relatively constant in these early stages discussed here. The frequency and surface lengths are affected by concentration of the environment and temperature as well as the value of  $\beta$ . The most persistent pattern here is the relatively large number of small cracks that are produced.

Figure 68 shows data for the occurrence of microcracks in carbon steel weld metal at 250°C. For two steels the frequency distribution of microcracks is the same as shown in Figure 68a and 68b. Figure 68c indicates that the length of microcracks does not change significantly over time; Figure 68d shows that, above a threshold of about 400MPa, the rate of initiation of microcracks increases rapidly.

### 6.3 Effect of Pitting on SCC Initiation

Pits can provide initiation sites for SCC. In Figure 69 from Nakanishi et al.<sup>107</sup> a relationship between pitting and SCC is shown. Figure 69a shows a minimum diameter of pits that can initiate SCC in both negative pulse wave loading and static loading. Here, lower stresses produce SCC in the negative-pulse wave mode of loading for carbon steel weld metal at 250°C and 8 ppm of dissolved oxygen. It seems that a stress intensity can be developed from the pit geometry as shown in Figure 69b above which cracks can nucleate at the base of the pit.

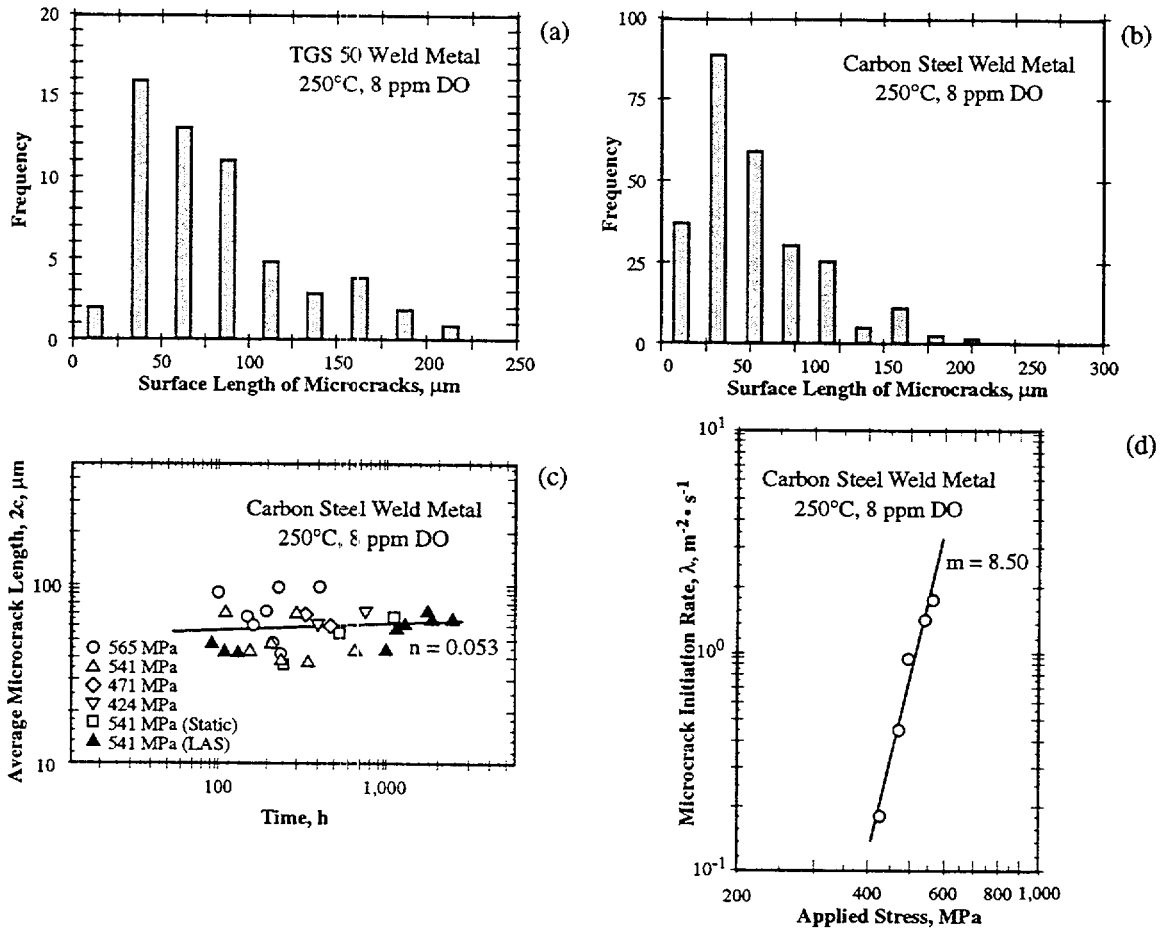


Figure 68: Results from exposure of stressed specimens of steel weld metal to 250°C in high purity water with 8 ppm dissolved oxygen. Specimens stressed with uniaxial constant load. (a) and (b) frequency vs. surface length of microcracks for two weld metals. (c) Length of microcracks vs. time. (d) Microcrack initiation rate vs. applied stress. From Nakanishi et al.<sup>107</sup>

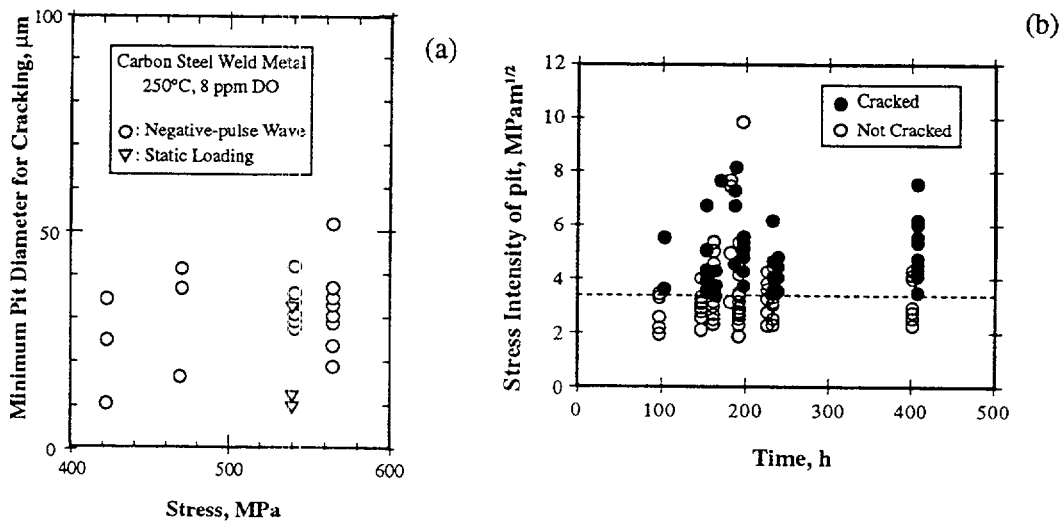


Figure 69: (a) Stress vs. minimum pit diameter for SCC of carbon steel weld metal at 250°C in high purity water with 8 ppm of dissolved oxygen. From Nakanishi et al.<sup>106</sup> (b) Stress intensity associated with pitting vs. duration of test that produces SCC as shown above the dotted line. From Nakayama et al.<sup>107</sup>

## 7.0 MEANS AND MEASUREMENT

### 7.1 Scope

Variability of data is introduced by (a) the means for conducting experiments and (b) the sensitivity of the operator-device combination in measuring results. This topic is a large one and is introduced here briefly to identify the sources and the extent of variability that can be expected depending on means and measurements. The contributors to overall variability are identified in Figure 23, and the means of testing and the measurement of occurrence sometimes contribute importantly.

Figures 2 and 3a indicate the extent of variability that can occur when experiments are conducted by reputable laboratories with nominally the same materials, environments and methods of testing. Within a single laboratory large variabilities result when different heats of nominally the same material are tested, as for Figure 27. Small differences among laboratories are magnified by the large leverage exerted by environmental variables as discussed in Section 5.0.

The significance of means of testing depends also on the intention of the test as to whether it should represent a worst case, as for the  $MgCl_2$ . The accelerated or bounding experiments, with their nominal worst case intentions, are often not good indicators of future performance as for the case of the tests that evaluated the effect of nickel on the SCC of high nickel alloys performed by Copson and Cheng,<sup>85</sup> and Copson.<sup>86</sup> The principal objective of choosing testing should relate to design life

### 7.2 Types of Tests

Figure 70 shows major types of tests used to evaluate SCC, their advantages and their shortcomings. There is no perfect test. Further, the testing selected depends on the conditions expected in the application.


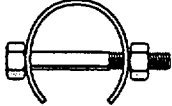

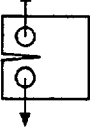
Type	Use	Problems
 Smooth Surface Constant Load	Measure initiation threshold	<ul style="list-style-type: none"> <li>• Failure time is combination of initiation and growth</li> </ul>
 Constant Strain	Inexpensive, many tests	<ul style="list-style-type: none"> <li>• Relaxed stress with time</li> <li>• Complex surface stresses</li> </ul>
 $\dot{\epsilon} = K$ Constant Extension Rate (CERT)	Measure worst case, determine boundaries	<ul style="list-style-type: none"> <li>• Crack tip environment not unique to tip but to outside surface</li> <li>• Not valid for crack growth rate</li> </ul>
 Compact Tension	Measure crack velocity	<ul style="list-style-type: none"> <li>• Crack fronts often uneven</li> </ul>

Figure 70: Principal types of tests for SCC and their applicability.



Figure 71 shows problems with smooth surface and pre-cracked specimens. Figure 71a shows the effect of static loading compared with negative pulse loading for tests of Alloy 182 in high purity water at 288°C from Nakayama and Akashi.<sup>162</sup> The negative pulse produces a  $\theta$  of 231 hours compared with the 655 hours for the static loading; values of  $\beta$  are 1.96 and 1.08, respectively, with the latter indicating more control by surface and random processes. Periodic unloading for measuring crack growth has also been found by Andresen to be effective in obtaining reliable results.<sup>42</sup>

Gangloff shows in Figure 71b a result similar to Figure 71a, where a rising load test produces the onset of hydrogen enhanced crack growth at much lower stress intensities, especially for lower strength steels, than a statically loaded test. These tests were conducted using a 2 1/4Cr-1Mo steel with a fracture toughness above 200 MPa m<sup>1/2</sup> at 25°C.

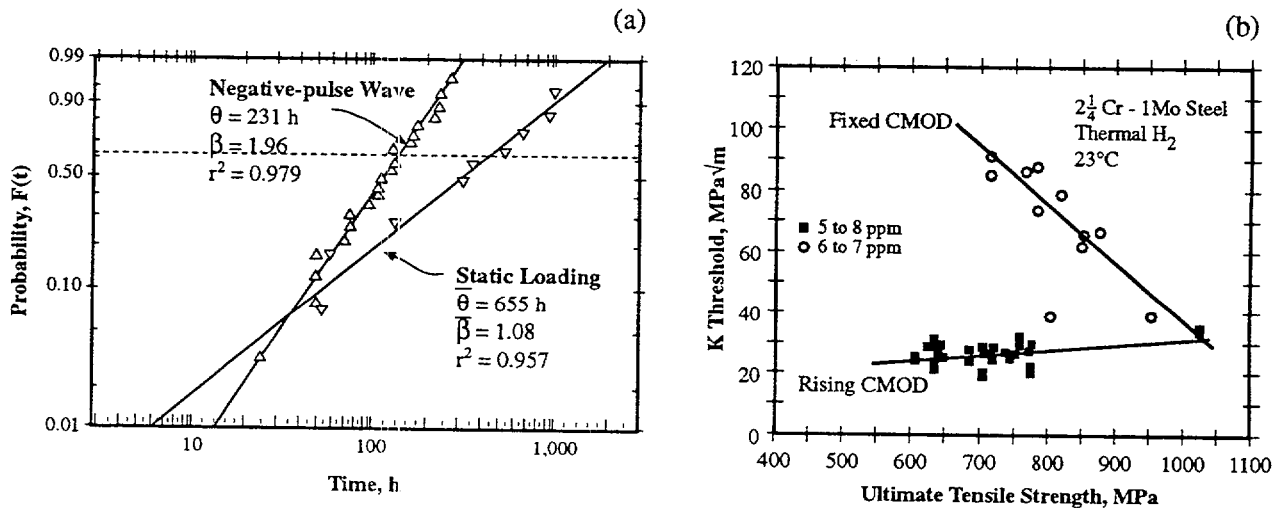


Figure 71: (a) Probability vs. time for two types of loading using Alloy 182 in high purity water at 288°C. CBB test with flow velocity of 0.056 cm/s. From Nakayama and Akashi.<sup>162</sup> (b) K threshold vs. ultimate strength for a 2 1/4Cr-1Mo steel measured using a crack opening displacement method (CMOD). Hydrogen charged thermally. From Gangloff.<sup>163</sup>

Results from various kinds of tests relative to field applications have been compared by Shibata<sup>14</sup> as shown in Figure 72. In Figure 72a he compares testing by four different methods with field experience. He shows generally that the more accelerated testing produces higher slopes, as discussed in connection with Figure 25, compared with field results. Figure 5a, which describes the SCC of welded BWR piping, also shows a  $\beta$  in the range of unity.

Figure 72b from Sato et al.<sup>164</sup> compares the values of  $\beta$  produced by three methods. Here, the constant extension rate experiment (CERT) produces a  $\beta=13.2$  compared with constant load tests that produce  $\beta=3.41$  for a MgCl<sub>2</sub> environment and  $\beta=1.90$  for a wet and dry environment using 0.5M NaCl.

### 7.3 Considerations in Means of Testing and Measurements

In considering the means and measurements:

- Accelerated tests are sometimes not applicable, as in the case of  $MgCl_2$  tests, for selecting high nickel alloys for resistance to SCC.<sup>85, 86</sup>
- The type of loading produces large differences in the scale and shape factors as shown in Figures 71 and 72. In Figure 72, the results in  $MgCl_2$  relative to the field are similar to the comparison of accelerated test and field experience in Figure 25.
- Testing in different laboratories with the same material, environment and testing arrangement produces sufficiently different results that the aggregate  $\beta_g$  is decreased relative to the local values of  $\beta_L$  as shown in Figure 22 and 27.
- Whether the test emphasizes surface-related failure processes or propagation-related processes, the values of  $\beta$  will vary from the  $\beta=1$  to the  $\beta=4$  cases.
- Uses of single vs. multiple heats affect the value of  $\beta$  as shown in Figures 22 and 27 and 38-40.
- If data are to be applied to a particular application, the features of the experiments need to be relevant, as indicated in Figure 3 which indicates a need for censoring.

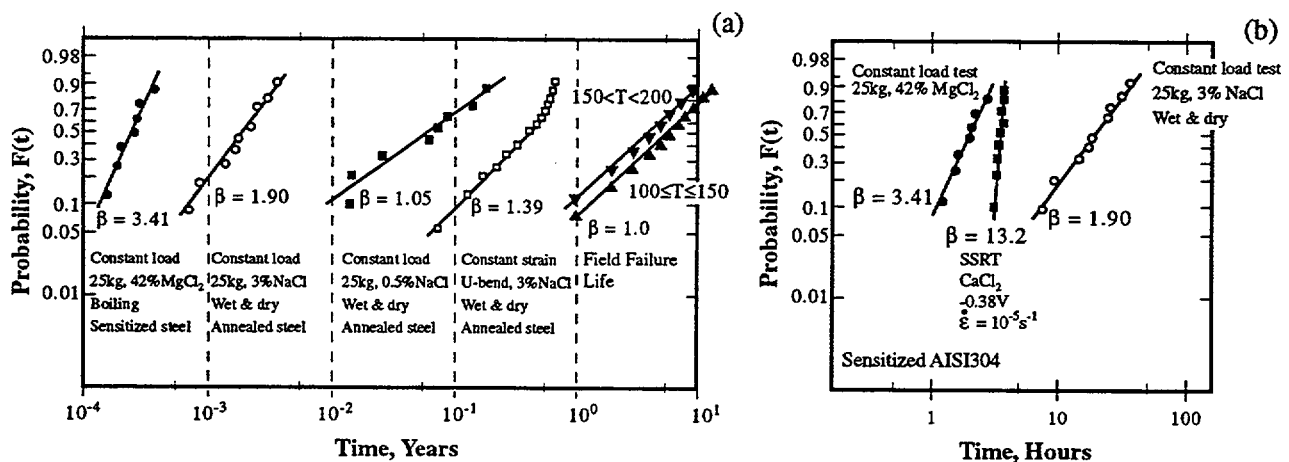


Figure 72: (a) Probability vs. time for various testing methods of Type 304 stainless steel compared with field experience. From Shibata.<sup>14</sup> (b) Probability vs. time comparing the CERT experiment on Type 304 stainless steel with results in (a). From Sato et al.<sup>164</sup>

## 8.0 MODELING AND APPLICATION

### 8.1 Scope

The objective of this report is to develop a useable framework for predicting the earliest failures that can occur by SCC in tubes of a SG. This objective is approached by developing a method of integrating physical bases with well established statistical distributions, mainly the Weibull distribution. Predicting the earliest failures depends primarily on the value of  $\beta$  and then on the value of  $\theta$ . As shown by the early failure ratio in Figure 24, values of  $\beta$  become important for early failures when they decrease below about  $\beta=4$ . Below  $\beta=1$ , the early failure ratio decreases rapidly, but the magnitudes of the early failure ratio seem impractically low. Thus, early failures depend mainly on the factors that control the value of  $\beta$ ; predicting this value is a central objective of this modeling.

There is no mechanistic nor metallurgical theory for predicting values and trends for  $\beta$ , and there is no significant body of literature where values of  $\beta$  have been examined experimentally except for the work of Akashi, e.g. Figure 17, which is reviewed in this report. There are also no theories that provide quantitative explanations for the dimensions of the submodes shown in Figures 11, 12, 13, and 14 except for some reasonable interpretations of patterns in the mode diagrams. There is no theory that provides quantitative bases for either initiation or propagation, nor the transition between these stages, aside from the lack of bases for each of the nine segments in Figure 6. While quantitative theories are lacking for the submodes, at least there is a body of consistent and relatively reproducible knowledge that permits engineers to assess performance. No such body of phenomenology exists for evaluating  $\beta$ ; further,  $\beta$ , as shown in Sections 4.0 and 5.0, does not seem to follow apparent nor consistent patterns related to either the stressors, the other statistical parameters nor to mechanisms although, on a case by case basis, there seems to be some relationship to one or the other of each of these influences.

In view of both the great importance of  $\beta$  to predicting early failures as well as the lack of theory or phenomenology, the development of a basis for this parameter is important, and approaches are suggested here.

An aim of developing quantitative bases for  $\theta$ ,  $\beta$ , and  $t_0$  relating to the seven principal variables, upon which SCC depends, is to permit evaluating Eqns. (24), (25), and (26). Such quantitative relationships can then be used for predicting cdfs that change with changing temperature, stress, and concentration and for organizing and interpreting accelerated tests.

At this point, the physically based statistical method described here assumes that the principal variables act independently as applied in Figure 5b and that multiple failures, which occur, are independent. To a first approximation this seems justified. However, such possible interdependencies need to be examined.

### 8.2 Choosing $\theta$ for Estimating Earliest Failures with No Prior Failures

The specific approach for evaluating  $\theta$  to be applied to predicting earliest failures involves the following:

1.  $\theta$  is taken as the same as the mean value that is commonly determined for correlating the dependence of SCC on principal variables. Many such data exist. Judgements are required as to selecting heats of material for bases and taking the mean.
2. Insert the appropriate values into Eqn. (24).

The data analyzed in this report show that  $\theta$  depends on temperature in Figures 54, 56, 57 and 62 and on stress in Figures 20, 28, 30, 59, 60, 62 and 63 in the same way as mean values depend on these variables. The dependencies of the data described in these figures are summarized in Tables 1 and 2. These patterns show that  $\theta$  depends in expected ways upon temperature and stress. The data in Figures 49a and 49b show that  $\theta$  decreases with increasing chloride concentrations as would be expected. A similar pattern is shown in Figure 50.  $\theta$  may be extrapolated and interpolated in the same manner as the mean values are conventionally handled. Such an approach has been extensively used by Gorman et al.<sup>20</sup>

### 8.3 Evaluation of $t_o$ for Estimating Earliest Failures with No Prior Failures

The location parameter,  $t_o$ , tends to follow the same patterns as  $\theta$  but at values 0.1 to 0.01 of  $\theta$  as shown in Tables 1 and 2. The same relationship occurs for the dependence of  $t_o$  on concentration of chloride as shown in Figure 49. For the case where no failure has been observed, choosing a value of  $t_o$  of  $0.1\theta$  is most consistent with the existing data.

### 8.4 Choosing $\beta$ for Estimating Earliest Failures with No Prior Failures

A conservative but realistic value to choose for predicting the earliest failure with no prior failures is  $\beta=1$ . This choice is suggested by the non-coherent bases for  $\beta_g=1$  from the following:

- Multiple heats including welds as indicated in Figure 5a from Eason and Shusto,<sup>44</sup> Figure 27 from Norring et al.,<sup>117</sup> Figure 37 from Webb,<sup>24</sup> Figure 38 from Scott,<sup>139</sup> Figure 40 from Clarke and Gordon,<sup>115</sup> and Figure 43 from Webb.<sup>24</sup>
- SCC occurring over a range of environmental variables, such as suggested by Figure 47, where there is also rapid change of rates of SCC as shown in Figure 13 and analyzed in Figure 28.
- Data obtained in multiple laboratories, producing non-coherent variability, where the experiments are not well coordinated as illustrated in Figures 2 from Jiang and Staehle<sup>41</sup> and from Jansson and Morin<sup>43</sup> in Figure 3a.
- The highly leveraged effects of the principal variables on the occurrence of SCC.
- The general pattern that combining a range of  $\theta$  values lowers the  $\beta$  of the aggregate to produce the aggregate  $\beta_g$  in Figures 22, 27 and 28 where  $\beta_g$  is lower than  $\beta_L$ .

Table 1  
Relationship of  $\theta$ ,  $\beta$ , and  $t_o$  to Temperature

Fig	Env't	Mat'l	°C	$\theta \sim 1/T$	$Q_{app} \times 10^{-3}$	$\beta \sim T$	$\beta \sim \theta$	$t_o \sim T$	$t_o \sim \theta$
54b	indust water	stainless steel	50-200	$\sim 0$	+0.15	$\sim 1/T$	$\sim \theta$	-	-
56b	MgCl <sub>2</sub>	304	126-138	$\sim T$	-12	$\sim 1/T$	$\sim 1/\theta$	$\sim T$	$\sim \theta$
57c	BWR water	304ss	25-300	$\sim T$	-4	$\sim 1/T$	$\sim 1/\theta$	$\sim T$	$\sim \theta$
58b	PWR water	600	288-360	$\sim 1/T$	+54	$\sim T$	$\sim 1/\theta$	$\sim 1/T$	$\sim \theta$
58d	PWR water	600	360-400	$\sim 1/T$	+32	$\sim T$	$\sim 1/\theta$	$\sim 1/T$	$\sim \theta$

Table 2  
Relationship of  $\theta$ ,  $\beta$ , and  $t_o$  to Stress

Fig	Env't	Mat'l	°C	MPa	$\theta \sim \sigma$	m	$t_o \sim \sigma$	$t_o \sim \theta$	$\beta \sim \sigma$	$\beta \sim \theta$
59b	Cu, SO <sub>4</sub>	304ss	100	100-400	$\sim 1/\sigma$	-3.8	$\sim 1/\sigma$	$\sim \theta$	$\sim \sigma$	$\sim 1/\sigma$
59d	0.35% NaCl	304ss	80	98-392	$\sim 1/\sigma$	-2.7	$\sim 1/\sigma$	$\sim \theta$	Vbl	Vbl
60c (S)	MgCl <sub>2</sub>	304	154	98-294	$\sim 1/\sigma$	-2.1	$\sim 1/\sigma$	$\sim \theta$	$\sim \sigma$	$\sim 1/\sigma$
60c (C)	MgCl <sub>2</sub>	310	154	206-413	$\sim 1/\sigma$	0.71	$\sim 1/\sigma$	$\sim \theta$	$\sim \sigma$	$\sim 1/\sigma$
61	MgCl <sub>2</sub>	304	138	-	$\sim 1/\sigma$	-1.2	-	-	$\sim \sigma$	$\sim 1/\sigma$
30c (A)	BWR	304ss	288	203-271	$\sim 1/\sigma$	-4	$\sim 1/\sigma$	$\sim \theta$	$\sim 1/\sigma$	$\sim \sigma$
30c (CG)	BWR	304ss	288	241-338	$\sim 1/\sigma$	-11	$\sim 1/\sigma$	$\sim \theta$	$\sim 1/\sigma$	$\sim \sigma$
63b	BWR	c.s.	250	424-565	-	-3.7	$\sim 1/\sigma$	$\sim \theta$	$\sim 1/\sigma$	$\sim \sigma$
63d	PWR	750	350	221-661	-	-3	$\sim 1/\sigma$	$\sim \theta$	$\sim 1/\sigma$	$\sim \sigma$
29	I <sub>2</sub>	Zr 2	350	240-310	$\sim 1/\sigma$	-	$\sim 1/\sigma$	$\sim \theta$	$\sim \sigma$	$\sim 1/\sigma$

Notes:

1. Proportionalities are general and are not given powers or precise dependency other than direct or inverse.
2.  $\theta$  and  $t_o$  taken in terms of time ( $t/a$ ) for this chart from Figure 57b.
3. BWR and PWR water is oxygenated and deoxygenated, respectively, with temperatures in the general range of 288°C and 290 to 325°C (depending on secondary and primary sides), also respectively.
4. ss = sensitized
5. Figure 63 d last point is opposite.
6. m = stress exponent;  $Q_{app}$  = apparent activation energy
7. Figure 56 exhibited increased failure time with increased temperature.

Choosing a value of  $\beta < 1$  does not seem practical in view of the patterns of early failures normally observed. The early failure ratio in Figure 24 shows that values of  $\beta < 1$  produce increasingly larger differences between the earliest failure and the mean.

There is a practical question in considering the applicability of  $\beta_g$  to predicting early failures in the sense that it is calculated in Figure 22. For example, the earliest failure of the first heat in Figure 27 is dominated by a  $\beta=4$  case; however, when the  $\beta_g$  is determined for the whole set as for the  $\beta_g$  of Figure 27, the time of the earliest failure is greatly reduced owing to the effect shown by the early failure ratio of Figure 24. This possible inconsistency for the  $\beta_g$  case suggests that the early failures that are predicted by a  $\beta_g$  should be truncated. An example of such a practical circumstance, aside from the experiments in Figure 27, is the occurrence of failures on the primary and secondary sides of SG tubing as shown in Figure 52 where the values of  $\beta$  observed in practice are in the range of  $\beta=4$  despite the many heats as shown in Figure 38. The  $\beta=4$  behavior of the examples in Figure 52

is consistent with the observation of Scott in Figure 38 where he shows that only the most susceptible heats produce the early failures. The extent to which a  $\beta_g$  should be truncated to account for the  $\beta=4$  behavior of the early failing heats is not clear but needs to be considered in the practical application of using a  $\beta=1$  basis for predicting the earliest failures in the absence of any failure data.

The use of  $\beta=1$  indicates that failure can occur randomly at any time and is the same value as the Poisson  $\beta=1$  for the coherent case. In the coherent case only a single set of homogeneous specimens in a controlled environment is being considered. The  $\beta$  is interpreted in Figures 15f and Eqn. 5 where it is shown that the probability of failure for  $\beta=1$  is constant over time independent of the physical processes that produce  $\beta=1$ , coherent or non-coherent. While  $\beta=1$  is interesting mechanistically, probably, most cases, where  $\beta=1$ , are actually expressions of the aggregate  $\beta_g$ .

## 8.5 Dependencies of $\beta$

Unlike the regular and predictable dependencies of  $\theta$  and  $t_o$  on temperature and stress in Tables 1 and 2 as well as for concentration and other variables where data are not so extensive, dependencies of  $\beta$  on principal variables do not follow consistent patterns. The data suggest that  $\beta$ , aside from the integrating effects that lead to  $\beta_g$ , is affected by three main influences:

- Mechanistic processes that produce the Poissonian and accumulation cases as illustrated in Figure 26 and as argued in connection with Figure 17.
- Effects of the increasing intensity of stressors as they favor failure in more narrow range ratios.
- Competition of initiation and propagation processes as indicated in Figure 31 and 32.

Tables 1 and 2 summarize the results from figures showing that the dependencies of  $\beta$  on stress and temperature do not follow consistent patterns as do  $\theta$  and  $t_o$ .

### 8.5.1 General Features of $\beta$

The early suggestion of Shibata in Figure 31a indicated that the overall value of  $\beta$  for time-to-failure would approach  $\beta=1$  when initiation processes dominate the time-to-failure and that initiation processes are essentially  $\beta=1$  in their dependence in accordance with the arguments illustrated in Figure 17.  $\beta=1$  behavior related to the dominance of initiation is illustrated in Figures 31b, 31d, 31e, 31f, 32, and 55. Shibata analyzed a set of values for  $\beta_i$ ,  $\beta_p$ , and  $\beta_r$  as defined in Figure 31e and 31f and also illustrated in Figures 50 and 55, as shown in Figure 73. The mean value of  $\beta_i$  was about 1.5 and the mean value of  $\beta_p$  was about 2.3 with the  $\beta_r$  approaching the initiation case; these patterns are based on the behavior of stainless steels in concentrated chloride solutions such as  $\text{CaCl}_2$  and  $\text{MgCl}_2$ .

Shibata<sup>150</sup> has also shown, as in Figure 73b, that  $\beta$  tends toward higher values with increasing concentrations as also shown in Figure 49a for dilute solutions but is opposite to the trend in Figure 49b for concentrated solutions. Figure 73b also shows that  $\beta$  is reduced as temperature increases for concentrated solutions; this trend is opposite to any proportionality to stressors but is consistent with the trends at lower temperatures in Table 1.

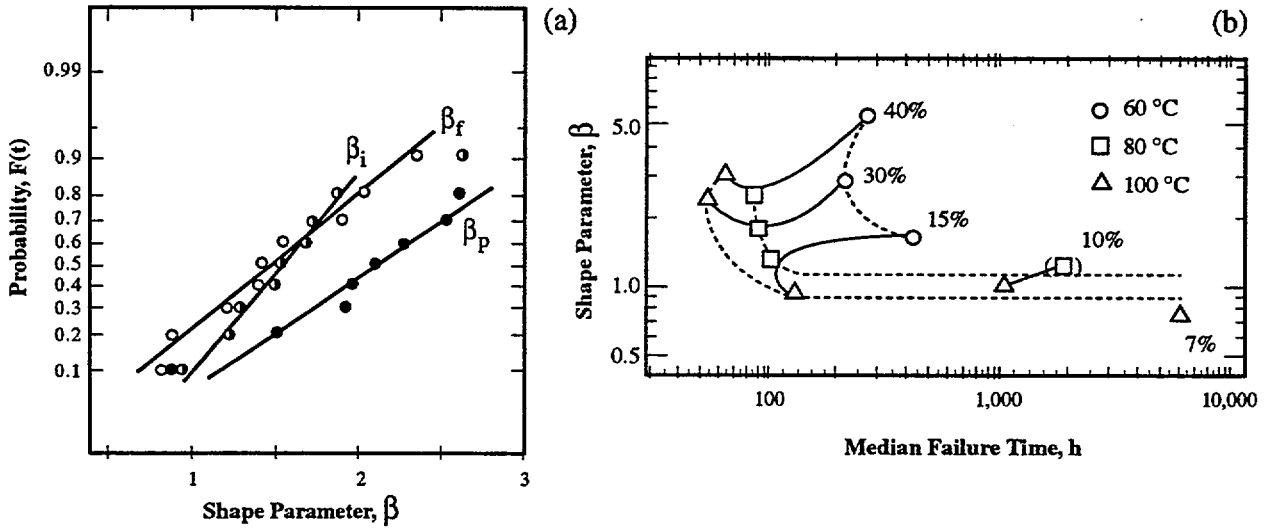


Figure 73: (a) Probability vs.  $\beta$ : for initiation,  $\beta_i$ , propagation,  $\beta_p$ , and failure,  $\beta_f$ , for data from various investigations in Prof. Shibata's laboratory. From Shibata.<sup>16</sup> (b) Shape parameter vs. median failure time for Type 304 stainless steel exposed to  $\text{CaCl}_2$  at three temperatures and three concentrations. From Shibata et al.<sup>150</sup>

### 8.5.2 Analysis for Dependence of $\beta$ on Temperature and Stress

Expectations for the trends of  $\beta$  have been analyzed by Stavropoulos et al.<sup>165</sup> for temperature and stress. In the case of temperature and stress, the times-to-failure are related usually to the absolute temperature and to stress by the well known relationships in Eqns. (28) and (29):

$$t_f = C \exp\left(\frac{Q_{app}}{RT}\right) \quad (28)$$

$$t_f = \frac{C}{\sigma^m} \quad (29)$$

where:

- $Q_{app}$  = apparent activation energy
- $T$  = temperature in absolute degrees
- $R$  = gas constant
- $\sigma$  = stress
- $m$  = stress exponent

For the case of the temperature, by taking logarithms of both sides of Eqn. (28) and determining the variance of  $\ln t$ , a relationship between  $\beta$  and  $T$  can be developed, as in Eqn. (30):

$$\beta \approx \frac{RT^2}{Q\sqrt{\text{Var}(T)}} \quad (30)$$

If the variance is constant, i.e. independent of  $T$ , then  $\beta$  is expected to be approximately proportional to  $T^2$ . If, instead of the variance being constant, the coefficient of variation of the temperature distribution is constant, then  $\beta$  is proportional to the first power of  $T$ , i.e. in Eqn. (31):

$$\beta \propto T \quad (31)$$

The ratio of two values of  $\beta$  at different temperatures according to Eqn. (30) is given in Eqn. (32):

$$\frac{\beta_2}{\beta_1} = \left(\frac{T_2}{T_1}\right)^2 \sqrt{\frac{\text{Var}(T_1)}{\text{Var}(T_2)}} \quad (32)$$

For analyzing the expected effect of stress on  $\beta$  and starting from Eqn. (29), it can be shown that  $\beta$  is proportional to stress and inversely proportional to the stress exponent in Eqn (33); and the ratio of  $\beta$  at two stresses for the case of constant variance is shown in Eqn. (34):

$$\beta = \frac{\sigma}{m\sqrt{\text{Var}(\sigma)}} \quad (33)$$

$$\frac{\beta_2}{\beta_1} = \left(\frac{\sigma_2}{\sigma_1}\right) \sqrt{\frac{\text{Var}(\sigma_1)}{\text{Var}(\sigma_2)}} \quad (34)$$

If the coefficient of variation is constant,  $\beta$  is independent of stress as shown in Eqn. (35)

$$\frac{\beta_2}{\beta_1} = 1 \dots [\text{If} \cdot \text{CV}(\sigma) = \text{const}] \quad (35)$$

In Table 1  $\beta$  is shown to be proportional to temperature for two cases in PWR water and therefore is consistent with the expectations of Eqns. (30) and (31). However,  $\beta$  is shown to be inversely proportional to  $T$  in more oxidizing cases of BWR water,  $\text{MgCl}_2$  solutions, and industrial water. This bi-modal pattern suggests domination by both the intensity of stressors and mechanistic influences depending on the environments.

In Table 2  $\beta$  is shown to be proportional to stress, according to the prediction of Eqn. (33), for lower temperatures including the  $\text{MgCl}_2$  environments as well as for  $I_2$ ; however,  $\beta$  depends inversely on stress for high temperature pure water.

The dependencies of  $\beta$  on temperature and stress summarized in Tables 1 and 2 show some consistency with the predictions of Eqns. (30) through (34); however, about half the cases exhibit opposite dependencies. This general pattern supports the idea that the dependencies of  $\beta$  are at least bi-modal with respect to influences of stressors and mechanisms, aside from the effects of aggregation.

### 8.5.3 Alloy Dependence

$\beta$  exhibits a linear dependence on  $\text{Cr}_{\text{eq}}$ , as in Figure 33b. Figure 34 shows that Pt, Rh and N additions to a Fe-15Ni-20Cr alloy lower  $\beta$  whereas Mo and P raise it. The effect of Cr on  $\beta$  coincides with improved passive films associated with increases in Cr. The effects of the alloy additions do not have clear bases. It is reasonable that the pattern of Figure 33b for the linear dependence of  $\beta$  on  $\text{Cr}_{\text{eq}}$  may apply more broadly to other dependencies of major alloying elements.

### 8.5.4 Alloy Structure

Data for effects of metallurgical structure in Figure 37 show that structures that increase values of  $\theta$  also increase values of  $\beta$  for two separate studies. The same is true for welds in Figure 43b, but the opposite is true for the welds in Figure 43a. For lower magnitudes of cold work, as shown in Figure 42a,  $\beta$  tends to increase with cold work but decreases at higher cold works as shown in Figure 42b. Various surface finishes produce  $\beta$  in the range of 1.1 to 5.6, but there is no regular pattern.

## 8.6 Overall Problem with $\beta$

Choosing a  $\beta=1$  for predicting the earliest failures essentially on a  $\beta_g$  basis can be easily supported.



This approach obviates the necessity to speculate about the inherent values of  $\beta$ . However, these inherent values of  $\beta$  that are not masked by the non-coherencies are important for prediction after the early failures occur and for comparing accelerated tests with long term performance.

While the dependencies of  $\theta$  and  $t_o$  on principal variables seem interpretable and follow expected patterns, the dependencies of  $\beta$  are much less so. While some of the dependencies, at least for temperature and stress, follow analytic predictions from Eqns (30) to (34), others do not, as noted in connection with the observations summarized in Tables 1 and 2.

Unfortunately, there is no mechanistic nor metallurgical theory for  $\beta$ ; while, on the other hand, it is the most critical of the statistical parameters. Available data analyzed for the present paper suggest that the least conservative approach is to assume that  $\beta$  is proportional to the intensity of stressors. However, this approach is more reliable analytically. The most conservative approach is to use the  $\beta=1$  case until alternate interpretations as to the other part of the bimodal dependence (i.e. other than proportionality to stressors) of  $\beta$  can be developed. For the present, the alternative mechanically based interpretation is epitomized in Figure 26 where it is suggested, based on the observed hazard functions, that  $\beta$  is bounded at the low end by Poissonian patterns of  $\beta=1$  and at the high end by accumulation patterns of  $\beta=4$ .

### 8.7 Choosing Parameters After First Failures Have Occurred

Once some early failures have occurred, the question of the earliest failure has been solved, and the question then remains as to how the rate of failures should be extrapolated to the future until a sufficient number of failures occur that the dependency is reasonably clarified. There are two basic choices here. One is to continue with the  $\beta=1$  assumption using the earliest failure as an intercept; the other is to use what is now a conservative assumption and that is to assume that the earliest failure is associated with a sensitive heat of material and that these failures will occur at a higher rate. Choosing  $\beta=4$ , following Figures 26, 27, 38 and 52, would apply for some time until the next and less sensitive heats exhibit SCC and cause the aggregate  $\beta_g$  to include values with larger  $\theta$  and decrease, as predicted in the calculation of Figure 22. Approaches to options for predicting subsequent failures after the earliest are shown in Figure 74 where the options are illustrated for choosing the  $\beta=1$  and  $\beta=4$  cases after the first failure.

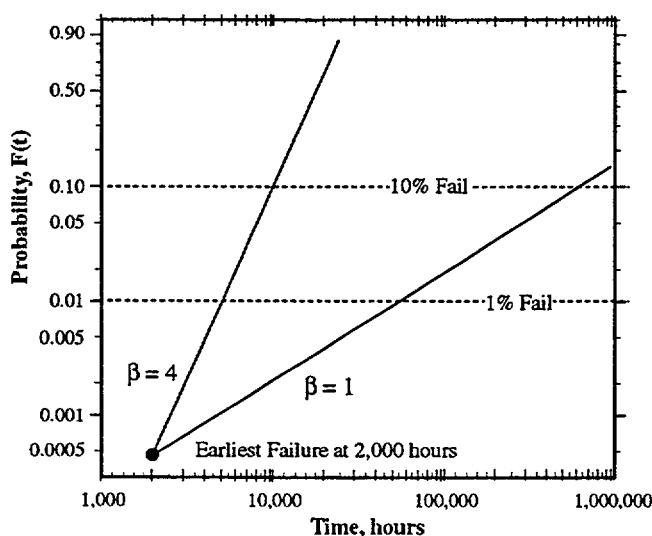


Figure 74: Schematic view of probability vs. time for case with early failure at 2000 hours and at 0.0005 probability showing options for extrapolating with slopes of  $\beta=1$  and  $\beta=4$ .

As more failures occur, better choices for predicting the course of the failure rate can be justified. However, it is not clear whether this rate would continue because the most sensitive early heats, having higher values of  $\beta$ , would fail early, following the implication of Scott's data in Figure 44;<sup>138</sup> and later failures of less sensitive material would cause  $\beta_g$  to decrease.

### 8.8 Existing Patterns of Early Failures

One means for estimating the occurrence of early failures is to determine the cdf for the early failures of components in the same class, e.g. at 0.01 probability, and examine their probability. Such a study of tubing in PWR SGs has been undertaken by Gorman et al.<sup>20</sup> He determined the time of 1% failure for a number of SGs for specific locations of failures in the SGs shown, for example, in Figure 4. The results of this investigation provided the data of Figure 75. With these data, it is possible to determine the mean time for initiation as defined by 1% failure from a set of SGs. This value is then used to anchor the prediction of failure rate vs. time following the approach of Figure 74.

This approach depends on the availability of sufficient prior information. However, it can be used when at least some prior history is available.

### 8.9 Multiple Failures

The discussions in this paper have considered single failures. The reality of engineering components such as SGs as shown in Figure 4 involves the occurrence of many failures by several different submodes at several locations. Such a multiplicity of mode-location cases is illustrated in Figure 76.

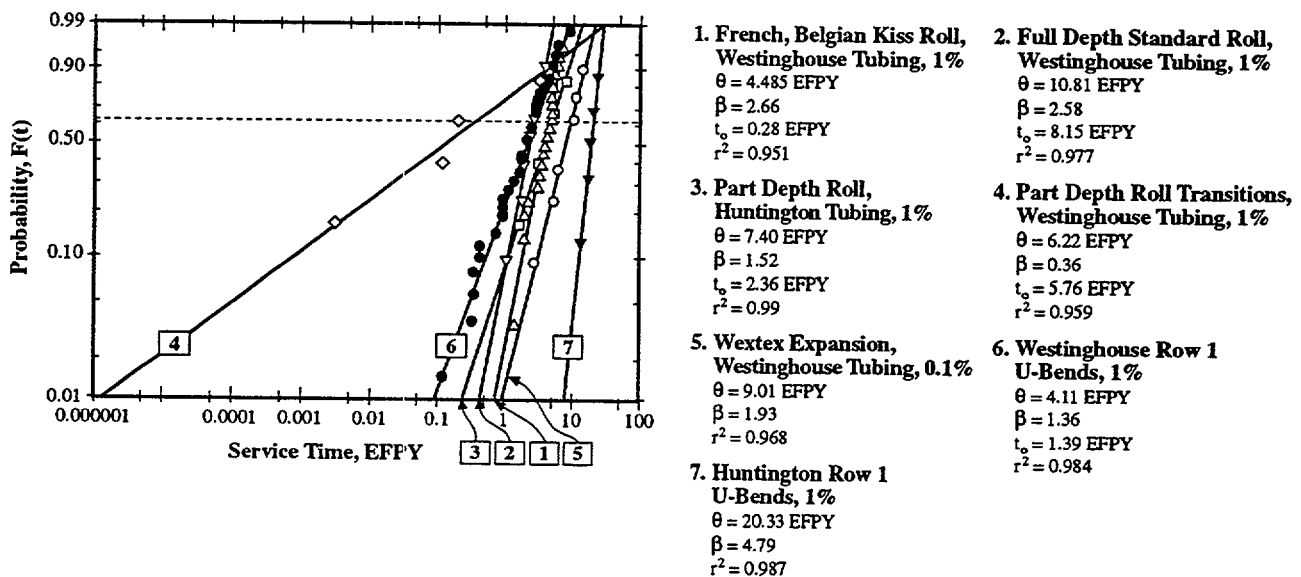


Figure 75: Probability vs. service time (equivalent full power years) for 0.1 or 1% for LPSCC at seven specific locations, using for each distribution data from SGs of multiple plants, each plot accounting for a single data point. Data adjusted to 316°C using an apparent activation energy of 50 kcal/mole. Adapted from Gorman et al.<sup>20</sup>

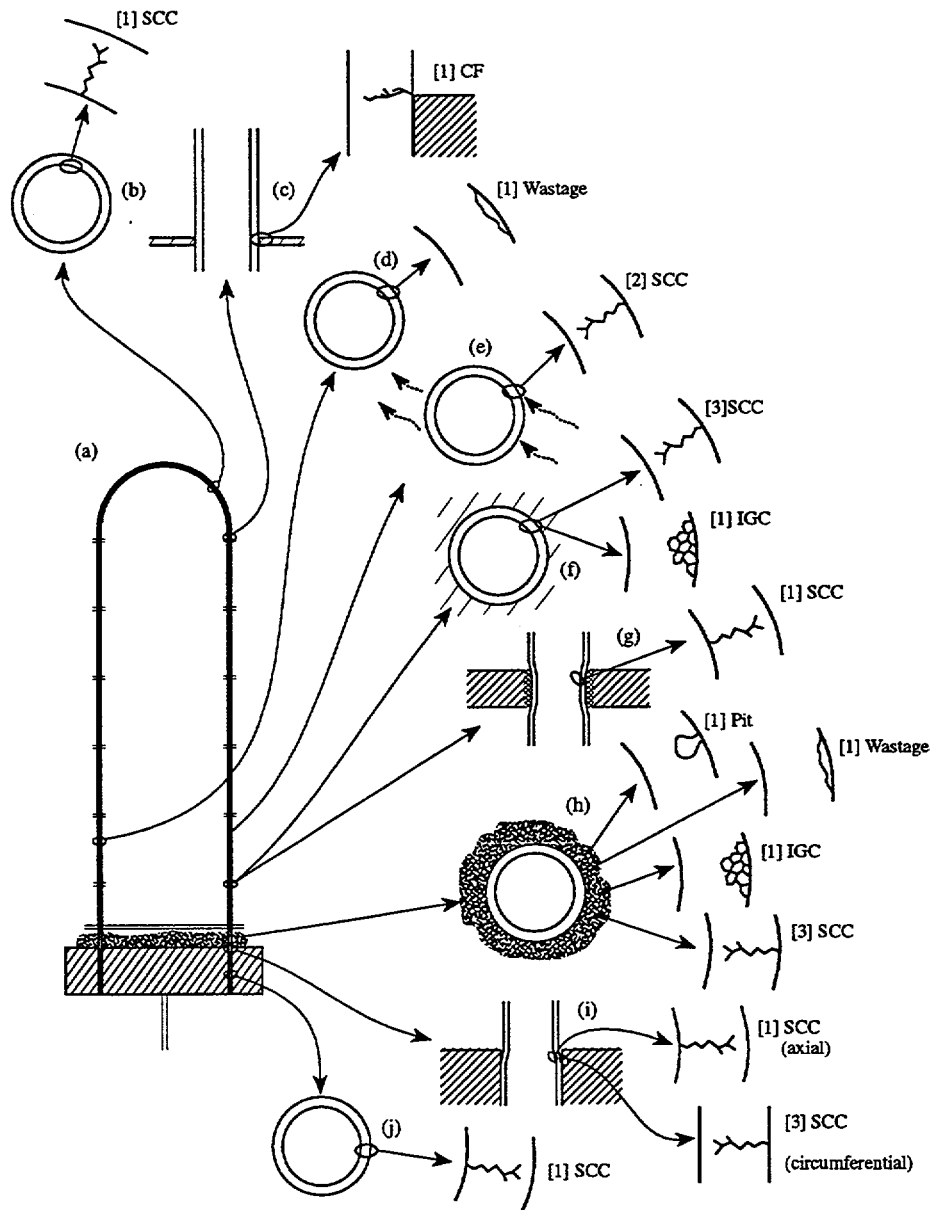


Figure 76: Schematic view of occurrence of different modes of SCC and localized corrosion at specific locations on the primary and secondary sides of PWR SGs. Details of SG locations shown in Figure 4. From Staehle.<sup>1</sup>

The occurrence of this multiplicity of mode-location cases is shown in Figure 5b for the case of an SG. Also, in Figure 5b a cumulative probability of failure is shown. This cumulative probability of failure is given by Eqn. (36)

$$F_T(t) = 1 - [1 - F_1(t)][1 - F_2(t)] \cdots [1 - F_n(t)] \quad (36)$$

where:  $F_T(t)$  and  $F_n(t)$  are the total failure probability and the failure probability due to the  $n$ th mode-location case.

Eqn. (36) assumes that the  $n$  mode-location cases are not interdependent. In fact, those in Figure 5b are connected to some extent, but the analysis has been used successfully for the SG application as noted in work by Gorman et al.<sup>20</sup> Eqn. (36) can be applied to predicting earliest failures for multiple mode-location cases using separate expressions based on Eqns (24) to (26). Figure 77 illustrates the approach using Eqn. (36).

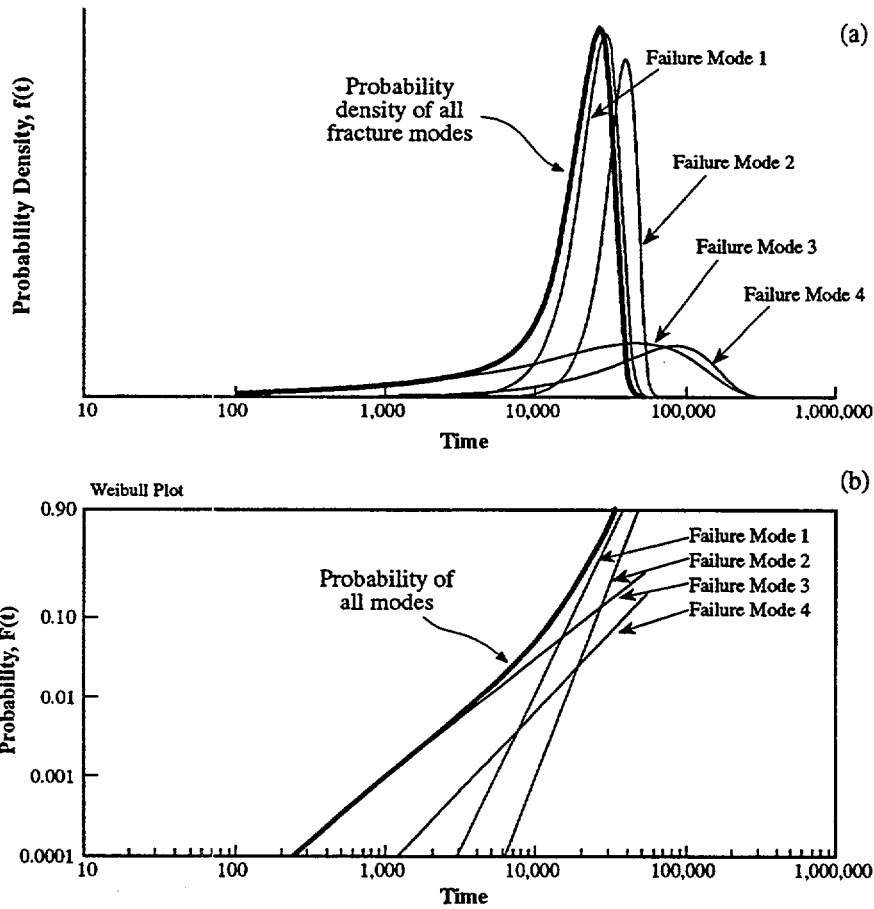


Figure 77: (a) pdfs for four separate failure modes occurring in the same subcomponent. Total pdf shown aggregating data from the four. (b) cdf for the four cases in (a) and the aggregate distribution is shown based on Eqn. (36).

### 8.10 Calculating the Probability of Failure Time Based on Initiation and Propagation

Once expressions for the statistical parameters are developed, the cumulative failure probability can be calculated from a knowledge of separate probabilities of initiation and propagation. Let the  $t_f$  be given as usual in Eqn. (37):

$$t_f = t_i + t_p \quad (37)$$

The probability densities are then defined:

$$f_i(t_i) = \text{probability density function of the initiation time, } t$$

$$f_p(t_p) = \text{probability density function of the propagation time, } t$$

$$f_f(t_f) = \text{probability density function of the time-to-failure, } t$$

The pdf and cdf for failure can be expressed as Eqns. (38) and (39):

$$f_f(t_f) = \int_0^{t_f} f_i(x) f_p(t_f - x) dx \quad (38)$$

$$F_f(t_f) = \int_0^{t_f} f_i(x) F_p(t_f - x) dx \quad (39)$$

These integrals can be determined numerically and the results for a sample calculation is shown in Figure 78.

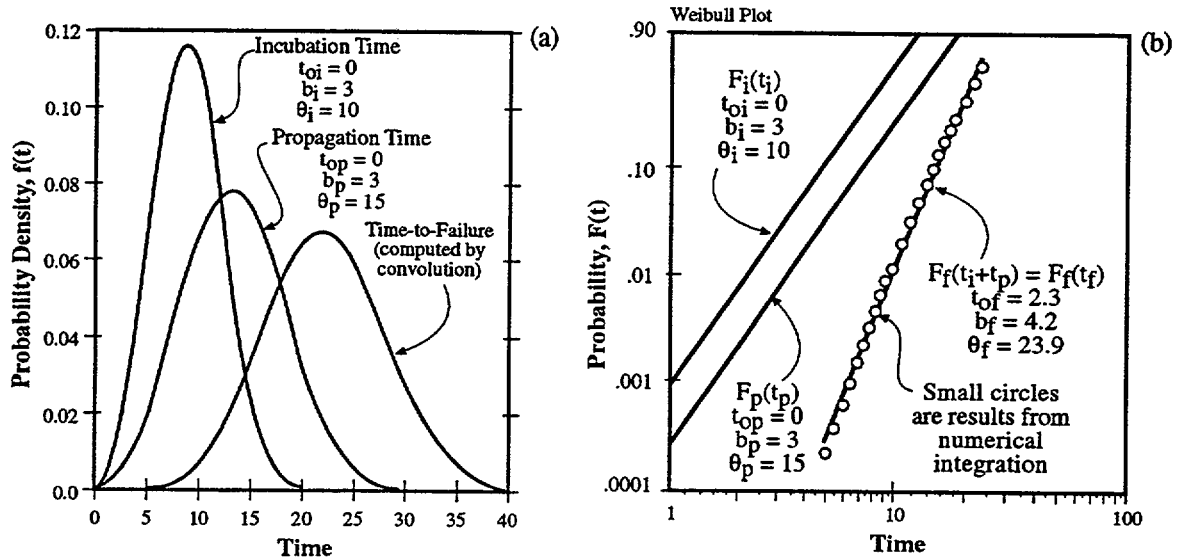


Figure 78: (a) pdf for initiation, propagation and failure calculated numerically from Eqn. (38). (b) cdf for initiation, propagation, and failure calculated numerically from Eqn. (39). Dots show locations of numerical calculations. From Staehle and Stavropoulos.<sup>2</sup>

### 8.11 Calculating cdf with Changing Variables

The probability of failure over time can be calculated when the dependencies of the statistical parameters on the principal variables is known as in Eqns. (24) to (26). One method for performing such a calculation was developed by Stavropoulos et al.<sup>165</sup> For a change of temperature from 100 to 20°C over time Figure 79 shows the resulting cdf based on a Weibull distribution. Figure 79 demonstrates that incorporating the dependencies of principal variables into the statistical parameters permits predictions over changing values of the variables.

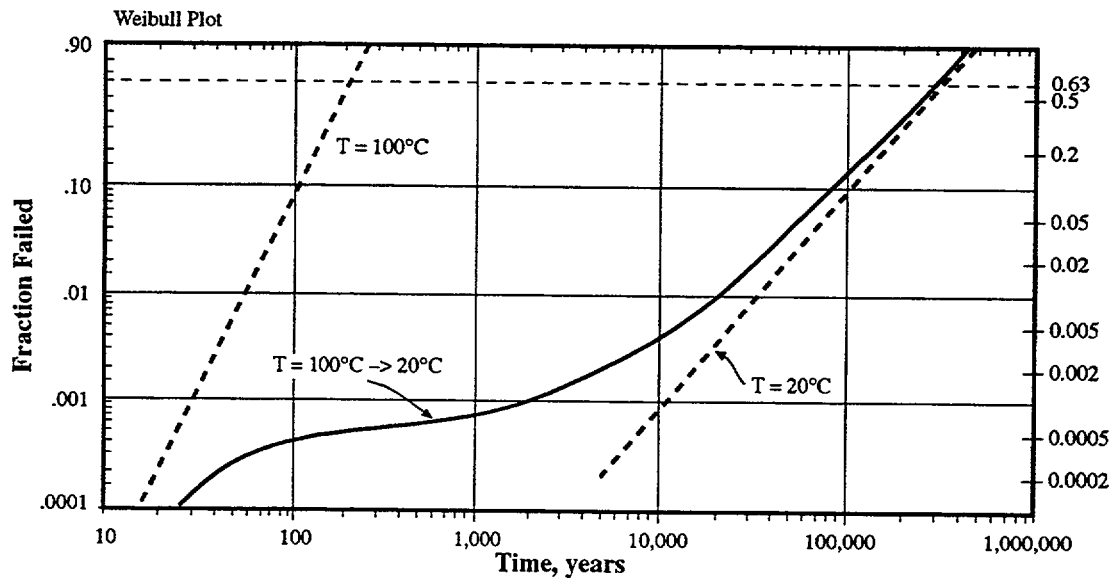


Figure 79: cdf calculated on the basis of temperature changing from  $T=100^\circ\text{C}$  initially to  $T=20^\circ\text{C}$  after 100 years following an exponential decay in temperature. From Stavropoulos et al.<sup>165</sup>

## 8.12 Accelerated Testing and Extrapolating Results

Problems with applying the results of accelerated testing to predicting future performance are discussed in connection with Figure 25. This figure notes that predictions in terms of comparing mean values can be quite flawed with respect to the need to predict the earliest failures. Such a problem can be remedied by the approach shown in Figure 80 where the values of pdfs and cdfs determined at accelerated conditions can be extrapolated to operating conditions.

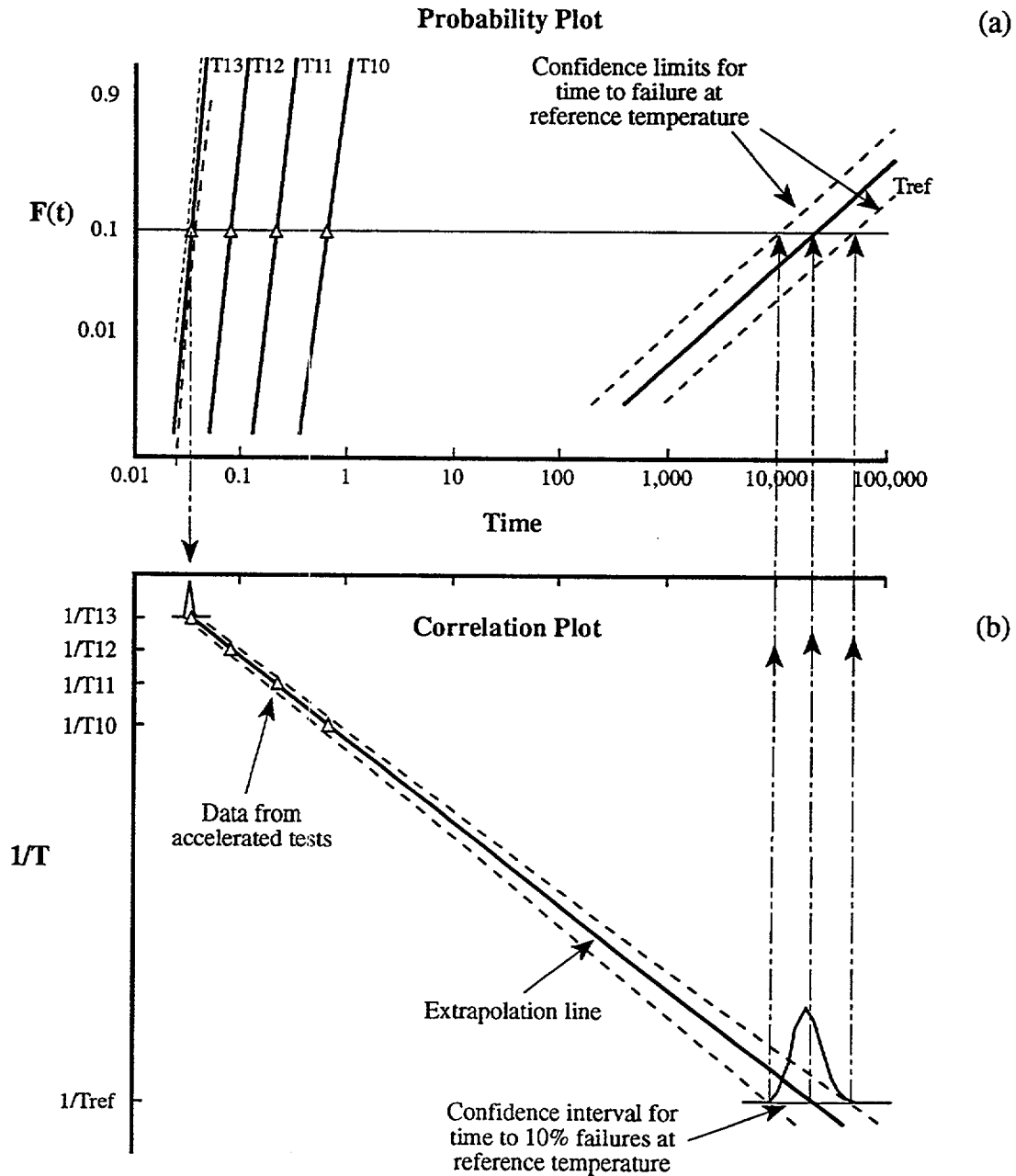


Figure 80: Schematic view of extrapolating statistical data obtained at accelerated conditions to the operating case.

### 8.13 Predicting Engineering Performance

Predicting performance is based on one of two problems: either there are no data or there is a plethora of non-coherent data as suggested in the extreme by Figures 2 and 3a. Practical approaches to developing predictions include the following:

1. Screening data as shown in Figure 3b.
2. Assuming that predictions based on mean value acceleration are adequate and the problem shown in Figure 25 does not occur.
3. Use a means for predicting early failures suggested in this paper as modified according to the suggestion of Figure 74.
4. Analyze prior data according to the method used in connection with Figure 75.
5. Using Monte Carlo methods to model cdfs as successfully applied to interpreting LPSCC by Scott et al.<sup>155</sup>
6. Recognize the nature of data scatter discussed in connection with Figures 19, 22, and 28 as well as the implications of  $\beta_g$  and apply the conclusions carefully.

Practically, combining some of each of these is often done. A rigorous method for predicting complex performance such as that shown in Figure 76 is discussed in various papers.<sup>1,2,3,4,5</sup>

## REFERENCES

1. R.W. Staehle, "Lifetime Prediction," Corrosion Control in the New Millennium, W. Revie and I. Al-Tai, Meeting Chairmen, National Association of Corrosion Engineers International, Houston, 1999, p. 1.
2. R.W. Staehle, "Combining Design and Corrosion for Predicting Life," Life Prediction of Corrodible Structures, R.N. Parkins, ed., National Association of Corrosion Engineers International, Houston, 1994, p. 138.
3. R.W. Staehle, "Lifetime Prediction of Materials in Environments," Uhlig's Corrosion Handbook, 2<sup>nd</sup> Edition, R.W. Revie, ed., John Wiley and Sons, New York, 2000, p. 27.
4. R.W. Staehle, "Framework for Predicting Stress Corrosion Cracking," Environmentally Assisted Cracking: Predictive Methods for Risk Assessment and Evaluation of Materials, Equipment, and Structures, STP 1401, R. Kane, ed., American Society for Testing and Materials, Philadelphia, 2000, p. 131.
5. R.W. Staehle, "Environmental Definition," Materials Performance Maintenance, R.W. Revie, V.S. Sastri, M. Elboudjaini, E. Ghali, D.L. Piron, P.R. Roberge, and P. Mayer, eds., Pergamon Press, Ottawa, 1991, p. 3.
6. U.R. Evans, "Notes on the Localized Corrosion Meeting and the Corrosion Studies at Cambridge," Localized Corrosion, NACE-3, R.W. Staehle, B.F. Brown, J. Kruger, and A. Agrawal, eds., National Association of Corrosion Engineers International, Houston, 1974, p. 44.
7. W.E. Berry, W.N. Stiegelmeier, V.W. Storhok, T.R. Emswiler, and W.K. Boyd, Examination of the Crack in the Stub Riser in Dresden 1 Nuclear Station, Final Report, Docket 50010 86, Battelle Memorial Institute, Columbus, Ohio, 1971.
8. C.F. Cheng and E.E. Potter, "Intergranular Stress-Assisted Corrosion Cracking of Type 304 Stainless Steel Piping in Dresden-1 BWR Systems," Metallurgical Society of AIME 19, 1973, p. 273.
9. W. Nelson, Applied Life Data Analysis, John Wiley and Sons, New York, 1982.
10. A. Stuart and J.K. Ord, Kendall's Advanced Theory of Statistics, Volume 1, Distribution Theory, Oxford University Press, New York, 1987.
11. J.B. Kennedy and A.M. Neville, Basic Statistical Methods for Engineers and Scientists, Third Edition, Harper and Row, New York, 1986.
12. P.D. O'Connor, Practical Reliability Engineering; Third Edition, John Wiley and Sons, New York, 1991.
13. H.M. Wadsworth, ed., Handbook of Statistical Methods for Engineers and Scientists, McGraw-Hill, New York, 1990.
14. T. Shibata, "Corrosion Probability and Statistical Evaluation of Corrosion Data," Uhlig's Corrosion Handbook, 2<sup>nd</sup> Edition, W.R. Revie, ed., John Wiley and Sons, New York, 2000, p. 367.
15. T. Shibata, "1996 W.R. Whitney Award Lecture: Statistical and Stochastic Approaches to Localized Corrosion," Corrosion 37, 11, 1996, p. 813.



16. T. Shibata, "Probability Distribution of the Failure Time Due to Stress Corrosion Cracking," Localized Corrosion, F. Hino, K. Komai, and K. Yamakawa, eds., Elsevier Science Publishing Co., New York, 1988, p. 197.
17. M. Akashi, "An Exponential Distribution Model for Assessing the Stress Corrosion Cracking Lifetime of BWR Component Materials," Life Prediction of Corrodible Structures, R.N. Parkins, ed., National Association of Corrosion Engineers International, Houston, 1994, p. 1040.
18. M. Akashi and G. Nakayama, "A Process Model for the Initiation of Stress Corrosion Crack Growth in BWR Plant Materials," Effects of the Environment on the Initiation of Crack Growth, STP 1298, W.A. Van Der Sluys, R.S. Piascik, and R. Zawierucha, eds., American Society for Testing and Materials, Philadelphia, 1997, p. 150.
19. M. Akashi and G. Nakayama, "Effects of Acceleration Factors on the Probability Distribution of Stress Corrosion Crack Initiation Life for Alloys 600, 182, and 82 in High Temperature and High Purity Water Environments," The Ninth International Conference on Environmental Degradation of Materials in Nuclear Power Systems – Water Reactors, S. Bruemmer, P. Ford, and G. Was, eds., TMS (The Minerals, Metals and Materials Society), Warrendale, Pennsylvania, 1999, p. 389.
20. J.A. Gorman, K.D. Stavropoulos, W.S. Zemitis, and M.E. Dudley, PWSCC Prediction Guidelines, TR-104030, Final Report, Electric Power Research Institute, Palo Alto, 1994.
21. J.A. Gorman, R.W. Staehle, and K.D. Stavropoulos, Statistical Analysis of Steam Generator Tube Degradation, NP-7493, Electric Power Research Institute, Palo Alto, 1991.
22. G.L. Webb and M.G. Burke, "Stress Corrosion Cracking Behavior of Alloy 600 in High Temperature Water," Seventh International Symposium on Environmental Degradation of Materials in Nuclear Power Systems - Water Reactors, G. Airey, et al., eds., National Association of Corrosion Engineers International, Houston, 1995, p. 41.
23. G.L. Webb and M.M. Hall, Jr., Pressurized Water Stress Corrosion Cracking of Alloy 600, WAPD-T-3059, Bettis Atomic Power Laboratory, Pittsburgh, Pennsylvania, 1994.
24. G.L. Webb, "Environmental Degradation of Alloy 600 and Welded Filler Metal EN82 in an Elevated Temperature Aqueous Environment," WAPD-T-2989, Bettis Atomic Power Laboratory, Pittsburgh, 1993.
25. S. Shimada and M. Nagai, "Analysis of the Distribution of Time-to-Failure in Stochastic Failure Process," Journal of the Society of Materials Science 32, 1983, p. 83.
26. S. Shimada and M. Nagai, "Variation of Initiation Time for Stress Corrosion Cracking in Zircaloy-2 Cladding Tube," Reliability Engineering 9, 1984, p. 19.
27. R.W. Staehle, J.A. Gorman, K.D. Stavropoulos, and C.S. Welty, Jr., "Application of Statistical Distributions to Characterizing and Predicting Corrosion of Tubing in Steam Generators of Pressurized Water Reactors," Life Prediction of Corrodible Structures, R.N. Parkins, ed., National Association of Corrosion Engineers International, Houston, 1994, p. 1374.
28. E.J. Gumbel, "Statistical Theory of Extreme Values and Some Practical Applications," Applied Mathematics 33, U.S. Dept. of Commerce, National Bureau of Standards, Washington, 1954, p. 1.
29. E.J. Gumbel, Statistics of Extremes, Columbia University Press, New York, 1958.

30. J. Galambos, J. Lechner, and E. Simiu, eds., Extreme Value Theory and Applications. Special Publication 866, National Institute of Standards and Technology, Gaithersburg, MD, 1994.
31. W. Weibull, "A Statistical Distribution Function of Wide Applicability," Journal of Applied Mechanics 10, 1951, p. 293.
32. W. Nelson, "Weibull Prediction of a Future Number of Failures," Quality and Reliability Engineering International 16, 2000, p. 23.
33. K.T. Chang, "Analysis of the Weibull Distribution Function," Journal of Applied Mechanics 49, 1982, p. 450.
34. R.K. Reeves and D.W. Hoepfner, "A Weibull Analysis of Center Cracked Panel Crack Growth Data of a 0.40/0.50 Carbon Steel," Engineering Fracture Mechanics 10, 1978, p. 571.
35. R.B. Abernethy, The New Weibull Handbook; Second Edition, R.B. Abernethy Publisher, North Palm Beach, Florida, 1996.
36. D.G. Harlow and R.P. Wei, "A Mechanistically Based Approach to Probability Modeling for Corrosion Fatigue Crack Growth," Engineering Fracture Mechanics 45, 1, 1993, p. 79.
37. R.P. Wei and D. G. Harlow, "A Mechanistically Based Probability Approach for Life Prediction," International Symposium on Plant Aging and Life Predictions of Corrodible Structures, T. Shibata and T. Shoji, eds., National Association of Corrosion Engineers International, Houston, 1995, p. 47.
38. N.R. Cawley, D. G. Harlow, and R. P. Wei, "Probability and Statistics Modeling of Constituent Particles and Corrosion Pits as a Basis for Multiple-Site Damage Analysis," FAA-NASA Symposium on the Continued Airworthiness of Aircraft Structures, A97-4010111-05, Office of Aviation Research, Washington, 1997, p. 531.
39. R.P. Wei, "Life Prediction: A Case for Multidisciplinary Research," Fatigue and Fracture Mechanics: Volume 27, STP 1296, R.S. Piascik, J.C. Newman, and N. E. Dowling, eds., American Society for Testing and Materials, Philadelphia, 1997, p. 3.
40. R. P. Wei, "Material Aging and Reliability of Engineered Systems," Environmentally Assisted Cracking: Predictive Methods for Risk Assessment and Evaluation of Materials, Equipment, and Structures, STP 1401, R. Kane, ed., American Society for Testing and Materials, Philadelphia, 2000, p. 3.
41. X.C. Jiang and R.W. Staehle, "Effects of Stress and Temperature on Stress Corrosion Cracking of Austenitic Stainless Steels in Concentrated Magnesium Chloride Solutions," Corrosion 53, 6, 1997, p. 448.
42. P.L. Andresen, "Effects of Testing Characteristics on Observed SCC Behavior in BWRs," Corrosion 98, Paper No. 137, National Association of Corrosion Engineers International, Houston, 1998, p. 137/1.
43. J. Jansson and U. Morin, "Assessment of Crack Growth Rates in Austenitic Stainless Steels in Operating BWRs," Eighth International Symposium on Environmental Degradation of Materials in Nuclear Power Systems - Water Reactors, A.R. McIlree, chair, American Nuclear Society, La Grange Park, 1997, p. 667.
44. E.D. Eason and L.M. Shusto, Analysis of Cracking in Small Diameter BWR Piping, EPRI NP 4394, Electric Power Research Institute, Palo Alto, 1986.

45. R.W. Staehle, "Initiation and Propagation of SCC in Inconels for Steam Generators," paper presented at Korea Atomic Energy Research Institute Second Seminar on Nuclear Materials, Taejon, Korea, June 13-14, 1996.
46. T.P. Hoar and J.G. Hines, "Stress Corrosion Cracking of Austenitic Stainless Steels," Journal of the Iron and Steel Institute 182, 2, 1956, p. 124.
47. G. Engelhardt and D.D. Macdonald, "Deterministic Prediction of Pit Depth Distribution," Corrosion 54, 1998, p. 469.
48. J.R. Galvele, "Transport Processes and the Mechanism of Pitting of Metals," Journal of the Electrochemical Society 4, 1976, p. 464.
49. G.G. Lang, K. Ueno, M. Ujvari and M. Seo, "Simultaneous Oscillations of Surface Stress and Potential in the Course of Galvanostatic Oxidation of Formic Acid," Phys. Chem. B 104, 13, 2000, p. 2785.
50. R.M. Latanision and R.W. Staehle, "The Effect of Continuous Hydrogenation on the Deformation of Nickel Single Crystals," Scripta Met. 2, 12, 1968, p. 667.
51. R.M. Latanision and R.W. Staehle, "Plastic Deformation of Electrochemically Polarized Nickel Single Crystals," Acta Met. 17, 3, 1969, p. 307.
52. T. Shibata and R.W. Staehle, "Application of High Speed Elongation Technique to Stress Corrosion Cracking of Fe-Cr-Ni Alloys," Proceedings of Fifth International Congress on Metallic Corrosion, N. Sato, ed., National Association of Corrosion Engineers International, Houston, 1972, p. 487.
53. P.R. Swann and J. Nutting "Stacking Faults and the Failure of Alloys in Corrosive Media," Journal of the Institute of Metals 88, 1960, p. 468.
54. F.P. Ford and P.L. Andresen, "Corrosion in Nuclear Systems: Environmentally Assisted Cracking in Light Water Reactors," Corrosion Mechanisms in Theory and Practice, P. Marcus and J. Oudar, eds., Marcel Dekker, New York, 1995, p. 501.
55. J.L. Leach and P. Neufeld, "Mechanical Effects During the Growth of Anodic Films," Corrosion Science 9, 1969, p. 225.
56. T.J. Smith and R.W. Staehle, "Role of Slip Step Emergence in the Early Stages of Stress Corrosion Cracking in Face Centered Iron-Nickel-Chromium Alloys," Corrosion 23, 1967, p. 117.
57. J.A. Davis and R.W. Staehle, "Local Dissolution Phenomena Occurring on Iron-Chromium-Nickel Alloys: An Electron Microscopic Study," Ohio State University Report #COO-1319-66 for U. S. Atomic Energy Commission, January 1968.
58. R.W. Staehle, "Predictions and Experimental Verification of the Slip Dissolution Model for SCC of Low Strength Alloys," Stress Corrosion Cracking and Hydrogen Embrittlement of Iron Base Alloys. NACE-5, J. Hochmann, J. Slater, and R.W. Staehle, eds., National Association of Corrosion Engineers International, Houston, 1977, p. 700.
59. N.A. Nielsen, "I. Nature of Initial Corrosion of Stressed Austenitic Stainless Steel by Chloride Ions. II. Platinum Decoration of Active Sites," Corrosion 20, 1964, p. 104.
60. M.F. Dean, F.H. Beck, and R.W. Staehle, "Tunnel Formation in Iron-Nickel-Chromium Alloys," Corrosion 23, 1967, p. 192.

61. M. Akashi and G. Nakayama, "Stress-Corrosion Crack Initiation Process Model for BWR Plant Materials," International Symposium on Plant Aging and Life Predictions of Corrodible Structures, T. Shibata and T. Shoji, eds., National Association of Corrosion Engineers International, Houston, 1995, p. 99.
62. H.W. Pickering, "Direct Observations of Etch Pits at Dislocations in Fe-3%Si," Acta Metallurgica 13, 1965, p. 437.
63. H. W. Pickering, "Characteristic Features of Alloy Polarization Curves," Corrosion Science 23, 1983, p. 1107.
64. H. W. Pickering and Y.S. Kim, "De-Alloying at Elevated Temperatures and at 298K—Similarities and Differences," Corrosion Science 22, 1982, p. 621.
65. P.M. Scott and M. LeCalvar, "Some Possible Mechanisms of Intergranular Stress Corrosion Cracking of Alloy 600 in PWR Primary Water," Proceedings of the Sixth International Symposium on Environmental Degradation of Materials in Nuclear Power Systems—Water Reactors, R.E. Gold and E.P. Simonen, eds., TMS (The Minerals, Metals and Materials Society), Warrendale, Pennsylvania, 1993, p. 657.
66. A.J. Forty, "The Metal Physics of Stress Corrosion," Fundamental Aspects of Stress Corrosion Cracking, R.W. Staehle, A.J. Forty, and D. van Rooyen, eds., National Association of Corrosion Engineers International, Houston, 1969, p. 64.
67. R.N. Parkins, "Stress Corrosion Cracking," Environment Induced Cracking of Metals: NACE-10, R.P. Gangloff and M.B. Ives, eds., National Association of Corrosion Engineers International, Houston, 1990, p. 1.
68. P.L. Andresen and F.P. Ford, "Fundamental Modeling of Environmental Cracking for Improved Design and Lifetime Evaluation in BWRs," International Journal of Pressure Vessels and Piping 50, 1994, p. 61.
69. R.N. Parkins, "Stress Corrosion Cracking," Environment-Induced Cracking of Metals, NACE-10, R.P. Gangloff and M.B. Ives, eds., National Association of Corrosion Engineers International, Houston, 1990, p. 1.
70. J.M. Gras, "Stress Corrosion Cracking of Steam Generator Tubing Materials, Review and Assessment," in S.M. Bruemmer, E.I. Meletis, R.H. Jones, W.W. Gerberich, F. P. Ford, and R.W. Staehle, eds, Parkins Symposium on Stress Corrosion Cracking, TMS (The Minerals, Metals and Materials Society), Warrendale, Pennsylvania, 1992, p. 411.
71. T.P. Hoar and J.G. Hines, "Stress Corrosion Cracking of Austenitic Stainless Steels," Journal of Iron and Steel Institute 182, 2, 1956, p. 124.
72. J.G. Hines, "The Development of Stress Corrosion Cracks in Austenitic Cr-Ni Steels," Corrosion Science 1, 1961, p. 1.
73. J.F. Eckel, "Stress Corrosion Crack Nucleation & Growth in Austenitic Stainless Steel," Corrosion 18, 7, 1962, p. 270.
74. N. Pessall, "Prediction of Stress Corrosion Cracking in 10% Caustic Soda Solutions at 315°C," Corrosion Science 20, 1980, p. 225.

75. R.W. Staehle, "Development and Application of Corrosion Mode Diagrams," Parkins Symposium on Stress Corrosion Cracking, S.M. Bruemmer, E. Meletis, R.H. Jones, W.W. Gerberich, F.P. Ford, and R.W. Staehle, eds, TMS (The Minerals, Metals and Materials Society), Warrendale, Pennsylvania, 1992, p. 447.
76. R.W. Staehle, "Understanding 'Situation-Dependent Strength'; A Fundamental Objective in Assessing the History of Stress Corrosion Cracking," Environment Induced Cracking of Metals, NACE-10, R.P. Gangloff and M.B. Ives, eds., National Association of Corrosion Engineers International, Houston, 1990, p. 561.
77. R.W. Staehle, "Stress Corrosion Cracking of Fe-Cr-Ni Alloy Systems," Theory of Stress Corrosion Cracking, J.C. Scully, ed., NATO Scientific Affairs Division, Brussels, 1971, p. 222.
78. R.W. Staehle and J.A. Gorman, "Development and Application of Intensity and Operating Diagrams for Predicting the Occurrence and Extent of Stress Corrosion Cracking," Corrosion Science and Engineering: Proceedings of an International Symposium in Honour of Marcel Pourbaix's 85th Birthday, R.A. Rapp, N.A. Gokchen, and A. Pourbaix, eds., Rapports Techniques CEBELCOR, Brussels, Vol. 157-158, 1989, p. 199.
79. R.H. Copson and S.W. Dean, "Effect of Contaminants on Resistance to Stress Corrosion Cracking of Ni-Cr Alloy 600 in Pressurized Water," Corrosion 21, 1965, p. 1.
80. B.P. Miglin and J.M. Sarver, "Preliminary Studies of Lead Stress Corrosion Cracking of Alloy 690," Proceedings of the Fourth International Symposium on Environmental Degradation of Materials in Nuclear Power Systems - Water Reactors, D. Cubicciotti, ed., National Association of Corrosion Engineers International, Houston, 1990, p. 11/32.
81. S.S. Hwang, K.M. Kim, and U.C. Kim, "Stress Corrosion Cracking Aspects of Nuclear Steam Generator Tubing Materials in the Water Containing Lead at High Temperature," Proceedings of the 8th International Symposium on Environmental Degradation of Materials in Nuclear Power Systems - Water Reactors, A.R. McIlree and S.M. Bruemmer, chairs, American Nuclear Society, La Grange Park, Illinois, 1997, p. 200.
82. M.D. Wright, "Establishing Threshold Conditions for Lead Induced Cracking of Steam Generator Tube Alloys," Water Chemistry of Nuclear Reactor Systems 7, T. Swan, chair, British Nuclear Energy Society, London, 1996, p. 435.
83. P. Berge and J.R. Donati, "Materials Requirements for Pressurized Water Reactor Steam Generator Tubing," Nuclear Technology 55, 1981, p. 88.
84. P. Berge, D. Noel, J. Gras, and B. Prieux, "Chloride Stress Corrosion Cracking of Alloy 600 in Boric Acid Solutions," Proceedings of the 8th International Symposium on Environmental Degradation of Materials in Nuclear Power Systems - Water Reactors, A.R. McIlree and S.M. Bruemmer, chairs, American Nuclear Society, La Grange Park, Illinois, 1997, p.189.
85. H.R. Copson and C.F. Cheng "Some Case Histories of Stress Corrosion Cracking of Austenitic Stainless Steels Associated with Chlorides," Corrosion 13, 1957, p. 397.
86. H.R. Copson, "Effect of Nickel Content on the Resistance to Stress-Corrosion Cracking of Iron-Nickel-Chromium Alloys in Chloride Environments," Proceedings of the First International Congress on Metallic Corrosion, L. Kenworthy, ed., Butterworths, London, 1962, p. 328.

87. G.S. Was, J.L. Hertzberg, and V. Thaveeprungrasriorn, "Effects of Grain Boundary Composition and Structure on IGSCC of Alloy 600," Control of Corrosion on the Secondary Side of Steam Generators, R.W. Staehle, J.A. Gorman, and A.R. McIlree, eds., National Association of Corrosion Engineers International, Houston, 1996, p. 347.
88. R.W. Staehle, "Occurrence of Modes and Submodes of IGC and SCC," Control of Corrosion on the Secondary Side of Steam Generators, R.W. Staehle, J.A. Gorman, and A.R. McIlree, eds., National Association of Corrosion Engineers International, Houston, 1996, p. 135.
89. T. Cassagne and A. Gelpi, "Crack Growth Rate Measurements on Alloy 600 Steam Generator Tubing in Primary and Hydrogenated AVT Water," Proceedings of the Sixth International Symposium on Environmental Degradation of Materials in Nuclear Power Systems—Water Reactors, R.E. Gold and E.P. Simonen, eds., TMS (The Minerals, Metals and Materials Society), Warrendale, Pennsylvania, 1993, p. 679.
90. Z. Fang and R.W. Staehle, "Effects of the Valence of Sulfur on the Passivation of Alloys 600 and 690 at 25° and 95°C," Corrosion Journal 55, 4, 1999, p. 355.
91. R. Jacko, Effect of Lithium Hydroxide on Primary Water Stress Corrosion Cracking of Alloy 600 Tubing, NP-7396-M, Electric Power Research Institute, Palo Alto, 1991.
92. S. M. Dehmlow, "Development of Accelerated Test Methods: Application to a Fillet Welded Tube and Plate Geometry," EPRI Workshop on Primary Water Stress Corrosion Cracking of Alloy 600, Electric Power Research Institute, Palo Alto, 1994.
93. N. Totsuka and Z. Szklarska-Smialowska, "Effect of Electrode Potential on the Hydrogen-Induced IGSCC of Alloy 600 in an Aqueous Solution at 350°C," Corrosion 43, 1987, p. 734.
94. T. Shoji, "Mechanics and Mechanisms of Stress Corrosion Cracking of Alloy 600 in High Temperature Waters," Proceedings: Specialists Meeting on Environmental Degradation of Alloy 600: TR-104898, R.G. Ballinger, A.R. McIlree, and J.P.N. Paine, eds., Electric Power Research Institute, Palo Alto, 1996, p. 18/1.
95. R.N. Parkins, "Synthetic Solutions and Environment Sensitive Fracture," The Use of Synthetic Environments for Corrosion Testing: STP-970, P.E. Francis and T.S. Lee, eds., American Society of Testing and Materials, Philadelphia, 1988, p. 132.
96. C.J. Congleton, T. Shoji, and R. N. Parkins, "The Stress Corrosion Cracking of Reactor Pressure Vessel Steel in High Temperature Water," Corrosion Science 25, 1985, p. 633.
97. M.J. Pourbaix, Thermodynamics of Dilute Aqueous Solutions, Edward Arnold, London, 1949.
98. J. Tafel, "Über die Polarisation Bei Kathodischer Wasserstoffentwicklung," Z. Phys. Chem 50, 1904, p. 641.
99. J.V. Butler, "Studies in Heterogeneous Equilibria. Part II. The Kinetic Interpretation of the Nernst Theory of Electromotive Force," Trans. Faraday Soc. 19, 1924, p. 729
100. T. Erdey-Gruz and M. Volmer, "Zur Theorie der Wasserstoffüberspannung," Z. Physik., Chem. (Leipzig) 150, 1930, p. 203.
101. T. Shibata, J. Horikawa, and J. Nakata, "Effect of Sensitization on the Probability Distribution of Stress Corrosion Cracking Failure Times of Type 304 Stainless Steel," Boshoku Gijutsu 35, 1986, 83.

102. M. Akashi, T. Kenjyo, S. Matsukura, and T. Kawamoto, "The Probability Distribution of Intergranular Stress Corrosion Cracking Life for Sensitized 304 Stainless Steels in High Temperature, High Purity Water," Boshoku Gijutsu 33, 1984, p. 628.
103. A. Okamoto, M. Akashi, and M. Kitagawa, "Probabilistic Approach for the Defect Identification in BWR Piping, Pressure Vessel and Piping Conference, Paper 87-PVP-30, American Society of Mechanical Engineers, New York, 1987, p. 1.
104. M. Akashi and A. Ohtomo, "Evaluation of the Factor of Improvement for the Intergranular Stress Corrosion Cracking Life of Sensitized Stainless Alloys in High Temperature, High-Purity Water Environment," Society of Materials Science- Japan 36, 1987, p. 59.
105. G. Nakayama, M. Akashi, and A. Ohtomo, "A Probabilistic Assessment for the Stress Corrosion Cracking Lifetime of Sensitized 304 Stainless Steel in Sodium Chloride Solutions," ISIJ International 31, 1991, p. 223.
106. K. Nakanishi, Y. Tanaka, K. Yoshida, and M. Akashi, "Effects of Applied Stress on the Stress-Corrosion Cracking Lifetime of Carbon Steel Weld Metal in High-Purity Water Environment at 250°C," Proceedings of the International Symposium on Plant Aging and the Prediction of Corrodible Materials, T. Shoji and T. Shibata, eds., National Academy of Corrosion Engineers International, Houston, 1997, p. 691.
107. K. Nakanishi, Y. Tanaka, K. Yoshida, G. Nakayama, and M. Akashi, "Stress-Corrosion Crack Initiation Behavior of Carbon Steel in Simulated BWR Environment," Corrosion 94, Paper 156, National Academy of Corrosion Engineers International, Houston, 1994, p. 156/1.
108. T. Shibata, "Stochastic Approach to the Effect of Alloying Elements on the Pitting Resistance of Ferritic Stainless Steels," Transactions ISIJ 23, 1983, p. 785.
109. J.R. Balavage and S.J. Gardner, "Material Test Results on Thermally Treated Alloy 690 and Shot Peened Alloy 800 Steam Generator Tubing. Appendix C," Alloy 690 for Steam Generator Tubing Applications, NP-6997-SD, R.E. Gold, D.L. Harrod, R.G. Aspden, and A.J. Baum, eds., Electric Power Research Institute, Palo Alto, 1990, p. C-1.
110. T. Shibata and K. Okamoto, "Estimation of Maximum Pit Depth on the Oil Tank Base Plate by Extreme Value Analysis," Bositoku Gijutsu 30, 1981, p. 404.
111. T. Shibata, "Evaluation of Corrosion Failure by Extreme Value Statistics," ISIJ International 31, 1991, p. 115.
112. T. Shibata, M. Akashi, K. Ikematsu, H. Nakajima, and H. Tsuge, "Estimating Localized-Corrosion Maximum Depths by Extreme-Value Analysis," Corrosion Engineering 37, 1988, p. 699.
113. T. Shibata, "Evaluation of Corrosion Failure by Extreme Value Statistics," ISIJ International 31, 1991, p. 115.
114. T. Shibata, "Application of Extreme Value Statistics to Corrosion," Journal of Research National Institute of Standards Technology 99, 1994, p. 327.
115. W.L. Clarke and G.M. Gordon, "Investigation of Stress Corrosion Cracking Susceptibility of Fe-Ni-Cr Alloys in Nuclear Reactor Water Environments," Corrosion 29, 1973, p. 1.

116. T.B. Cassagne, P. Combrade, M.A. Foucault, and A. Gelpi, "The Influence of Mechanical and Environmental Parameters on the Crack Growth Behavior of Alloy 600 in PWR Primary Water," 12th Scandinavian Corrosion Congress & Eurocorr '92, P.J. Tunturi, ed., Corrosion Society of Finland, Helsinki, 1992, p. 55.
117. K. Noring, J. Engstrom, and P. Norberg, "Intergranular Stress Corrosion Cracking in Steam Generator Tubing. Testing of Alloy 690 and Alloy 600 Tubes," Proceedings of the Third International Symposium on Environmental Degradation of Materials in Nuclear Power Systems – Water Reactors, G.J. Theus and J.R. Weeks, eds., The Metallurgical Society, Warrendale, Pennsylvania, 1988, p.587.
118. Z. Fang and R.W. Staehle, Calculations with KalidaGraph Software, Version 3.0.
119. M. Akashi and A. Ohtomo, "Evaluation of the Factor of Improvement for the Intergranular Stress Corrosion Cracking Life of Sensitized Stainless Alloys in High-Temperature, High-Purity Water Environment," Journal of the Society of Materials Science of Japan 36, 59, 1987, p. 59.
120. T. Shibata and T. Takeyama, "Analysis of Stress Corrosion Cracking Failure Times of Type 316 Stainless Steel by the Weibull Distribution," Boshoku Gijutsu 30, 1, 1981, p. 47.
121. T. Shibata, S. Fujimoto, A. Asada, and J. Nakata, "Effect of CaCl<sub>2</sub> Concentration on the Probability Distribution of Stress Corrosion Cracking Failure Time of Type 304 Stainless Steel," 10<sup>th</sup> International Congress on Metallic Corrosion, K.I. Vasu, Chair, Trans Tech Publications, Switzerland, 1987, p. 1892.
122. WINSMITH™ Weibull 3.0U Version.
123. T. Shibata and T. Takeyama, "Probability Distribution of Failure Times of Stress Corrosion Cracking of 17Cr-11Ni Stainless Steel," Tetsu-To-Hagane 66, 1980, p. 693.
124. M. Ichikawa, T. Takura, and S. Tanaka, "A Statistical Aspect of Stress Corrosion Cracking of a High Strength Steel in NaCl Solution," International Journal of Fracture 16, 1980, p. 251.
125. M. Ichikawa, T. Takura, and S. Tanaka, "A Statistical Study of Stress Corrosion Cracking Life," Bulletin of the JSME 26, 1983, p. 1857.
126. R.W. Staehle, J.J. Royuela, T.L. Raredon, E. Serrate, C.R. Morin, and R.V Farrar, "Effect of Alloy Composition on Stress Corrosion Cracking of Fe-Cr-Ni Base Alloys," Corrosion 26, 11, 1970, p. 451.
127. D. van Rooyen, "Some Aspects of Stress Corrosion Cracking in Austenitic Stainless Steels," Proceedings of the First International Congress on Metallic Corrosion, L. Kenworthy, ed., Butterworths, London, 1962, p. 309.
128. S. Barnartt, R. Stickler, and D. van Rooyen, "Stress Corrosion Cracking Mechanism in Purified 16% Cr- 10% Ni Stainless Steels," Corrosion Science 3, 1963, p. 9.
129. H.H. Uhlig, A. White, and J. Lincoln, "Austenitic Cr-Fe-Ni Alloys Resistant to Stress Corrosion Cracking in Magnesium Chloride," Acta Metallurgica 5, 1957, p. 473.
130. H.H. Uhlig and R.A. White, "Some Metallurgical Factors Affecting Stress Corrosion Cracking of Austenitic Stainless Steel," Trans. ASM 52, 1960, p. 830.
131. H.H. Uhlig and J.P. Sava, Massachusetts Institute of Technology, Topical Report, 1966.

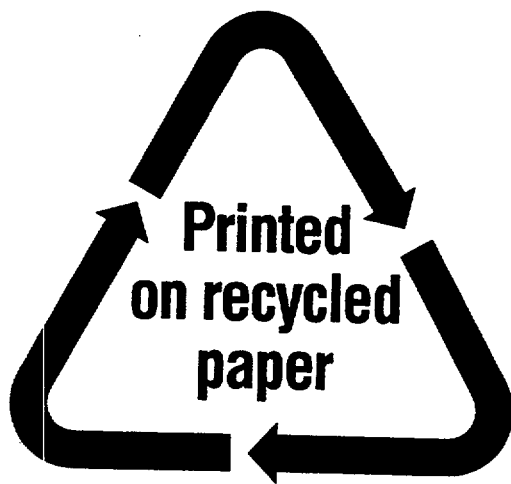


132. F.S. Lang, "Effects of Trace Elements on Stress Corrosion Cracking of Austenitic Stainless Steels in Chloride Solutions," Corrosion 18, 1962, p. 378.
133. A.P. Bond and H.J. Dundas, "Effects of Composition on the Stress Corrosion Cracking of Ferritic Stainless Steels," Corrosion 24, 10, 1968, p. 344.
134. P.R. Swann and J. Nutting, "Stacking Faults and the Failure of Alloys in Corrosive Media," Journal of the Institute of Metals 88, 1960, p. 478.
135. D.L. Douglass, G. Thomas and W. R. Roser, "Ordering, Stacking Faults, and Stress Corrosion Cracking in Austenitic Alloys," Proceedings 2nd International Congress on Metallic Corrosion, E.C. Greco, president, National Association of Corrosion Engineers International, Houston, 1966, p. 66.
136. R.J. Jacko, Evaluation of Thermally Treated Alloy 600 in Faulted Secondary and Primary Water Environments, NP-3051 (ext.), Electric Power Research Institute, Palo Alto, 1985.
137. J. Blanchet, H. Coriou, L. Grall, C. Mahieu, C. Otter, and G. Turlur, "Historical Review of the Principal Research Concerning the Phenomena of Cracking of Nickel Base Austenitic Alloys," Stress Corrosion Cracking and Hydrogen Embrittlement of Iron Base Alloys, NACE-5, R.W. Staehle, J. Hochmann, R.D. McCright, and J.E. Slater, eds., National Association of Corrosion Engineers International, Houston, 1977, p. 1149.
138. P.M. Scott, "2000 F.N. Speller Award Lecture: Stress Corrosion Cracking in Pressurized Water Reactors - Interpretation, Modeling, and Remedies," Corrosion 56, 8, 2000, p.771.
139. W.L. Clarke and V.M. Romero, Detection of Sensitization in Stainless Steel: II. EPR Method for Nondestructive Field Tests, GEAP-12697, General Electric, San Jose, February 1978.
140. D.O. Harris, D.D. Dedhia, and E.D. Eason, "Probabilistic Analysis of Initiation and Early Growth of Stress Corrosion Cracks in BWR Piping," 86-PVP-11, presented at the ASME Pressure Vessels and Piping Conference, American Society of Mechanical Engineers, New York, 1986, p. 1.
141. R.W. Cochran and R.W. Staehle, "Effects of Surface Preparation on Stress Corrosion Cracking of Type 310 Stainless Steel in Boiling 42% Magnesium Chloride," Corrosion 24, 11, 1968, p. 369.
142. M. Akashi and G. Nakayama, "Effects of Acceleration Factors on the Probability Distribution of Stress Corrosion Crack Initiation Life for Alloys 600, 182, and 82 in High Temperature and High Purity Water Environments," The Ninth International Conference on Environmental Degradation of Materials in Nuclear Power Systems – Water Reactors, S. Bruemmer and P. Ford, eds., TMS (The Minerals, Metals and Materials Society), Warrendale, Pennsylvania, 1999, p. 389.
143. P. Berge, "The Importance of Surface Preparation for the Control of Corrosion in Nuclear Power Stations," Materials Performance 36, 11, 1997, p. 56.
144. G.V. Rao, "Methodologies to Assess PWSCC Susceptibility of Primary Component Alloy 600 Locations in Pressurized Water Reactors," Proceedings of the Sixth International Symposium on Environmental Degradation of Materials in Nuclear Power Systems—Water Reactors, R.E. Gold and E.P. Simonen, eds., TMS (The Minerals, Metals and Materials Society), Warrendale, Pennsylvania, 1993, p. 871.

145. T. Shibata and T. Takeyama, "Stochastic Theory of Pitting Corrosion," Corrosion 33, 7, 1977, p. 248.
146. Z. Szklarska Smialowska and R. B. Rebak "Stress Corrosion Cracking of Alloy 600 in High Temperature Aqueous Solutions: Influencing Factors, Mechanisms and Models," Control of Corrosion on the Secondary Side of Steam Generators, R.W. Staehle, J.A. Gorman, and A.R. McIlree, eds., National Association of Corrosion Engineers, Houston, 1996, p. 223.
147. M.E. Indig and A.R. McIlree, "High Temperature Electrochemical Studies of the Stress Corrosion of Type 304 Stainless Steel," Corrosion 35, 7, p. 288.
148. G. Salvago, G. Fumagalli, and G. Taccani, "Corrosion Potential and Breakdown Potential Distributions for Stainless Steels in Seawater," Corrosion 96, Paper No. 511, National Association of Corrosion Engineers, Houston, 1996, p.511/1.
149. H. Takamatsu, K. Matsueda, E. Kadokami, K. Arioka, T. Tsuruta, S. Okamoto, and T. Ueno, "Evaluation of SG Crevice Environment by Directly Sampled Method Using an On-Site Autoclave Facility," Proceedings of the Fifth International Symposium on Environmental Degradation of Materials in Nuclear Power Systems - Water Reactors, D. Cubicciotti, chair, American Nuclear Society, La Grange Park, Illinois, 1992, p. 752.
150. T. Shibata, J. Nakata, and S. Fujimoto, "Probability Distribution of SCC Failure Time Type 304 Stainless Steel in CaCl<sub>2</sub> Solution," Lifetime Prediction of Corrodible Structures, R.N. Parkins, ed., National Association of Corrosion Engineers International, Houston, 1994, p. 1064.
151. T. Shibata and Y.-C. Zhu, "A Stochastic Analysis of Flow Velocity Effects on the Pit Generation Process on Anodized Titanium," Corrosion Science 37, 5, 1995, p. 853.
152. E.D. Eason and J. Padmanaban, "A Model of Expected Time-to-failure by IGSCC in 304 Stainless Steel," Report FAA-M-82-12-4, Failure Analysis Associates, Palo Alto, December 14, 1982.
153. R.J. Jacko, Corrosion Evaluation of Thermally Treated Alloy 600 Tubing in Primary and Faulted Secondary Water Environments, NP-6721-SD, Electric Power Research Institute, Palo Alto, 1990.
154. D. van Rooyen, "Update on SCC of Alloy 600 in High Temperature Water," Paper 10, Proceedings: 1985 Workshop on Primary Side Stress Corrosion Cracking of PWR Steam Generator Tubing, NP 5158, A.A. Stein and A.R. McIlree, eds., Electric Power Research Institute, Palo Alto, 1985, p. 10/1.
155. P. Scott, Y. Meyzaud, and C. Benhamou, "Prediction of Stress Corrosion Cracking of Alloy 600 Components Exposed to PWR Primary Water," International Symposium on Plant Aging and Life Predictions of Corrodible Structures, T. Shibata and T. Shoji, eds., National Association of Corrosion Engineers International, Houston, 1995, p. 285.
156. G.J. Theus, "Summary of the Babcock and Wilcox Company's Stress Corrosion Cracking Tests of Alloy 600, Workshop Proceedings: U-Bend Tube Cracking in Steam Generators, WS-80-136, C.E. Shoemaker, ed., Electric Power Research Institute, Palo Alto, 1981, p.15/1.
157. R. Magdowski and M.O. Speidel, "Effect of Cold Work on the Growth Rates of Stress Corrosion Cracks in Structural Materials of Nuclear Systems," Corrosion 96, Paper No. 112, National Association of Corrosion Engineers, Houston, 1996, p. 112/1.

158. C. Amzallag, F. Vaillant, and A. Teissier, "Derivation of Stress Corrosion Crack Growth Laws for Alloy 600 PWR Components," Paper B4, Proceedings: 1997 EPRI Workshop on PWSCC of Alloy 600 in PWRs, EPRI TR-109138, S. Hunt, ed., Electric Power Research Institute, Palo Alto, 1997, p. 3/7.
159. K. Yamauchi, S. Kimura, T. Katori, K. Sigehiro, and T. Shindo, "Analysis of Stress Corrosion Cracking Life Based on Reactor Model," Nuclear Engineering and Design, 138, 1992, p. 239.
160. T. Shibata, K. Furusaki, and J. Nakata, "Probability Distribution of Crack Initiation and Propagation Times for Stress Corrosion Cracking of Type 304 Stainless Steel," Boshoku Gijutsu 33, 1984, p. 223.
161. R.N. Parkins and P.M. Singh, "Stress Corrosion Crack Coalescence," Corrosion 46, 6, 1990, p 485.
162. G. Nakayama and M. Akashi, "Stress Corrosion Crack Initiation Process for Alloy 182 Weld Metal in Simulated BWR Environments," Corrosion 95, Paper No. 406, National Association of Corrosion Engineers International, Houston, 1995, p. 406/1.
163. R.P. Gangloff, "Fracture Mechanics Characterization of Hydrogen Embrittlement in Cr-Mo Steel," Present Situation on Steels for Hydrogen Pressure Vessels, Creusot-Loire Industrie, Le Creusot, France, 1998.
164. E. Sato, H. Abo, and T. Murata, "Lifetime Estimation and Accelerated Stress Corrosion Cracking Test of Stainless Steel in a Neutral Chloride Environment," Corrosion 46, 11, 1990, p. 924.
165. K.D. Stavropoulos, R.W. Staehle, and J.A. Gorman, Statistical Prediction of Performance of Containers for Radioactive Waste, Topical Report DEI-313, Dominion Engineering, McLean, Virginia, November 7, 1991.
166. R.W. Staehle and K.D. Stavropoulos, Elements and Issues in Predicting the Life of Containers for Radioactive Waste, Topical Report DEI-335, Dominion Engineering, McLean, Virginia, March 30, 1992.
167. P.M. Scott, "Prediction of Alloy 600 Component Failures in PWR Systems," Proceedings of Corrosion 96: Research Topical Symposia, F.P. Ford and R. Baboian, chairs, National Association of Corrosion Engineers, Houston, 1996, p. 135.
168. E. Pierson and C. Laire "The Influence of Copper on the SCC of Alloy 600 and Alloy 690 Steam Generator Tubes," Proceedings of International Symposium, Fontevraud IV, French Nuclear Society, 1998, p. 381.
169. R. Rentler and I. Welinsky, "Effect of HNO<sub>3</sub>- HF Pickling on Stress Corrosion Cracking of Ni-Cr-Fe Alloy 600 in High Purity Water at 660°F," WAPD-TM-944, Bettis Atomic Power Laboratory, Pittsburg, PA, October, 1970.

NRC FORM 335 (2-89) NRCM 1102, 3201, 3202	U. S. NUCLEAR REGULATORY COMMISSION  <b>BIBLIOGRAPHIC DATA SHEET</b> <i>(See instructions on the reverse)</i>	1. REPORT NUMBER <i>(Assigned by NRC. Add Vol., Supp., Rev., and Addendum Numbers, if any.)</i>  NUREG/CR- 6737 ANL-01/20 , RWS 151		
2. TITLE AND SUBTITLE  Bases for Predicting the Earliest Penetrations Due to SCC for Alloy 600 on the Secondary Side of PWR Steam Generators	3. DATE REPORT PUBLISHED			
	MONTH September	YEAR 2001		
	4. FIN OR GRANT NUMBER W6487			
5. AUTHOR(S)  R. W. Staelhle	6. TYPE OF REPORT Technical; Topical			
	7. PERIOD COVERED <i>(Inclusive Dates)</i>			
8. PERFORMING ORGANIZATION - NAME AND ADDRESS <i>(If NRC, provide Division, Office or Region, U.S. Nuclear Regulatory Commission, and mailing address; if contractor, provide name and mailing address.)</i>  <table style="width: 100%; border: none;"> <tr> <td style="width: 50%; border: none;">           Argonne National Laboratory through a subcontract to            9700 South Cass Avenue            Argonne, IL 60439         </td> <td style="width: 50%; border: none;">           Dr. R. W. Staelhle            22 Red Fox Road            North Oaks, MN 55127         </td> </tr> </table>			Argonne National Laboratory through a subcontract to 9700 South Cass Avenue Argonne, IL 60439	Dr. R. W. Staelhle 22 Red Fox Road North Oaks, MN 55127
Argonne National Laboratory through a subcontract to 9700 South Cass Avenue Argonne, IL 60439	Dr. R. W. Staelhle 22 Red Fox Road North Oaks, MN 55127			
9. SPONSORING ORGANIZATION - NAME AND ADDRESS <i>(If NRC, type "Same as above": if contractor, provide NRC Division, Office or Region, U.S. Nuclear Regulatory Commission, and mailing address.)</i>  Division of Engineering Technology Office of Nuclear Regulatory Research U.S. Nuclear Regulatory Commission Washington, DC 20555-0001				
10. SUPPLEMENTARY NOTES  J. Muscara, NRC Project Manager				
11. ABSTRACT (200 words or less)  The purpose of this report is to define the bases for predicting the earliest failures in a set of tubes in steam generators where the mode of failure is stress corrosion cracking. By "earliest failure" is meant the first that occur at a probability in the range of 0.0001 to 0.01, depending on the number of tubes at risk for a particular mode-location failure. Such early failures are removed from the mean time-to-failure where the probability of failure is 0.5. Most testing for the purpose of predicting performance is directed intentionally or not, toward determining the mean; however, using the mean time-to-failure as a measure of design life implies that 50% of the tubes would have failed during the design life. Failure times at probabilities of 0.0001 to 0.01 may be less than $10^{-4}$ to $10^{-2}$ of the mean time-to-failure when the shape parameter of the Weibull distribution, $\beta$ , is unity. In developing predictions of the earliest failures. In developing predictions of the earliest failures, knowledge of both the mean, whether measures as $\mu$ or the Weibull scale parameter, $\theta$ , and the shape parameter, $\beta$ , are necessary. In general, data obtained that are taken as the mean values are the same as correlations that are usually developed from testing; however, there are few data and no theory for predicting the shape parameter although certain inferences are possible with respect to the critical failure processes being random or subject to accumulation processes. To a first approximation, a conservative shape parameter for predicting the earliest failure is unity. Information is available that permits developing useful inferences about the mechanistic bases for statistical parameters.				
12. KEY WORDS/DESCRIPTORS <i>(List words or phrases that will assist researchers in locating this report.)</i>  Steam Generator Stress Corrosion Cracking	13. AVAILABILITY STATEMENT Unlimited			
	14. SECURITY CLASSIFICATION <i>(This Page)</i> Unclassified <i>(This Report)</i> Unclassified			
	15. NUMBER OF PAGES			
	16. PRICE			



Federal Recycling Program

**UNITED STATES  
NUCLEAR REGULATORY COMMISSION  
WASHINGTON, DC 20555-0001**

---

OFFICIAL BUSINESS  
PENALTY FOR PRIVATE USE, \$300